UNIVERSITY OF LIVERPOOL

DOCTORAL THESIS

Classification of Non-Supersymmetric Heterotic String Vacua

Author:
Benjamin PERCIVAL

Supervisor:
Prof. Alon FARAGGI

Thesis submitted in accordance with the requirements of the University of Liverpool for the degree of Doctor in Philosophy

in the

School of Physical Sciences

June 22, 2022

Abstract of thesis entitled

Classification of Non-Supersymmetric Heterotic String Vacua

Submitted by

Benjamin PERCIVAL

for the degree of Doctor of Philosophy

at The University of Liverpool

in June, 2022

This thesis centres around the classification of different types of non-supersymmetric $\mathbb{Z}_2 \times \mathbb{Z}_2$ heterotic string vacua in four dimensions according to certain phenomenological characteristics. Of notable interest are models that descend from the tachyonic heterotic string in ten dimensions. It is shown that tachyon-free models can be classified and their observable matter content studied, as well as their one-loop cosmological constants evaluated. A similar analysis can also be performed for non-supersymmetric vacua descending from the more widely studied $SO(16) \times SO(16)$ tachyon-free heterotic string in ten dimensions. Exploration in these spaces of models gives rise to uncovering novel string vacua, Type 0 and Type $\bar{0}$ strings, that are free from massless fermions and untwisted massless bosons, respectively.

A key tool to help in this investigation are the sophisticated computation algorithms SAT/SMT solvers, which are highly optimised for dealing with large constraint systems and deciding satisfiability. These solvers are shown to be useful in both efficiently solving phenomenological constraint systems and declaring when certain characteristics in classes of models are in contradiction.

The classification of non-supersymmetric vacua with asymmetric shifts is further introduced. In this setup several important phenomenological effects are noted arising from the asymmetric shifts. Worth special emphasis is their impact on fixing moduli in the internal space, which is suspected to be instrumental when seeking to deduce general features of the string vacua throughout the moduli space.

Classification of Non-Supersymmetric Heterotic String Vacua

by

Benjamin PERCIVAL

A Thesis Submitted in Partial Fulfilment
of the Requirements for the Degree of
Doctor of Philosophy

at

University of Liverpool
June, 2022

Declaration

The work in this thesis is based on research carried out in the String and BSM Phenomenology Group at the University of Liverpool. I, Benjamin Percival, declare that no material presented in this thesis has previously been submitted by myself in whole or in part for consideration for any other degree or qualification at this or any other University. The research described in this thesis has been carried out in collaboration with my supervisor, Professor Alon Faraggi. Parts of this thesis therefore have been published in collaborative works given in the 'List of Publications' section.

Signed: Benjamin Percival

Date: June 22, 2022

Acknowledgements

I would like to thank my supervisor Prof. Alon Faraggi, first and foremost, for his unwavering support throughout my PhD. It has been a pleasure to be welcomed into the world of string phenomenology with your perspective to guide me. I have particularly appreciated your quick feedback, as well as regular alerts of opportunities and advice for applications. A notable treat I remember is to have been invited by you to attend the small meal with Nobel Prize winner Didier Queloz prior to the 2019 Barkla lecture. I also always appreciated the regular meetings, in which I learned so much and improved my navigation of the literature.

To my family: thanks for all your support and understanding throughout the ups and down of the PhD. I am especially grateful for letting me stay during Covid lockdown for a couple of months and for help with my home in Liverpool.

Even though she is included in my family, Cinzia deserves a special mention for being by my side and supporting me throughout the PhD. I thank you for sharing these years with me- it's a joy to stumble through life with you. *Ti voglio bene*. Thanks also to your family for always welcoming me so warmly in Limbiate.

The TP department at Liverpool has made me feel very at home and I really have appreciated the independence granted to us in doing our research. I give a special mention to Susha for offering me advice and support at a difficult point in my PhD. I have also been very lucky to find colleagues who would become close friends over the years. With me right from the start, Flavio, was always there for me to meet at the cinema, Cambridge or Caledonia, as well as inspire me to be a better researcher. Viktor has been wonderful at juggling the mix of roles: collaborator, friend and office mate. Louis was a great ally and master of maintaining perspective. Stefano certainly shaped and brightened my experience of Liverpool. It was a delight sharing my office with Ulserik and going to lunches together- you also inspired me and brought so much kindness into my PhD life. Bruno, Max, John, Francesco and Jamie I am also delighted to have (had) as colleagues and friends.

Outside the University, I am still shocked by the incredible people I can call my friends. Of special mention: Julyan, Murray, Megan, Ed, Thomas, Anna, Rory, Sylvia, Ioana, Rob, Zoë, George, Johny, Clarky, Niamh, Tash, Teej and Kate. I love you all. Three of you deserve a special additional mention for 'technical support' work you did when I lost the thread: Murray, Ioana and Ed, I'm very grateful.

Benjamin PERCIVAL
University of Liverpool
June 22, 2022

List of Publications

Journals:

[1] A.E. Faraggi, G. Harries, B. Percival and J. Rizos (2020), *Doublet-Triplet Splitting in Fertile Left-Right Symmetric Heterotic String Vacua*, *Nucl. Phys.* **B953** (2020) 114969, doi: https://doi.org/10.1016/j.nuclphysb.2020.114969.

[2] A.E. Faraggi, V. G. Matyas and B. Percival (2020), *Stable Three Generation Standard–like Model From a Tachyonic Ten Dimensional Heterotic–String Vacuum*, *Eur. Phys. Jour.* **C80** (2020) 4, doi: https://doi.org/10.1140/epjc/s10052-020-7894-x.

[3] A.E. Faraggi, V.G. Matyas and B. Percival (2020), *Towards the Classification of Tachyon-Free Models From Tachyonic Ten-Dimensional Heterotic String Vacua*, *Nucl. Phys.* **B0550-3213** (2020) 115231, https://doi.org/10.1016/j.nuclphysb.2020.115231.

[4] A.E. Faraggi, V. G. Matyas and B. Percival (2021), *Type 0 Z_2 x Z_2 Heterotic String Orbifolds and Misaligned Supersymmetry*, Int. J. Mod. Phys. A **36** 2150174, doi: https://doi.org/10.1142/S0217751X21501748

[5] A.E. Faraggi, V.G. Matyas and B. Percival (2021), *Classification of Non-Supersymmetric Pati-Salam Heterotic String Models*, Phys. Rev. D **104** (2021) 046002, doi: https://doi.org/10.1103/PhysRevD.104.046002.

[6] A.E. Faraggi, V.G. Matyas and B. Percival (2021), *Type $\bar{\mathbf{0}}$ Heterotic String Orbifolds*, Phys. Lett. B **814** (2021) 136080, doi: https://doi.org/10.1016/j.physletb.2021.136080.

[7] A.E. Faraggi, B. Percival, S. Schewe and D. Wojtczak (2021), *Satisfiability Modulo Theories and Chiral Heterotic String Vacua with Positive Cosmological Constant*, Phys. Lett. B **816** (2021), 136187. doi: https://doi.org/10.1016/j.physletb.2021.136187.

[8] A.E. Faraggi, V. Matyas and B. Percival (2022), *Towards Classification of $\mathcal{N} = 1$ and $\mathcal{N} = 0$ Flipped $SU(5)$ Asymmetric $\mathbb{Z}_2 \times \mathbb{Z}_2$ Heterotic String Orbifolds*, arXiv:2202.04507.

Conference Proceedings:

[1] A.E. Faraggi, G. Harries, B. Percival and J. Rizos, *Towards machine learning in the classification of Z_2 x Z_2 orbifold compactifications (2020)*, arXiv:1901.04448, doi: https://doi.org/10.1088/1742-6596/1586/1/012032, *J. Phys. Conf. Series* 1586 vol. 1.

Contents

List of Figures

List of Tables

Chapter 1

Introduction

Picture a vacuum.
An endless and unmoving blackness.
Peace, or the absence at least, of terror.
I see, and amongst all this space,
That speck of light in the furthest corner,
Gold as a pharaoh's coffin,
Now follow that light with your tired eyes,
Its been a long day, I know, but look.
Watch as it flickers and it roars into
fullness and fills the whole frame blazing a
fire you can't bear the majesty of.
Here is our Sun.
And look.
See how the planets are dangled around it
And held in that intricate dance.
There is our Earth.
Our Earth.

Kae Tempest

1.1 Motivation

At least since the 1970s much work has gone into successful unification of General Relativity (GR) and the Standard Model (SM) of particle physics within a single framework. The key reason for trying to move beyond these two theories into a unified framework is to address a range of mysteries that remain unanswered by GR and the SM. Some of these mysteries are motivated by theory and some by experimental observation. More concretely, the discovery of dark matter and right-handed neutrinos require some form of extension of the SM. There is a long list of additional mysteries unexplained by the SM, perhaps the two most notable being the hierarchy problem and the cosmological constant problem. The latter problem speaks to the deeper issue of how a theory of gravity can be unified with our understand of particle physics coming from the SM.

The leading candidate and most powerful framework for trying to understand all four fundamental forces within a single framework is, still, string theory. The crucial fact in this regard is that string theory can naturally unify gravitational and gauge interactions within a single theory. In particular, it evades the problem of perturbative non-renormalisability of GR under quantisation and embeds a spin-2 representation of the Poincaré group automatically, giving rise to the graviton: the particle generating gravitational interactions. In order to realise the gauge sectors of the SM requires the incorporation of chiral fermions in the theory and for them to have representations under a gauge group consistent with the SM. The introduction of spacetime fermions induces some supersymmetry (SUSY) into the string theory, which is a symmetry between bosons and fermions. The study of SUSY predates string theory and is the most widely postulated resolution to some of the aforementioned mysteries left open by the SM. In particular, SUSY gives a natural way to resolve the radiative corrections that destabilise the Higgs mass and, thus, resolve the hierarchy problem. Furthermore, SUSY automatically allows for the cosmological constant to be zero (although the small positive value still needs explanation). A final key motivation in the history of SUSY was that, when combined with a Grand Unified Theory (GUT) gauge group, such as $SU(5)$ or $SO(10)$ in which the SM gauge group is contained, allows for the gauge couplings of strong and electroweak forces from the SM to naturally unify at a higher energy scale. Both SUSY GUTs and string theory also allow for several routes for understanding the origin of dark matter.

Perhaps the key stumbling block for string theory and SUSY GUTs is the question of falsifiability [1]. In one sense this is somewhat unavoidable since they are naturally constructed to explain physics at higher energies than those currently probed at particle colliders. However, SUSY theorists have been able to essentially build models where the undetected superpartners to the SM particle content are at higher and higher energies so as to evade the upper limit at the LHC. Similarly, string theory gives rise to a vast landscape of vacua, large classes of which are consistent with the SM (or, usually more specifically, the Minimally SUSY Standard Model- the MSSM). Despite there being some model-independent results and predictions arising from string theory, it still suffers from difficulties finding concrete predictions and, thus, the unfalsifiability problem [2]. This large space of vacua is referred to as the string landscape [3] and can be thought of as arising due to the fact that the superstring can only be consistently embedded within 10 spacetime dimensions and so, in order to reproduce realistic 4D models, is required to be compactified in 6 of its dimensions. Choosing this 6D compactification manifold gives rise to a vast choice of 4D theories, in fact there are, *a priori*, an (uncountable) infinity of ways to construct this manifold.

To constrain this large space of possibilities one approach is to study promising specific classes of compactifications, motivated by known physics. One such promising class of models are those generated by $\mathbb{Z}_2 \times \mathbb{Z}_2$ orbifold compactifications of the heterotic string, which are investigated in this thesis. The key attraction of this class

of models is that the appearance of three particle generations is tied to the orbifold structure- providing a fascinating natural geometric origin for this feature of the SM. Even through specifying a promising class of string models, one still has to deal with vast spaces of vacua. Handling such large spaces brings string theory into the realms of Big data, Machine learning (ML) [4] and other advanced computing tools such as the Satisfiability Modulo Theories (SMTs) that will also be studied in this thesis.

Another important set of, still emerging, ideas is to find general sets of constraints from a theory of quantum gravity (QG) consistent with known physics. These constraints are called swampland conjectures and include the Weak Gravity Conjecture, de-Sitter conjecture and Distance conjecture and are the subject of much active research within the string phenomenology community at present. The fundamental idea is that such constraints can dump large areas of the string landscape into the so-called swampland, where such constraints are unsatisfied [5, 6]. Such investigations may help shine a light on promising parts of the landscape.

Having mentioned the role of SUSY in the development of string theory, a deep question persists as to what relationship string theory ought to now have with (spacetime) SUSY, given it's increasingly shakey foundation observationally. Although worldsheet SUSY is a necessary ingredient to building consistent string theories, the issue of SUSY breaking and study of non-SUSY strings is a more pressing issue for string theory now than ever.

Despite being worked on for at least 40 years, it is fair to say that our understanding of string theory remains in its infancy. This is testament to the depth and profound subtlety of the mathematics embroiled within it. There is a strong case to be made for taking an instrumental approach and effectively see string theory as a web of tools to approach novel questions and mysteries within physics. Where the theory may lead once its dualities, geometries and new symmetries are better understood is yet to be determined. I hope that my small contribution in this thesis to the exploration of novel regions of the string landscape can form some part of a baby step within the general direction of determining where this wonderful theory leads.

1.2 Outline

In Chapter 2 we begin with a fast, and accelerating, overview of the key aspects of the bosonic string and classical superstrings. Chapter 3 introduces the free fermionic formulation for model building in 10 and 4 dimensions and uses it to complete the explanation of some fundamental results of (perturbative closed) superstring theory. Special attention is given to non-supersymmetric strings and key features for the kind of model building done in the rest of the thesis. Chapter 4 presents a general overview of the classification program for $\mathbb{Z}_2 \times \mathbb{Z}_2$ orbifolds. Chapter 5 is largely based on the paper [7], in which a classification of tachyon-free non-SUSY models with unbroken $SO(10)$ gauge

group descending from a tachyonic 10D heterotic string is presented. Following this, Chapter 6 is based on refs. [8, 9] and explores some novel string models, the Type 0 and Type $\bar{0}$, arising from studies of non-supersymmetric $\mathbb{Z}_2 \times \mathbb{Z}_2$ orbifold models. Chapter 7 is based on ref. [10] and presents a first application of SAT/SMT solvers to the string landscape, in regard to the Type $\bar{0}$ models discussed in Chapter 6. In Chapter 8 we turn to extending the classification methodology to Classes of Flipped $SU(5)$ string vacua with asymmetric shifts, which is work presented in ref. [11]. Finally, Chapter 9 presents final reflections on classifying the string landscape and non-supersymmetric string model building.

Chapter 2

Key Aspects of String Theory

In this chapter some basic aspects of perturbative string theory are quickly reviewed, beginning with the bosonic string and then introducing spacetime fermions to explore the superstring. We will focus on highlighting some key elements with a view towards later topics in this work. Some of the presentation in this chapter is based around refs. [12, 13, 14, 15, 16, 17].

2.1 Overview of the Bosonic String

In analogy to a point particle with the fundamental property of mass which carves out a one-dimensional worldline in spacetime, we can consider a string with fundamental property tension, T, generating a 2D surface as it propagates in spacetime. This 2D surface is called the *worldsheet*, Σ, and can be parametised by a local spacelike coordinate σ and a local timelike coordinate τ such that $\Sigma \ni \{\sigma^a\} = \{\tau, \sigma\}$, $a = 0, 1$. The string is then embedded[1] in spacetime via the spacetime coordinates $X^\mu(\sigma^a)$, $\mu = 0, ..., D-1$, which is a vector field mapping the worldsheet to the target space, $\mathcal{M}$.

The Nambu-Goto action

We can lean on the analogy with the point particle, whose action is given by the proper length of its worldline, in order to construct an action for our string. The natural quantity to use is the proper worldsheet *area* and we therefore postulate the action

$$S = -T \int dA, \tag{2.1}$$

where the string tension T has units of mass per unit length.

In order to write the area in terms of the spacetime coordinates $X^\mu(\sigma^a)$ we can identify the induced metric on the worldsheet, g_{ab}, as the pullback of the spacetime metric $G^{\mu\nu}$

$$g_{ab}(\sigma^c) = G_{\mu\nu}(X)\partial_a X^\mu \partial_b X^\nu \tag{2.2}$$

[1] As noted in ref. [18], it is more precise to talk about the map $\Sigma \to \mathcal{M}$ as an *immersion*, rather than an embedding, to allow for self-intersections of the string but embedding is more intuitive.

and then the area can be expressed in terms of the determinant of this induced metric

$$S_{NG} = -T \int d\sigma d\tau \sqrt{-\det\{g_{ab}\}}, \tag{2.3}$$

which is called the Nabu-Goto action. The characteristic string scale is connected to the string tension via

$$T = \frac{1}{2\pi\alpha}, \quad M_s = \alpha'^{-1/2} = \frac{1}{l_s}. \tag{2.4}$$

The introduction of α' has a historical origin in the application of string theory to the theory of strong interactions, where it was identified as the 'universal Regge slope'[19].

The Polyakov action

The square root in the Nabu-Goto action (2.3) ends up causing difficulties when quantising and making calculations, so it is preferable to write the action of the theory in polynomial form using an auxiliary field, h_{ab}, which can be identified as a dynamical metric for the worldsheet Σ. This action is called the Polyakov action[2] and takes the form

$$S_P[X,h] = -T \int_\Sigma d^2\sigma \sqrt{-h}\, h^{ab} \partial_a X^\mu \partial_b X^\nu G_{\mu\nu}(X), \tag{2.5}$$

where $h := \det\{h_{ab}\}$. We can therefore see we have a theory for D massless, real scalar fields X^μ coupled to gravity in two-dimensions, described through the worldsheet dynamical metric, h_{ab}. String theory can then be considered as the study of consistent quantisations of these fields on the 2D Riemann worldsheet surface, Σ[3]. Varying the Polyakov action with respect to the metric h_{ab} generates the energy-momentum tensor

$$T_{ab} = -\frac{1}{T}\frac{1}{\sqrt{-h}}\frac{\delta S}{\delta h^{ab}} = \frac{1}{2}\partial_a X^\mu \partial_b X_\mu - \frac{1}{4} h_{ab} h^{cd} \partial_c X^\mu \partial_d X_\mu = 0, \tag{2.6}$$

solving for h_{ab} gives

$$h_{ab} = 2f(\sigma^c)\partial_a X^\mu \partial_b X_\mu, \tag{2.7}$$

where we introduce the conformal factor given through

$$f(\sigma^c)^{-1} = g^{ab}\partial_a X^\mu \partial_b X_\mu. \tag{2.8}$$

This illustrates the difference between h_{ab} and the pullback metric g_{ab} from equation 2.2. Substituting this expression for h_{ab} back into the Polyakov action reduces it to the Nambu-Goto action- showing their equivalence, at least at the classical level.

[2] Incidentally, Polyakov did not discover the action he just understood how to work with it and perform the path integral quantisation.

[3] We note here that there are a couple of extra terms that can be added to the Polyakov action consistent with Poincaré invariance and power counting renormalizability for closed strings. The most relevant one is a 2D Gauss-Bonnet term which does play a role in string perturbation theory. This will not be discussed here but more details can, for example, be found in ref. [14].

The equations of motion for X^μ can be found through the action variation

$$\frac{\delta S}{\delta X_\mu} = \sqrt{-h}h^{ab}n_a\partial_b X^\mu \Big\|_{\sigma=\sigma_L}^{\sigma=\sigma_R} + \partial_a\left(\sqrt{-h}h^{ab}\partial_b X^\mu\right) = 0 \tag{2.9}$$

where n_a is normal to the boundary of Σ. The boundary term will vanish for strings that are closed loops, *i.e.* closed strings, but give rise to non-trivial boundary conditions for open strings. In this work we will not consider open strings.

Symmetries of the Polyakov action

So far we have not specified a metric for the target space $\mathcal{M}$. To begin investigating the properties of the Polyakov action we can now specify a D-dimensional (flat) Minkowskian target-space so that $G_{\mu\nu} = \eta_{\mu\nu}$[4]. We can identify 3 symmetries of the resultant Polyakov action

- **Poincaré invariance**: arises as the global symmetry of the spacetime such that

$$\delta X^\mu = \omega^\mu_{\ \nu} X^\nu + a^\mu, \quad \delta h_{ab} = 0, \tag{2.10}$$

  where $\omega_{\mu\nu}$ are the (antisymmetric) infinitesimal generators of Lorentz transformations

- **Diffeomorphism invariance**: this is simply the basic requirement that the physics of our theory is unaffected by (local) reparameterisation of Σ. This is a gauge symmetry as it speaks to a redundancy in the labelling of worldsheet coordinates σ^a. Infinitesimally this can be written $\sigma^a \to \tilde{\sigma}^a = \sigma^a - \xi^a(\sigma^a)$ such that the fields transform according to

$$\begin{aligned} \delta X^\mu &= \xi^a \partial_a X^\mu \\ \delta h_{ab} &= -(\nabla_a \xi_b + \nabla_b \xi_a). \end{aligned} \tag{2.11}$$

- **Weyl Invariance**: is less familiar and rather novel. It leaves X^μ unchanged and induces a scale factor to the worldsheet metric and infinitesimally can be written

$$\delta X^\mu = 0, \quad \delta h_{ab} = 2\Lambda(\sigma^a)h_{ab}. \tag{2.12}$$

  An important consequence of this symmetry is that it ensures that the stress-energy tensor is traceless. Furthermore, it allows for the worldsheet metric to be rescaled to the 2D flat Minkowski metric to simplify the theory. Weyl symmetry will also give rise to important consistency constraints once the theory is

[4]The generalised action with a curved background can be considered, in which the theory is a non-linear sigma model and the massless excitations we derive through quantisation, the graviton, anti-symmetric tensor and the dilaton, become dynamical fields. The case $G^{\mu\nu} = \eta^{\mu\nu}$ can be considered as the zeroth order term in an expansion around a flat background. More details can be found in Chap. 14 of [14].

quantised, in particular because the aforementioned stress-energy tensor trace, T^a_a, becomes non-zero at the quantum level.

Path Integral Approach to Bosonic String

A powerful formalism to employ for quantisation and calculation of scattering amplitudes is the path integral formulation. In particular, such a path integral will include an integration over the fields X^μ and h_{ab}, modulo gauge transformations. As a starting point we can take the partition function of the bosonic string with Euclidean worldsheet signature

$$Z = \int \frac{DhDX}{V_{gauge}} e^{-S_P[h,X]} = \int \frac{DhDX}{V_{gauge}} e^{T \int_\Sigma d^2\sigma \sqrt{-h}\, h^{ab} \partial_a X^\mu \partial_b X^\nu \eta_{\mu\nu}} \tag{2.13}$$

where the V_{gauge} ensures the modding out by X^μ and h_{ab}'s related by gauge transformations (Diffeomorphisms and Weyl). In order to define the integration measures for X^μ and h_{ab}, which preserve all symmetries of the classical theory, we can write the norms

$$\begin{aligned} ||\delta h|| &= \int d^2\sigma \sqrt{h} h^{ab} h^{cd} \delta h_{ad} \delta h_{bc} \\ ||\delta X^\mu|| &= \int d^2\sigma \sqrt{h} h^{ab} \delta X^\mu \delta X_\mu, \end{aligned} \tag{2.14}$$

but these are not Weyl invariant. If we take a general gauge transformation, Ξ, of the metric

$$\Xi : \; h_{ab}(\sigma) \to h'_{ab}(\sigma') = e^{2\Lambda(\sigma)} \frac{\partial \sigma^c}{\partial \sigma'^a} \frac{\partial \sigma^d}{\partial \sigma'^b} h_{c\delta}, \tag{2.15}$$

we can put the metric into a gauge fixed form $\hat{h}$, called the fiducial metric. Infinitesimally we can write this transformation as

$$\delta h_{ab} = \nabla_a \xi_b + \nabla_b \xi_a + 2\Lambda h_{ab} = (\hat{P}\xi)_{ab} + 2\tilde{\Lambda} h_{ab}, \tag{2.16}$$

where $(\hat{P}\xi)_{ab} = \nabla_a \xi_b + \nabla_b \xi_a - (\nabla_c \xi^c) h_{ab}$ maps vectors into symmetric traceless tensors and $\tilde{\Lambda} = \Lambda + \frac{1}{2} \nabla_c \xi^c$. In this form we can see that there is a traceless symmetric part independent of the scale factor Λ and a pure trace part. In these components we can write the integration measure for h_{ab} as

$$Dh = D(\hat{P}\xi) D(\tilde{\Lambda}) = D\xi D\Lambda \Big| \frac{\partial(\hat{P}\xi, \tilde{\Lambda})}{\partial(\xi, \Lambda)} \Big|, \tag{2.17}$$

where the Jacobian is called the Fadeev-Popov determinant and is equal to

$$\Big| \frac{\partial(\hat{P}\xi, \tilde{\Lambda})}{\partial(\xi, \Lambda)} \Big| = \Big| \det \left\{ \begin{pmatrix} P & * \\ 0 & 1 \end{pmatrix} \right\} \Big| = \Big| \det \{ \hat{P} \} \Big|, \tag{2.18}$$

where $*$ doesn't affect the determinant value. This determinant can be rewritten in exponential form through an integration over two new fields we introduce called $b_{\alpha\beta}$ and

c^α, which are both necessarily (anti-commuting) Grassman-valued fields. Doing this, we now have a gauge fixed partition function where the Polykov action is augmented by the action of these new *ghost fields* b and c

$$Z[\hat{h}] = \int DXDbDc \exp\Big\{-S_P[X,\hat{h}] - S_{\text{ghost}}[b,c,\hat{h}]\Big\}, \tag{2.19}$$

such that

$$S_{\text{ghost}}[b,c,\hat{h}] = \frac{1}{2\pi}\int d^2\sigma\sqrt{\hat{h}}b_{ab}\nabla^a c^b. \tag{2.20}$$

In order to explore this further we can choose a convenient fiducial metric

$$\hat{h}_{ab} = \delta_{ab}, \tag{2.21}$$

where we have used Weyl symmetry with Euclidean signature. We can now employ a conformal map from the Euclidean cylinder to the complex plane via $z = e^{\tau_E + i\sigma}$ and $\bar{z} = e^{\tau_E - i\sigma}$, where the τ_E emphasises that we are in Euclidean signature. In terms of these coordinates we can write the measure as $d^2\sigma = \frac{1}{2}d^2z$, the covariant derivative becomes the normal partial derivative and our partition function becomes

$$Z = \int DXDbDc \exp\left\{\left(\frac{T}{2}\int_{\mathbb{C}} dz^2(\partial_z X\partial_{\bar{z}}X) + \frac{1}{4\pi}\int_{\mathbb{C}} d^2z(b_{zz}\partial_{\bar{z}}c^z + b_{\bar{z}\bar{z}}\partial_z c^{\bar{z}})\right)\right\}. \tag{2.22}$$

This is a theory of two decoupled CFTs relating to the matter theory (X^μ) and the ghost theory (b and c). The ghost CFT is universal, resulting from the impact of gauge fixing the Polyakov action, whereas the matter CFT arises from a specific choice of background. We can note that the ghost theory has equations of motion

$$\bar{\partial}b = \partial\bar{b} = \bar{\partial}c = \partial\bar{c} = 0, \tag{2.23}$$

where $b = b_{zz}$, $\partial = \partial_z$, $c = c^z$ and so on. We can thus observe that b and c are holomorphic and $\bar{b}, \bar{c}$ are antiholomorphic.

The Ghost CFT and $D = 26$

The total energy-momentum tensor of the theory is the sum of the (normal-ordered) contributions to it from the matter sector and the ghost sector, *i.e.* $T = T^M + T^{gh}$, where T^M has two non-zero components

$$T^M(z) := T_{zz} = -2 : \partial_z X\partial_z X : \quad \text{and} \quad T^M(\bar{z}) := T_{\bar{z}\bar{z}} = -2 : \partial_{\bar{z}} X\partial_{\bar{z}} X : . \tag{2.24}$$

For which we note the Laurent expansion

$$T^M(z) = \sum_{n\in\mathbb{Z}} \frac{L_n}{z^{n+2}} \tag{2.25}$$

and similarly on the antiholomorphic side with Laurent modes $\bar{L}_n$. Meanwhile, we also have the ghost contribution

$$T^{gh}(z) = 2 : (\partial c)b : + : c\partial b :, \quad \text{and} \quad T^{gh}(\bar{z}) = 2 : (\bar{\partial}\bar{c})\bar{b} : + : \bar{c}\bar{\partial}\bar{b} : . \tag{2.26}$$

Taking variations of the ghost action with respect to b and c results in the OPEs

$$c(z)b(w) = \frac{1}{z-w} + ..., \tag{2.27}$$

where the ... refer to regular terms. We can show that b and c are in fact primary fields of the ghost CFT by taking their OPEs with the holomorphic ghost energy-momentum tensor

$$T^{gh}(z)c(w) = -\frac{c(w)}{(z-w)^2} + \frac{\partial c(w)}{z-w} + ..., \tag{2.28}$$

which corresponds to an OPE for a conformal primary of weight -1 and

$$T^{gh}(z)b(w) = -\frac{2b(w)}{(z-w)^2} + \frac{\partial b(w)}{z-w} + ..., \tag{2.29}$$

which corresponds to a OPE of a conformal primary weight 2. In order to calculate the central charge, c, of the ghost CFT we can take the OPE of the ghost energy-momentum tensor which can be calculated to equal

$$T^{gh}(z)T^{gh}(w) = \frac{-13}{(z-w)^4} + \frac{2T(w)}{(z-w)^2} + \frac{\partial T(w)}{z-w} + ..., \tag{2.30}$$

which implies that that ghost central charge is $c = -26$. In order to cancel this (for the preservation of the Weyl symmetry) we require the matter CFT to be $c^M = 26$. This can be done by having X^μ live in $D = 26$, the so-called critical dimension of the bosonic string.

BRST Quantisation

The Hilbert space of our matter-ghost theory can be decomposed as

$$\mathcal{H} = \mathcal{H}^M \otimes \mathcal{H}^{gh}. \tag{2.31}$$

In order to build states we must examine the residual symmetry of the theory after we used the Fadeev-Popov method to gauge fix our action. The residual symmetry is

called the BRST transformation and is generated by

$$\begin{aligned}
\delta_B X^\mu &= -i\kappa(c\partial X^\mu + c\partial X^\mu) \\
\delta_B c &= -i\kappa \bar{c}\bar{\partial}\bar{c} \\
\delta_B \bar{c} &= i\kappa c\partial c \\
\delta_B b &= -i\kappa T \\
\delta_B \bar{b} &= -i\kappa \bar{T},
\end{aligned} \tag{2.32}$$

where T and $\bar{T}$ are the holomorphic and antiholomorphic total energy-momentum tensors, respectively. By Noether's theorem there exists a corresponding BRST current

$$j_B(z) = c(z)T^M(z) + :b(z)c(z)\partial c(z): + \frac{3}{2}\partial^2 c(z) \tag{2.33}$$

and correspondingly for the antiholomorphic part. Additionally this comes with the Noether charge Q_B

$$Q_B = \frac{1}{2\pi}\oint dz \left(c(z)T^M(z) + :b(z)c(z)\partial c(z):\right), \tag{2.34}$$

which is just the contour integral of the BRST current without the total derivative term which is inserted by hand into (2.33) to ensure that j_B transforms as a conformal primary when $c^M = 26$.

Writing the Laurent expansion of the ghost fields as

$$\begin{aligned}
b(z) &= \sum_{m=-\infty}^{\infty} \frac{b_m}{z^{m+2}} \\
c(z) &= \sum_{m=-\infty}^{\infty} \frac{c_m}{z^{m-1}}.
\end{aligned} \tag{2.35}$$

We can rewrite the BRST charge in terms of the modes (Virasoro generators) of the matter theory's energy-momentum tensor, L_m, of eq. (2.25) and the modes b_m, c_m of the ghost theory

$$Q_B = \sum_{m=-\infty}^{\infty} (L_{-m} - \delta_{m,0})\, c_m - \sum_{m,n=-\infty}^{\infty} (m-n) :c_{-m}c_{-n}b_{m+n}:, \tag{2.36}$$

and similarly for the antiholomorphic $\bar{Q}_B$. The Hilbert space of physical states contains those states $|phys\rangle$ that are BRST invariant

$$(Q_B + \bar{Q}_B)\,|phys\rangle = 0. \tag{2.37}$$

We must ensure that the BRST charge remains conserved under a change in gauge-fixing condition. To check this we can compute that it commutes with the full Hamiltonian H under a BRST variation $\delta_B H$. Doing this proves the important fact that Q_B is

nilpotent, that is

$$Q_B^2 = 0, \tag{2.38}$$

otherwise the theory becomes anomalous under gauge changes. This nilpotency implies that any state $Q_B |\chi\rangle$ will be annihilated by Q_B and so naively is physical. However, this state is orthogonal to all physical states, including itself, and is therefore called a *null state* and should be ignored when exploring quantum dynamics.

The upshot is that the Hilbert space of physical states are given by the cohomology of Q_B. In other words, physical states are the BRST *closed* states modulo the BRST *exact* states.

In order to begin building the Hilbert space we need to define the full vacuum of the theory $|0^X\rangle \otimes |0\rangle^{gh}$. The Hilbert space of the CFT for the free scalar fields X^μ is built from primary highest weight states $|p^\mu\rangle$ of conformal dimensions

$$L_0 |p\rangle = \bar{L}_0 |p\rangle = \frac{\alpha'}{4} p_\mu p^\mu |p\rangle \tag{2.39}$$

and its descendents obtained by acting with creation operators associated with X^μ

$$|\Phi\rangle = ...(\bar{\alpha}_{-2}^{\mu_2})^{\bar{N}_2^{\mu_2}} (\alpha_{-2}^{\nu_2})^{N_2^{\nu_2}} (\bar{\alpha}_{-1}^{\mu_1})^{\bar{N}_1^{\mu_1}} (\alpha_{-1}^{\nu_1})^{N_1^{\nu_1}} |p\rangle , \tag{2.40}$$

such that the conformal dimension for a state is

$$L_0 |\Phi\rangle = \left(\frac{\alpha'}{4} p^2 + N^X \right) |\Phi\rangle , \quad N^X = \sum_{\nu_r, r} r N_r^{\nu_r} \tag{2.41}$$

and similarly for the antiholomorphic side, where we call N^X (and $\bar{N}^X$) the holomorphic (and antiholomorphic) level(s) of the states in the module.

For the ghost CFT, we can define $|0\rangle^{gh}$ in the standard way as annihilated by the modes b_n, c_n for $n \geq 1$. Inspecting the zero modes b_0, c_0, we see they satisfy anticommutation relations

$$\{b_0, c_0\} = 1, \tag{2.42}$$

generating a Clifford algebra and, thus, an $SL(2, \mathbb{C})$ doubly degenerate vacuum with spin up $|\uparrow\rangle$ and spin down $|\downarrow\rangle$ states such that

$$b_0 |\uparrow\rangle = |\downarrow\rangle , \quad b_0 |\downarrow\rangle = 0, \quad c_0 |\uparrow\rangle = 0, \text{ and } c_0 |\downarrow\rangle = |\uparrow\rangle . \tag{2.43}$$

Once we try to build physical amplitudes it turns out that the $|\uparrow\rangle$ generates null states and typically unphysical amplitudes. Another way to implement this choice is through imposing

$$b_0 |phys\rangle = 0, \tag{2.44}$$

which is called the 'Siegel gauge' as a new condition on physical states. Now that we have $|\downarrow\rangle$ as the ghost vacuum acting with the negative modes of the ghosts will create

our states

$$|\Phi\rangle_{gh} = \left(...(b_{-1})^{N_1}(c_{-1})^{M_1}\,|{\downarrow}\rangle^{gh}\right) \otimes \left(...(\bar{b}_{-1})^{\bar{N}_1}(\bar{c}_{-1})^{\bar{M}_1}\left|\overline{\downarrow}\right\rangle^{gh}\right). \tag{2.45}$$

We can now deduce the spectrum level by level for closed strings according to the levels of the full CFT, which is allowed since from (2.36) we see that Q_B does not mix terms of different levels.

At level zero there is a unique state of the form

$$|p^\mu\rangle_T = |p\rangle \otimes |{\downarrow}\rangle^{gh} \otimes \left|\overline{\downarrow}\right\rangle^{gh} \tag{2.46}$$

and acting with the BRST charge gives

$$Q_B\,|p^\mu\rangle_T = \left(\frac{\alpha'}{4}p^2 - 1\right)|p\rangle \otimes |{\uparrow}\rangle^{gh} \otimes \left|\overline{\downarrow}\right\rangle^{gh} \tag{2.47}$$

and similarly for the antiholomorphic side. Therefore the constraint for physical states (2.37) holds when

$$\frac{\alpha'}{4}p^2 = 1, \tag{2.48}$$

which corresponds to a tachyon, indicating that our bosonic string theory has not been constructed at a true vacuum.

The next level to consider is $N = \bar{N} = 1$ due to *level matching*[5]. At this level, we can write a general physical state as the following linear combination of operators acting on the level 0 state

$$\begin{aligned}\left|\Psi^1\right\rangle = \Big(&e_{\mu\nu}\alpha^\mu_{-1}\bar{\alpha}^\nu_{-1} + \zeta_\mu\alpha^\mu_{-1}\bar{b}_{-1} + v_\mu\alpha^\mu_{-1}\bar{c}_{-1} + \bar{\zeta}_\mu\bar{\alpha}^\mu_{-1}b_{-1} + \bar{v}_\mu\bar{\alpha}^\mu_{-1}c_{-1} \\ &+ \lambda_1 b_{-1}\bar{b}_{-1} + \lambda_2 c_{-1}\bar{c}_{-1} + \lambda_3 b_{-1}\bar{c}_{-1} + \lambda_4 c_{-1}\bar{b}_{-1}\Big)\,|p^\mu\rangle_T\,.\end{aligned} \tag{2.49}$$

Now acting with Q_B tells us that physical states at this level are massless. Being careful to remove null states we find that the BRST invariant states simplify to being of the form

$$\left|\Psi^1\right\rangle = e_{\mu\nu}\alpha^\mu_{-1}\bar{\alpha}^\nu_{-1}\,|p\rangle \otimes |{\downarrow}\rangle^{gh} \otimes \left|\overline{\uparrow}\right\rangle^{gh} \tag{2.50}$$

subject to the conditions

$$p^\mu p_\mu = 0, \tag{2.51}$$

$$p^\mu e_{\mu\nu} = p^\nu e_{\mu\nu} = 0, \tag{2.52}$$

$$e_{\mu\nu} \sim e_{\mu\nu} + a_\mu p_\nu + b_\nu p_\mu, \quad a_\mu p^\mu = b_\nu p^\nu = 0. \tag{2.53}$$

[5] Level-matching implies that, for a closed string, holomorphic and antiholomorphic excitations contribute equally to the mass. This can be viewed as a consequence of translation invariance in σ.

In order to interpret these states as spacetime particles we consider that (2.52) imposes that the polarisation vector $e_{\mu\nu}$ satisfies transversality and we can decompose it into irreducible representations of the Poincaré group in the standard way. There is a symmetric traceless part corresponding to the graviton $G_{\mu\nu}$, an antisymmetric part corresponding to the Kalb-Ramond tensor $B_{\mu\nu}$ and a trace part corresponding to the dilaton Φ.[6]

This BRST procedure can be continued to higher levels to give massive string states. A couple of important facts one finds doing this are that the masses are of the string scale and there is an exponential increase in the degeneracy of states with the level N.

2.2 The Classical Fermionic String

There is a fundamental omission from the bosonic string theory when thinking from the perspective of it being related to real world physics: the absence of spacetime fermions. As mentioned previously, the physical tachyon that arises in the spectrum indicates that a stable background for the bosonic string needs to be found, whether this is possible is still an open question. A true vacuum has been found in string field theory for the case of the open string tachyon (see review [20] and references therein) but it is still unknown how to roll the theory to a true vacuum for the closed string tachyon within closed string field theory.

A natural way to introduce fermions is to append the action of a free boson X^μ with that of a Majorana fermion, Ψ^μ, which with a Euclidean 2D flat metric generates the action

$$S = T \int dz d\bar{z} (\partial_a X^\mu \partial^\alpha X_\mu + \Psi \bar{\partial} \Psi + \overline{\Psi} \partial \overline{\Psi}), \tag{2.54}$$

where $\Psi^\mu(z, \bar{z}) = \binom{\Psi^\mu(z)}{\Psi^\mu(\bar{z})} = \binom{\Psi}{\overline{\Psi}}$ has two real Weyl components, one holomorphic and the other antiholomorphic.

Since the worldsheet fermions Ψ^μ are taken to be real their possible closed string boundary conditions are

$$\Psi(e^{2\pi i} z) = e^{\pi i \nu} \Psi(z), \tag{2.55}$$

with $\nu = 0, 1$ being periodic and antiperiodic which we will rename Neveu-Schwarz (NS) and Ramond (R), respectively, from now on. With these boundary conditions we

[6] As mentioned in footnotes 3 and 4, the bosonic string, as defined through the Polyakov action, is dependent on background fluctuations from these massless fields $(G_{\mu\nu}, B_{\mu\nu}, \Phi)$. By considering the Polyakov action (2.5) with $G_{\mu\nu} = \eta_{\mu\nu}$ we are choosing to set the background fluctuations of $B_{\mu\nu}$ and Φ to zero. The full action would be a non-linear sigma model incorporating their contributions. A consistent background for the bosonic string must be Weyl invariant, which generates equations of motion for these background fields given through beta functions $\beta_{\mu\nu}(G) = \beta_{\mu\nu}(B) = \beta(\Phi) = 0$. More details can be found in [14, 16], for example.

can write the Laurent expansion

$$\Psi(z) = \sum_r z^{-r-\frac{1}{2}} \quad \text{with} \quad \begin{cases} \text{NS} & \leftrightarrow \quad r \in \mathbb{Z} + \frac{1}{2} \\ \text{R} & \leftrightarrow \quad r \in \mathbb{Z} \end{cases} \tag{2.56}$$

and similar for the antiholomorphic side. Quantising these fields is achieved through imposing the anticommutation relations

$$\{\Psi_r, \Psi_s\} = \delta_{r+s,0}. \tag{2.57}$$

The (holomorphic) energy momentum tensor in this theory is

$$T(z) = -\frac{1}{\alpha'} : \partial X^\mu \partial X_\mu : -\frac{1}{2} : \Psi^\mu \partial \Psi_\mu : . \tag{2.58}$$

There is a important enhancement to the symmetry of the theory now that the fermionic contribution has been added. This is $(1,1)$ worldsheet supersymmetry generated by the infinitesimal transformations

$$\delta X \propto \epsilon \psi \tag{2.59}$$

$$\delta \Psi \propto \epsilon \gamma^\alpha \partial_a X, \tag{2.60}$$

where ϵ is an infinitesimal spinor and γ^α generate a Clifford algebra. Using the OPE

$$\Psi^\mu(z)\Psi^\nu(w) = \frac{\eta^{\mu\nu}}{z-w}, \tag{2.61}$$

one can use the OPE $: T(z)\Psi^\mu(w) :$ to verify that the conformal weight of the free fermion $\Psi(z)$ is $(\frac{1}{2}, 0)$, which is consistent with the structure of the (Dirac-like) kinetic term in the action (2.54). The superpartner of the energy-momentum tensor is

$$G(z) =: \partial X \Psi : (z) \tag{2.62}$$

and can be Laurent expanded as

$$G(z) = \sum_{r \in \mathbb{Z}+\frac{1}{2}} G_r z^{-r-\frac{3}{2}}. \tag{2.63}$$

The central charge of the theory is then determined in the usual way by taking the OPEs

$$: T(z)G(w) : = \frac{3/2}{(z-w)^2} G(w) + \frac{1}{z-w} \partial G(w) \tag{2.64}$$

$$: G(z)G(w) : = \frac{\hat{c}}{(z-w)^3} + \frac{2}{z-w} T(w), \tag{2.65}$$

with $\hat{c} = \frac{2}{3}c$. These OPEs generate a $N = 1$ superconformal algebra for the holomorphic degrees of freedom and we have an analogous result for the antiholomorphic sector. These OPEs furthermore imply that $G(z)$ is a primary field of conformal weight $\frac{3}{2}$.

Superghosts and $D = 10$

For the superstring just defined, the ghost fields b, c arising in the bosonic string through the Fadeev-Popov prescription are accompanied by (commuting) superghost fields β, γ required for the gauge fixing and new superparameterisation invariance. These superghosts contribute a similar term $\sim \int \beta\bar{\partial}\gamma$ to the action and give contributions to the ghost energy-momentum tensor and supercurrent:

$$T^{gh}(z) = -(\partial b)c - 2b\partial c - \frac{1}{2}(\partial\beta)\gamma - \frac{3}{2}\beta\partial\gamma \tag{2.66}$$

$$G^{gh}(z) = (\partial\beta)c + \frac{3}{2}\beta\partial c - 2b\gamma. \tag{2.67}$$

By doing the OPEs of these with $T(z)$ we find the conformal dimensions of β and γ are $\frac{3}{2}$ and $-\frac{1}{2}$, respectively, making them superpartners of the b, c ghost system. Taken altogether, these give rise to a ghost supermultiplet contributing a total of $c^{gh} = c_{\beta\gamma} + c_{bc} = 11 - 26 = -15$ such that $c_{matter} = 15$ or $\hat{c} = 10$. Therefore the matter fields of the superstring $X^\mu(z, \bar{z}), \Psi^\mu(z, \bar{z})$ have critical dimension $D = 10$.

Superstring BRST

We can follow similar steps as in the bosonic case to perform the BRST procedure to construct physical states through the cohomology of BRST charge Q_B. On the holomorphic side we have contributions to the conserved Noether current from $X^\mu(z), \Psi^\mu(z), b, c, \beta$ and γ giving

$$j_B = cT^M + \gamma G^M(z) + bc\partial c + \frac{3}{4}(\partial c)\beta\gamma + \frac{1}{4}c(\partial\beta)\gamma - \frac{3}{4}c\beta\partial\gamma - b\gamma^2 \tag{2.68}$$

and then Q_B is the zero mode of this current. The superconformal anomaly cancellation again imposes the nilpotency condition $Q_B^2 = 0$. There is an analogous Siegel gauge condition as well $b_0 |\chi\rangle = \beta_0 |\chi\rangle = 0$, which ensures only physical amplitudes remain in the spectrum. This condition leads to the following constraints on physical states:

$$L_0 |\chi\rangle = \{Q_B, b_0\} |\chi\rangle = 0 \tag{2.69}$$

$$G_0 |\chi\rangle = [Q_B, \beta_0] |\chi\rangle = 0, \tag{2.70}$$

where L_0 is the zero mode of the total (matter plus ghost) energy-momentum tensor. The low lying states of the superstring can be found in an analogous way as with the bosonic string. We will leave the derivation of the massless spectrum for the Type IIA/B and heterotic strings to Chapter 3 once we define the free fermionic construction.

2.3 CFT Representation theory and Current Algebras

From the bosonic string we saw that the modes L_n ($\bar{L}_n$) of the stress-energy tensor $T(z)$ ($T(\bar{z})$) satisfy the Virasoro algebra. The introduction of fermionic fields in the last section resulted in the presence of an additional primary field $G(z)$ of conformal weight $\frac{3}{2}$ that enhanced the theory to a superconformal algebra. In general, we can discuss $c \geq 1$ CFTs built from the Virasoro algebra that get enhanced by some additional set of chiral operators.The set of these operators generate an operator product algebra that depends on h with: $h = \frac{1}{2}$ being free fermions; $h = 1$ being Kac-Moody algebras; $h = \frac{3}{2}$ being superconformal algebras; $h = 2$ including the Virasoro algebra and $h = 3$ being the so-called W-algebra.

Free Fermion Current Algebras

As seen in the discussion of the classical superstring, the superconformal algebra is central to the superstring. The situation of free fermions is also of interest in the forthcoming discussion of the heterotic string and so we will present some of the key ingredients of how to deal with them in a CFT. In order to discuss the details of their representation theory we take a theory of just N holomorphic and N antiholomorphic real fermions given by the Euclidean action

$$S = \frac{1}{4\pi} \int d^2z \left(\delta_{ij} \Psi^i \bar{\partial} \Psi^j + \delta_{ij} \bar{\Psi}^i \partial \bar{\Psi}^j \right). \tag{2.71}$$

This action has a symmetry under $SO(N)$ chiral rotations

$$\Psi \to R^i{}_j \Psi^i, \quad R \in SO(N) \tag{2.72}$$

and similarly for the antiholomorphic side. The corresponding Noether currents are

$$J^{ij}(z) = - : \Psi^i \Psi^j : (z), \quad i < j, \tag{2.73}$$

with conformal weight $(1, 0)$. Using the fundamental OPE

$$\Psi^i(z)\Psi(w) = \frac{\delta^{ij}}{z - w}, \tag{2.74}$$

we can calculate the OPE of two currents

$$J^{ij}(z)J^{kl}(w) = -\frac{\kappa^{ijkl}}{(z-w)^2} + f^{ijkl}_{mn} \frac{J^{mn}}{(z-w)} + ..., \tag{2.75}$$

where κ^{ijkl} is the Killing form and f^{ijkl}_{mn} are the structure constants of the Lie algebra $\mathfrak{so}(N)$.

We can further construct the affine-Sugawara stress-tensor from these currents

$$T(z) = \frac{1}{2(N-1)} \sum_{i<j}^{N} : J^{ij} J^{ij} : (z). \tag{2.76}$$

Any such $(2,0)$ operator from such a current obeys the general OPE

$$T(z)T(w) = \frac{c_G/2}{(z-w)^4} + \frac{2T(w)}{(z-w)^2} + \frac{\partial T(w)}{z-w}, \tag{2.77}$$

such that the central charge is determined by the level k, dual Coxeter number $\tilde{h}$ and dimension D_G of the group G through

$$c_G = \frac{kD_G}{k+\tilde{h}}. \tag{2.78}$$

We are interested here in level one $k = 1$ for the group $SO(N)$ with $\tilde{h} = N-2$ and $D = \frac{1}{2}N(N-1)$ so that

$$c_G = \frac{N}{2}, \tag{2.79}$$

verifying what we found in Section 2.2 that each fermion contributes $\frac{1}{2}$ to the central charge.

We can now consider the Hilbert Space of the free fermion CFT as given by the irreducible representations of the $SO(N)$ current algebra. At $k = 1$ this gives rise to 3 possibilites: the Unit/Trivial representation obtained by acting on the vacuum with negative current modes; the vector representation and the spinor representation(s). Typically in string theory applications N is even, $N = 2k$, and there are two dimensional 2^{k-1} spinorial representations of the $Spin(2k)$ group that is the double-cover of $SO(N)$. We call these the spinor, S, and the conjugate, C, representations.

To understand these representations we first define primary states of the affine algebra which should be annihilated by the positive modes of the currents, $J^{ij}_n,\ n > 0$. In particular, we consider the algebra of the zero modes

$$[J^{ij}_0, J^{kl}_0] = f^{ijkl}_{mn} J^{mn}_0, \tag{2.80}$$

which is a (horizontal) subalgebra coinciding with the Lie algebra $\mathfrak{so}(N)$. Therefore we can classify states in terms of representations of this zero-mode algebra. Sets of states $|R_i\rangle$ that transform in a representation R and are annihilated by the positive modes of the current will have some local operator counterparts $R_i(z,\bar{z})$ with the OPE

$$J^{ij}(z) R_\alpha(w,\bar{w}) = \frac{R(T^{ij})^\beta_\alpha R_\beta}{z-w}, \tag{2.81}$$

which defines *affine primary* fields. By acting with the Virasoro zero-mode L_0 on $|R_i\rangle$ we can deduce the conformal dimension for an affine primary to be

$$h = \frac{C_R}{k+\tilde{h}}, \tag{2.82}$$

where C_R is the quadratic Casimir of the representation R. For $SO(N)$ we see that affine primaries have

$$h = \frac{C_R}{2(N-1)}. \tag{2.83}$$

With this technology we can better understand the three aforementioned representations of the $\mathfrak{so}(N)$ subalgebra (2.80).

- **The Trivial Representation:** is associated with the Neveu-Schwarz vacuum $|0\rangle_{NS}$ such that

$$\forall i,\ \ \forall r \in \mathbb{N} + \frac{1}{2}, \quad \Psi^i_r |0\rangle_{NS} = 0, \tag{2.84}$$

  and descendent states are obtained by acting with negative modes of the currents J^{ij}.

- **The Vector Representation:** From eq. (2.72) we observe that $\Psi(z)$ transforms as a vector of $SO(N)$ and so we can consider the set of states

$$|i\rangle := \Psi^i_{-1/2} |0\rangle, \quad i \in \{1, ..., N\} \tag{2.85}$$

  to define the vector representation of the horizontal subalgebra. This can be seen to have $h = \frac{1}{2}$. As usual, descendents can be obtained by acting with negative modes of currents J^{ij}.

- **The Spinorial Representation:** From eq. (2.83), we use that $C_R = \frac{N(N-1)}{8}$ for the spinorial representation of $SO(N)$ to observe that

$$h = \frac{N}{16}. \tag{2.86}$$

  In eq. (2.56) we noted the case of integer moded Ramond fermions which can be seen to arise from the action (2.71) through the $\mathbb{Z}_2$ symmetry

$$\Psi^i \to -\Psi^i, \tag{2.87}$$

  which commutes with the $SO(N)$ symmetry. We note that there are anticommuting zero modes from the Ramond fermions giving the $SO(N)$ Clifford algebra

$$\{\Psi^i, \Psi^j\} = \delta^{ij}, \tag{2.88}$$

  which is realised by Hermitean $SO(N)$ γ matrices. We thus expect the Ramond 'vacuum' to be a Dirac spinor with $2^{N/2}$ components. We expect the R vacua,

$|S_\alpha\rangle$, corresponding to the S and C representations, to be generated by the action of some local affine primary field on the NS vacuum

$$|S_\alpha\rangle = \lim_{z\to 0} S_\alpha(z)\,|0\rangle_{NS}\,. \tag{2.89}$$

This operator, $S_\alpha(z)$, is called the *spin field*, which can be constructed through the OPE

$$\Psi^i(z)S_\alpha(w) = \frac{1}{\sqrt{2(z-w)}}(\gamma^i)^\beta_\alpha S^\beta(w) + ..., \tag{2.90}$$

which we note incurs a branch cut in the complex plane that needs to be considered carefully in constructing the Hilbert space of the theory and will be considered in relation to the GSO projection in the following subsection. Despite this branch cut, one can take the OPE with the currents J^{ij} and see that the spin field is indeed the desired affine primary of the spinorial representation. The spin field can be split into fields of positive and negative chirality and then be used to define the S and C Ramond vacua as distinct, $|S_\alpha\rangle$ and $|S_{\dot\alpha}\rangle$.

2.4 GSO Projection

In [21, 22] Gliozzi, Scherk and Olive introduced a consistent requirement on the construction of the Hilbert space of fermionic strings. It can be seen to arise either from considerations of modular invariance or as a way to ensure the correlation functions involving fermions with Ramond boundary conditions are free from branch cuts. The idea is to introduce a projection such that only states with even total (matter plus ghost) worldsheet Fermion number, $\mathcal{F}$, remain in the Hilbert space of the theory.

Acting on the NS and Ramond vacua with the worldsheet fermion number operator gives

$$(-)^{\mathcal{F}}\,|0\rangle_{NS} = -\,|0\rangle_{NS} \tag{2.91}$$

$$(-)^{\mathcal{F}}\,|0\rangle_{R} = \Gamma^D\,|0\rangle_{R}\,, \tag{2.92}$$

where

$$\Gamma^D = i^{\pm\frac{D}{2}}\prod_{m=1}^{D}\gamma^m \tag{2.93}$$

is the D-dimensionality chirality operator. The GSO projection is such that it fixes the chirality of states in the theory to even fermion number

$$(-)^{\mathcal{F}}\,|\chi\rangle = +\,|\chi\rangle \tag{2.94}$$

and similarly on the antiholomophic side with operator $(-)^{\tilde{\mathcal{F}}}$.

Therefore, the GSO projection can be viewed as ensuring that only states with even number of fermionic excitations survive from the NS sector, whilst in the R sector it

fixes the chirality of the spin field (2.89). It can be seen as directly related to ensuring spactime supersymmetry since the projection results in the vertex operator of the gravitino being local with respect to the other vertex operators of the theory.

Imposing the projection independently on both sides of the theory we will see results in the Type IIA and Type IIB superstrings, which are tachyon-free and supersymmetric. However, a projection onto states with total (left plus right) even worldsheet fermion number, given through the operator $(-)^{\mathcal{F}+\bar{\mathcal{F}}}$ gives the so-called Type 0A and Type 0B theories which are tachyonic and non-supersymmetric. We illustrate this in Section 3.4 in the free fermionic formulation.

2.5 One-Loop Partition Function and Modular Invariance

The simplest quantum corrections in string theory are from the vacuum to vacuum one-loop amplitude which gives the first quantum correction to the vacuum energy. For closed strings this one-loop amplitude is the torus amplitude and will be our focus in this section.

The one-loop amplitude, when interpreted in Euclidean time, corresponds to the statistical partition function of the string theory. This object is of fundamental importance and relevance to model builders in string phenomenology since the structure of the string spectrum is manifest through the partition function and it allows for the one-loop string potential to be calculated, which generates the leading order contribution to the cosmological constant. Constructing our (S)CFT on the two-torus leads to a crucial fact about the partition function called modular invariance, which means our amplitude must be invariant under the modular group $PSL(2,\mathbb{Z})$. This provides rather stringent consistency constraints on our (super)string theories, especially when we compactify to four-dimensions.

In this section, we will see how to build the partition function, which will require considering both compact and non-compact bosonic and fermionic contributions. Once modular invariance is explained, we will then compute these different contributions from the Hamiltonian perspective.

Modular Invariance

A key result from the study of Riemann surfaces is the Riemann-Roch theorem, which relates the Euler characteristic, χ, of the surface to the number of, so-called, *moduli*, n_μ, and the number of conformal Killing vectors, n_k, through

$$n_\mu - n_k = -3\chi = 6(g-1), \tag{2.95}$$

where g is the genus of the surface. The moduli are defined as parameters for gauge-inequivalent metrics on the surface, while the (conformal) Killing vectors are gauge

transformations that leave the gauge-fixed metric form invariant. We can define the *Teichmüller space*, $\mathbb{T}$, of the surface as the quotient of the space of metrics with respect to the gauge transformations, continuously connected to the identity

$$\mathbb{T} = \frac{\text{metrics}}{\text{Diff. } \times \text{ Weyl}}. \tag{2.96}$$

However, in general there will be additional gauge transformations on the Riemann surface not connected to the identity, *i.e.* 'large' diffeomorphisms, that will usually be given by some discrete group Γ. Considering these allows us to define the true moduli space as

$$\mathcal{M} = \frac{\text{metrics}}{\text{Diff. } \times \text{ Weyl} \times \Gamma}, \tag{2.97}$$

so called because it is generated by the space of the moduli for the surface.

We can now apply this to the case of $g = 1$ ($\chi = 0$) Riemann surfaces that are topologically equivalent to T^2. The translations along the two non-contractible cycles of the torus correspond to two Killing vector fields generating a conformal Killing group $U(1) \times U(1)$. From the Riemann-Roch theorem we expect the torus to have two real moduli. We can define a complex parameter $\tau = \tau_1 + i\tau_2$ to parameterise the torus metric, through conformal invariance we can choose to set the surface area of the torus to 1 and then we can write the metric as

$$g^{ij} = \frac{1}{\tau_2} \begin{pmatrix} |\tau|^2 & -\tau_1 \\ -\tau_1 & 1 \end{pmatrix}, \tag{2.98}$$

where we have picked coordinates on the torus $\sigma_1, \sigma_2 \in [0, 1]$. With this choice we can identify the space of τ as giving the Teichmüller space, which will be the upper half plane, $\mathbb{H}$. We can then consider the additional symmetries of the torus parameter τ not connected to the identity that generate the group Γ. These symmetries of τ are given by global operations called Dehn twists. An obvious such Dehn twist is to consider cutting the torus open along its first cycle, rotating it by 2π and then glueing it back together. This is given by taking $\tau \to \tau + 1$. Additionally, the transformation $\tau \to -1/\tau$ can be seen to only change the metric by an overall scale factor and so is equivalent by Weyl transformations.

Together these two transformations act on τ according to

$$\tau \to \frac{a\tau + b}{c\tau + d}, \quad a, b, c, d \in \mathbb{Z}, \tag{2.99}$$

where we can identify the action of the group $SL(2, \mathbb{Z})$ with elements

$$M = \begin{pmatrix} a & b \\ c & d \end{pmatrix}, \quad ad - bc = 1, \quad a, b, c, d \in \mathbb{Z}, \tag{2.100}$$

quotiented by its centre: the $\mathbb{Z}_2$ identification $(a, b, c, d) \to (-a, -b, -c, -d)$, which clearly leaves the action (2.99) unchanged. Therefore we have found that $\Gamma = PSL(2, \mathbb{Z})$ and we can define the moduli space $\mathcal{M}$ as the *fundamental domain* $\mathcal{F}$ defined by

$$\mathcal{F} = \left\{ \tau \in \mathbb{H} \,|\, \Big| \, |\tau_1| \leq 1, \; |\tau| \geq 1 \right\}. \tag{2.101}$$

We can locate the origin of UV finiteness for string theory in the fact that, since the one-loop toroidal amplitude is integrated over $\mathcal{F}$, the UV limit, which corresponds to $\tau_2 \to 0$, is excluded from the integration region. In the analagous limit for one-dimensional QFT we have the well-known UV singularities at one-loop that ultimately restrict these QFTs to being effective theories.

Partition Function in Hamiltonian formalism

As mentioned above, the one loop amplitude corresponds to a statistical partition function when considered in Euclidean time. For T^2 with local coordinates $\sigma_1, \sigma_2 \in [0, 1)$ such that σ_2 is spacelike and σ_1 is given the interpretation of Euclidean time on the string worldsheet. Considering the torus as a cylinder with its ends identified along the time direction, we note this corresponds to setting the initial and final states as the same and the amplitude will correspond to summing all states in the physical Hilbert space, which will give us a trace. Before gluing the ends, the real part of the modular parameter τ_1 induces a rotation or, analogously, a translation along σ_2. On the cylinder such translations are generated by the momentum operator

$$P = -2\pi i (L_0 - \bar{L}_0) \tag{2.102}$$

and we have already seen that the Hamiltonian of a CFT is given by

$$H = 2\pi \left(L_0 + \bar{L}_0 - \frac{c + \bar{c}}{24} \right), \tag{2.103}$$

which, as usual, can be associated to time translations, in particular along the σ_1 direction of the cylinder. We note that the prefactors in these equations (2.102) and (2.103) would be absent had we chosen the conventional $\sigma_1, \sigma_2 \in [0, 2\pi)$.

With all these considerations the torus amplitude can be restated as the following partition function

$$Z(\tau, \bar{\tau}) = \mathrm{Tr} \left[e^{-2\pi\tau_2 (L_0 + \bar{L}_0 - \frac{c+\bar{c}}{24})} e^{-2\pi\tau_1 (L_0 - \bar{L}_0)} \right], \tag{2.104}$$

which can be rewritten as

$$Z(\tau, \bar{\tau}) = \mathrm{Tr} \left[q^{L_0 - \frac{c}{24}} \bar{q}^{\bar{L}_0 - \frac{\bar{c}}{24}} \right], \tag{2.105}$$

where we have defined $q = e^{2\pi i \tau}$, sometimes called the 'nome' to number theorists.

This is a very useful form of the partition because it will have the form of an expansion of Fourier modes

$$Z = \sum_{m,n} a_{mn} q^m \bar{q}^n, \tag{2.106}$$

also known as a q-expansion. The exponents m, n will count the mass level in CFT units and a_{mn} gives the degeneracy of states at that level.

Partition Function for free scalar CFT

For the $X^\mu(\sigma^a)$ spacetime scalar fields of the bosonic string we have seen $\mu = 0, ..., 25$. A general state constructed out of the creation operators α_n, $n > 0$ can be written

$$|\Phi\rangle = \prod_{\mu=0}^{25} \prod_{n=1}^{\infty} (\alpha^\mu_{-n})^{N_n} (\bar{\alpha}^\mu_{-n})^{\bar{N}_n} |p\rangle \,, \tag{2.107}$$

which is just a rewriting of eq. (2.40). We note that the $N_i \in \mathbb{N}$ completely specify the state and that the conformal weights of states are given by eq. (2.41). Then, computing the trace corresponds to performing the integration

$$iV_{26} \int \frac{d^{26}k}{(2\pi)^{26}} e^{-2\pi\tau_2 k^2} q^{-\frac{c}{24}} \bar{q}^{-\frac{\bar{c}}{24}} \left[\prod_{r=1}^{\infty} \sum_{N=0}^{\infty} \sum_{\bar{N}=0}^{\infty} q^{rN} \bar{q}^{r\bar{N}} \right]^{26}, \tag{2.108}$$

where the imaginary unit arises due to us employing Euclidean space such that $k^0 \to ik^0$. Performing the integration results in

$$Z_X(\tau, \bar{\tau}) = \frac{iV_{26}}{(4\pi^2\alpha'\tau_2)^{13}} \frac{1}{\eta^{26}(\tau)\bar{\eta}^{26}(\bar{\tau})}, \tag{2.109}$$

where

$$\eta(\tau) = q^{1/24} \prod_{n=0}^{\infty} (1 - q^n), \tag{2.110}$$

is the Dedekind eta function with the nice modular transformation properties

$$\eta(\tau + 1) = e^{i\pi/12} \eta(\tau), \quad \eta(-\frac{1}{\tau}) = \sqrt{-i\tau}\eta(\tau). \tag{2.111}$$

It is interesting to note that we could have done this calculation without setting $c = 26$ and then using these modular transformation properties of $\eta(\tau)$ to prove it. In other words, modular invariance alone could have been used to fix the central charge of the CFT. In general, modular invariance is strongly related to unitarity and, thus, the consistency of the theory and the constraints it imposes at one-loop from the torus CFT, as well the constraints at higher genus (although these can be considered as minor additions to those from the torus), can be used as the general guiding principle for constructing consistent string vacua.

Partition Function of the ghost CFT

The scalar fields $X^\mu(\sigma^a)$ we saw were accompanied by the ghost system (b, c) for the full bosonic string theory. We may naturally wish to take a trace over states, where we have now two raising operators b_n and c_n, which we note are anticommuting. From the path integral perspective, this trace would give a path integral over antiperiodic boundary conditions in the time direction. In order to calculate the Faddeev–Popov determinant, we require that the ghosts must have the same periodicity as the original coordinate transformations, which were periodic. Hence we require that

$$Z(\tau) = \mathrm{Tr}\left[(-1)^F e^{(2\pi i \tau_1 P - 2\pi\tau_2 H)}\right] = 0. \tag{2.112}$$

The non-vanishing contribution arises due to the zero modes b_0 and c_0. These can be soaked up by insertions, the simplest choice being two b and two c insertions that can be fixed at the origin such that the partition function is augmented as

$$\begin{aligned} Z(\tau) &= \mathrm{Tr}\left[(-1)^F c_0 b_0 \bar{c}_0 \bar{b}_0 e^{(2\pi i \tau_1 P - 2\pi\tau_2 H)}\right] && (2.113)\\ &= (q\bar{q})^{26/24}\mathrm{Tr}\left[(-1)^F c_0 b_0 \bar{c}_0 \bar{b}_0 q^{L_0}\bar{q}^{\bar{L}_0}\right] && (2.114)\\ &= \eta^2\bar{\eta}^2. && (2.115)\end{aligned}$$

The full one-loop amplitude for the bosonic string is then

$$Z_1 = \frac{iV_{26}}{(4\pi^2\alpha')^{13}}\int_{\mathcal{F}}\frac{d^2\tau}{4\tau_2^2}\frac{1}{(\sqrt{\tau_2}\eta(\tau)\bar{\eta}(\bar{\tau}))^{24}}, \tag{2.116}$$

which can be shown to be modular invariant as it should be. Interestingly we can see that the contribution from the ghosts essentially cancels two of the scalar fields in X^μ. This can be interpreted as meaning we are left with the contributions only from transverse fields $X^i(\sigma^a)$, $i = 1, ..., 24$, which is related to the fact we can formulate the bosonic string theory in the light-cone gauge.

Using our amplitude (2.116) we can consider the IR limit $\tau_2 \to \infty$ where we could potentially have a divergence. By expanding the Dedekind η functions it is easy to check that the tachyon will, as expected, cause a divergence precisely in this limit.

Partition Function for Fermions

For our torus with local coordinates $\sigma_1, \sigma_2 \in [0, 1)$ we can consider the boundary conditions of a complex fermion Ψ around the two non-contractible cycles

$$\begin{aligned}\Psi(\sigma_1 + 1, \sigma_2) &= e^{i\pi(1-a)}\Psi(\sigma_1, \sigma_2) && (2.117)\\ \Psi(\sigma_1, \sigma_2 + 1) &= e^{i\pi(1-b)}\Psi(\sigma_1, \sigma_2). && (2.118)\end{aligned}$$

The partition function will split into sectors for each boundary condition possibility. More specifically, the modding of states and the value of the zero-point constant in the Hamiltonian will differ depending on a, whilst $b = 1$ will introduce an operator $e^{i\pi F}$ into the trace. For our single holomorphic complex fermion we have

$$Z_\Psi[{}^a_b] = \mathrm{Tr}_a\left[e^{i\pi bF} q^{L_0[a]-1/24}\right] = \frac{\theta[{}^a_b]}{\eta}, \tag{2.119}$$

where we have introduced the Jacobi theta functions

$$\theta[{}^a_b] = \sum_{n\in\mathbb{Z}} q^{(n+a/2)^2/2} e^{2\pi i(n+a/2)b/2}, \tag{2.120}$$

with $a, b \in \{0, 1\}$. We note that $a, b = 1$ correspond to Ramond boundary conditions and $a, b = 0$ to NS. We can in general allow for more general boundary conditions $a, b \in \mathbb{R}$, however, for complex fermions.

It will be useful to introduce the following definitions as we seek to construct consistent partition functions

$$\theta_1 := \theta[{}^0_0] = \mathrm{Tr}_{NS}\, q^{L_0 - \frac{c}{24}} \tag{2.121}$$

$$\theta_2 := \theta[{}^1_0] = \mathrm{Tr}_{R}\, q^{L_0 - \frac{c}{24}} \tag{2.122}$$

$$\theta_3 := \theta[{}^0_1] = \mathrm{Tr}_{NS}(-1)^F q^{L_0 - \frac{c}{24}} \tag{2.123}$$

$$\theta_4 := \theta[{}^1_1] = \mathrm{Tr}_{R}(-1)^F q^{L_0 - \frac{c}{24}} = 0. \tag{2.124}$$

We recall that the superstring theory contained the superghost system (β, γ). It can be shown with appropriate consideration of how to define the trace and operator insertions for different sectors of the superghost system that the contribution to the partition function from these superghosts is

$$Z_{\beta,\gamma} = (-)^{b+\mu ab} \frac{\eta}{\theta[{}^a_b]}, \tag{2.125}$$

where $\mu = 0, 1$ gives the chirality of the R vacuum. For $D = 10$, for example, we can see that the supeghosts are acting to cancel the contribution of longitudinal fermions, similar to the bosonic string case with the ghost contribution (2.113). This again means that we could have written the partition function of the transverse fermionic fields and ignored the superghosts, which is exactly what one does in the lightcone gauge approach.

Partition Function for Compact Scalars

If we consider d compact scalars that can be said to parameterise a d-dimensional torus T^d. The fields can be given the boundary conditions

$$X^I(\sigma^1 + 2\pi, \sigma^2) = X^I(\sigma^1, \sigma^2) + 2\pi n^I \tag{2.126}$$

$$X^I(\sigma^1, \sigma^2 + 2\pi) = X^I(\sigma^1, \sigma^2) + 2\pi \tilde{m}^I, \tag{2.127}$$

where $n, \tilde{m} \in \mathbb{Z}$ are winding numbers. The partition function will be given by the d-dimensional non-compact bosonic partition multiplied by a part, $Z_{n,m}$, given by tracing over the winding and internal Kaluza-Klein (KK) degrees of freedom. In the Hamiltonian representation it takes the form

$$Z_d = Z_{non-comp.} Z_{n,m} = \frac{1}{\eta^d \bar{\eta}^d} \sum_{n^I, m_I} q^{\frac{1}{2}P_L^2} \bar{q}^{\frac{1}{2}P_R^2} = \frac{1}{\eta^d \bar{\eta}^d} \Gamma_{(d,d)}(G, B), \tag{2.128}$$

where m_I are the momentum space versions of $\tilde{m}^I$ and

$$(P_{L,R})_I = \frac{\sqrt{\alpha'}}{\sqrt{2}} \left(m_I + (\alpha')^{-1} (B_{IJ} \pm G_{IJ} n^J \right), \tag{2.129}$$

are the compact momenta and we see the appearance of the metric of T^d, G_{IJ} and its antisymmetric tensor B_{IJ}.

For $d = 1$ we consider the partition function as a boson compactified on a circle of radius R

$$Z(R) = \frac{1}{\eta \bar{\eta}} \sum_{n,m \in \mathbb{Z}} q^{\frac{1}{2}P_L^2} \bar{q}^{\frac{1}{2}P_R^2}, \tag{2.130}$$

where

$$P_L = \frac{1}{\sqrt{2}} \left(\frac{m}{R} + nR \right), \quad P_R = \frac{1}{\sqrt{2}} \left(\frac{m}{R} - nR \right). \tag{2.131}$$

We can note here the emergence of T-duality through the interchanges $R \to 1/R$ and $m \to n$.

Bosonisation/Fermionisation

Using the partition function result for a single complex fermion (2.119) we can write the partition function of two holomorphic and two anti-holomorphic fermions on the torus as

$$Z_f = \frac{1}{2} \sum_{a,b=0,1} \left| \frac{\theta[\begin{smallmatrix} a \\ b \end{smallmatrix}]}{\eta} \right|^2, \tag{2.132}$$

which, through a Poisson resummation and some relabelling can be shown to equal

$$Z_f = \frac{1}{\sqrt{2\tau_2}\eta\bar{\eta}} \sum_{n,m \in \mathbb{Z}} e^{-\frac{\pi}{2\tau_2}|m - n\tau|^2}, \tag{2.133}$$

which we can see is equal to $Z(R = \frac{1}{\sqrt{2}})$ from eq. (2.130). This is an example of the phenomenon of bosonisation/fermionisation where the partition functions for bosons and fermions are related at a specific value of moduli parameters. This result can be extended, for example to a compactification on the complex torus T^2. In this case, we can introduce the complex structure modulus T and Kähler modulus U and construct the lattice defined in (2.128) $\Gamma_{(2,2)}(T, U)$. It can then be seen that at the specific point $(T, U) = (i, i)$ in the moduli space, the T^2 compactified bosonic partition function coincides exactly with that of four holomorphic and four antiholomorphic fermions.

Chapter 3

Free Fermionic Superstrings

Having reviewed some of the key aspects of string theory in Chapter 2 we are ready to describe some superstring theories. To do this we can introduce the free fermionic formulation (FFF), which provides us with a general framework in which to describe consistent perturbative superstrings. We will focus on heterotic strings in 10D and then 4D, as well as a brief description of the Type IIA/B and Type 0A/B superstrings.

3.1 The Heterotic String

In Section 2.2 we described a classical fermionic string in which we introduced a Majorana-Weyl fermion $\Psi^\mu(z,\bar{z})$ that generated the action (2.54). This theory possessed $(1,1)$ worldsheet supersymmetry with an underlying $N=1$ superconformal algebra for both the holomorphic (or 'Left', as we will often refer to it as) and antiholomorphic ('Right') side. We wish now to consider a modified approach in which there is, say, only a holomorphic Majorana fermion $\Psi^\mu(z)$ such that the local worldsheet supersymmetry is $(1,0)$. This theory will then have an antiholomorphic sector equivalent to the bosonic string defined through the Virasoro algebra and have a SCFT on the holomorphic side. The resultant theory is called the heterotic string, first uncovered in refs. [23, 24, 25]. Since all of the string models explored in this thesis derive from the heterotic string, it will be our main focus.

We have already seen that the absence of a Weyl anomaly for the system of fields $X^\mu, \Psi^\mu, b, c, \beta, \gamma$ in the holomorphic SCFT requires critical dimension $\hat{c} = D = 10$. On the antiholomorphic side we have the bosonic fields $X^\mu(\bar{z})$ and the ghosts b and c, which altogether contribute a $\bar{c} = -16$, necessitating some additional antiholomorphic fields with $\bar{c} = 16$. This can be achieved with 32 Majorana-Weyl fermionic fields, $\bar{\lambda}^A$, producing a flat gauge action in $D = 10$ of:

$$S \sim \int d^2z \left[\partial_z X^\mu \partial_{\bar{z}} X_\mu - 2i\Psi^\mu(z)\partial_z \Psi_\mu(z) - 2i \sum_{A=1}^{32} \bar{\lambda}^A \bar{\partial}_{\bar{z}} \bar{\lambda}^A \right], \tag{3.1}$$

Note the $\bar{\lambda}^A$ do not carry a spacetime index and so are considered as purely internal. Through bosonisation we could have also chosen 16 chiral bosons $\bar{X}^I$ to generate the $\bar{c} = 16$ internal, compact CFT. From (2.128) we can write the partition function contribution for these compact chiral bosons in terms of their momenta $\bar{P}^I$ that take discrete values on a 16D lattice $\bar{\Gamma}_{16}$

$$Z_{\bar{X}^I} = \frac{1}{\bar{\eta}^{16}} \sum_{\bar{P}^I \in \bar{\Gamma}} e^{\frac{1}{2}(\bar{P}^I)^2} = \frac{\bar{\Gamma}_{16}}{\bar{\eta}^{16}}. \tag{3.2}$$

The full partition function of the 10D heterotic string can be written as

$$Z_{het} = Z_{X^\mu} Z_{\psi^\mu} Z_{\bar{X}^I} \tag{3.3}$$

$$= \frac{1}{\tau_2^4 \eta^8 \bar{\eta}^8} \frac{1}{\eta^4} \left(\sum_{a,b=0,1} (-)^{a+b+ab} \theta[{}^a_b]^4 \right) \frac{\bar{\Gamma}_{16}}{\bar{\eta}^{16}}, \tag{3.4}$$

where we employ results from Section 2.5. Modular invariance now constrains the possible $\bar{\Gamma}_{16}$. The transformation $T : \tau \to \tau + 1$ on Z_{het} necessitates that $\bar{P}^I \in 2\mathbb{Z}$ and $S : \tau \to -\frac{1}{\tau}$ requires that

$$S : \bar{\Gamma}_{16} \to \bar{\tau}^8 \bar{\Gamma}_{16}\,, \tag{3.5}$$

is true. These two conditions impose that $\bar{\Gamma}_{16}$ is an even and self-dual ($\Gamma = \Gamma^*$) lattice. In 16 dimensions there are just two such lattices formed from the root lattices of the groups $SO(32)$ and $E_8 \times E_8$[1]. We can now write the one-loop vacuum to vacuum amplitude for the heterotic string as

$$\Lambda = \frac{iV_{10}}{(4\pi^2\alpha')^5} \int_{\mathcal{F}} \frac{d^2\tau}{\tau_2^2} \frac{\sum_{a,b=0,1} (-1)^{1+b+ab} \theta[{}^a_b]^4}{\tau_2^4 (\eta\bar{\eta})^8 \eta^4} \frac{\bar{\Gamma}_{16}}{\bar{\eta}^{16}}, \tag{3.6}$$

where $\bar{\Gamma}_{16}$ is one of these two consistent root lattices.

In terms of the Majorana-Weyl fermionic formulation of the heterotic string the $SO(32)$ corresponds to choosing the same boundary conditions for the 32 (real) Majorana-Weyl fermions. We can then write the partition function for the $SO(32)$ theory as

$$Z^{\bar{\lambda}}_{SO(32)} = \frac{1}{\bar{\eta}^{16}} \left(\sum_{a,b=0,1} \bar{\theta}[{}^a_b]^{16} \right), \tag{3.7}$$

whereas $E_8 \times E_8$ corresponds to splitting the fermions into two groups of 16 and choosing independent boundary conditions for the two groups

$$Z^{\bar{\lambda}}_{E_8 \times E_8} = \frac{1}{\bar{\eta}^{16}} \left(\sum_{a,b=0,1} \bar{\theta}[{}^a_b]^8 \right)^2. \tag{3.8}$$

[1]Further details on the E_8 and $Spin(32)/\mathbb{Z}_2$ root lattices, and root lattices in general, can be found in ref. [13], for example.

We note that the 32 antiholomorphic Majorana-Weyl fermions form a current algebra of the type discussed in Section 2.3. In particular, we have the currents

$$J^{ij} =: \bar{\lambda}^i(z)\bar{\lambda}^j(z) :, \quad i > j. \tag{3.9}$$

Taking NS boundary conditions for all 32 fermions, for example, generates the affine algebra of $SO(32)$ and the results of Section 2.3 apply.

3.2 10D Heterotic Model Building in the Free Fermionic Formalism

Having discussed modular invariance of the one-loop partition function in Section 2.5, we now turn our attention to building modular invariant models within the free fermionic realisation of the heterotic string. In addition to the bosonic coordinates $X^\mu(z), X^\mu(\bar{z})$ we have the holomorphic spacetime fermion $\Psi^\mu(z)$, which in the light-cone gauge has 8 transverse polarisations as degrees of freedom.

From now on, we will complexify the 32 Majorana free fermions into 16 complexified fermionic degrees of freedom through applying

$$f = \frac{1}{\sqrt{2}}(f_1 + if_2). \tag{3.10}$$

We will label these 16 complexified fields as:

$$\bar{\Phi}^a : \quad \bar{\psi}^{1,\dots,5},\ \bar{\eta}^{1,2,3},\ \bar{\phi}^{1,\dots,8}. \tag{3.11}$$

These groupings are introduced with an eye towards future GUT model building, where we will see the $\bar{\phi}^{1,\dots,8}$ as relating to the rank 8 hidden degrees of freedom, the $\bar{\psi}^{1,\dots,5}$ as generating an $SO(10)$ GUT and the $\bar{\eta}^{1,2,3}$ as generating three $U(1)$ currents in this sense discussed in Section 2.3 and in eq. (3.9). Indeed, each fermion generates a worldsheet current, which, in turn, produce the Cartan generators of the relevant gauge group. Each fermion is endowed with a charge with respect to the group given in terms of its boundary condition in the sector and its fermion number

$$Q(f) = \frac{1}{2}\alpha(f) + F(f), \tag{3.12}$$

where the action of the fermion number operator is

$$F : \begin{cases} f\,|0\rangle_{NS} = +1 \\ f^*\,|0\rangle_{NS} = -1 \\ |+\rangle = 0 \\ |-\rangle = -1 \end{cases}, \tag{3.13}$$

where we simplify the notation for the different chiralities of the Ramond vacuum to $|\pm\rangle$.

In order to group together boundary condition choices for the fermions, a key ingredient of models are vectors of boundary conditions

$$\boldsymbol{\alpha} = \{\alpha(\Psi^1), ..., \alpha(\Psi^8) \mid \alpha(\bar{\psi}^1), ..., \alpha(\bar{\psi}^5), \alpha(\bar{\eta}^1), \alpha(\bar{\eta}^2), \alpha(\bar{\eta}^3), \alpha(\bar{\phi}^1), ..., \alpha(\bar{\phi}^8)\}, \quad (3.14)$$

which defines a *sector* in free fermionic models. The boundary conditions of the complex fermions as they propagate around one of the two non-contractable loops of the torus in this notation are given through

$$f \to -e^{-i\pi\alpha(f)} f, \quad f \to -e^{+i\pi\alpha(f)} f. \quad (3.15)$$

Real boundary conditions simply implies $\alpha(\psi) \in \{0, 1\}$, but other values in the range $(-1, +1]$ can be considered, which allows for generating complex phase factors so long as modular invariance rules (to be defined shortly) are obeyed. By convention, we omit those fermions with antiperiodic (NS) boundary conditions in the sectors and only write explicitly the periodic (R) fermions, as well as specifying any more general boundary conditions.

Such sectors in the FFF arise through the definition of basis vectors $\boldsymbol{v_i} \in \mathcal{B}$ as linear combinations spanning an additive group Ξ. A complete *spin structure* can then be defined for two of these sectors through

$$\begin{bmatrix} \boldsymbol{\alpha} \\ \boldsymbol{\beta} \end{bmatrix} \quad (3.16)$$

and to these spin structure we can then associate a partition function using eq. (2.119). The full partition function can be written as

$$Z = \int_{\mathcal{F}} \frac{d^2\tau}{\tau_2^2} Z_B \sum_{\boldsymbol{\alpha},\boldsymbol{\beta}\in\Xi} C\begin{bmatrix} \boldsymbol{\alpha} \\ \boldsymbol{\beta} \end{bmatrix} \prod_f Z\begin{bmatrix} \alpha(f) \\ \beta(f) \end{bmatrix} \quad (3.17)$$

$$= \int_{\mathcal{F}} \frac{d^2\tau}{\tau_2^2} Z_B \sum_{\boldsymbol{\alpha},\boldsymbol{\beta}\in\Xi} C\begin{bmatrix} \boldsymbol{\alpha} \\ \boldsymbol{\beta} \end{bmatrix} \prod_f \left(\frac{\theta\begin{bmatrix} \alpha(f) \\ \beta(f) \end{bmatrix}}{\eta} \right)^{1/2} \prod_{\bar{f}} \left(\frac{\bar{\theta}\begin{bmatrix} \alpha(\bar{f}) \\ \beta(\bar{f}) \end{bmatrix}}{\bar{\eta}} \right)^{1/2}, \quad (3.18)$$

where we have the modular invariant measure and bosonic partition function

$$Z_B = \frac{1}{\tau_2^4} \frac{1}{\eta^8 \bar{\eta}^8}, \quad (3.19)$$

as discussed in Section 2.5. The fermionic part of the partition function we see is simply products of Jacobi-Theta functions. As also noted in Section 2.5, the modular transformations S and T will transform one theta function product to another and motivate

the introduction of the coefficients $C[\begin{smallmatrix}\alpha\\ \beta\end{smallmatrix}]$, which weight spin structures related by these transformations equally. These GGSO phases relate to discrete torsions in the orbifold formalism [26, 27, 28].

We will focus on the fermionic part of the partition function

$$Z_f = \sum_{\boldsymbol{\alpha},\boldsymbol{\beta}\in\Xi} C\begin{bmatrix}\boldsymbol{\alpha}\\ \boldsymbol{\beta}\end{bmatrix} \prod_f Z\begin{bmatrix}\alpha(f)\\ \beta(f)\end{bmatrix}, \tag{3.20}$$

in order to derive modular invariance constraints on the basis vectors and $C[\begin{smallmatrix}\alpha\\ \beta\end{smallmatrix}]$, which we call the Generalised GSO (GGSO) phases. A free fermionic model can be thought of as a choice of specific choice for these basis vectors and GGSO phases consistent with modular invariance.

The modular invariance constraints we call the ABK rules worked out in refs. [29, 30][2] and we will reproduce them below.

The first condition is simply that the possibility of both antiperiodic and periodic boundary conditions for the fermions is necessary for modular invariance which means starting a consistent basis with the vector $\mathbb{1}$, where all fermions are periodic. The NS sector then automatically belongs in Ξ since $NS = 2\mathbb{1}$.

The choice of other basis vectors have the further modular invariance constraints

$$N_i \boldsymbol{v_i}\cdot\boldsymbol{v_i} = 0 \bmod 8 \tag{3.21}$$

$$N_{ij}\boldsymbol{v_i}\cdot\boldsymbol{v_j} = 0 \bmod 4 \tag{3.22}$$

$$\prod_f \boldsymbol{v_i}(f)\boldsymbol{v_j}(f)\boldsymbol{v_k}(f)\boldsymbol{v_l}(f) = 0 \bmod 2, \tag{3.23}$$

where the (Lorentzian) dot product is defined as

$$\boldsymbol{v_i}\cdot\boldsymbol{v_j} = \left\{\left(\sum_{\text{cx. Left}} + \frac{1}{2}\sum_{\text{real Left}}\right) - \left(\sum_{\text{cx. Right}} + \frac{1}{2}\sum_{\text{real Right}}\right)\right\}\boldsymbol{v_i}(f)\boldsymbol{v_j}(f) \tag{3.24}$$

and where N_i is the smallest positive integer for which $N_i\boldsymbol{v_i} = 0$ and N_{ij} is the least common multiple of N_i and N_j.

[2] These rules were worked out in a slightly different notation at the same time in ref. [31]

The ABK rules on the GGSO phases are

$$C\begin{bmatrix}\boldsymbol{v_i}\\ \boldsymbol{v_j}\end{bmatrix} = \delta_{\boldsymbol{v_i}} e^{2\pi i \frac{n}{N_j}} = \delta_{\boldsymbol{v_j}} e^{2\pi i \frac{m}{N_i}} e^{i\pi \frac{\boldsymbol{v_i}\cdot\boldsymbol{v_j}}{2}} \tag{3.25}$$

$$C\begin{bmatrix}\boldsymbol{v_i}\\ \boldsymbol{v_i}\end{bmatrix} = -e^{i\pi \frac{\boldsymbol{v_i}\cdot\boldsymbol{v_i}}{4}} C\begin{bmatrix}\boldsymbol{v_i}\\ \mathbb{1}\end{bmatrix} \tag{3.26}$$

$$C\begin{bmatrix}\boldsymbol{v_i}\\ \boldsymbol{v_j}\end{bmatrix} = e^{i\pi \frac{\boldsymbol{v_i}\cdot\boldsymbol{v_j}}{2}} C\begin{bmatrix}\boldsymbol{v_j}\\ \boldsymbol{v_i}\end{bmatrix}^* \tag{3.27}$$

$$C\begin{bmatrix}\boldsymbol{v_i}\\ \boldsymbol{v_j}+\boldsymbol{v_k}\end{bmatrix} = \delta_{\boldsymbol{v_i}} C\begin{bmatrix}\boldsymbol{v_i}\\ \boldsymbol{v_j}\end{bmatrix} C\begin{bmatrix}\boldsymbol{v_i}\\ \boldsymbol{v_k}\end{bmatrix}, \tag{3.28}$$

where we have introduced the spin statistics operator

$$\delta_{\boldsymbol{\alpha}} = \begin{cases} +1 \text{ if } \alpha(\psi^\mu) = 0 \\ -1 \text{ if } \alpha(\psi^\mu) = 1. \end{cases} \tag{3.29}$$

Additionally, a general GGSO phase between sectors $\boldsymbol{\alpha} = m_i \boldsymbol{v_i}$ and $\boldsymbol{\beta} = n_j \boldsymbol{v_j}$ can be decomposed into the GGSO phases between basis vectors, $\boldsymbol{v_i}$, through the equation

$$C\begin{bmatrix}\boldsymbol{\alpha}\\ \boldsymbol{\beta}\end{bmatrix} = \Gamma(\boldsymbol{\alpha},\boldsymbol{\beta}) \prod_{i,j} C\begin{bmatrix}\boldsymbol{v_i}\\ \boldsymbol{v_j}\end{bmatrix}^{m_i n_i}, \tag{3.30}$$

where the prefactor is

$$\Gamma(\boldsymbol{\alpha},\boldsymbol{\beta}) = \delta_{\boldsymbol{\alpha}}^{\sum_j n_j - 1} \delta_{\boldsymbol{\beta}}^{\sum_i m_i - 1} e^{-\pi i r(\boldsymbol{\alpha})\cdot\boldsymbol{\beta}} \tag{3.31}$$

such that we have made use of the 'reduced representation'

$$2r(\boldsymbol{\alpha}) := \boldsymbol{\alpha} - [\boldsymbol{\alpha}], \tag{3.32}$$

where $[\boldsymbol{\alpha}]$ is the sector with entries in the range $(-1, +1]$.

We note that for all $\boldsymbol{\alpha} \in \Xi$ there is a Hilbert space obtained by acting on the NS vacuum or the (doubly-degenerate) Ramond vacua. All states in each sector, $\boldsymbol{\alpha}$, are subject to the generalised GSO projection

$$e^{i\pi \boldsymbol{v_i}\cdot F_{\boldsymbol{\alpha}}} |S_{\boldsymbol{\alpha}}\rangle = \delta_{\boldsymbol{\alpha}} C\begin{bmatrix}\boldsymbol{\alpha}\\ \boldsymbol{v_i}\end{bmatrix}^* |S_{\boldsymbol{\alpha}}\rangle\,, \tag{3.33}$$

which can be seen to arise also through demanding modular invariance. The full Hilbert space of models can now be constructed by direct summing over the sector Hilbert spaces subject to the GGSO projection

$$\mathcal{H} = \bigoplus_{\boldsymbol{\alpha}\in\Xi} \prod_{i=1}^{k} \left\{ e^{i\pi \boldsymbol{v_i}\cdot F_{\boldsymbol{\alpha}}} |S_{\boldsymbol{\alpha}}\rangle = \delta_{\boldsymbol{\alpha}} C\begin{bmatrix}\boldsymbol{\alpha}\\ \boldsymbol{v_i}\end{bmatrix}^* |S_{\boldsymbol{\alpha}}\rangle \right\}, \tag{3.34}$$

The sectors in the model can be characterised according to the left and right moving vacuum separately

$$M_L^2 = -\frac{1}{2} + \frac{\boldsymbol{\alpha}_L \cdot \boldsymbol{\alpha}_L}{8} + N_L \tag{3.35}$$
$$M_R^2 = -1 + \frac{\boldsymbol{\alpha}_R \cdot \boldsymbol{\alpha}_R}{8} + N_R,$$

where N_L and N_R are sums over holomorphic (L) and antiholomorphic (R) oscillator frequencies, respectively

$$N_L = \sum_f \nu_f + \sum_{f^*} \nu_{f^*} \tag{3.36}$$
$$N_R = \sum_{\bar{f}} \nu_{\bar{f}} + \sum_{\bar{f}^*} \nu_{\bar{f}^*}, \tag{3.37}$$

where f is a holomophic oscillator and $\bar{f}$ is an antiholomorphic oscillator and the frequency is defined through the boundary condition in the sector $\boldsymbol{\alpha}$. For real fermions, f we have

$$\nu_f = \frac{1+\alpha(f)}{2}, \quad \nu_{\bar{f}} = \frac{1+\alpha(f)}{2}, \tag{3.38}$$

whilst for complex fermions, $\bar{\lambda}$, and their complex conjugates we have

$$\nu_{\bar{\lambda}} = \frac{1+\alpha(\bar{\lambda})}{2}, \quad \nu_{\bar{\lambda}^*} = \frac{1-\alpha(\bar{\lambda})}{2}. \tag{3.39}$$

Physical states must then additionally satisfy the Virasoro matching condition: $M_L^2 = M_R^2$, states not satisfying this correspond to off-shell states. It will often be useful to define the vacuum energy of a sector as

$$\alpha_V = \left(-\frac{1}{2} + \frac{\boldsymbol{\alpha}_L \cdot \boldsymbol{\alpha}_L}{8}, -1 + \frac{\boldsymbol{\alpha}_R \cdot \boldsymbol{\alpha}_R}{8} \right). \tag{3.40}$$

3.3 Some 10D Heterotic Models

We are now ready to show some examples of how 10D heterotic string models look in the free fermionic formulation.

Tachyonic $SO(32)$ Model, $\mathcal{B} = \{\mathbb{1}\}$

The simplest basis we can choose consistent with modular invariance is $\mathcal{B} = \{\mathbb{1}\}$. This model has just two sectors: the Ramond sector, $\mathbb{1}$, and the NS sector $\mathbb{1} + \mathbb{1} = |0\rangle_{NS}$. Since the vacuum energy of $\mathbb{1}$ is $\alpha_V = (0, 1)$ it only gives rise to massive states. On the other hand the NS sector has $\alpha_V = (-\frac{1}{2}, -1)$ and so we can consider on-shell states arising from it for $M^2 \leq 0$.

At mass level $M^2 = -\frac{1}{2}$ we can consider an oscillator contributing $N_R = -\frac{1}{2}$ to give the on-shell tachyonic states

$$\bar{\Phi}^a \left|0\right\rangle_{NS} . \tag{3.41}$$

Next we can consider the massless level such that $N_L = \frac{1}{2}$ and $N_R = 1$. This gives us the following states:

- First of all we have

$$\Psi^i \partial \bar{X}^j \left|0\right\rangle_{NS} , \tag{3.42}$$

  where i labels the 8 transverse fermionic excitations and j the 8 transverse bosonic excitations. These states are gravitational and model-independent. They decompose into the irreducible representations of the transverse rotation group $SO(8)$ to give the graviton, antisymmetric tensor and dilaton as we would expect to see from earlier discussion in Chapter 2.

- Then we have gauge bosons of the form

$$\Psi^i \bar{\Phi}^a \bar{\Phi}^b \left|0\right\rangle_{NS} , \tag{3.43}$$

  with $a, b \in \{1, ..., 16\}$. The $\bar{\Phi}^a$ anticommute so that $a \neq b$ and we then associate these states to the **496** adjoint representation of $SO(32)$.

We note that all these sectors survive the GGSO projection (3.33) since $C[\begin{smallmatrix} NS \\ \mathbb{1} \end{smallmatrix}] = -1$, from the rule of eq. (3.25).

We will finally note the appearance of the following off-shell tachyonic state from the NS sector

$$\Psi^i \left|0\right\rangle_{NS} , \tag{3.44}$$

at mass level $(0, -1)$. This state was first discussed in [32] and given the name the 'protograviton'. It appears in a model-independent way in non-supersymmetric models. Its presence in the string spectrum can be understood at the CFT level by noting that it appears in the same Verma module as the graviton state which is always present in the massless NS sector.

Supersymmetric $SO(32)$ Model, $\mathcal{B} = \{\mathbb{1}, S\}$

In addition to $\mathbb{1}$, we will now add the basis vector

$$\boldsymbol{S} = \{\Psi^i\}, \tag{3.45}$$

which we call, with foresight, the SUSY generator. Now we can consider the sectors that can generate massless states. Along with the NS sector, we note that the sector $\boldsymbol{S}$ has $\alpha_V = (0, -1)$ and so generates massless states of the form

$$\partial \bar{X}^j \left|\boldsymbol{S}\right\rangle , \tag{3.46}$$

and

$$\bar{\Phi}^a\bar{\Phi}^b\,|\boldsymbol{S}\rangle\,, \tag{3.47}$$

where the $|\boldsymbol{S}\rangle$ means the Ramond vacua for the 8 real transverse fermionic degrees of freedom Ψ^i, which can be thought of as 4 complexified degrees of freedom. The GGSO phase $C\left[\begin{smallmatrix}\mathbb{1}\\ \boldsymbol{S}\end{smallmatrix}\right] = \pm 1$ then fixes whether we have the spinor or conjugate representation. We can observe that the states (3.46) are spin $\frac{3}{2}$ and identify as one gravitino so that this model enjoys $\mathcal{N} = 1$ spacetime supersymmetry. We then further note that the states (3.47) are spin $\frac{1}{2}$ and, as such, identify as the superpartners of the gauge bosons from the NS Sector (3.43) and so are the gaugini of $SO(32)$.

In this model, we further note that the NS tachyon (3.41) will automatically be GGSO projected by $\boldsymbol{S}$ since $C\left[\begin{smallmatrix}\boldsymbol{S}\\ NS\end{smallmatrix}\right] = -1$. It is now clear why we called $\boldsymbol{S}$ the SUSY generator, although we can illustrate this still further by considering the partition function. First, we recall from Chapter 2 the theta functions (2.121) and that the Ramond-Ramond theta function, θ_1, vanishes. There are then 9 non-zero terms in the $\mathcal{B} = \{\mathbb{1}, \boldsymbol{S}\}$ partition function

$$C\begin{bmatrix}\mathbb{1}\\ NS\end{bmatrix}Z\begin{bmatrix}\mathbb{1}\\ NS\end{bmatrix}, \qquad C\begin{bmatrix}\boldsymbol{S}\\ NS\end{bmatrix}Z\begin{bmatrix}\boldsymbol{S}\\ NS\end{bmatrix}, \qquad C\begin{bmatrix}\boldsymbol{S}\\ \mathbb{1}+\boldsymbol{S}\end{bmatrix}Z\begin{bmatrix}\boldsymbol{S}\\ \mathbb{1}+\boldsymbol{S}\end{bmatrix}, \tag{3.48}$$

$$C\begin{bmatrix}NS\\ NS\end{bmatrix}Z\begin{bmatrix}NS\\ NS\end{bmatrix}, \qquad C\begin{bmatrix}NS\\ \mathbb{1}+\boldsymbol{S}\end{bmatrix}Z\begin{bmatrix}NS\\ \mathbb{1}+\boldsymbol{S}\end{bmatrix}, \qquad C\begin{bmatrix}\mathbb{1}+\boldsymbol{S}\\ NS\end{bmatrix}Z\begin{bmatrix}\mathbb{1}+\boldsymbol{S}\\ NS\end{bmatrix}, \tag{3.49}$$

$$C\begin{bmatrix}NS\\ \boldsymbol{S}\end{bmatrix}Z\begin{bmatrix}NS\\ \boldsymbol{S}\end{bmatrix}, \qquad C\begin{bmatrix}\mathbb{1}+\boldsymbol{S}\\ \boldsymbol{S}\end{bmatrix}Z\begin{bmatrix}\mathbb{1}+\boldsymbol{S}\\ \boldsymbol{S}\end{bmatrix}, \qquad C\begin{bmatrix}NS\\ \mathbb{1}\end{bmatrix}Z\begin{bmatrix}NS\\ \mathbb{1}\end{bmatrix}. \tag{3.50}$$

Using the ABK rules (3.25-3.28) to calculate the GGSO phases[3] we can write the contribution of the first 3 terms (3.48) as

$$\propto \theta_2^4\left(-\bar{\theta}_2^{16} - \bar{\theta}_3^{16} - \bar{\theta}_4^{16}\right) \tag{3.51}$$

then the second 3 terms (3.49)

$$\propto \theta_3^4\left(\bar{\theta}_2^{16} + \bar{\theta}_3^{16} + \bar{\theta}_4^{16}\right) \tag{3.52}$$

and the final 3 terms (3.50)

$$\propto \theta_4^4\left(-\bar{\theta}_2^{16} - \bar{\theta}_3^{16} - \bar{\theta}_4^{16}\right). \tag{3.53}$$

Putting this all together we can write the fermionic partition function in factorised form is

$$Z_{\{\mathbb{1},\boldsymbol{S}\}} = \frac{1}{\eta^4\bar{\eta}^{16}}\left(\theta_3^4 - \theta_2^4 - \theta_4^4\right)\left[\bar{\theta}_2^{16} + \bar{\theta}_3^{16} + \bar{\theta}_4^{16}\right], \tag{3.54}$$

and we see the emergence of the 'Abstrusa' identity for Jacobi-theta functions which ensures this partition function vanishes as expected from supersymmetry.

[3]Modular invariance dictates that the only free phase is $C\left[\begin{smallmatrix}\boldsymbol{S}\\ \mathbb{1}\end{smallmatrix}\right]$ which then fixes the other GGSO phases. This choice, however, we can easily see does not impact on this analysis of the partition function.

The $E_8 \times E_8$ and $SO(16) \times SO(16)$ Models

In Section 3.1 we introduced the $E_8 \times E_8$ heterotic string in ten dimensions so now let's see how it looks in the free fermionic formulation. This will allow us to inspect its massless spectrum as promised. We start with the basis vectors

$$\begin{aligned}\mathbb{1} &= \{\Psi^i, \mid \overline{\eta}^{1,2,3}, \overline{\psi}^{1,\dots,5}, \overline{\phi}^{1,\dots,8}\},\\ \boldsymbol{x} &= \{\overline{\psi}^{1,\dots,5}, \overline{\eta}^{1,2,3}\},\\ \boldsymbol{H} &= \{\overline{\phi}^{1,\dots,8}\},\end{aligned}$$

We observe that now the supersymmetry generator arises from the combination

$$\boldsymbol{S} = \mathbb{1} + \boldsymbol{x} + \boldsymbol{H}. \tag{3.55}$$

Firstly, we can observe that the possible tachyons in this model coming from the NS sector (3.41) will again be GGSO projected by $\boldsymbol{S}$ automatically. Next we turn to the massless spectrum. The possible states, prior to considering GGSO projections, are summarised in Table 3.1

Sector	α_V	Possible States	Interpretation
NS	$(-1/2,-1)$	$\Psi^i\partial\bar{X}^j\,\lvert 0\rangle_{NS}$ $\Psi^i\bar{\Phi}^a\bar{\Phi}^b\,\lvert 0\rangle_{NS}$	Graviton, Antisymmetric tensor and Dilaton Gauge bosons giving the $SO(16)\times SO(16)$ representations: $(\mathbf{120},\mathbf{1})$ for $a,b=1,\dots,8$ $(\mathbf{1},\mathbf{120})$ for $a,b=9,\dots,16$ $(\mathbf{16},\mathbf{16})$ for $a=1,\dots,8,\ b=9,\dots,16$
$\boldsymbol{S}$	$(0,-1)$	$\partial\bar{X}^j\,\lvert\boldsymbol{S}\rangle$ $\bar{\Phi}^a\bar{\Phi}^b\,\lvert\boldsymbol{S}\rangle$,	Gravitino Gaugini of gauge bosons from NS
$\boldsymbol{x}$	$(-1/2,0)$	$\Psi^i\,\lvert\boldsymbol{x}\rangle$	Gauge bosons in $(\mathbf{128},\mathbf{1})$ spinorial of $SO(16)\times SO(16)$
$\boldsymbol{H}$	$(-1/2,0)$	$\Psi^i\,\lvert\boldsymbol{H}\rangle$	Gauge bosons in $(\mathbf{1},\mathbf{128})$
$\boldsymbol{S}+\boldsymbol{x}$	$(0,0)$	$\lvert\boldsymbol{S}+\boldsymbol{x}\rangle$	Gaugini of the $(\mathbf{128},\mathbf{1})$
$\boldsymbol{S}+\boldsymbol{H}$	$(0,0)$	$\lvert\boldsymbol{S}+\boldsymbol{H}\rangle$	Gaugini of the $(\mathbf{1},\mathbf{128})$

Table 3.1: *Possible massless states of the $\mathcal{B}=\{\mathbb{1},\boldsymbol{x},\boldsymbol{H}\}$ model.*

There are just 3 independent GGSO phases in this basis, which are

$$C\begin{bmatrix}\mathbb{1}\\ \boldsymbol{x}\end{bmatrix},\ C\begin{bmatrix}\mathbb{1}\\ \boldsymbol{H}\end{bmatrix}\ \text{and}\ C\begin{bmatrix}\boldsymbol{x}\\ \boldsymbol{H}\end{bmatrix}. \tag{3.56}$$

giving us, *a priori*[4], 8 possibilities. However, we can observe that the phase $C[\frac{\boldsymbol{x}}{\boldsymbol{H}}]=\pm 1$ is what counts for the charateristics of the spectrum.

[4] At this point we can note that distinct GGSO configurations can, and often do, correspond to models with the same partition function. Although not ideal, we often will say 'model' when it would be more accurate to say 'GGSO configuration' and reserve 'model' to be defined by a distinct partition function.

In the case $C[\frac{\boldsymbol{x}}{\boldsymbol{H}}] = +1$, the GGSO projections ensure that the gravitino is retained as well as the additional gauge bosons $\Psi^i |\boldsymbol{x}\rangle$ and $\Psi^i |\boldsymbol{H}\rangle$ that provide the $(\mathbf{128}, \mathbf{1})$ and $(\mathbf{1}, \mathbf{128})$ representations that induce the enhancement $SO(16) \times SO(16) \to E_8 \times E_8$. However, $C[\frac{\boldsymbol{x}}{\boldsymbol{H}}] = -1$ projects the gravitino and projects out these additional gauge bosons. Therefore we see how the supersymmetric $E_8 \times E_8$ heterotic string and non-supersymmetric, tachyon-free $SO(16) \times SO(16)$ are distinguished solely by a choice of GGSO phase. This was originally shown in refs. [33, 34]. Further it was shown in [35] that these vacua can be connected via interpolation.

The $\tilde{S}$-Map and a tachyonic 10D Heterotic String

We can now construct additional 10D heterotic strings that come with tachyons from the NS sector by taking a basis such as

$$\mathcal{B} = \{\mathbb{1}, \tilde{\boldsymbol{S}}\}, \tag{3.57}$$

where we introduce the vector

$$\tilde{\boldsymbol{S}} = \{\Psi^i \mid \bar{\phi}^{1,\dots,4}\}, \tag{3.58}$$

which takes the SUSY generator $\boldsymbol{S}$ and augments it by 4 periodic antiholomorphic fermions. This was introduced in refs. [36, 37] to explore tachyonic 10D vacua and their descendent 4D models.

By taking the GGSO projection with $\tilde{\boldsymbol{S}}$ on the NS tachyon (3.41) we have the surviving tachyons

$$\bar{\phi}^{1,\dots,4} |0\rangle_{NS}, \tag{3.59}$$

and we note that there is no gravitino state since $\boldsymbol{S}$ is absent from the basis. The gauge bosons from the NS sector are

$$\begin{cases} \Psi^i \bar{\phi}^{1,\dots,4} \bar{\phi}^{1,\dots,4} |0\rangle_{NS}, \\ \Psi^i \bar{\Phi}^a \bar{\Phi}^b |0\rangle_{NS}, \quad \bar{\Phi}^a, \bar{\Phi}^b \notin \{\bar{\phi}^{1,\dots 4}\}, \end{cases} \tag{3.60}$$

generating the gauge group $SO(24) \times SO(8)$. Such a non-supersymmetric, tachyonic vacua with this gauge group is one of the original modular invariant heterotic strings found first in [33]. In ref. [38] all these possibilities are summarised in Table 1 with the other tachyonic, non-supersymmetric heterotics strings having the gauge groups: $O(16) \times E_8, (E_7 \times SU(2))^2, U(16)$ and E_8.

3.4 Type II Superstrings from Free Fermions

So far, we have limited our discussion to heterotic superstrings but now let's install supersymmetry on both sides of the theory with the fermionic field $\Psi^i(z, \bar{z})$ with

$i = 1, ..., 8$ labelling the transverse degrees of freedom. In the free fermionic language things are simpler than in the heterotic case as our basis vectors specify the boundary conditions of 8 real holomorphic and 8 real antiholomorphic fermions, or just 4 on each side once we complexify. We have just 4 sectors to consider in this case

$$\boldsymbol{\alpha}_1 = \{\Psi^i \mid \bar{\Psi}^i\} \tag{3.61}$$
$$\boldsymbol{\alpha}_2 = \{\Psi^i\} \tag{3.62}$$
$$\boldsymbol{\alpha}_3 = \{\bar{\Psi}^i\} \tag{3.63}$$
$$\boldsymbol{\alpha}_4 = \{\}, \tag{3.64}$$

generating the R-R, R-NS, NS-R and NS-NS sectors of the theory. We can create a free fermionic model with these sectors using the basis

$$\begin{aligned} \mathbb{1} &= \{\Psi^i \mid \bar{\Psi}^i\} \\ \boldsymbol{S} &= \{\Psi^i\}. \end{aligned} \tag{3.65}$$

The modular invariance constraints will work as for the heterotic case but the spacetime statistics operator will be modified to $\delta_{\boldsymbol{\alpha}} = e^{i\pi(\alpha(\Psi^i)+\alpha(\bar{\Psi}^i))}$ in the GGSO projection and the mass formula (3.35) will take the supersymmetric form on both sides. For this model we first note that the NS tachyon, which has no oscillators since $\alpha_V = (-\frac{1}{2}, -\frac{1}{2})$, will be automatically projected by $\boldsymbol{S}$. We have the massless states from NS

$$\Psi^i \overline{\Psi}^j \left|0\right\rangle_{NS}, \tag{3.66}$$

which gives the gravitational states. Next we can consider the sector $\boldsymbol{S}$ which, as usual, gives the gravitino

$$\bar{\Psi}^i \left|\boldsymbol{S}\right\rangle, \tag{3.67}$$

with the chirality determined by the GGSO phase $C[\frac{\mathbb{1}}{\boldsymbol{S}}]$. Similarly the sector $\mathbb{1} + \boldsymbol{S}$ gives another gravitino

$$\Psi^i \left|\mathbb{1} + \boldsymbol{S}\right\rangle \tag{3.68}$$

and again the chirality is determined by the phase $C[\frac{\mathbb{1}}{\boldsymbol{S}}]$ and is the same as that of the $\boldsymbol{S}$ gravitino. The final massless sector is $\mathbb{1}$ which gives massless states of the form

$$\left|\Psi^i\right\rangle \otimes \left|\overline{\Psi}^j\right\rangle \tag{3.69}$$

and this time the $C[\frac{\mathbb{1}}{\boldsymbol{S}}]$ determines whether the two sides have the same or opposite chirality.

This choice of the phase $C[\frac{\mathbb{1}}{\boldsymbol{S}}]$ gives rise, then, to two superstrings with $\mathcal{N} = 2$ spacetime supersymmetry: Type IIA and Type IIB. We can note that a perfectly modular invariant theory is given by just the basis $\mathcal{B} = \{\mathbb{1}\}$. In this case the $\boldsymbol{S}$ sector is not present to generate the gravitinos or project the NS tachyon. The states from the sector

$\mathbb{1}$ (3.69) are still subject to a chirality projection from $C\left[\begin{smallmatrix}\mathbb{1}\\ \mathbb{1}\end{smallmatrix}\right] = \pm 1$ and so, again, we have two distinct models. Both are without supersymmetry and are called the Type 0A and Type 0B strings, alluded to already in Section 2.4 on the GSO projection.

More details on Type II string models can be found in ref. [39] where 4D $\mathcal{N} = 2$ Type II strings from $\mathbb{Z}_2 \times \mathbb{Z}_2$ orbifolds are classified.

3.5 4D Heterotic Strings

After having discussed a range of 10D superstrings in the previous section, we can now discuss the construction of models in four dimensions. In 10D, we saw that to cancel the Weyl anomaly for the heterotic string we chose the holomorphic central charge matter contribution of $c = 15$, in order to cancel the ghost contributions. However, this is just one choice where we privilege the spacetime degrees of freedom over internal fermions. For $D = 4$ we can take the 4D spacetime fields $X^\mu(z, \bar{z}), \psi^\mu(z)$, with $\mu = 1, 2$ for the lightcone gauge. These contribute $c = 6$ on the supersymmetric side and $\bar{c} = 4$ to the bosonic CFT. The additional $c = 9$ on the holomorphic side can be generated by introducing 18 free real fermions

$$\chi^{1,\dots,6}, y^{1,\dots,6}, w^{1,\dots,6}(z), \tag{3.70}$$

and the required $\bar{c} = 6$ can be generated by the antiholomorphic real free fermions

$$\bar{y}^{1,\dots,6}, \bar{w}^{1,\dots,6}(\bar{z}). \tag{3.71}$$

Model building then follows the same modular invariance rules as the 10D case except the basis vectors also include boundary conditions for these additional free fermions.

In order to maintain the $N = 1$ SCFT algebra on the worldsheet required to eliminate unphysical states we must ensure that the supercurrent $T_F(z)$ can be realised in terms of our free fermionic fields. The choice

$$T_F(z) = i\psi^\mu \partial X^\mu(z) + i \sum_{I=1}^{6} \chi^I y^I w^I(z), \tag{3.72}$$

realises local worldsheet supersymmetry non-linearly and corresponds to choosing the 18 holomorphic free fermions to transform under the Lie Group $SU(2)^6$ as explained in [40].

Having constructed this 4D heterotic construction we can note that the term 'critical dimension' for $D = 10$ is somewhat misleading. In fact, this 4D heterotic string is the same heterotic string as the 10D case just expanded around a different background given by a 4D Minkowski spacetime and some internal 6D torus generated by the fermionic degrees of freedom $\{y^I, w^I \,|\bar{y}^I, \bar{w}^I\}$ introduced above. We note that these fermionic degrees of freedom describe a torus where the radii are all fixed at the

special self-dual point in which bosonisation/fermionisation is possible, as discussed in Section 2.5. We can make contact with the bosonic coordinates through the bosonisation $i\partial X^i_L = y^i w^i$, and similarly on the antiholomorphic side. From this, we can observe that the way we assign boundary conditions to the internal fermionic coordinates $\{y^I, w^I \,|\bar{y}^I, \bar{w}^I\}$ will determine the geometry of this internal 6D space and with these fermions we can naturally realise non-geometric spaces by asymmetric pairings. We will return to this in Chapter 8 where asymmetric orbifold models are classified. One restriction of the free fermionic construction is that we are fixed at this particular point in the moduli space. We can however move away from this point by turning on Thirring interactions in terms of the free worldsheet fermions along the lines of ref. [41]. Another approach is to translate the free fermionic models to the bosonic orbifold formalism using the tools of refs. [26, 42, 43, 44], where the incorporation of moduli is manifest and phenomenological features such as SUSY breaking can be studied.

Chapter 4

Overview of the Classification Program for $\mathbb{Z}_2 \times \mathbb{Z}_2$ Orbifold Heterotic String Vacua

The classification of $\mathbb{Z}_2 \times \mathbb{Z}_2$ orbifold [26, 45, 46, 47, 48] heterotic string vacua in the free fermionic formulation is an ongoing endeavour after its origins over two decades ago in ref. [49] for the heterotic string and in ref. [39] for Type II. In this chapter we will review the classification program with a focus on recent developments extended in the rest of this thesis.

4.1 $\mathcal{N} = 1$ Symmetric $\mathbb{Z}_2 \times \mathbb{Z}_2$ Orbifold Classification

The classification methodology was first constructed in the context of symmetric $\mathbb{Z}_2 \times \mathbb{Z}_2$ orbifolds with $\mathcal{N} = 1$ supersymmetry and unbroken $SO(10)$ gauge symmetry in [50, 51]. The starting point of this construction is the basis set

$$\begin{aligned}
\mathbb{1} &= \{\psi^\mu,\ \chi^{1,\dots,6}, y^{1,\dots,6}, \omega^{1,\dots,6} \mid\ \overline{y}^{1,\dots,6}, \overline{\omega}^{1,\dots,6}, \overline{\eta}^{1,2,3}, \overline{\psi}^{1,\dots,5}, \overline{\phi}^{1,\dots,8}\},\\
\boldsymbol{S} &= \{\psi^\mu, \chi^{1,\dots,6}\},\\
\boldsymbol{e_i} &= \{y^i, w^i \mid \overline{y}^i, \overline{w}^i\},\ i = 1,\dots,6,\\
\boldsymbol{b_1} &= \{\chi^{34}, \chi^{56}, y^{34}, y^{56} \mid \overline{y}^{34}, \overline{y}^{56}, \overline{\eta}^1, \overline{\psi}^{1,\dots,5}\},\\
\boldsymbol{b_2} &= \{\chi^{12}, \chi^{56}, y^{12}, y^{56} \mid \overline{y}^{12}, \overline{y}^{56}, \overline{\eta}^2, \overline{\psi}^{1,\dots,5}\},\\
\boldsymbol{z_1} &= \{\overline{\phi}^{1,\dots,4}\},\\
\boldsymbol{z_2} &= \{\overline{\phi}^{5,\dots,8}\}.
\end{aligned} \tag{4.1}$$

The untwisted vector bosons present due to this choice of basis vectors generate the gauge group

$$SO(10) \times U(1)^3 \times SO(8)^2 \tag{4.2}$$

in the adjoint representation. The observable GUT $SO(10)$ group here is associated to the $\bar{\psi}^{1,\dots,5}$ complex fermions, while the $U(1)$'s are generated from the currents $: \bar{\eta}^j \bar{\eta}^{*j} :$ and gauge bosons associated to $\bar{\phi}^{1,\dots,8}$ generate the hidden $SO(8)^2$ group.

A key role is played by the vectors $\boldsymbol{b_1}$ and $\boldsymbol{b_2}$ in these models as they define the $SO(10)$ gauge symmetry and correspond to $\mathbb{Z}_2 \times \mathbb{Z}_2$ orbifold twists which break the $\mathcal{N} = 4$ supersymmetry, obeyed by the other 10 vectors, to $\mathcal{N} = 1$. Meanwhile the $\boldsymbol{e_i}$ vectors generate all symmetric shifts of the internal $\Gamma_{6,6}$ lattice given by the six internal bosonic coordinates, which are bosonised through the equation $i\partial X_L^I = y^I w^I$. We note that this basis imposes symmetric pairings of the internal fermionised coordinates $\{y^I, w^I \mid \bar{y}^I, \bar{w}^I\}$ generating 12 Ising operators and giving the minimal rank gauge group of the heterotic string since no antiholomorphic currents are generated from asymmetrically pairings of the $\bar{y}^I, \bar{w}^I$.

The 12 basis vectors of (4.1) generate a 12×12 matrix of GGSO phases $C\left[\begin{smallmatrix} v_i \\ v_j \end{smallmatrix}\right]$, which we can consider as having just $2^{12(11)/2} \sim 7.4 \times 10^{19}$ indepedent phases from the upper triangle; with the rest fixed by modular invariance rules (3.25-3.28). In order to specifically classify $\mathcal{N} = 1$ string vacua, the following GGSO phases must be fixed in order to retain the gravitino from the state $\partial X^\mu \left|\boldsymbol{S}\right\rangle$

$$C\begin{bmatrix}\boldsymbol{S}\\ \boldsymbol{e_i}\end{bmatrix} = C\begin{bmatrix}\boldsymbol{S}\\ \boldsymbol{z_1}\end{bmatrix} = C\begin{bmatrix}\boldsymbol{S}\\ \boldsymbol{z_2}\end{bmatrix} = -1 \tag{4.3}$$

and the additional following choices ensure the presence of the gravitino and fix its chirality consistently

$$C\begin{bmatrix}\mathbb{1}\\ \boldsymbol{S}\end{bmatrix} = C\begin{bmatrix}\boldsymbol{S}\\ \boldsymbol{S}\end{bmatrix} = C\begin{bmatrix}\boldsymbol{S}\\ \boldsymbol{b_1}\end{bmatrix} = C\begin{bmatrix}\boldsymbol{S}\\ \boldsymbol{b_2}\end{bmatrix} = -1. \tag{4.4}$$

Considering these constraints, we can deduce that the space of independent $\mathcal{N} = 1$ GGSO configurations is $2^{55} \sim 3.6 \times 10^{16}$.

The idea of the classification methodology is to scan over this space of independent phases and collect data for each configuration as we do so. This data can be written in the form of a set of classification numbers relating to the representations of states in the spectrum of each model. In the $\mathcal{N} = 1$ $SO(10)$ case we consider here, the important data will relate to the observational representations in which the content of the Standard Model ought to arise, in particular the spinorial **16**, $\overline{\mathbf{16}}$ and vectorial **10**. The details of how these representations arise are detailed in the following subsection. Further important data to collect as we scan GGSO configurations is whether there are additional gauge bosons that enhance the untwisted gauge group (4.2).

4.1.1 Observable $SO(10)$ Sectors

The fermion generations of the Standard Model reside within the spinorial states from the $\mathbf{16}/\overline{\mathbf{16}}$ of $SO(10)$, which in this construction are given by

$$\begin{aligned}
\boldsymbol{F}^1_{pqrs} =& \boldsymbol{S}+\boldsymbol{b_1}+p\boldsymbol{e_3}+q\boldsymbol{e_4}+r\boldsymbol{e_5}+s\boldsymbol{e_6}\\
=&\{\psi^\mu,\chi^{1,2},(1-p)y^3\bar{y}^3,pw^3\bar{w}^3,(1-q)y^4\bar{y}^4,qw^4\bar{w}^4\\
&(1-r)y^5\bar{y}^5,rw^5\bar{w}^5,(1-s)y^6\bar{y}^6,sw^6\bar{w}^6,\bar{\eta}^1,\bar{\psi}^{1,\dots,5}\}\\
\boldsymbol{F}^2_{pqrs} =& \boldsymbol{S}+\boldsymbol{b_2}+p\boldsymbol{e_1}+q\boldsymbol{e_2}+r\boldsymbol{e_5}+s\boldsymbol{e_6}\\
\boldsymbol{F}^3_{pqrs} =& \boldsymbol{S}+\boldsymbol{b_3}+p\boldsymbol{e_1}+q\boldsymbol{e_2}+r\boldsymbol{e_3}+s\boldsymbol{e_4},
\end{aligned} \tag{4.5}$$

where $\boldsymbol{b_3}=\boldsymbol{b_1}+\boldsymbol{b_2}+\boldsymbol{x}$ such that the $\boldsymbol{x}$ vector is the important combination:

$$\boldsymbol{x}=\mathbb{1}+\boldsymbol{S}+\sum_{i=1}^{6}\boldsymbol{e_i}+\sum_{k=1}^{2}\boldsymbol{z_k}=\{\bar{\eta}^{123},\bar{\psi}^{12345}\}. \tag{4.6}$$

We note that the orbifold action of $\mathbb{Z}_2$ from $\boldsymbol{b_k}$ on each T^2 has four fixed points. Therefore, when considering $\mathbb{Z}_2\times\mathbb{Z}_2$ twists on two of the two-tori, *i.e.* $T^4=T^2\times T^2$ there are $4\times4=16$ fixed points. These sixteen fixed points are represented in the free fermionic formulation by the choices $p,q,r,s=0,1$ appearing in the twisted sectors.

In order to determine whether a particular sector survives the GGSO projections and remains in the massless spectrum we can construct a projector. For example, taking a sector with no oscillators $|\boldsymbol{\alpha}\rangle$ and employing the notation of [44], the survival/projection condition is encapsulated in the generalised projector

$$\mathbb{P}_{\boldsymbol{\alpha}}=\prod_{\boldsymbol{\xi}\in\mathrm{Y}(\boldsymbol{\alpha})}\frac{1}{2}\left(1+\delta_{\boldsymbol{\alpha}}C\begin{bmatrix}\boldsymbol{\alpha}\\ \boldsymbol{\xi}\end{bmatrix}\right), \tag{4.7}$$

where

$$\delta_{\boldsymbol{\alpha}}=\begin{cases}+1 \text{ if } \alpha(\psi^\mu)=0 & \Longleftrightarrow \quad \text{sector is bosonic}\\ -1 \text{ if } \alpha(\psi^\mu)=1 & \Longleftrightarrow \quad \text{sector is fermionic.}\end{cases} \tag{4.8}$$

The $\mathrm{Y}(\boldsymbol{\alpha})$ is defined as a minimal linearly independent set of vectors $\boldsymbol{\xi}$ such that $\boldsymbol{\xi}\cap\boldsymbol{\alpha}=\emptyset$. To check whether the sector $\boldsymbol{\alpha}$ is projected simply amounts to checking $\mathbb{P}_{\boldsymbol{\alpha}}=0$.

Accounting for oscillators in the projectors can be done by additional operators relating to the oscillator. For example, in the presence of a single right-moving oscillator $\bar{\lambda}$ with $\nu_f=\frac{1}{2}$, this generalised projector is modified to

$$\mathbb{P}_{\boldsymbol{\alpha}}=\prod_{\boldsymbol{\xi}\in\mathrm{Y}(\boldsymbol{\alpha})}\frac{1}{2}\left(1+\delta_{\boldsymbol{\alpha}}\delta^{\bar{\lambda}}_{\boldsymbol{\xi}}C\begin{bmatrix}\boldsymbol{\alpha}\\ \boldsymbol{\xi}\end{bmatrix}\right), \tag{4.9}$$

such that

$$\delta_{\boldsymbol{\beta}}^{\bar{\lambda}} = \begin{cases} +1 \text{ if } \bar{\lambda} \in \boldsymbol{\beta} \\ -1 \text{ if } \bar{\lambda} \notin \boldsymbol{\beta} \end{cases} \tag{4.10}$$

and there would be an analogous insertion of $\delta_{\boldsymbol{\beta}}^{\lambda}$ for a left-moving oscillator with frequency $\nu_\lambda = \frac{1}{2}$.

We can now apply this to the observable spinorial sectors (4.5), to find the projectors $\mathbb{P}_{\boldsymbol{F}^{\boldsymbol{k}}_{\boldsymbol{pqrs}}}$, which will have the form of (4.7) with the sets

$$\begin{aligned} \Upsilon(\boldsymbol{F}^1_{pqrs}) &= \{\boldsymbol{z_1}, \boldsymbol{z_2}, \boldsymbol{e_1}, \boldsymbol{e_2}\} \\ \Upsilon(\boldsymbol{F}^2_{pqrs}) &= \{\boldsymbol{z_1}, \boldsymbol{z_2}, \boldsymbol{e_3}, \boldsymbol{e_4}\} \\ \Upsilon(\boldsymbol{F}^3_{pqrs}) &= \{\boldsymbol{z_1}, \boldsymbol{z_2}, \boldsymbol{e_5}, \boldsymbol{e_6}\}. \end{aligned} \tag{4.11}$$

These projectors only tell us whether the sector remains in the massless spectrum or not. In order to determine whether a particular $\boldsymbol{F}^k_{pqrs}$ produces a **16** or $\overline{\mathbf{16}}$ we must construct the chirality phases

$$\begin{aligned} \boldsymbol{X}^1_{pqrs} &= -\mathrm{ch}(\psi^\mu) C \begin{bmatrix} \boldsymbol{F}^1_{pqrs} \\ \boldsymbol{S} + \boldsymbol{b_2} + (1-r)\boldsymbol{e_5} + (1-s)\boldsymbol{e_6} \end{bmatrix}^* \\ \boldsymbol{X}^2_{pqrs} &= -\mathrm{ch}(\psi^\mu) C \begin{bmatrix} \boldsymbol{F}^2_{pqrs} \\ \boldsymbol{S} + \boldsymbol{b_1} + (1-r)\boldsymbol{e_5} + (1-s)\boldsymbol{e_6} \end{bmatrix}^* \\ \boldsymbol{X}^3_{pqrs} &= -\mathrm{ch}(\psi^\mu) C \begin{bmatrix} \boldsymbol{F}^3_{pqrs} \\ \boldsymbol{S} + \boldsymbol{b_1} + (1-p)\boldsymbol{e_3} + (1-q)\boldsymbol{e_4} \end{bmatrix}^*, \end{aligned} \tag{4.12}$$

where $\mathrm{ch}(\psi^\mu) = \pm 1$ is the spacetime chirality, which we will take as $+1$ for the states and -1 for their CPT conjugates.

We can now define the classification numbers $N_{16}, N_{\overline{16}}$ as

$$\begin{aligned} N_{16} &= \frac{1}{2} \sum_{\substack{k=1,2,3 \\ p,q,r,s=0,1}} \mathbb{P}_{\boldsymbol{F}^k_{pqrs}} \left(1 + \boldsymbol{X}^k_{pqrs}\right) \\ N_{\overline{16}} &= \frac{1}{2} \sum_{\substack{k=1,2,3 \\ p,q,r,s=0,1}} \mathbb{P}_{\boldsymbol{F}^k_{pqrs}} \left(1 - \boldsymbol{X}^k_{pqrs}\right). \end{aligned} \tag{4.13}$$

The other key classification number for the $SO(10)$ models is that concerning the vectorial representations, which are of great importance in this class of symmetric $\mathbb{Z}_2 \times \mathbb{Z}_2$ orbifolds since they accommodate the light Standard Model Higgs doublets. In the class of models under consideration, massless $SO(10)$ vectorial states arise from the sectors

$$\boldsymbol{V}^k_{pqrs} = \boldsymbol{S} + \boldsymbol{F}^k_{pqrs} + \boldsymbol{x}, \tag{4.14}$$

which contain four periodic antiholomorphic complex fermions and consequently they admit one Neveu-Schwarz fermionic oscillator, which for the **10** is given by $\overline{\psi}^a_{1/2}/\overline{\psi}^{*a}_{1/2}$, $a=1,...5$. In order to determine which of these sectors survive the GGSO projections we can write the projector of the form given in eq. (4.9)

$$\mathbb{P}_{\{\overline{\psi}^{(*)a}\}\boldsymbol{V}^k_{pqrs}}=\prod_{\boldsymbol{\xi}\in\Upsilon(\boldsymbol{V}^k_{pqrs})}\frac{1}{2}\left(1+\delta^{\bar{\psi}^a}_{\boldsymbol{\xi}}C\begin{bmatrix}\boldsymbol{V}^k_{pqrs}\\ \boldsymbol{\xi}\end{bmatrix}\right), \tag{4.15}$$

such that, as in eq. (4.11) we have

$$\begin{aligned}\Upsilon(\boldsymbol{V}^1_{pqrs})&=\{\boldsymbol{z_1},\boldsymbol{z_2},\boldsymbol{e_1},\boldsymbol{e_2}\}\\ \Upsilon(\boldsymbol{V}^2_{pqrs})&=\{\boldsymbol{z_1},\boldsymbol{z_2},\boldsymbol{e_3},\boldsymbol{e_4}\}\\ \Upsilon(\boldsymbol{V}^3_{pqrs})&=\{\boldsymbol{z_1},\boldsymbol{z_2},\boldsymbol{e_5},\boldsymbol{e_6}\}.\end{aligned} \tag{4.16}$$

The number of such vectorial **10** representations gives the number of Higgs doublets and is of the simple form

$$N_{10}=\sum_{\substack{k=1,2,3\\ p,q,r,s=0,1}}\mathbb{P}_{\{\overline{\psi}^{(*)a}\}\boldsymbol{V}^k_{pqrs}}. \tag{4.17}$$

At the $SO(10)$ level the classification numbers are simply $(N_{16},N_{\overline{16}},N_{10})$ and a statistical analysis of these numbers in this construction uncovered the fascinating Spinor-Vector Duality (SVD) [52, 53, 54, 55, 56] relating vacua under the exchange $(\mathbf{16}+\overline{\mathbf{16}})\leftrightarrow\mathbf{10}$.

4.1.2 $\mathcal{N}=1$ $SO(10)$ Subgroup Classification

This $SO(10)$ construction was extended to $\mathcal{N}=1$ models in which the $SO(10)$ GUT is broken directly at the string scale to various subgroups[1]:

- Pati-Salam, $SO(6)\times SO(4)$ (PS) [58]
- Flipped $SU(5)$, $SU(5)\times U(1)$ (FSU5) [59]
- Standard-like Models, $SU(3)\times SU(2)\times U(1)^2$ (SLM) [60]
- Left-Right Symmetric, $SU(3)\times SU(2)^2\times U(1)$ (LRS) [61].

These subgroups are generated through the addition of $SO(10)$ breaking vector(s), in which the boundary conditions of $\bar{\psi}^{1,...,5}$ are

- $\alpha(\bar{\psi}^{1,...,5})=\{11100\}$ (PS)
- $\alpha(\bar{\psi}^{1,...,5})=\{\frac{1}{2}\frac{1}{2}\frac{1}{2}\frac{1}{2}\frac{1}{2}\}$ (FSU5)

[1] Another possibility than those listed is the subgroup $SU(4)\times U(1)$, which was investigated in ref. [57] and shown to not give rise to three generation models.

- $\begin{cases} \alpha(\bar{\psi}^{1,\cdots,5}) = \{11100\} \\ \beta(\bar{\psi}^{1,\cdots,5}) = \{\frac{1}{2}\frac{1}{2}\frac{1}{2}\frac{1}{2}\frac{1}{2}\} \end{cases}$ (SLM)
- $\alpha(\bar{\psi}^{1,\cdots,5}) = \{\frac{1}{2}\frac{1}{2}\frac{1}{2}00\}$ (LRS).

Of course, once the $SO(10)$ is broken to these subgroups we now need to collect classification data relating to the representations under the subgroup. An additional complication is the emergence of exotic sectors, *i.e.* those transforming under both the observable and the hidden groups, which arise through combinations of the $SO(10)$ breaking vector(s) and are generic in string compactifications [62, 63, 64, 65, 66]. If such fractionally charged states are present and chiral under some gauge factor then the model is phenomenologically untenable. If exotic states are present then they are required to form vector-like representations so they may be pushed to higher mass scales. It has been shown in [67, 68, 69] that in supersymmetric Pati-Salam models, GGSO phase configurations exist such that these massless fractionally charged states are projected out. Such models are termed exophobic. In the FSU5 classification of [59] exophobic vacua were only found for even number of fermion generations. In the SLM and LRS cases no such configurations can be found. In fact, in these cases since there are in fact two breaking vectors (note the LRS vector multiplied by two gives the PS breaking vector) the number of exotic sectors appearing in the massless spectra tend to proliferate. This results in there being a general scarcity of phenomenologically viable SLM and LRS string vacua once the absence of chiral exotics (along with other phenomenological constraints) is imposed. In the LRS case for example, in a sample of 10^{11} GGSO configurations classified in [61], just 4 vacua were found to satisfy the phenomenological criteria imposed. Since scanning through samples of 10^{11} for longwinded criteria such as the absence of chiral exotics can take large amounts of computating time, this scarcity is somewhat prohibitive to landscape studies and this was a strong motivating factor for the application of new computational techniques, which we discuss further in Section 4.3.

4.2 $\mathcal{N} = 0$ Classification Overview

The absence of evidence from particle colliders of supersymmetry motivates the study of non-supersymmetric string theories. In the context of free fermionic classification, two distinct routes toward $\mathcal{N} = 0$ classification from symmetric $\mathbb{Z}_2 \times \mathbb{Z}_2$ orbfiolds have been studied. The first, and most obvious, is to keep the basis (4.1) as a starting point and break SUSY by projecting the gravitino through a GGSO phase by breaking the condition (4.3). Such models still contain the SUSY generating vector $\boldsymbol{S}$ and, as such, we dub '$\boldsymbol{S}$-models'. These can be viewed as descending from the 10D non-tachyonic $SO(16) \times SO(16)$ non-supersymmetric heterotic string discussed in Section 3.3.

The second route to $\mathcal{N} = 0$ is less well travelled in the literature and involves the $\tilde{\boldsymbol{S}}$-map discussed in Section 3.3. The essential point is that we modify $\boldsymbol{S}$ from the basis

(4.1) by augmenting it with 4 antiholomorphic hidden fermions such as

$$\tilde{\boldsymbol{S}} = \{\psi^{\mu}, \chi^{1,\dots,6} \mid \bar{\phi}^{3,4,5,6}\} \tag{4.18}$$

this vector ensures the absence of massless gravitinos and, additionally, the untwisted tachyonic states

$$|0\rangle_L \otimes \bar{\phi}^{3,\cdots,6}|0\rangle_R \tag{4.19}$$

are invariant under the $\tilde{\boldsymbol{S}}$–vector projection. These untwisted tachyons are those that descend from the ten dimensional vacuum, hence confirming that the model can be regarded as a compactification of a ten dimensional tachyonic vacuum. A first example of a notable tachyon-free model resulting from the $\tilde{\boldsymbol{S}}$ setup was given in [37] which obtained as the $\tilde{\boldsymbol{S}}$-map of a well-studied semi-realistic $\mathcal{N} = 1$ model given in [70].

We can observe that the $\tilde{\boldsymbol{S}}$-map is reminiscent of the map used to induce SVD in ref. [52, 56], in the sense that both utilise a block of four periodic right–moving worldsheet fermions. We may term these sorts of maps as modular maps, in the sense that they involve a block of four periodic complex worldsheet fermions. We therefore have another instance where such a modular map is reflected in the symmetry structure of the string vacua. Be it the spacetime supersymmetry in the models in which the $\boldsymbol{S}$–basis vector is the supersymmetry spectral flow operator, or in the SVD models in which a similar spectral flow operator operates in the observable E_8 sector and induces the spinor-vector duality map [52, 53, 56]. Here, a similar operation is at play in the four dimensional models inducing the transformation from the supersymmetric (and non-supersymmetric) models that contain the $\boldsymbol{S}$ basis vector, to the non–supersymmetric models that contain the $\tilde{\boldsymbol{S}}$ basis vector. As discussed in refs. [71, 72], this may be a reflection of a larger symmetry structure that underlies these models and string compactifications in general.

Although in general non-SUSY strings introduce a range of new issues compared to SUSY models, from the classification perspective the primary issue to address is the possible appearance of (on-shell) tachyonic sectors in the Fock space of the string vacua in both the case of $\boldsymbol{S}$ and $\tilde{\boldsymbol{S}}$-models. In the next chapter we will classify the space of $SO(10)$ $\tilde{\boldsymbol{S}}$-models, where we will demonstrate how to project tachyonic sectors in this setup. A couple of notable additional features to the analysis of $\mathcal{N} = 0$ vacua are introduced: the calculation of the one-loop cosmological constant for samples of models and the 'super no-scale' property $N_b^0 = N_f^0$. There has been significant interest in 'super no-scale' models in the literature [73, 74] where it has been conjectured that such models in which SUSY is broken via a stringy version [75, 76, 77, 78, 79] of the Scherk-Schwarz mechanism [80, 81] will have the leading (massless) contribution to the one-loop cosmological constant exponentially suppressed.

A further step in the classification program for $\mathcal{N} = 0$ models was taken in [82] where both $\boldsymbol{S}$ and $\tilde{\boldsymbol{S}}$-models were classified with PS subgroup. In this setup it was

noted that the presence of a 'Heavy Higgs' to break the PS subgroup was impacted by the $\tilde{S}$-map. From this analysis, the SLM $\tilde{S}$ models are the only ones not suffering from this absence of an intermediate GUT breaking mechanism- at least in these classes of $\tilde{S}$ models.

So far all classifications discussed, both $\mathcal{N} = 0$ and $\mathcal{N} = 1$, have been constructed for symmetric $\mathbb{Z}_2 \times \mathbb{Z}_2$ orbifolds. However, the heterotic string in general, and the free fermionic models in particular, allow for more general assignments of boundary conditions, which are asymmetric between the holomorphic and antiholomorphic worldsheet fermions. These can be complicated assignments that realise the non-Abelian gauge symmetries at higher level Kac–Moody algebra [83, 84, 85], or more mundane assignments that leave the gauge symmetries at level $k = 1$. These asymmetric assignments produce asymmetric orbifold models, which amount to non-geometric compactifications, a review of which is given by [86]. Completing a first step towards the extension of the classification methodology to such asymmetric orbifolds is tackled in Chapter 8.

4.3 Computational Analysis of the $\mathbb{Z}_2 \times \mathbb{Z}_2$ Orbifold Landscape

As discussed above, the SLM and LRS classifications brought to light the need for the introduction of more sophisticated techniques than random classification into the classification methodology, in order to deal with the scarcity of phenomenologically viable models. This inspired the implementation of fertility conditions at the $SO(10)$ level in the SLM [60] and LRS [87] constructions. The idea of these fertility conditions is that, although exact knowledge of the observable particle content of a model will require analysis at the subgroup level, there are necessary conditions that can be imposed on the $SO(10)$ classification numbers $(N_{16}, N_{\overline{16}}, N_{10})$ in order for a model to be phenomenologically viable at the subgroup level. Restricting classification to the $SO(10)$ level is more computationally manageable and only models satisfying the fertility conditions can be collected for further exhaustive analysis at the subgroup level. In the LRS fertility analysis [87], the probability of finding phenomenologically viable models was increased by some nine orders of magnitude compared with the random classification method.

In the $\mathcal{N} = 0$ $SO(10)$ $\tilde{S}$-classification, we will find in the next chapter that tachyon-free configurations arise with probability of just 5×10^{-3}. This, again, motivates the use of sophisticated classification methods such as the fertility analysis. In [88], the machine learning (ML) technique of genetic algorithms were introduced into the classification program for the case of Pati-Salam models. It was shown that the genetic algorithm is especially efficient in fishing out good models, although is not suited to classifying large spaces of vacua. In recent years, there has been a flurry of interest in the general

area of applying machine learning techniques to the string landscape. For a general overview of such ML applications see [4] and for a book on Machine learning in the Calabi-Yau landscape see [89].

In the free fermionic classification, advanced SAT/SMT algorithms have surfaced as an extremely effective tool in various aspects of investigating the landscape of $\mathbb{Z}_2 \times \mathbb{Z}_2$ orbifolds. In Chapter 7 we retrace the work of [10], where we will see that such an SAT/SMT algorithm improves efficiency within a certain class of models by 3 orders of magnitude. Although promising as an efficient way to scan large spaces of models, the SAT/SMT algorithms are especially good as fishing tools, similar to the case of genetic algorithms, and, perhaps even more exciting as a tools to demonstrate no-go theorems in classes of string vacua. In particular, it has been a common feature of all $\mathbb{Z}_2 \times \mathbb{Z}_2$ orbifold classes that certain phenomenological constraints can be in contradiction. For example, the aforementioned absence of exophobic vacua in odd generation FSU5 models uncovered in [59] or that the presence of spinorial **16**'s for tachyon-free Type $\bar{0}$ models uncovered in [10] that we will see in Chapter 7. In the language of SAT/SMTs these no-go results are equivalent to the unsatisfiability of constraints inputted into some SAT/SMT solver program, such as Microsoft's Z3 [90], which will be utilised throughout this work.

The fact that free fermionic models take GGSO phases as their primary inputs, which are essentially binary inputs, makes them readily amenable to translation into Boolean language and we will see expicitly in Chapters 7 and 8 how phenomenological constraints can easily be recast into standard Boolean expressions. It is not necessary to form only Boolean expressions, since SMT solvers allow for operations over non-Boolean types such as integers, reals, bitvectors, and arrays. However, there is a well-known trade off between efficiency and expressibility, with a Boolean encoding of a problem drastically increasing efficiency compared with even a simple encoding in terms of integers. This too is demonstrated for the free fermionic constraints in [10] that we discuss further in Chapter 7.

The scope of problems that SMT solvers may be of use in tackling within string phenomenology is potentially vast. For decades computer scientists have worked on various tools and optimisations that make solvers such as Z3 extremely powerful in solving a wide range of problems efficiently. It will certainly be exciting to see future applications such as finding no-go theorems from constraints on geometric data from different string compactification constructions, which will certainly be feasible for cases where input variables can be taken as integers.

Having now given this overview of the classification program up to the present day, we will move towards the central work in this thesis which is the classification of non-SUSY models, starting with the study of $\tilde{\boldsymbol{S}}$ models with unbroken $SO(10)$ symmetric in the next chapter and finishing with the extension of the classification methodology to $\boldsymbol{S}$-models endowed with asymmetric shifts in Chapter 8.

Chapter 5

Classification of Tachyon-Free Heterotic String Orbifolds from the 10D Tachyonic Heterotic String

In this chapter a systematic classification of 4D string vacua descending from a 10D tachyonic heterotic string called $\tilde{\boldsymbol{S}}$-Models is presented. This is work taken from the paper [7] with some minor notational adjustments for consistency.

5.1 Ten Dimensional Vacua and the $\tilde{S}$ - Map

Following the discussion of Section 3.3, we can observe that, in the free fermionic formulation, four dimensional models that descend from the ten dimensional tachyonic vacua arise from the absence of the SUSY generating vector $\boldsymbol{S}$ in the basis. We can naturally extend the discussion of models from Section 3.3 with basis $\{\mathbb{1}, \boldsymbol{x}, \boldsymbol{H}\}$ to four spacetime dimensions. Constructing models in which the gravitini from $\boldsymbol{S}$ are projected allows us to consider non-supersymmetric models that we can think of as 'descending' from the $SO(16) \times SO(16)$ heterotic string. We will refer to such models as $\boldsymbol{S}$-models. Another route to non-supersymmetric models is through the $\tilde{\boldsymbol{S}}$-map á la eq. (3.58) in place of a supersymmetric construction with $\boldsymbol{S}$. For this chapter we will take this vector to be of the form

$$\tilde{\boldsymbol{S}} = \{\psi^{1,2}, \chi^{1,2}, \chi^{3,4}, \chi^{5,6} \mid \bar{\phi}^{3,\ldots,6}\} \tag{5.1}$$

Models descending from bases with $\tilde{\boldsymbol{S}}$ we will label as $\tilde{\boldsymbol{S}}$-models and we can think of them as corresponding to compactifications of a tachyonic 10D vacuum. Supersymmetry is explictly broken such that models will have no massless gravitinos. As in eq.

(3.59) the untwisted tachyonic states will be

$$|0\rangle_L \otimes \bar{\phi}^{3,\cdots,6}|0\rangle_R, \tag{5.2}$$

since they are invariant under the $\tilde{\boldsymbol{S}}$-vector projection.

We note that this $\tilde{\boldsymbol{S}}$-map was discussed and used in the construction of the $\overline{\text{NAHE}}$-based model in ref. [37] and that it is reminiscent of the map used to induce the spinor-vector duality in ref. [52, 53, 56], in the sense that both utilise a block of four periodic right-moving worldsheet fermions. We may term such maps as modular maps and we therefore have another instance where such a modular map is reflected in the symmetry structure of the string vacua. In the case of spinor-vector dual models a spectral flow operator operates in the observable E_8 sector and induces the spinor-vector duality map [52, 53, 56]. Here, a similar operation is at play in the four dimensional models inducing the transformation from the supersymmetric (and non-supersymmetric) models that contain the $\boldsymbol{S}$-basis vector, to the non-supersymmetric models that contain the $\tilde{\boldsymbol{S}}$-basis vector. As discussed in ref. [71, 72], this may be a reflection of a larger symmetry structure that underlies these models and string compactifications in general.

5.2 Non-Supersymmetric $SO(10)$ Models in 4D

Let us now define the classification structure for the $SO(10)$ models we consider, which employ the $\tilde{\boldsymbol{S}}$-map. The first ingredient we need is a set of basis vectors that generate the space of $SO(10)$ $\tilde{\boldsymbol{S}}$-models. We can choose the set

$$\begin{aligned}
\mathbb{1} &= \{\psi^\mu,\ \chi^{1,\ldots,6}, y^{1,\ldots,6}, w^{1,\ldots,6} \mid \overline{y}^{1,\ldots,6}, \overline{w}^{1,\ldots,6}, \overline{\psi}^{1,\ldots,5}, \overline{\eta}^{1,2,3}, \overline{\phi}^{1,\ldots,8}\},\\
\tilde{\boldsymbol{S}} &= \{\psi^\mu, \chi^{1,\ldots,6} \mid \overline{\phi}^{3,4,5,6}\},\\
\boldsymbol{e_i} &= \{y^i, w^i \mid \overline{y}^i, \overline{w}^i\}, \quad i = 1,\ldots,6\\
\boldsymbol{b_1} &= \{\psi^\mu, \chi^{12}, y^{34}, y^{56} \mid \overline{y}^{34}, \overline{y}^{56}, \overline{\eta}^1, \overline{\psi}^{1,\ldots,5}\},\\
\boldsymbol{b_2} &= \{\psi^\mu, \chi^{34}, y^{12}, y^{56} \mid \overline{y}^{12}, \overline{y}^{56}, \overline{\eta}^2, \overline{\psi}^{1,\ldots,5}\},\\
\boldsymbol{b_3} &= \{\psi^\mu, \chi^{56}, y^{12}, y^{34} \mid \overline{y}^{12}, \overline{y}^{34}, \overline{\eta}^3, \overline{\psi}^{1,\ldots,5}\},\\
\boldsymbol{z_1} &= \{\overline{\phi}^{1,\ldots,4}\},
\end{aligned} \tag{5.3}$$

which is a similar basis set to $\overline{\text{NAHE}}$=$\{\mathbb{1}, \tilde{\boldsymbol{S}}, \boldsymbol{b_1}, \boldsymbol{b_2}, \boldsymbol{b_3}\}$ employed in [37], except with the inclusion of $\boldsymbol{z_1}$ to break the hidden gauge group and of $\boldsymbol{e_i}$ to obtain all symmetric shifts of the internal $\Gamma_{6,6}$ lattice. We note that the vector $\boldsymbol{b_3}$, which spans the third twisted plane and facilitates the analysis of the obervable spinorial representations, is typically formed as a linear combination in previous supersymmetric classifications [50, 51, 59, 60, 61, 67, 87]. Furthermore we note the existence of a vector combination

$$\boldsymbol{z_2} = \mathbb{1} + \sum_{i=1}^{6} \boldsymbol{e_i} + \sum_{k=1}^{3} \boldsymbol{b}_k + \boldsymbol{z_1} = \{\bar{\phi}^{5,6,7,8}\} \tag{5.4}$$

in our models, which is typically its own basis vector.

Models may then be defined through the specification of GGSO phases $C\binom{v_i}{v_j}$, which for our $SO(10)$ models are 66 free phases with all others specified by modular invariance. Hence, the full space of models is of size $2^{66} \sim 10^{19.9}$ models. This is a notably enlarged space compared with the supersymmetric $SO(10)$ case where the requirement that the spectrum is supersymmetric fixes some GGSO phases.

The untwisted sector gauge vector bosons for this choice of basis vectors give rise to a gauge group

$$SO(10) \times U(1)_1 \times U(1)_2 \times U(1)_3 \times SO(4)^4, \tag{5.5}$$

where our desired GUT $SO(10)$ is generated by the spacetime vector bosons $\psi^\mu \bar{\psi}^a \bar{\psi}^b |0\rangle$, the $U(1)_{k=1,2,3}$ are those generated by the worldsheet currents $: \bar{\eta}^k \bar{\eta}^{k*} :$ and the $SO(4)^4$ is the hidden sector generated by spacetime vector bosons from the pairs of $\bar{\phi}^a$ with common boundary conditions for each basis vector: $\{\bar{\phi}^{1,2}, \bar{\phi}^{3,4}, \bar{\phi}^{5,6}, \bar{\phi}^{7,8}\}$.

The gauge group of a model may be enhanced by additional gauge bosons arising from the $\boldsymbol{z_1}, \boldsymbol{z_2}$ and $\boldsymbol{z_1} + \boldsymbol{z_2}$ sectors with appropriate oscillators, i.e.

$$\left\{ \begin{array}{c} \psi^\mu |\boldsymbol{z_1}\rangle_L \otimes \bar{\lambda}^i |\boldsymbol{z_1}\rangle_R \\ \psi^\mu |\boldsymbol{z_2}\rangle_L \otimes \bar{\lambda}^i |\boldsymbol{z_2}\rangle_R \\ \psi^\mu |\boldsymbol{z_1} + \boldsymbol{z_2}\rangle_L \otimes |\boldsymbol{z_1} + \boldsymbol{z_2}\rangle_R \end{array} \right\}, \tag{5.6}$$

where $\bar{\lambda}^i$ are all possible right moving Neveu-Schwarz oscillators.

Whether these gauge bosons appear is model-dependent since it depends on their survival under the GGSO projections. These enhancement sectors are also present in the familiar supersymmetric classification set-ups used in [50, 59, 60, 61, 67, 87]. However in those cases there is also an observable enhancement from the vector $\boldsymbol{x} = \{\overline{\psi}^{1,\ldots,5}, \overline{\eta}^{1,2,3}\}$, which arises as a linear combination in these models. If present, this vector induces the enhancement $SO(10) \times U(1) \to E_6$, where the $U(1) = U(1)_1 + U(1)_2 + U(1)_3$ combination is typically anomalous [91], unless such an enhancement is present. This result was first discussed in the context of the NAHE models, where including $\boldsymbol{x}$ in the basis was shown to similarly produce E_6 GUT models [92]. We therefore can see that one effect of our $\tilde{\boldsymbol{S}}$-models with the basis (5.3) is to preclude the possibility of an E_6 enhancement in these models.

From (5.6) we can deduce that enhancements of the observable $SO(10)$ gauge group may arise from $\psi^\mu \{\bar{\psi}^a\} |\boldsymbol{z_1}\rangle, \psi^\mu \{\bar{\psi}^a\} |\boldsymbol{z_2}\rangle$, $a = 1, \ldots, 5$. Interestingly, the sectors: $|\boldsymbol{z_1}\rangle, |\boldsymbol{z_2}\rangle$ (with no oscillators) produce level-matched tachyons with conformal weight $(-1/2, -1/2)$ and so the appearance of these enhancements is correlated with the projection of level-matched tachyons. The full analysis of the level-matched tachyonic sectors is presented in the following section.

5.3 Tachyonic Sectors Analysis

Due to the absence of the supersymmetry generating vector $\boldsymbol{S}$ in our construction, analysing whether on-shell tachyons arise in the spectrum of our models becomes paramount. On-shell tachyons will arise when

$$M_L^2 = M_R^2 < 0, \tag{5.7}$$

which corresponds to left and right products of $\boldsymbol{\alpha}_L \cdot \boldsymbol{\alpha}_L \leq 3$ and $\boldsymbol{\alpha}_R \cdot \boldsymbol{\alpha}_R \leq 7$. The presence of such tachyonic sectors in the physical spectrum indicates the instability of the string vacuum. There are 126 of these sectors in our models which are summarised compactly in Table 1. We will find that models in which all 126 on-shell tachyons are

Mass Level	Vectorials	Spinorials
$(-1/2,-1/2)$	$\{\bar{\lambda}^m\}\,\|0\rangle$	$\boldsymbol{z_1},\ \boldsymbol{z_2}$
$(-3/8,-3/8)$	$\{\bar{\lambda}^m\}\boldsymbol{e_i}$	$\boldsymbol{e_i}+\boldsymbol{z_1},\ \boldsymbol{e_i}+\boldsymbol{z_2}$
$(-1/4,-1/4)$	$\{\bar{\lambda}^m\}\boldsymbol{e_i}+\boldsymbol{e_j}$	$\boldsymbol{e_i}+\boldsymbol{e_j}+\boldsymbol{z_1},\ \boldsymbol{e_i}+\boldsymbol{e_j}+\boldsymbol{z_2}$
$(-1/8,-1/8)$	$\{\bar{\lambda}^m\}\boldsymbol{e_i}+\boldsymbol{e_j}+\boldsymbol{e_k}$	$\boldsymbol{e_i}+\boldsymbol{e_j}+\boldsymbol{e_k}+\boldsymbol{z_1},\ \boldsymbol{e_i}+\boldsymbol{e_j}+\boldsymbol{e_k}+\boldsymbol{z_2}$

Table 5.1: *Level-matched tachyonic sectors and their mass level, where $i \neq j \neq k = 1,...,6$ and $\bar{\lambda}^m$ is any right-moving complex fermion with NS boundary condition for the relevant tachyonic sector.*

projected by the GGSO projections appear with probability $\sim$ 0.0054 and so in our classification we will throw away all but around 1 in 185 models.

In ref. [43] a basis was chosen such that, rather than having the six internal shift vectors $\boldsymbol{e_i}$, the combinations $T_1 = \boldsymbol{e_1}+\boldsymbol{e_2}$, $T_2 = \boldsymbol{e_3}+\boldsymbol{e_4}$ and $T_3 = \boldsymbol{e_5}+\boldsymbol{e_6}$ were employed. Such a grouping does not allow for sectors to arise for all shifts in the internal space and, for example, means that spinorial $\mathbf{16}/\overline{\mathbf{16}}$ sectors have a degeneracy of 4 making 3 particle generations impossible once the $SO(10)$ group is broken. However, choosing $T_{i=1,2,3}$ did have the advantage of restricting the number of tachyonic sectors and allowing for a more simplified set-up to perform an analysis of the structure of the 1-loop potential in these models.

Since finding models in which all on-shell tachyons are projected is of utmost importance for all questions of stability of our string vacua we will delineate the methodology used in our analysis. In order to perform this analysis an efficient computer algorithm had to be developed which could scan samples of $\mathcal{O}(10^9)$ models or more for on-shell tachyons within a reasonable computing time. The code we developed in Python when running in parallel across 64 cores could check a sample of 10^9 models for tachyons in approximately 12 hours. A more detailed analysis of how to check whether our on-shell tachyons are projected is presented in the next section.

5.3.1 Tachyons of conformal weight $(-\frac{1}{2}, -\frac{1}{2})$

The first on-shell tachyons we will inspect are those with conformal weight $(-\frac{1}{2}, -\frac{1}{2})$. Firstly, we have the aforementioned untwisted tachyons (5.2), which are always projected since $C[\frac{\boldsymbol{z_1}}{NS}] = C[\frac{\boldsymbol{z_2}}{NS}] = -C[\frac{\boldsymbol{b_i}}{NS}] = 1$. Then there are two spinorial tachyonic sectors at this mass level: $\boldsymbol{z_1}$ and $\boldsymbol{z_2}$. The conditions for their survival are displayed in Tables 5.2 and 5.3.

Sector	$C[\frac{\boldsymbol{z_1}}{\boldsymbol{e_1}}]$	$C[\frac{\boldsymbol{z_1}}{\boldsymbol{e_2}}]$	$C[\frac{\boldsymbol{z_1}}{\boldsymbol{e_3}}]$	$C[\frac{\boldsymbol{z_1}}{\boldsymbol{e_4}}]$	$C[\frac{\boldsymbol{z_1}}{\boldsymbol{e_5}}]$	$C[\frac{\boldsymbol{z_1}}{\boldsymbol{e_6}}]$	$C[\frac{\boldsymbol{z_1}}{\boldsymbol{b_1}}]$	$C[\frac{\boldsymbol{z_1}}{\boldsymbol{b_2}}]$	$C[\frac{\boldsymbol{z_1}}{\boldsymbol{b_3}}]$	$C[\frac{\boldsymbol{z_1}}{\boldsymbol{z_2}}]$
$\boldsymbol{z_1}$	+	+	+	+	+	+	+	+	+	+

Table 5.2: *Conditions on GGSO coefficients for survival of the on-shell tachyons* $|\boldsymbol{z_1}\rangle$

Sector	$C[\frac{\boldsymbol{z_2}}{\boldsymbol{e_1}}]$	$C[\frac{\boldsymbol{z_2}}{\boldsymbol{e_2}}]$	$C[\frac{\boldsymbol{z_2}}{\boldsymbol{e_3}}]$	$C[\frac{\boldsymbol{z_2}}{\boldsymbol{e_4}}]$	$C[\frac{\boldsymbol{z_2}}{\boldsymbol{e_5}}]$	$C[\frac{\boldsymbol{z_2}}{\boldsymbol{e_6}}]$	$C[\frac{\boldsymbol{z_2}}{\boldsymbol{b_1}}]$	$C[\frac{\boldsymbol{z_2}}{\boldsymbol{b_2}}]$	$C[\frac{\boldsymbol{z_2}}{\boldsymbol{b_3}}]$	$C[\frac{\boldsymbol{z_2}}{\boldsymbol{z_1}}]$
$\boldsymbol{z_2}$	+	+	+	+	+	+	+	+	+	+

Table 5.3: *Conditions on GGSO coefficients for survival of the on-shell tachyons* $|\boldsymbol{z_2}\rangle$

These tables tell us that only when all 10 of the column phases are $+1$ do the sectors remain in the spectrum. Interestingly, this has a bearing on the existence of the gauge group enhancements mentioned in the previous section. In particular, the only observable enhancements: $\psi^\mu |\boldsymbol{z_1}\rangle_L \otimes \bar{\psi}^a |\boldsymbol{z_1}\rangle_R$ and $\psi^\mu |\boldsymbol{z_2}\rangle_L \otimes \bar{\psi}^a |\boldsymbol{z_2}\rangle_R$ have the same survival conditions as the $\boldsymbol{z_1}, \boldsymbol{z_2}$ tachyonic sectors. Therefore we find that for our construction, there are no tachyon-free models in which the $SO(10)$ is enhanced. This is evident in the classification results shown in Table 5.15 of Section 5.6.

5.3.2 Tachyons of conformal weight $(-\frac{3}{8}, -\frac{3}{8})$

Now moving up the mass levels to $(-\frac{3}{8}, -\frac{3}{8})$, we have vectorial tachyons from the 6 sectors: $\{\bar{\lambda}^i\} |\boldsymbol{e_i}\rangle$, $i = 1, ..., 6$ and spinorial tachyons from 12 sectors: $|\boldsymbol{e_i} + \boldsymbol{z_1}\rangle$ and $|\boldsymbol{e_i} + \boldsymbol{z_2}\rangle$. To demonstrate how to check the survival of these sectors we take the case of $\{\bar{\lambda}^i\} |\boldsymbol{e_1}\rangle$, $|\boldsymbol{e_1} + \boldsymbol{z_1}\rangle$ and $|\boldsymbol{e_1} + \boldsymbol{z_2}\rangle$, which we show in the Tables 5.4, 5.5 and 5.6. The other cases with $\boldsymbol{e_{2,...,6}}$ are much the same except for a simple permutation of the projection phases.

$\lvert e_1\rangle$ **Oscillator**	$C\binom{e_1}{\tilde{S}}$	$C\binom{e_1}{e_2}$	$C\binom{e_1}{e_3}$	$C\binom{e_1}{e_4}$	$C\binom{e_1}{e_5}$	$C\binom{e_1}{e_6}$	$C\binom{e_1}{b_1}$	$C\binom{e_1}{\tilde{x}}$	$C\binom{e_1}{z_1}$	$C\binom{e_1}{z_2}$
$\{\bar{y}^2\}$	+	-	+	+	+	+	-	+	+	+
$\{\bar{w}^2\}$	+	-	+	+	+	+	+	+	+	+
$\{\bar{y}^3\}$	+	+	-	+	+	+	-	+	+	+
$\{\bar{w}^3\}$	+	+	-	+	+	+	+	+	+	+
$\{\bar{y}^4\}$	+	+	+	-	+	+	-	+	+	+
$\{\bar{w}^4\}$	+	+	+	-	+	+	+	+	+	+
$\{\bar{y}^5\}$	+	+	+	+	-	+	-	+	+	+
$\{\bar{w}^5\}$	+	+	+	+	-	+	+	+	+	+
$\{\bar{y}^6\}$	+	+	+	+	+	-	-	+	+	+
$\{\bar{w}^6\}$	+	+	+	+	+	-	+	+	+	+
$\{\bar{\psi}^{1/2/3/4/5(*)}\}$ / $\{\bar{\eta}^{1(*)}\}$	+	+	+	+	+	+	-	-	+	+
$\{\bar{\eta}^{2,3(*)}\}$	+	+	+	+	+	+	+	-	+	+
$\{\bar{\phi}^{1,2(*)}\}$	+	+	+	+	+	+	+	+	-	+
$\{\bar{\phi}^{3,4(*)}\}$	-	+	+	+	+	+	+	+	-	+
$\{\bar{\phi}^{5,6(*)}\}$	-	+	+	+	+	+	+	+	+	-
$\{\bar{\phi}^{7,8(*)}\}$	+	+	+	+	+	+	+	+	+	-

Table 5.4: *Conditions on GGSO coefficients for survival of the on-shell vectorial tachyons* $\{\bar{\lambda}^i\}\lvert e_1\rangle$. *We have made use of the combination* $\tilde{x} = b_1 + b_2 + b_3 = \{\psi^\mu, \chi^{1,\dots,6} \mid \bar{\psi}^{1,2,3,4,5}, \bar{\eta}^{1,2,3}\}$, *which will be discussed more in the next section.*

Sector	$C\binom{e_1+z_1}{e_2}$	$C\binom{e_1+z_1}{e_3}$	$C\binom{e_1+z_1}{e_4}$	$C\binom{e_1+z_1}{e_5}$	$C\binom{e_1+z_1}{e_6}$	$C\binom{e_1+z_1}{b_1}$	$C\binom{e_1+z_1}{\tilde{x}}$	$C\binom{e_1+z_1}{z_2}$
$\lvert e_1+z_1\rangle$	+	+	+	+	+	+	+	+

Table 5.5: *Conditions on GGSO coefficients for survival of the on-shell tachyons* $\lvert e_1 + z_1\rangle$

Sector	$C\binom{e_1+z_2}{e_2}$	$C\binom{e_1+z_2}{e_3}$	$C\binom{e_1+z_2}{e_4}$	$C\binom{e_1+z_2}{e_5}$	$C\binom{e_1+z_2}{e_6}$	$C\binom{e_1+z_2}{b_1}$	$C\binom{e_1+z_2}{\tilde{x}}$	$C\binom{e_1+z_2}{z_1}$
$\lvert e_1+z_2\rangle$	+	+	+	+	+	+	+	+

Table 5.6: *Conditions on GGSO coefficients for survival of the on-shell tachyons* $\lvert e_1 + z_2\rangle$

5.3.3 Tachyons of conformal weight $(-\frac{1}{4}, -\frac{1}{4})$

Carrying on up the mass levels we have $(-\frac{1}{4}, -\frac{1}{4})$, in which vectorial tachyons arise from 15 sectors: $\{\bar{\lambda}^i\}\lvert e_i + e_j\rangle$, $i \neq j = 1,\dots,6$ and spinorial tachyons arise from 30 sectors: $\lvert e_i + e_j + z_1\rangle$ and $\lvert e_i + e_j + z_2\rangle$. Again, we will present the conditions on the survival of $\{\bar{\lambda}^i\}\lvert e_1 + e_2\rangle$, $\lvert e_1 + e_2 + z_1\rangle$ and $\lvert e_1 + e_2 + z_2\rangle$ in Tables 5.7, 5.8 and 5.9 below and note that the other sectors with other e_i combinations are easily obtainable from these.

$\lvert e_1+e_2\rangle$ **Oscillators**	$C\binom{e_1+e_2}{\tilde{S}}$	$C\binom{e_1+e_2}{e_3}$	$C\binom{e_1+e_2}{e_4}$	$C\binom{e_1+e_2}{e_5}$	$C\binom{e_1+e_2}{e_6}$	$C\binom{e_1+e_2}{b_1}$	$C\binom{e_1+e_2}{\tilde{x}}$	$C\binom{e_1+e_2}{z_1}$	$C\binom{e_1+e_2}{z_2}$
$\{\bar{y}^3\}$	+	-	+	+	+	-	+	+	+
$\{\bar{w}^3\}$	+	-	+	+	+	+	+	+	+
$\{\bar{y}^4\}$	+	+	-	+	+	-	+	+	+
$\{\bar{w}^4\}$	+	+	-	+	+	+	+	+	+
$\{\bar{y}^5\}$	+	+	+	-	+	-	+	+	+
$\{\bar{w}^5\}$	+	+	+	-	+	+	+	+	+
$\{\bar{y}^6\}$	+	+	+	+	-	-	+	+	+
$\{\bar{w}^6\}$	+	+	+	+	-	+	+	+	+
$\{\bar{\psi}^{1/\dots/5(*)}\}$ $/\{\bar{\eta}^{1(*)}\}$	+	+	+	+	+	-	-	+	+
$\{\bar{\eta}^{2,3(*)}\}$	+	+	+	+	+	+	-	+	+
$\{\bar{\phi}^{1,2(*)}\}$	+	+	+	+	+	+	+	-	+
$\{\bar{\phi}^{3,4(*)}\}$	-	+	+	+	+	+	+	-	+
$\{\bar{\phi}^{5,6(*)}\}$	-	+	+	+	+	+	+	+	-
$\{\bar{\phi}^{7,8(*)}\}$	+	+	+	+	+	+	+	+	-

Table 5.7: *Conditions on GGSO coefficients for survival of the on-shell vectorial tachyons* $\{\bar{\lambda}^i\}\,\lvert e_1+e_2\rangle$. *We have made use of the combination* $\tilde{x} = b_1+b_2+b_3 = \{\psi^\mu, \chi^{1,\dots,6} \mid \bar{\psi}^{1,2,3,4,5}, \bar{\eta}^{1,2,3}\}$, *which will be discussed more in the next section.*

Sector	$C\binom{e_1+e_2+z_1}{e_3}$	$C\binom{e_1+e_2+z_1}{e_4}$	$C\binom{e_1+e_2+z_1}{e_5}$	$C\binom{e_1+e_2+z_1}{e_6}$	$C\binom{e_1+e_2+z_1}{b_1}$	$C\binom{e_1+e_2+z_1}{\tilde{x}}$	$C\binom{e_1+e_2+z_1}{z_2}$
$\lvert e_1+e_2+z_1\rangle$	+	+	+	+	+	+	+

Table 5.8: *Conditions on GGSO coefficients for survival of the on-shell tachyons* $\lvert e_1+e_2+z_1\rangle$.

Sector	$C\binom{e_1+e_2+z_2}{e_3}$	$C\binom{e_1+e_2+z_2}{e_4}$	$C\binom{e_1+e_2+z_2}{e_5}$	$C\binom{e_1+e_2+z_2}{e_6}$	$C\binom{e_1+e_2+z_2}{b_1}$	$C\binom{e_1+e_2+z_2}{\tilde{x}}$	$C\binom{e_1+e_2+z_2}{z_1}$
$\lvert e_1+e_2+z_2\rangle$	+	+	+	+	+	+	+

Table 5.9: *Conditions on GGSO coefficients for survival of the on-shell tachyons* $\lvert e_1+e_2+z_2\rangle$.

5.3.4 Tachyons of conformal weight $(-\frac{1}{8},-\frac{1}{8})$

The final mass level we obtain on-shell tachyons from is $(-\frac{1}{8},-\frac{1}{8})$, where vectorial tachyons arise from 20 sectors: $\{\bar{\lambda}^i\}\,\lvert e_i+e_j+e_k\rangle$, $i\neq j\neq k=1,\dots,6$ and spinorial tachyons arise from 40 sectors: $\lvert e_i+e_j+e_k+z_1\rangle$ and $\lvert e_i+e_j+e_k+z_2\rangle$. We present the conditions on the survival of $\{\bar{\lambda}^i\}\,\lvert e_1+e_2+e_3\rangle$, $\lvert e_1+e_2+e_3+z_1\rangle$ and $\lvert e_1+e_2+e_3+z_2\rangle$ in the Tables 5.10, 5.11 and 5.12 below and note again that the conditions for other sectors with other e_i combinations are easily obtainable from these.

$\lvert e_1+e_2+e_3\rangle$ **Oscillator**	$C\binom{e_1+e_2+e_3}{\tilde{S}}$	$C\binom{e_1+e_2+e_3}{e_4}$	$C\binom{e_1+e_2+e_3}{e_5}$	$C\binom{e_1+e_2+e_3}{e_6}$	$C\binom{e_1+e_2+e_3}{\tilde{x}}$	$C\binom{e_1+e_2+e_3}{z_1}$	$C\binom{e_1+e_2+e_3}{z_2}$
$\{\bar{y}^4/\bar{w}^4\}$	+	-	+	+	+	+	+
$\{\bar{y}^5/\bar{w}^5\}$	+	+	-	+	+	+	+
$\{\bar{y}^6/\bar{w}^6\}$	+	+	+	-	+	+	+
$\{\bar{y}^{1/\ldots/5}\}$ $/\{\bar{\eta}^{1/2/3(*)}\}$	+	+	+	+	-	+	+
$\{\bar{\phi}^{1,2(*)}\}$	+	+	+	+	+	-	+
$\{\bar{\phi}^{3,4(*)}\}$	-	+	+	+	+	-	+
$\{\bar{\phi}^{5,6(*)}\}$	-	+	+	+	+	+	-
$\{\bar{\phi}^{7,8(*)}\}$	+	+	+	+	+	+	-

Table 5.10: *Conditions on GGSO coefficients for survival of the on-shell vectorial tachyons* $\{\bar{\lambda}^i\}\,\lvert e_1+e_2+e_3\rangle$.

Sector	$C\binom{e_1+e_2+e_3+z_1}{e_4}$	$C\binom{e_1+e_2+e_3+z_1}{e_5}$	$C\binom{e_1+e_2+e_3+z_1}{e_6}$	$C\binom{e_1+e_2+e_3+z_1}{\tilde{x}}$	$C\binom{e_1+e_2+e_3+z_1}{z_2}$
$\lvert e_1+e_2+e_3+z_1\rangle$	+	+	+	+	+

Table 5.11: *Conditions on GGSO coefficients for survival of the on-shell tachyons* $\lvert e_1+e_2+e_3+z_1\rangle$.

Sector	$C\binom{e_1+e_2+e_3+z_2}{e_4}$	$C\binom{e_1+e_2+e_3+z_2}{e_5}$	$C\binom{e_1+e_2+e_3+z_2}{e_6}$	$C\binom{e_1+e_2+e_3+z_2}{\tilde{x}}$	$C\binom{e_1+e_2+e_3+z_2}{z_1}$
$\lvert e_1+e_2+e_3+z_2\rangle$	+	+	+	+	+

Table 5.12: *Conditions on GGSO coefficients for survival of the on-shell tachyons* $\lvert e_1+e_2+e_3+z_2\rangle$.

Using this structure of the conditions on the GGSO phases for the survival of tachyonic sectors at each mass level our computer algorithm runs through and checks whether any configuration of the phases that leaves the tachyon in the spectrum is satisfied. If none are satisfied then all 126 are projected and the model is retained for further analysis.

Having dealt now with the $M_L^2 = M_R^2 < 0$ level-matched sectors we turn our attention to the more familiar discussion of the structure of the massless sectors $M_L^2 = M_R^2 = 0$ in the following section where we can discern the phenomenological features of our models.

5.4 Massless Sectors

Now that we have a way to generate models free of on-shell tachyons, we can turn our attention to the massless sectors and their representations. Although some aspects of the massless spectrum look similar to the supersymmetric case, the structure of our $\tilde{S}$-models is very different. In particular, we can contrast our models with those in which supersymmetry is spontaneously broken (by a GGSO phase) where in general some parts of the spectrum remain supersymmetric. This was, for example, demonstrated in [93] in terms of invariant orbits of the partition function for orbifold models with spontaneously broken supersymmetry. Similarly, our models are very different than those

of the broken supersymmetry models discussed in [94] where observable spinorial sectors of the models still exhibit a supersymmetric-like structure, *i.e.* in these sectors the bosonic and fermionic states only differ by their charges under some $U(1)$ symmetries that are broken at a high scale.

As we explore this new structure in the massless spectrum we will see that the role of the $\tilde{\boldsymbol{S}}$-map is of central importance. Further to this, we will also uncover the importance of a vector combination $\tilde{\boldsymbol{x}}$ which induces another interesting map. Without the presence of the supersymmetry generator $\boldsymbol{S}$ we must also handle a number of extra massless sectors which would not arise in supersymmetric setups due to the GGSO projections induced by $\boldsymbol{S}$.

5.4.1 The Observable Sectors and the $\tilde{S}$ and $\tilde{x}$ -maps

The chiral spinorial $\mathbf{16}/\overline{\mathbf{16}}$ representations are very similar to those given in Section 4.1.1, arising from the 48 sectors (16 from each orbifold plane)

$$\begin{aligned}
\boldsymbol{F}^1_{pqrs} &= \boldsymbol{b_1} + p\boldsymbol{e_3} + q\boldsymbol{e_4} + r\boldsymbol{e_5} + s\boldsymbol{e_6} \\
&= \{\psi^\mu, \chi^{1,2}, (1-p)y^3\bar{y}^3, pw^3\bar{w}^3, (1-q)y^4\bar{y}^4, qw^4\bar{w}^4, \\
&\quad (1-r)y^5\bar{y}^5, rw^5\bar{w}^5, (1-s)y^6\bar{y}^6, sw^6\bar{w}^6, \bar{\eta}^1, \bar{\psi}^{1,\dots,5}\} \qquad (5.8)\\
\boldsymbol{F}^2_{pqrs} &= \boldsymbol{b_2} + p\boldsymbol{e_1} + q\boldsymbol{e_2} + r\boldsymbol{e_5} + s\boldsymbol{e_6} \\
\boldsymbol{F}^3_{pqrs} &= \boldsymbol{b_3} + p\boldsymbol{e_1} + q\boldsymbol{e_2} + r\boldsymbol{e_3} + s\boldsymbol{e_4},
\end{aligned}$$

where $p,q,r,s = 0,1$ account for all combinations of shift vectors of the internal fermions $\{y^I, w^I \mid \bar{y}^I, \bar{w}^I\}$. As in previous classifications, we can now write down generic algebraic equations to determine the number $\mathbf{16}$ and $\overline{\mathbf{16}}$, of N_{16} and $N_{\overline{16}}$, as a function of the GGSO coefficients. To do this, we first utilize the projectors defined through eqs (4.7) and (4.11) to determine which of the 48 spinorial sectors survive. Then we define the chirality phases as in eq. (4.12) such that

$$\begin{aligned}
X^1_{pqrs} &= -C\begin{bmatrix} \boldsymbol{F}^1_{pqrs} \\ \boldsymbol{b_2} + (1-r)\boldsymbol{e_5} + (1-s)\boldsymbol{e_6} \end{bmatrix}^* \\
X^2_{pqrs} &= -C\begin{bmatrix} \boldsymbol{F}^2_{pqrs} \\ \boldsymbol{b_1} + (1-r)\boldsymbol{e_5} + (1-s)\boldsymbol{e_6} \end{bmatrix}^* \qquad (5.9)\\
X^3_{pqrs} &= -C\begin{bmatrix} \boldsymbol{F}^3_{pqrs} \\ \boldsymbol{b_1} + (1-r)\boldsymbol{e_3} + (1-s)\boldsymbol{e_4} \end{bmatrix}^*
\end{aligned}$$

to determine whether a sector will give rise to a $\mathbf{16}$ or a $\overline{\mathbf{16}}$. With these definitions we can write compact expressions for N_{16} and $N_{\overline{16}}$ as given by eq. (4.13). As we see, up until here, these equations are familiar from previous supersymmetric classifications. However there is a fundamental difference from the supersymmetric case where $\boldsymbol{F}^{1,2,3}$, along with all model sectors, appear in supermultiplets with superpartners obtained through the addition of $\boldsymbol{S}$, which exchanges spacetime bosons with spacetime fermions

but leaves the gauge group representations unchanged. In our set-up, the fermionic $\boldsymbol{F}^{1,2,3}$ sectors have no such bosonic sector counterparts. Indeed, the addition of our basis vector $\tilde{\boldsymbol{S}}$ would give rise to massive states with non-trivial representations under the hidden sector gauge group. As mentioned above, we can also compare with the broken supersymmetry models of [94] where the bosonic counterparts of $\boldsymbol{F}^{1,2,3}$ only differ from their fermionic superpartners by their charges under some $U(1)$ symmetries that are broken at a high scale.

A further new important feature of our construction is the inclusion of the vector

$$\tilde{\boldsymbol{x}} = \boldsymbol{b_1} + \boldsymbol{b_2} + \boldsymbol{b_3}, \tag{5.10}$$

which we name in analogy to the $\boldsymbol{x}$-vector from previous work in free fermionic models [51, 59, 61, 67, 87, 92]. We note that $\tilde{\boldsymbol{x}}$ is the same as the vector $\boldsymbol{S} + \boldsymbol{x}$ which arises in supersymmetric models. In these models the states from the $\boldsymbol{x}$-sector enhance the observable gauge symmetry from $SO(10)$ to E_6, so $\boldsymbol{S} + \boldsymbol{x}$ arises when such an enhancement is present as their gauginos. The vector $\tilde{\boldsymbol{x}}$ is important in our models since it plays the role of mapping between the observable spinorial and vectorial representations of $SO(10)$, as well as generally being a map between bosonic and fermionic states. More specifically, the $\tilde{\boldsymbol{x}}$-vector maps sectors that produce spacetime fermions in the spinorial representation of $SO(10)$, from which the Standard Model matter states are obtained, to sectors that produce spacetime bosons in its vectorial representation, from which the Standard Model Higgs state is obtained. Thus, the $\tilde{\boldsymbol{x}}$-map induces simultaneously the fermion-boson map of the $\boldsymbol{S}$-vector, as well as the spinor-vector map of the $\boldsymbol{x}$-vector. Without $\boldsymbol{S}$ to provide the simple symmetry at each mass level between bosons and fermions the question of the relationship between bosons and fermions is unclear. It appears that the structure is controlled in some sense by the $\tilde{\boldsymbol{S}}$-map and the $\tilde{\boldsymbol{x}}$-map taking us between mass levels as both these maps often change the mass level of the sector they act on. We also note that the $\tilde{\boldsymbol{x}}$-sector also affects the observable spectrum since its presence in the Hilbert space results in an extra 4 $\mathbf{16}$'s and $\overline{\mathbf{16}}$'s of $SO(10)$.

5.4.2 Vectorial Sectors

As mentioned above, the vector $\tilde{\boldsymbol{x}}$ in (5.10) maps between the spinorial sectors $\boldsymbol{F}^{1,2,3}_{pqrs}$ and vectorial sectors:

$$\begin{aligned}
\boldsymbol{V}^{(1)}_{pqrs} &= \boldsymbol{F}^{(1)}_{pqrs} + \tilde{\boldsymbol{x}} \\
&= \boldsymbol{b_2} + \boldsymbol{b_3} + p\boldsymbol{e_3} + q\boldsymbol{e_4} + r\boldsymbol{e_5} + s\boldsymbol{e_6} \\
&= \{\chi^{3,4,5,6}, (1-p)y^3\bar{y}^3, pw^3\bar{w}^3, (1-q)y^4\bar{y}^4, qw^4\bar{w}^4, \\
&\quad (1-r)y^5\bar{y}^5, rw^5\bar{w}^5, (1-s)y^6\bar{y}^6, sw^6\bar{w}^6, \bar{\eta}^{2,3}\} \\
\boldsymbol{V}^{(2)}_{pqrs} &= \boldsymbol{F}^{(2)}_{pqrs} + \tilde{\boldsymbol{x}} \\
\boldsymbol{V}^{(3)}_{pqrs} &= \boldsymbol{F}^{(3)}_{pqrs} + \tilde{\boldsymbol{x}},
\end{aligned} \tag{5.11}$$

The observable vectorial **10** representations of $SO(10)$ then arise when the right-moving oscillator is a $\overline{\psi}^{a(*)}$, $a = 1, ..., 5$. To determine the number of such observable vectorial sectors we use projectors given through eqs. (4.9) and (4.16). Using these we can write the number of vectorial **10**'s arising from these sectors as in eq. (4.17). Further to these observable vectorials arising from $\boldsymbol{V}^{1,2,3}$ there are the additional states arising for the other choices of oscillator $\bar{y}^i_{NS}, \bar{w}^i_{NS}, \bar{\phi}^{1,2}, \bar{\phi}^{3,4}, \bar{\phi}^{5,6}, \bar{\phi}^{7,8}$, which, we observe, only transform under the hidden group.

Our models come with additional vectorial sectors not present in the supersymmetric classifications, which can give rise to states transforming under the observable gauge group as well as the hidden. Firstly, we observe 4 additional sectors that can give rise to vectorial states transforming under both the observable and the hidden or solely the hidden. These sectors are

$$\tilde{\boldsymbol{V}} = \{\{\bar{\lambda}^i\}\left|\tilde{\boldsymbol{S}}\right\rangle, \{\bar{\lambda}^i\}\left|\tilde{\boldsymbol{S}} + \boldsymbol{z_1}\right\rangle, \{\bar{\lambda}^i\}\left|\tilde{\boldsymbol{S}} + \boldsymbol{z_2}\right\rangle, \{\bar{\lambda}^i\}\left|\tilde{\boldsymbol{S}} + \boldsymbol{z_1} + \boldsymbol{z_2}\right\rangle\}, \tag{5.12}$$

which are spacetime fermions. There are two cases to distinguish when one of these sectors is present:

- $\{\bar{y}^i/\bar{w}^i\}\left|\tilde{V}\right\rangle$ which are charged under the hidden sector only.
- $\{\bar{\psi}^{1,\dots,5}, \bar{\eta}^{1,2,3}, \bar{\phi}_{NS}\}\left|\tilde{V}\right\rangle$ with $\bar{\phi}_{NS}$ being the four Neveu-Schwarz oscillators such that $\bar{\phi}_{NS} \cap \tilde{V} = \emptyset$. These transform in mixed representations of the observable and hidden sectors which means we should analyse them further. We realise that the condition for one of these to remain in the spectrum is:

$$C\begin{bmatrix}\tilde{V}\\ \boldsymbol{e_i}\end{bmatrix} = -1, \quad \forall\, i \in \{1,2,3,4,5,6\}, \tag{5.13}$$

  for one of the $\tilde{V}$. In ref. [37] it was suggested that such states appearing in these models may be instrumental in implementing electroweak symmetry breaking by hidden sector condensates.

Further to these sectors, there are vectorials that may be observable or hidden arising from the 15 sectors

$$\boldsymbol{\gamma}^{k=1,\dots,15} = \{\bar{\lambda}^i\}\left|\boldsymbol{e_i} + \boldsymbol{e_j} + \boldsymbol{e_k} + \boldsymbol{e_l}\right\rangle, \tag{5.14}$$

for $i \neq j \neq k \neq l = 1, ..., 6$.

We note that these sectors can give rise to vectorial **10**'s when the oscillators $\bar{\psi}^a$, $a = 1, ..., 5$, are present. In this case the projector is of the form (4.9) but also can be written as

$$\mathbb{P}_{\boldsymbol{\gamma}^k} = \frac{1}{2^5}\prod_{i=m,n}\left(1 + C\begin{bmatrix}\boldsymbol{\gamma}^k\\ \boldsymbol{e_i}\end{bmatrix}\right)\prod_{a=1,2}\left(1 + C\begin{bmatrix}\boldsymbol{\gamma}^k\\ \boldsymbol{z_a}\end{bmatrix}\right)\left(1 - C\begin{bmatrix}\boldsymbol{\gamma}^k\\ \tilde{\boldsymbol{x}}\end{bmatrix}\right), \tag{5.15}$$

where $m \neq n \neq i \neq j \neq k \neq l$. We can count the number of such sectors through the expression

$$N_{\gamma}^{\{\bar{\psi},\bar{\eta}\}} = \sum_{k=1}^{15} \mathbb{P}_{\boldsymbol{\gamma}^k}. \tag{5.16}$$

These additional vectorials can evidently play a role in the phenomenology of our models, so their couplings and charge contributions must be considered carefully for specific models. We can note that $\boldsymbol{\gamma}^k$ will not couple at leading order to the observable spinorial representations due to their additional charges, and so at leading order the only vectorial **10** representations to generate realistic Standard Model fermion mass spectrum remain those from $\boldsymbol{V}^{1,2,3}$.

5.4.3 Hidden Sectors

We find that there are a large number of hidden massless sectors in our models, which is another effect of the $\tilde{\boldsymbol{S}}$-map we have chosen.

Firstly, we can identify 96 spinorial sectors that give rise to spacetime bosons arising through the addition of $\boldsymbol{z_1}$ or $\boldsymbol{z_2}$ onto the vectorial sectors $\boldsymbol{V}^{1,2,3}$

$$\begin{aligned} \boldsymbol{H}_{pqrs}^{(k)} &= \boldsymbol{V}_{pqrs}^{(k)} + \boldsymbol{z_1} \\ \boldsymbol{H}_{pqrs}^{(3+k)} &= \boldsymbol{V}_{pqrs}^{(k)} + \boldsymbol{z_2}, \end{aligned} \tag{5.17}$$

for $k = 1, 2, 3$, which evidently transform under the hidden $SO(4)^4$ only. A further four groups of 48 sectors are generated through the addition of the combinations $\{\tilde{\boldsymbol{S}}, \tilde{\boldsymbol{S}} + \boldsymbol{z_1}, \tilde{\boldsymbol{S}} + \boldsymbol{z_2}, \tilde{\boldsymbol{S}} + \boldsymbol{z_1} + \boldsymbol{z_2}\}$ which give rise to spacetime fermionic hidden sectors:

$$\begin{aligned} \boldsymbol{H}_{pqrs}^{(6+k)} &= \tilde{\boldsymbol{S}} + \boldsymbol{V}_{pqrs}^{(k)} \\ \boldsymbol{H}_{pqrs}^{(9+k)} &= \tilde{\boldsymbol{S}} + \boldsymbol{V}_{pqrs}^{(k)} + \boldsymbol{z_1} \\ \boldsymbol{H}_{pqrs}^{(12+k)} &= \tilde{\boldsymbol{S}} + \boldsymbol{V}_{pqrs}^{(k)} + \boldsymbol{z_2} \\ \boldsymbol{H}_{pqrs}^{(15+k)} &= \tilde{\boldsymbol{S}} + \boldsymbol{V}_{pqrs}^{(k)} + \boldsymbol{z_1} + \boldsymbol{z_2}. \end{aligned} \tag{5.18}$$

Essentially we see that by adding on the combinations: $\{\boldsymbol{z_1}, \boldsymbol{z_2}, \tilde{\boldsymbol{S}}, \tilde{\boldsymbol{S}} + \boldsymbol{z_1}, \tilde{\boldsymbol{S}} + \boldsymbol{z_2}, \tilde{\boldsymbol{S}} + \boldsymbol{z_1} + \boldsymbol{z_2}\}$ we generate the 6 ways of having 2 doublet representations of the four hidden $SO(4)$ groups. Knowing the number of hidden sectors will mainly be useful when looking at the size of massless coefficient in the q-expansion of the partition function, which is equivalent to a counting of the number of massless states. We will return to this in Section 5.5.

There are additional hidden sectors, on top of those counted by N_H, that do not live on the orbifold planes. These 30 sectors are:

$$\boldsymbol{\delta}^{1,\ldots,30} = \begin{cases} \boldsymbol{e_i} + \boldsymbol{e_j} + \boldsymbol{e_k} + \boldsymbol{e_l} + \boldsymbol{z_1} \\ \boldsymbol{e_i} + \boldsymbol{e_j} + \boldsymbol{e_k} + \boldsymbol{e_l} + \boldsymbol{z_2} \end{cases}, \tag{5.19}$$

for $i \neq j \neq k \neq l = 1, ..., 6$. Similar to (5.12), (5.14) these are examples of sectors which are not found in supersymmetric models since the $\boldsymbol{S}$-vector would project them out. Again, in order to evaluate the massless contribution to the q-expansion we will need to count the states arising from these sectors.

5.5 Partition Function and Cosmological Constant

Having detailed the construction of the partition function in free fermionic models in Section 3.2 we can recall eq. (3.17) and write the full partition function for models in our construction as the integral

$$Z = \int_{\mathcal{F}} \frac{d^2\tau}{\tau_2^2} Z_B \sum_{\boldsymbol{\alpha},\boldsymbol{\beta}\in\Xi} C\begin{bmatrix}\boldsymbol{\alpha}\\ \boldsymbol{\beta}\end{bmatrix} \prod_f Z\begin{bmatrix}\alpha(f)\\ \beta(f)\end{bmatrix}, \tag{5.20}$$

where the bosonic contribution in four dimensions is

$$Z_B = \frac{1}{\tau_2}\frac{1}{\eta^2\bar{\eta}^2}. \tag{5.21}$$

The expression (5.20) specifically represents the one-loop vacuum energy of our theory, which we will refer to as the cosmological constant Λ.

The practical way to perform this integral is as presented in [32] using the expansion of the η and θ functions in terms of the modular parameter, or more conveniently in terms of the nomes $q \equiv e^{2\pi i\tau}$ and $\bar{q} \equiv qe^{-2\pi i\bar{\tau}}$. This leads to a series expansion of the one-loop partition function which converges quickly as demonstrated in Figure 5.1. As in eq. (2.106), we can observe that all terms in the partition function sum (5.20) are modular functions of the variable τ and so we can rewrite the expression in terms of a q-expansion as

$$Z = \sum_{n.m} a_{mn} \int_{\mathcal{F}} \frac{d^2\tau}{\tau_2^3} q^m \bar{q}^n = \sum_{n.m} a_{mn} \int_{\mathcal{F}} \frac{d^2\tau}{\tau_2^3} e^{-2\pi\tau_2(m+n)} e^{2\pi i\tau_1(n-m)}. \tag{5.22}$$

where the a_{mn} physically represent the difference between bosonic and fermionic degrees of freedom at each mass level, i.e. $a_{mn} = N_b - N_f$. Since the fundamental domain $\mathcal{F}$ is symmetric with respect to τ_1, only the even part of the τ_1 exponential will contribute giving

$$Z = \sum_{n.m} a_{mn} \int_{\mathcal{F}} \frac{d^2\tau}{\tau_2^3} e^{-2\pi\tau_2(m+n)} \cos(2\pi\tau_1(m-n)) =: \sum_{m,n} a_{mn} I_{mn}. \tag{5.23}$$

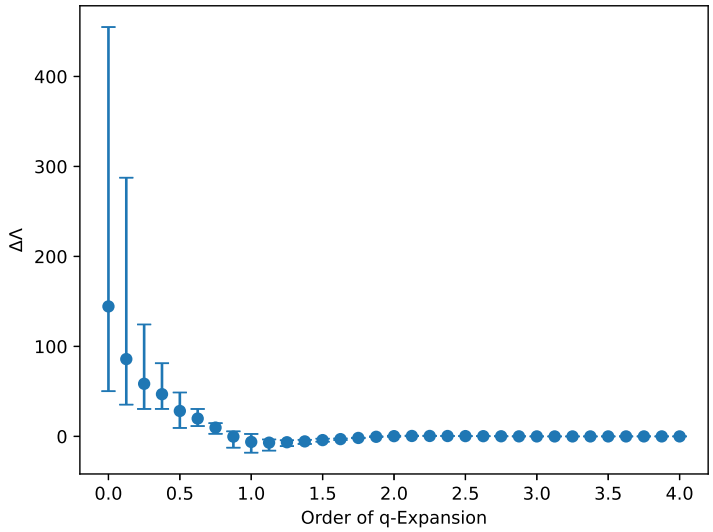

Figure 5.1: *The convergence of Λ order-by-order in the q-expansion, where $\Delta\Lambda$ is the difference between Λ at a specific order and Λ at 4th order. The dots represent the average over a sample of 2000 tachyon-free models and the bars give the maximum deviation from this average.*

The integral over τ_1 can be done analytically while the τ_2 integral has to be done numerically. The analytic integral is calculated by splitting $\mathcal{F}$ into the two regions

$$\begin{cases} \mathcal{F}_1 = \{\tau \in \mathbb{C} \,|\, \tau_2 \geq 1 \ \wedge \ |\tau_1| < 1/2\} \\ \mathcal{F}_2 = \{\tau \in \mathbb{C} \,|\, |\tau|^2 > 1 \ \wedge \ \tau_2 < 1 \ \wedge \ |\tau_1| < 1/2\}, \end{cases}$$

such that $\mathcal{F} = \mathcal{F}_1 \cup \mathcal{F}_2$. Performing the integration over τ_2 in this way also gives insight into what terms can and cannot contribute to the partition function. The integral over $\mathcal{F}_2$ is always finite however, the integral over $\mathcal{F}_1$ diverges for specific values of m, n. We specifically find that the following cases arise:

$$I_{mn} = \begin{cases} \infty & \text{if} \quad m+n < 0 \ \wedge \ m-n \notin \mathbb{Z}\backslash\{0\} \\ \text{Finite} & \text{Otherwise.} \end{cases} \tag{5.24}$$

The numerical values of the integrals I_{mn} can be found in Table 5.13.

We learn that, as expected, on-shell tachyonic states, i.e. states with $m = n < 0$, have an infinite contribution. On the other hand, it is important to note that some off-shell tachyonic states may contribute a finite value to the partition function. The above result also shows that not only on-shell tachyonic states can cause a divergence, but some off-shell tachyonic states as well. These states, however, do not arise due to the modular invariance constraints on the coefficients $C[^{\alpha}_{\beta}]$, which only allows states with $m - n \in \mathbb{Z}$.

$q\backslash\bar{q}$	-1	-3/4	-1/2	-1/4	0	1/4	1/2	3/4	1
-1	∞	∞	∞	∞	-1.22×10^{1}	∞	∞	∞	9.90×10^{-3}
-3/4	∞	∞	∞	∞	∞	-6.17×10^{-1}	∞	-1.34×10^{-1}	-8.55×10^{-3}
-1/2	∞	∞	∞	∞	∞	∞	-3.15×10^{-2}	-1.78×10^{-2}	-2.98×10^{-3}
-1/4	∞	∞	∞	∞	∞	3.35×10^{-1}	1.30×10^{-2}	-1.63×10^{-3}	-6.47×10^{-4}
0	-1.22×10^{1}	∞	∞	∞	5.49×10^{-1}	5.56×10^{-2}	5.61×10^{-3}	2.25×10^{-4}	-8.46×10^{-5}
1/4	∞	-6.17×10^{-1}	∞	3.35×10^{-1}	5.56×10^{-2}	1.00×10^{-2}	1.54×10^{-3}	1.70×10^{-4}	3.21×10^{-6}
1/2	∞	∞	-3.15×10^{-2}	1.30×10^{-2}	5.61×10^{-3}	1.54×10^{-3}	3.30×10^{-4}	5.52×10^{-5}	6.05×10^{-6}
3/4	∞	-1.34×10^{-1}	-1.78×10^{-2}	-1.63×10^{-3}	2.25×10^{-4}	1.70×10^{-4}	5.52×10^{-5}	1.29×10^{-5}	2.22×10^{-6}
1	9.90×10^{-3}	-8.55×10^{-3}	-2.98×10^{-3}	-6.47×10^{-4}	-8.46×10^{-5}	3.21×10^{-6}	6.05×10^{-6}	2.22×10^{-6}	5.47×10^{-7}

Table 5.13: *The values of the integral I_{mn} for $m, n \leq 1$. The first column and row denotes the value of m and n respectively.*

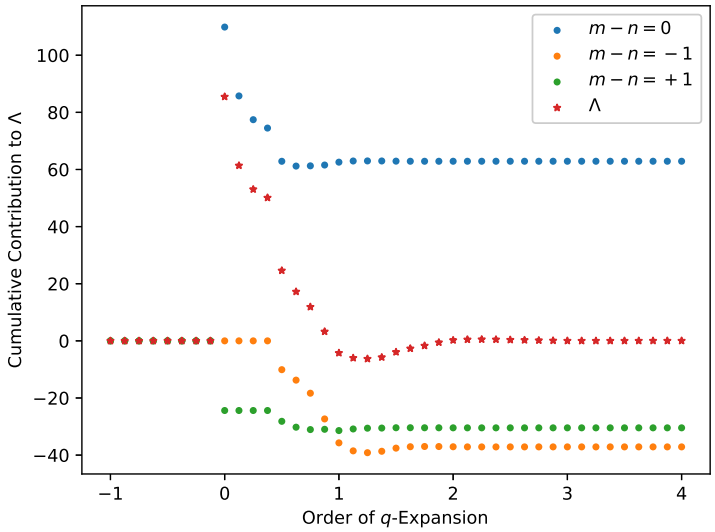

Figure 5.2: *A comparison of different contributions to* Λ *for a model with* $\Lambda = 0.03$ *arranged as in (5.25). We see that the large positive contributions of the on-shell states are compensated by the negative contributions of the off-shell states.*

The modular invariance constraint $m - n \in \mathbb{Z}$ means that the q-expansion of the partition function (5.22) neatly arranges into the form

$$a_{mn} = \begin{pmatrix} 0 & 0 & a_{-\frac{1}{2}-\frac{1}{2}} & 0 & 0 & 0 & a_{-\frac{1}{2}\frac{1}{2}} & 0 & 0 & 0 \\ 0 & 0 & 0 & a_{-\frac{1}{4}-\frac{1}{4}} & 0 & 0 & 0 & a_{-\frac{1}{4}\frac{3}{4}} & 0 & 0 \\ a_{0-1} & 0 & 0 & 0 & a_{00} & 0 & 0 & 0 & a_{01} & 0 \\ 0 & a_{\frac{1}{4}-\frac{3}{4}} & 0 & 0 & 0 & a_{\frac{1}{4}\frac{1}{4}} & 0 & 0 & 0 & \ddots \\ 0 & 0 & a_{\frac{1}{2}-\frac{1}{2}} & 0 & 0 & 0 & a_{\frac{1}{2}\frac{1}{2}} & 0 & 0 & 0 \\ 0 & 0 & 0 & a_{\frac{3}{4}-\frac{1}{4}} & 0 & 0 & 0 & a_{\frac{3}{4}\frac{3}{4}} & 0 & 0 \\ a_{1-1} & 0 & 0 & 0 & a_{10} & 0 & 0 & 0 & a_{11} & 0 \\ 0 & \ddots & 0 & 0 & 0 & \ddots & 0 & 0 & 0 & \ddots \end{pmatrix} \tag{5.25}$$

i.e. into series of states with $n - m = p \in \mathbb{Z}$. This gives a convenient way to examine the different contributions to the cosmological constant (5.23) and compare the effect of on and off-shell states. As an example we consider a model with a small value for the cosmological constant as shown in Figure 5.2. We see that the suppressed value of Λ is due to the cancellation between the large positive contributions from the on-shell states and the negative contributions from the off-shell states. Indeed, in general we find that for our set of models, the only positive contributions to Λ come from on-shell states and so these states can give us a handle on the expected value of the cosmological constant.

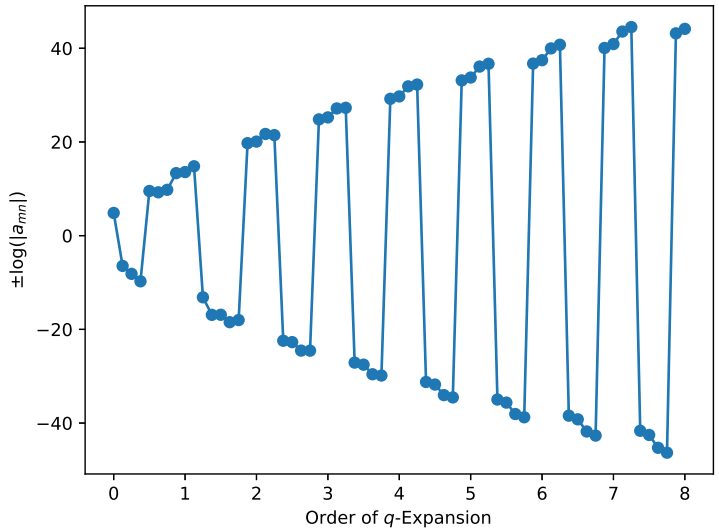

Figure 5.3: *The boson-fermion oscillation of misaligned supersymmetry for the on-shell states of one of our models to 8^{th} order in the q-expansion. The overall sign of $\pm\log(|\ a_{mn}\ |)$ is chosen according to the sign of a_{mn}.*

As we have seen in Figure 5.1, for our tachyon-free models, Λ always converges and does so rapidly starting from 2nd order in q. It is often stated that the finiteness of string theory is due to supersymmetry, which in our case is not present, thus one may wonder how the partition function of non-supersymmetric theories manages to remain finite. For supersymmetric free fermionic theories the $\boldsymbol{S}$-vector ensures that the bosonic and fermionic degrees of freedom are exactly matched at each mass level. That is, for a supersymmetric theory we necessarily have that $a_{mn} = 0$ for all m and n, which in turn causes the vanishing of the cosmological constant as one expects. For our non-supersymmetric models, the lack of an $\boldsymbol{S}$-vector means that such cancellations are not ensured and so such theories in general produce a non-zero value for Λ. It is, however, not obviously clear that they should produce finite partition functions. Such finiteness is achieved through a mechanism called misaligned supersymmetry as uncovered in [95, 96] and whose mathematical and conceptual footing is extended in [97, 98, 99].

The Hagedorn phenomena [100] tells us that the degeneracy of states grows rapidly going up the infinite tower of massive states. This growth, in theory, could counteract the suppression received from the decreasing contributions from the integrals in Table 5.13 and cause divergences. The mechanism of misaligned supersymmetry, however, causes the states in the massive tower to oscillate between an excess of bosons and an excess of fermions. This behaviour is referred to as boson-fermion oscillation. Our models indeed present this behaviour as shown in Figure 5.3. Instead of cancelling level-by-level as in the supersymmetric case, the cancellation is misaligned causing the oscillation to give a large positive contribution followed by an even larger

negative contribution and so on. This mechanism ensures that the partition function of our non-supersymmetric models remains finite.

5.5.1 $N_b = N_f$ at the Massless Level

The discussion above shows that, while for non-supersymmetric theories there is no mechanism which ensures the vanishing of a_{mn} at any allowed level, there is, however, nothing preventing it from happening. It is indeed possible to find models within our classification set-up detailed in Section 5.2 which have $a_{00} = 0$, *i.e.* $N_b^0 = N_f^0$. Such models have been dubbed 'super no-scale' models [73, 74] when SUSY is broken via Scherk-Schwarz [75, 76, 77, 78, 79, 80] it has been argued that their leading order cosmological constant is exponentially suppressed.

In the analysis of the one-loop potential in [43, 44], no models are found which exhibit $N_b^0 = N_f^0$ at the free fermionic point in the sample explored. Instead they use techniques developed in [42] to move away from the free fermionic point by translating to an analogous $\mathbb{Z}_2^n$ orbifold and rewriting the partition function at a generic point to find models with $N_b^0 = N_f^0$. In our analysis we stay at the free fermionic point and it turns out that we do find models with $N_b^0 = N_f^0$ and an example model is presented in Section 5.6.3.

It is convenient to summarise the various contributions to a_{00} in the form of Table 5.14. We use the notation for sectors laid out in Section 5.4. For simplicity, and since we restrict our classification to models with no enhancements, the contributions of vector bosons from sectors $\boldsymbol{z_1}, \boldsymbol{z_2}, \boldsymbol{z_1}+\boldsymbol{z_2}$ are ignored.

Sector	$N_b - N_f$	Sector	$N_b - N_f$
NS	304	$\bar{y}^i, \bar{w}^i \left\vert \tilde{\boldsymbol{V}} \right\rangle$	-8
$\left\vert \boldsymbol{F}^{1,2,3} \right\rangle$	-32	$\boldsymbol{\delta}^{1,\ldots,30}$	16
$\left\vert \tilde{\boldsymbol{x}} \right\rangle$	-256	$\bar{\psi}^{a(*)}, \bar{\eta}^{b(*)} \left\vert \boldsymbol{\gamma}^{1,\ldots,15} \right\rangle$	64
$\bar{\psi}^{a(*)} \left\vert \boldsymbol{V}^{1,2,3} \right\rangle$	32	$\{\bar{y}^i, \bar{w}^i\} \left\vert \boldsymbol{\gamma}^{1,\ldots,15} \right\rangle$	4
$\bar{\phi}^{\{1,2\},\{3,4\},\{5,6\},\{7,8\}(*)} \left\vert \boldsymbol{V}^{1,2,3} \right\rangle$	8	$\bar{\phi}^{\{1,2\},\{3,4\},\{5,6\},\{7,8\}(*)} \left\vert \boldsymbol{\gamma}^{1,\ldots,15} \right\rangle$	8
$\bar{y}^i, \bar{w}^i \left\vert \boldsymbol{V}^{1,2,3} \right\rangle$	4	$\{y^i, w^i\}\{\bar{y}^j, \bar{w}^j\} \left\vert \boldsymbol{z_{1,2}} \right\rangle$	8
$\left\vert \boldsymbol{H}^{1,\ldots,6} \right\rangle$	16	$\{y^i, w^i\}\bar{\eta}^{b(*)} \left\vert \boldsymbol{z_{1,2}} \right\rangle$	32
$\left\vert \boldsymbol{H}^{7,\ldots,18} \right\rangle$	-8	$\{y^i, w^i\}\{\bar{\phi}^{\{5,6,7,8\},\{1,2,3,4\}(*)}\} \left\vert \boldsymbol{z_{1,2}} \right\rangle$	16
$\bar{\psi}^{a(*)}, \bar{\eta}^{b(*)}, \bar{\phi}_{NS}^{(*)} \left\vert \tilde{\boldsymbol{V}} \right\rangle$	-192	$\{y^i, w^i\} \left\vert \boldsymbol{z_1}+\boldsymbol{z_2} \right\rangle$	8

Table 5.14: *Contributions of massless sectors to a_{00} when present in Hilbert space of a model. As noted $a_{00} = N_b^0 - N_f^0$, so bosonic contributions are positive and fermionic are negative. The superscripts used here are $i \neq j = 1, \ldots, 6$, $a = 1, \ldots, 5$ and $b = 1, 2, 3$. The NS subscript means that the oscillator has Neveu-Schwarz boundary conditions in the sector.*

5.6 Results of Classification

Having discussed how to determine key features of the massless spectrum and how to calculate the partition function and cosmological constant for our $\tilde{S}$-models we can now present some statistics derived from a sample in the space of models. As mentioned in Section 5.2, the space of all models is $2^{66} \sim 10^{19.9}$ and so a complete classification is far beyond the computing power at our disposal. Instead, we explore a sample of 2×10^9 models of which only around 1 in 185 are tachyon-free that we take forward for further analysis. We will start with some results of key aspects of the massless spectrum.

5.6.1 Results from Massless Spectrum

From our sample of 2×10^9 models we choose 10^7 tachyon-free models and display the results for their $SO(10)$ observable representations. In Figure 5.4 the net chirality, $N_{16} - N_{\overline{16}}$, distribution is displayed and in Figure 5.5 the distribution of their number of vectorial **10** representations is displayed. The familiar normal distribution also found

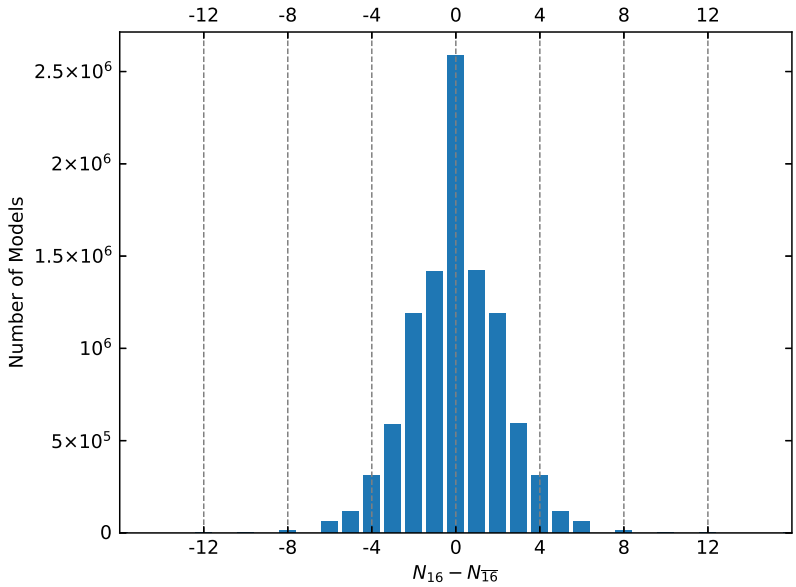

Figure 5.4: *Number of models versus net chiral generations from a random sample of* 10^7 *tachyon free* $SO(10)$ *models.*

in all other classifications for the supersymmetric cases is uncovered, which is hardly surprising since the structure of the fermionic $\mathbf{16}/\overline{\mathbf{16}}$ is unchanged. From Figure 5.5 we see that the large majority of models contain at least 1 vectorial **10** which may be used to generate a bidoublet Higgs representation when the $SO(10)$ is broken.

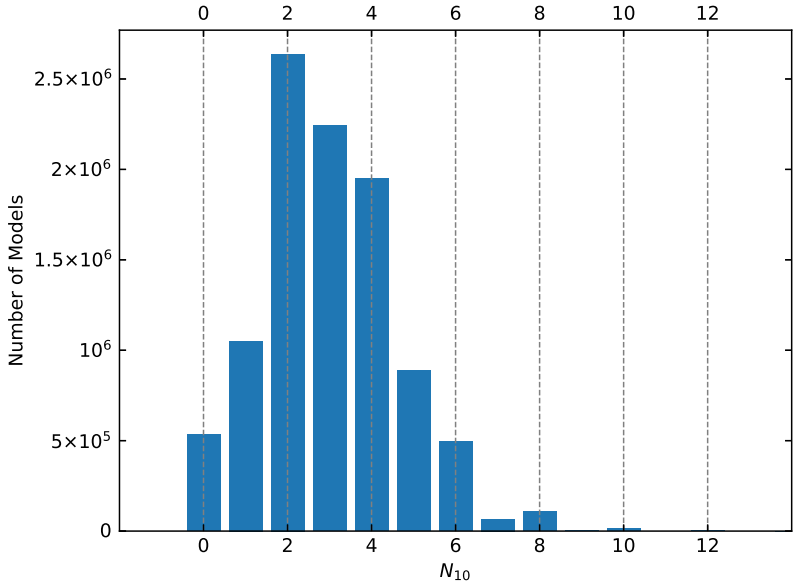

Figure 5.5: *Number of models versus number of vectorial* **10** *sectors from a random sample of* 10^7 *tachyon free* $SO(10)$ *models.*

In order to see more clearly the statistics from our 2×10^9 sample we display the frequency of $SO(10)$ models as several phenomenological constraints are considered in Table 5.15.

	Constraints	Total models in sample	Probability
	No Constraints	2×10^9	1
(1)	+ Tachyon-Free	10741667	5.37×10^{-3}
(2)	+ No Observable Enhancements	10741667	5.37×10^{-3}
(3)	+ No Hidden Enhancements	9921843	4.96×10^{-3}
(4)	+ $N_{16} - N_{\overline{16}} \geq 6$	69209	3.46×10^{-5}
(5)	+ $N_{10} \geq 1$	69013	3.45×10^{-5}
(6)	+ $a_{00} = N_b^0 - N_f^0 = 0$	3304	1.65×10^{-6}

Table 5.15: *Phenomenological statistics from sample of* 2×10^9 $SO(10)$ $\tilde{\boldsymbol{S}}$ *-models.*

These results confirm the observation made in previous sections that there are no tachyon-free models in our construction which have observable enhancements. In phenomenological terms, we do not need to worry about enhancements of the hidden sector gauge group, but they are included in the table for completeness. The next constraints we add are much like the so-called 'fertility constraints' implemented in [60, 87]. The constraint on the net chirality $N_{16} - N_{\overline{16}} \geq 6$ is a necessary, but not sufficient, condition for the existence of 3 or more chiral generations at the level of the standard model. The condition $N_{10} \geq 1$ ensures at least one state exists that can produce a Standard Model Higgs doublet and can be used to break the electroweak symmetry. Finally,

we implement a condition on the q-expansion coefficient $a_{00} = 0$ which corresponds to finding models with $N_b = N_f$ at the massless level as discussed in Section 5.5.

The 3304 models satisfying all these constraints are notable, particularly in regard to this final condition of $N_b^0 = N_f^0$. Inspecting the patterns in the spectra of these 3304 models revealed that $\sim 58\%$ contain the vector $\tilde{\boldsymbol{x}}$ in their spectrum. In these cases the large negative contribution of -256 that $\tilde{\boldsymbol{x}}$ contributes to a_{00} is helpful in ensuring $N_b^0 = N_0^f$ since the large positive NS contribution can often dominate. Of those models not containing $\tilde{\boldsymbol{x}}$ approximately 70% obtained the large negative contribution of -192 from one of the additional vectorials $\tilde{V} = \tilde{\boldsymbol{S}}, \tilde{\boldsymbol{S}} + \boldsymbol{z_1}, \tilde{\boldsymbol{S}} + \boldsymbol{z_2}, \tilde{\boldsymbol{S}} + \boldsymbol{z_1} + \boldsymbol{z_2}$ with mixed charges under the observable and hidden groups, i.e. the sectors $\{\bar{\psi}^{1,\dots,5}, \bar{\eta}^{1,2,3}, \bar{\phi}_{NS}\} \left|\tilde{V}\right\rangle$. Again this large negative contribution helps in matching the number of massless fermions to massless bosons.

5.6.2 Results for Cosmological Constant and $N_b - N_f$

As the value of the constant term $a_{00} = N_b^0 - N_f^0$ and the cosmological constant Λ vary from model-to-model, it is interesting to see what range of values these non-supersymmetric models can produce.

The distribution of the cosmological constant Λ is shown in Figure 5.6, for a sample of 10^4 non-tachyonic and 10^4 fertile models. By non-tachyonic we mean that only condition (1) of Table 5.15 is satisfied, while fertile models satisfy all conditions (1)-(5). It is important to note that values presented in Figure 5.6 are at the special free fermionic point in moduli space. This means that moving away from this point will change these values and if there are unfixed moduli, there is nothing preventing this from happening. This is indeed the case for our class of models.

As discussed in Section 5.5, the on-shell states provide the majority of positive contributions to the partition function, the largest of which is the massless term. Thus the value of a_{00} gives a dominant contribution on the value of the cosmological constant. It is also, of course, interesting for the discussion of phenomenological features and stability as explained in Section 5.5.1. The distribution of values of $a_{00} = N_b^0 - N_f^0$ for a sample of 10^4 non-tachyonic and 10^4 fertile models is shown in Figure 5.7.

From Figures 5.6 and 5.7 we see that the fertility conditions have a measurable effect on the distribution of Λ and a_{00}, that is, they slightly shift the values of both to the negative. This is an interesting effect and is likely due to condition (4) in Table 5.15. Even though the fertility condition (4) is directed at ensuring the difference $N_{16} - N_{\overline{16}}$ is greater than 6, in doing this it also results in fertile models having a larger average total $N_{16} + N_{\overline{16}}$ compared to non-fertile models. As specified in Table 5.14, these sectors contribute a value of -32 to a_{00} and thus appear to cause the shift toward smaller values for a_{00} and as a consequence also for Λ.

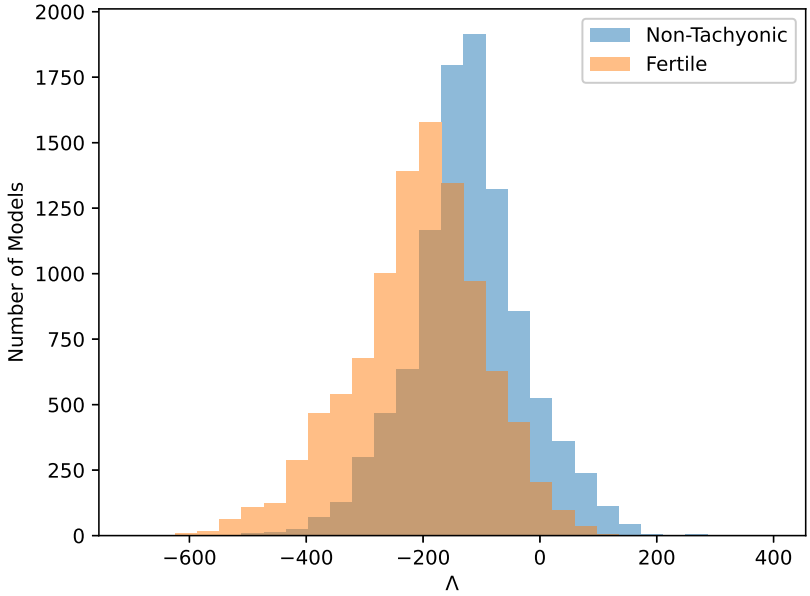

Figure 5.6: *The distribution of the cosmological constant for a sample of* 10^4 *non-tachyonic and* 10^4 *fertile models models.*

5.6.3 A Model with $N_b = N_f$

From the 3304 fertile models with $N_b^0 = N_f^0$ we present an analysis of the key features of the massless spectrum for one example model, as well as presenting its partition function and cosmological constant. The model we choose has the GGSO matrix

$$C\begin{bmatrix} v_i \\ v_j \end{bmatrix} = \begin{array}{c} \\ \mathbf{1} \\ \tilde{\boldsymbol{S}} \\ \boldsymbol{e_1} \\ \boldsymbol{e_2} \\ \boldsymbol{e_3} \\ \boldsymbol{e_4} \\ \boldsymbol{e_5} \\ \boldsymbol{e_6} \\ \boldsymbol{b_1} \\ \boldsymbol{b_2} \\ \boldsymbol{b_3} \\ \boldsymbol{z_1} \end{array} \begin{array}{c} \begin{array}{cccccccccccc} \mathbf{1} & \tilde{\boldsymbol{S}} & \boldsymbol{e_1} & \boldsymbol{e_2} & \boldsymbol{e_3} & \boldsymbol{e_4} & \boldsymbol{e_5} & \boldsymbol{e_6} & \boldsymbol{b_1} & \boldsymbol{b_2} & \boldsymbol{b_3} & \boldsymbol{z_1} \end{array} \\ \begin{pmatrix} -1 & -1 & 1 & -1 & -1 & -1 & 1 & 1 & 1 & 1 & -1 & -1 \\ -1 & 1 & -1 & -1 & -1 & 1 & 1 & 1 & 1 & -1 & -1 & 1 \\ 1 & -1 & -1 & -1 & -1 & -1 & -1 & -1 & -1 & -1 & -1 & 1 \\ -1 & -1 & -1 & 1 & -1 & 1 & 1 & -1 & 1 & -1 & 1 & -1 \\ -1 & -1 & -1 & -1 & 1 & -1 & -1 & 1 & 1 & 1 & -1 & -1 \\ -1 & 1 & -1 & 1 & -1 & 1 & 1 & 1 & 1 & -1 & 1 & 1 \\ 1 & 1 & -1 & 1 & -1 & 1 & -1 & 1 & -1 & 1 & 1 & -1 \\ 1 & 1 & -1 & -1 & 1 & 1 & 1 & -1 & -1 & 1 & 1 & 1 \\ 1 & -1 & -1 & 1 & 1 & 1 & -1 & -1 & 1 & -1 & 1 & 1 \\ 1 & 1 & -1 & -1 & 1 & -1 & 1 & 1 & -1 & 1 & -1 & 1 \\ -1 & 1 & -1 & 1 & -1 & 1 & 1 & 1 & 1 & -1 & -1 & -1 \\ -1 & -1 & 1 & -1 & -1 & 1 & -1 & 1 & 1 & 1 & -1 & -1 \end{pmatrix} \end{array} \tag{5.26}$$

This model has $N_{16} = 7$, $N_{\overline{16}} = 1$ and $N_{10} = 8$ and thus satisfies the constraints imposed in Table 5.15. Furthermore, in this model the $\tilde{\boldsymbol{x}}$-sector produces massless states, which in the supersymmetric models would correspond to the presence of the $\boldsymbol{S} + \boldsymbol{x}$

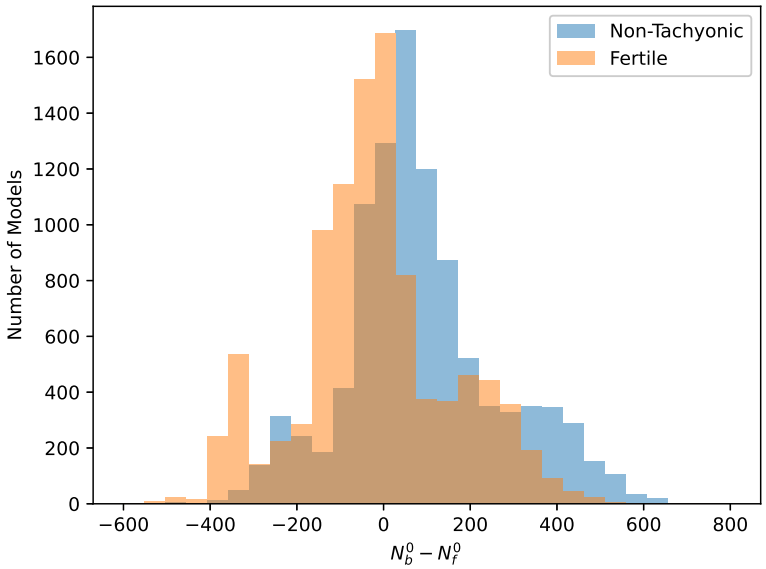

Figure 5.7: *The distribution of the constant term* $a_{00} = N_b^0 - N_f^0$ *for a sample of* 10^4 *non-tachyonic and* 10^4 *fertile models.*

sector when $\boldsymbol{x}$ enhances the $SO(10)$ symmetry to E_6. In that case, the $\boldsymbol{S} + \boldsymbol{x}$ include the superpartners of the gauge vector bosons of the sector $\boldsymbol{x}$, i.e. the gauginos. So in this case, we have the gauginos but not the vector bosons.

Our model also contains 6 bosonic hidden states from the sectors $\boldsymbol{H}^{1,\dots,6}$ and 48 fermionic hidden states from the $\boldsymbol{H}^{7,\dots,18}$. There are additional vectorials from the sectors $\boldsymbol{e_3} + \boldsymbol{e_4} + \boldsymbol{e_5} + \boldsymbol{e_6}$, $\boldsymbol{e_1} + \boldsymbol{e_2} + \boldsymbol{e_3} + \boldsymbol{e_6}$ and $\boldsymbol{e_1} + \boldsymbol{e_2} + \boldsymbol{e_3} + \boldsymbol{e_4}$ with observable oscillators $\{\bar{\psi}^a, \bar{\eta}^b\}$, $a = 1, \dots, 5$, $b = 1, 2, 3$ which cannot couple with observable states from $\boldsymbol{F}^{1,2,3}$ since it cannot conserve the charges of the $U(1)_{1,2,3}$ in particular. However, these three sectors may provide couplings at higher order.

The partition function is calculated in terms of its q-expansion and so it can be specified by a matrix of coefficients a_{mn} as in (5.25). For our example model these values are presented in Table 5.16. We see that indeed this model has $a_{00} = N_b^0 - N_f^0 = 0$ as advertised and the series of states arrange according to (5.25). The absence of on-shell tachyons is explicit and the contribution from off-shell tachyonic states is non-zero as expected. We also find that the consistency condition $a_{0-1} = 2$ for the proto-graviton (3.44) as described in [32, 101] is also satisfied.

The cosmological constant can also be calculated according to (5.23) with the modular integral quickly converging after 2^{nd} order in q. In this case it takes the value

$$\Lambda = \sum_{m,n} a_{mn} I_{mn} = -149.77 \tag{5.27}$$

	-1	-7/8	-3/4	-5/8	-1/2	-3/8	-1/4	-1/8	0	1/8	1/4	3/8	1/2	5/8	3/4	7/8
-1/2	0	0	0	0	0	0	0	0	0	0	0	0	320	0	0	0
-3/8	0	0	0	0	0	0	0	0	0	0	0	0	0	896	0	0
-1/4	0	0	0	0	0	0	0	0	0	0	0	0	0	0	5696	0
-1/8	0	0	0	0	0	0	0	0	0	0	0	0	0	0	0	29312
0	2	0	0	0	0	0	0	0	0	0	0	0	0	0	0	0
1/8	0	0	0	0	0	0	0	0	0	-288	0	0	0	0	0	0
1/4	0	0	0	0	0	0	0	0	0	0	-4512	0	0	0	0	0
3/8	0	0	0	16	0	0	0	0	0	0	0	-9808	0	0	0	0
1/2	0	0	0	0	224	0	0	0	0	0	0	0	1344	0	0	0
5/8	0	0	0	0	0	416	0	0	0	0	0	0	0	36640	0	0
3/4	0	0	0	0	0	0	576	0	0	0	0	0	0	0	78080	0
7/8	0	0	0	0	0	0	0	-320	0	0	0	0	0	0	0	212928
1	32	0	0	0	0	0	0	0	-1440	0	0	0	0	0	0	0

Table 5.16: *The q-expansion of the partition function for our example model. Each entry in the table represents the coefficient a_{mn} in the partition function sum (5.22), with the first column and row being the mass levels for the left and right moving sectors respectively.*

at the free fermionic point. As we see it is negative which is the case for most models with $N_b^0 = N_f^0$. This is due to the fact that the largest positive contributions to the partition function come from the light on-shell states and in particular from the massless states. If $N_b^0 - N_f^0 = 0$, this is zero and the negative contributions from the light off-shell tachyons produce a negative value for Λ. This is indeed the case for all 3304 such models in our scan.

5.7 Discussion and Conclusion

In this chapter we have developed systematic computerised tools to classify large spaces of free fermionic heterotic string vacua that correspond to compactifications of ten dimensional tachyonic vacua. From the point of view of the four dimensional constructions this is achieved by the general $\tilde{S}$-map. Our previous $\overline{\text{NAHE}}$-based model [37] was similarly constructed from the model published in [70], which raises the question: what are the consequences of applying the map to generic models? That is to say, what are the relations between the spectra of the two mapped models, and what are the general patterns? Through the connection to modular maps, it appears to be of the same nature as the spinor-vector duality map, and the two may in fact be manifestations of a much larger symmetry structure [71].

We have seen that adopting the classification methodology developed for supersymmetric free fermionic models entails the proliferation of tachyon producing sectors in the $\tilde{S}$-mapped models. The systematic classification therefore requires detailed analysis of these sectors that was discussed in Section 5.3. In the analysis of the massless sectors, separate attention to bosonic and fermionic sectors is required and was discussed in Section 5.4. In Section 5.5 we discussed the general analysis of the partition function and its q-expansion in left and right-moving energy modes. The analysis of the partition function is particularly illuminating in the case of non-supersymmetric string

vacua as it gives a direct handle on the physical states at different mass levels. Of particular interest in the q-expansion is the $a_{00} = N_b^0 - N_f^0$ term, which counts the difference between massless bosons and fermions in the spectrum of the string vacuum. In supersymmetric models the number of fermionic and bosonic degrees of freedom are matched at all mass levels, and hence the partition function and the vacuum energy are identically zero. In non-supersymmetric models there is a generic mismatch at different mass levels, which is partially compensated by the so-called misaligned supersymmetry [95, 96, 97, 98, 99].

These results in Section 5.6 reveal that extracting interesting phenomenological models motivates the development of more sophisticated computerised methods than the random generation method due to tachyon-free models occurring with $\sim 5 \times 10^{-3}$ probability. This is particularly true in light of the fact that generating viable symmetry breaking pattern may necessitate breaking the $SO(10)$ symmetry to the Standard Model subgroup direct because the $\tilde{\boldsymbol{S}}$-map entails that scalar degrees of freedom in the spinorial sixteen representation of $SO(10)$ are shifted to the massive spectrum. The consequence of this is that the spectrum does not contain the neutral component in the 16 of $SO(10)$ required to break the remnant unbroken gauge symmetry down to the Standard Model gauge group. The only available states are exotic states that carry fractional $U(1)_{Z'}$ charge and appear in the heterotic Standard-like Models (SLMs) [65, 102, 103]. This assertion is made more concrete in the classification of $\tilde{\boldsymbol{S}}$ and $\boldsymbol{S}$ models with Pati Salam subgroup in [82]. The lesson may be that quasi-realistic models in this class may only be possible for a very restricted and narrow set of models, rather than the more generic set, which is the prevalent experience with supersymmetric constructions. In forthcoming work these questions are investigated in tachyon-free Pati Salam models, including the inclusion of fertility conditions. The increased space of vacua, in particular in the case of LRS and SLMs, requires adaptation of novel computational techniques [60, 87].

Following from our previous paper [37] the analysis and results presented in this work open up new vistas in string phenomenology. It reveals the potential relevance of string vacua that have been previously considered irrelevant. One avenue to explore is the interpolation between the supersymmetric vacua and our tachyon-free constructions, as well as with the two dimensional MSDS constructions [104, 105, 106], that may shed some light on the problem of supersymmetry breaking and vacuum energy in string theory. Another question of interest is the question of stability of the tachyon-free models. This question is necessarily tied up with the non-vanishing one-loop vacuum energy in these models. In this respect it will be interesting to analyse the one-loop diagram that arises in these models due to the existence of an anomalous $U(1)$ symmetry [107] and to examine whether two diagrams can be cancelled against each other. Finally, further understanding of the symmetries that underlie the partition function at all mass levels will be interesting to understand, especially with respect to the $\tilde{\boldsymbol{S}}$ and $\tilde{\boldsymbol{x}}$ maps.

Chapter 6

Novel 4D String Vacua: Type 0 and Type $\bar{0}$

In this chapter two extremes of the $\mathbb{Z}_2 \times \mathbb{Z}_2$ heterotic string landscape are studied: Type 0 and Type $\bar{0}$ vacua. These are models that at the massless level are free of fermions and free of twisted bosons, respectively. This is work taken from the papers [8] and [9] with some minor notational adjustments. We will start with the Type 0 case.

6.1 Type 0

Our interest here is in the existence of models that do not contain massless fermions. Such models are known in the literature as Type 0 models and have been of interest in other string theory limits [108, 109, 110, 111, 112, 113, 114, 115, 116], although the term generally refers to models free from fermions at all mass levels. Such models are of particular interest in regard to exploring the boundaries of the space of $\mathbb{Z}_2 \times \mathbb{Z}_2$ orbifold compactifications. It is plausible that progress on some of the phenomenological issues in string theory, in particular in relation to the cosmological evolution and vacuum selection, will be obtained by improved understanding of these vacua. Moreover, it is likely that further insight can be achieved by exploring some of the features of these vacua in connection with the phenomenological string vacua. We therefore pursue this line of investigation. We present several Type 0 models in this Class. We further adapt the systematic classification methodology discussed in Chapter 4 and developed in refs. [7, 39, 50, 51, 59, 60, 61, 67, 87] to this Class of models. This requires careful analysis of tachyonic states that proliferate in these configurations. While we do not find any models completely free of tachyonic states, we present a model with a minimal set of tachyonic states. Although we won't explore this further here, these tachyonic states do not render these models irrelevant since techniques such as tachyon condensation may connect these theories to lower dimensional vacua. Additionally, the analysis of ref. [43, 44] suggest that tachyonic states may become massive when we move away from the free fermionic point in the moduli space. An issue that we analyse in detail

is the calculation of the vacuum energy and the finiteness properties of the string one-loop amplitude. Naturally, these are divergent due to the existence of tachyonic states. However, once the tachyonic states are removed by hand the amplitudes are finite and exhibit a form of misaligned supersymmetry.

6.1.1 Example Type 0 $\mathbb{Z}_2 \times \mathbb{Z}_2$ Heterotic String Orbifold Model

The first model that we present uses the $\overline{\text{NAHE}}$-set that was introduced in [36, 37]. The set of basis vectors is given by

$$\begin{aligned}
\mathbb{1} &= \{\psi^\mu,\ \chi^{1,\dots,6}, y^{1,\dots,6}, w^{1,\dots,6} \mid \overline{y}^{1,\dots,6}, \overline{w}^{1,\dots,6}, \overline{\psi}^{1,\dots,5}, \overline{\eta}^{1,2,3}, \overline{\phi}^{1,\dots,8}\},\\
\tilde{\boldsymbol{S}} &= \{\psi^\mu, \chi^{1,\dots,6} \mid \overline{\phi}^{3,4,5,6}\},\\
\boldsymbol{b_1} &= \{\chi^{34}, \chi^{56}, y^{34}, y^{56} \mid \overline{y}^{34}, \overline{y}^{56}, \overline{\eta}^{1}, \overline{\psi}^{1,\dots,5}\},\\
\boldsymbol{b_2} &= \{\chi^{12}, \chi^{56}, y^{12}, w^{56} \mid \overline{y}^{12}, \overline{w}^{56}, \overline{\eta}^{2}, \overline{\psi}^{1,\dots,5}\},\\
\boldsymbol{b_3} &= \{\chi^{12}, \chi^{34}, w^{12}, w^{34} \mid \overline{w}^{12}, \overline{w}^{34}, \overline{\eta}^{3}, \overline{\psi}^{1,\dots,5}\},\\
\boldsymbol{z_1} &= \{\overline{\phi}^{1,\dots,4}\},\\
\boldsymbol{x} &= \{\overline{\psi}^{1,\dots,5}, \overline{\eta}^{1,2,3}\}.
\end{aligned} \tag{6.1}$$

A model may then be specified through the assignment of modular invariant GGSO phases $C\binom{v_i}{v_j}$ between the basis vectors. One Type 0 configuration arises from the assignment

$$C\begin{bmatrix}\boldsymbol{v_i}\\ \boldsymbol{v_j}\end{bmatrix} = \begin{array}{c} \\ \mathbb{1} \\ \tilde{\boldsymbol{S}} \\ \boldsymbol{b_1} \\ \boldsymbol{b_2} \\ \boldsymbol{b_3} \\ \boldsymbol{z_1} \\ \boldsymbol{x} \end{array} \begin{array}{c} \begin{array}{ccccccc} \mathbb{1} & \tilde{\boldsymbol{S}} & \boldsymbol{b_1} & \boldsymbol{b_2} & \boldsymbol{b_3} & \boldsymbol{z_1} & \boldsymbol{x} \end{array} \\ \begin{pmatrix} 1 & 1 & -1 & -1 & -1 & -1 & -1 \\ 1 & -1 & -1 & -1 & -1 & 1 & 1 \\ -1 & 1 & -1 & -1 & -1 & 1 & 1 \\ -1 & 1 & -1 & -1 & -1 & 1 & 1 \\ -1 & 1 & -1 & -1 & -1 & 1 & 1 \\ -1 & -1 & 1 & 1 & 1 & -1 & 1 \\ -1 & 1 & -1 & -1 & -1 & 1 & 1 \end{pmatrix} \end{array}. \tag{6.2}$$

All models in this basis will have gauge bosons arising from the NS sector that produce the vector bosons of a

$$SO(10) \times U(1)^3 \times SO(4)^3 \times SU(2)^8 \tag{6.3}$$

gauge symmetry. Additional vector bosons may arise from the sectors $\boldsymbol{z_1}$, $\boldsymbol{z_3} = \mathbb{1} + \tilde{\boldsymbol{S}} + \boldsymbol{b_1} + \boldsymbol{b_2} + \boldsymbol{b_3} = \{\bar{\phi}^{1,2,7,8}\}$ and $\boldsymbol{z_4} = \mathbb{1} + \tilde{\boldsymbol{S}} + \boldsymbol{b_1} + \boldsymbol{b_2} + \boldsymbol{b_3} + \boldsymbol{z_1} = \{\bar{\phi}^{3,4,7,8}\}$, which can affect the observable if the right moving oscillator is $\bar{\psi}^a$ or solely the hidden gauge group factors otherwise. A solely observable gauge enhancement may also arise from the sector $\boldsymbol{x}$. In the above model, the hidden $SU(2)^8$ gauge symmetry is enhanced to $SO(16)$ by vector bosons arising in $\boldsymbol{z_1}$, $\boldsymbol{z_3}$ and $\boldsymbol{z_4}$. The four dimensional gauge group

is therefore

$$SO(10) \times U(1)^3 \times SO(4)^3 \times SO(16).$$

The NS-sector and the three sectors, $\boldsymbol{z_1}$, $\boldsymbol{z_3}$ and $\boldsymbol{z_4}$, that produce enhancements at the massless level also help to generate sixteen tachyonic states at mass level $(-\frac{1}{2}, -\frac{1}{2})$ that transform in the **16** representation of the hidden $SO(16)$ gauge symmetry.

The vectorial fermionic sectors in the model are

$$\begin{aligned} &\tilde{\boldsymbol{S}}; \\ &\tilde{\boldsymbol{S}} + \boldsymbol{z_1}; \\ &\tilde{\boldsymbol{S}} + \boldsymbol{z_4} \sim \boldsymbol{S} + \boldsymbol{z_2}, \end{aligned} \tag{6.4}$$

while the massless fermionic spinorial sectors are

$$\begin{aligned} &\tilde{\boldsymbol{S}} + \boldsymbol{b_{1,2,3}} + \boldsymbol{x}; \\ &\tilde{\boldsymbol{S}} + \boldsymbol{b_{1,2,3}} + \boldsymbol{x} + \boldsymbol{z_1}; \\ &\tilde{\boldsymbol{S}} + \boldsymbol{b_{1,2,3}} + \boldsymbol{x} + \boldsymbol{z_4}; \\ &\tilde{\boldsymbol{S}} + \boldsymbol{z_3} \sim \boldsymbol{S} + \boldsymbol{z_1} + \boldsymbol{z_2}; \end{aligned} \tag{6.5}$$

where we defined $\boldsymbol{z_2} = \{\bar{\phi}^{5,\cdots,8}\}$ and $\boldsymbol{S} = \{\psi^{1,2}, \chi^{1,\cdots,6}\}$, neither of which are basis vector combinations in the additive group. These definitions comply with the terminology used in the classification of the supersymmetric free fermionic heterotic string models.

The massless states from all the fermionic sectors are projected out from the physical spectrum by the choice of GGSO phases in eq. (6.2). In addition to the NS-sector, additional spacetime massless bosonic states arise from the sectors

$$\begin{aligned} &\boldsymbol{x}; \\ &\boldsymbol{z_{1,3,4}}; \\ &\boldsymbol{b_{1,2,3}}; \\ &\boldsymbol{b_{1,2,3}} + \boldsymbol{x}; \\ &\boldsymbol{b_{1,2,3}} + \boldsymbol{x} + \boldsymbol{z_1}; \\ &\boldsymbol{b_{1,2,3}} + \boldsymbol{x} + \boldsymbol{z_3}; \\ &\boldsymbol{b_{1,2,3}} + \boldsymbol{x} + \boldsymbol{z_1} + \boldsymbol{z_3}. \end{aligned} \tag{6.6}$$

These give rise to scalar spacetime bosons and we do not require further details for our analysis here.

In Section 6.1.3 and 6.1.4 we perform a more general search for similar Type 0 heterotic string models using the free fermionic classification methodology. In particular, we search for Type 0 models without tachyons. Our search is conducted using the $\tilde{\boldsymbol{S}}$

based models as well as models that use $\boldsymbol{S}$. First, however, it is interesting to study a bit more closely the basis (6.1), and what additional constraints Type 0 vacua may satisfy.

6.1.2 Analytic conditions on Type 0 vacua

Since we are interested in the construction and analysis of Type 0 vacua, we focus on the massless fermionic sectors and will seek to project them out, leaving only bosonic states at the massless level.

Therefore we can seek choices of GGSO phases for which the fermionic sectors may be projected out to leave Type 0 vacua and it turns out for this relatively simple basis we can find explicit analytic conditions on their projection. Another important part of the analysis will be to consider the presence of tachyonic sectors in our models which we turn to in Section 6.1.2.

By constructing projectors for the massless fermionic sectors and ensuring they all equal zero we find the following necessary and sufficient conditions on the projection of massless fermions within models derived from the basis (6.1)

$$\begin{aligned}
&C\begin{bmatrix}\tilde{\boldsymbol{S}}\\ \boldsymbol{x}\end{bmatrix} = 1, \quad C\begin{bmatrix}\boldsymbol{z_1}\\ \boldsymbol{x}\end{bmatrix} = 1, \quad C\begin{bmatrix}\boldsymbol{z_1}\\ \boldsymbol{b_1}\end{bmatrix} = C\begin{bmatrix}\boldsymbol{z_1}\\ \boldsymbol{b_2}\end{bmatrix} = C\begin{bmatrix}\boldsymbol{z_1}\\ \boldsymbol{b_3}\end{bmatrix} = 1\\
&C\begin{bmatrix}\tilde{\boldsymbol{S}}\\ \boldsymbol{b_1}\end{bmatrix} = -C\begin{bmatrix}\tilde{\boldsymbol{S}}\\ \boldsymbol{b_2}\end{bmatrix}C\begin{bmatrix}\tilde{\boldsymbol{S}}\\ \boldsymbol{b_3}\end{bmatrix}\\
&C\begin{bmatrix}\boldsymbol{x}\\ \mathbb{1}\end{bmatrix} = C\begin{bmatrix}\boldsymbol{x}\\ \boldsymbol{b_1}\end{bmatrix}C\begin{bmatrix}\boldsymbol{x}\\ \boldsymbol{b_2}\end{bmatrix}C\begin{bmatrix}\boldsymbol{x}\\ \boldsymbol{b_3}\end{bmatrix}\\
&C\begin{bmatrix}\boldsymbol{b_2}\\ \boldsymbol{b_3}\end{bmatrix} = -C\begin{bmatrix}\tilde{\boldsymbol{S}}\\ \boldsymbol{b_2}\end{bmatrix}C\begin{bmatrix}\boldsymbol{b_1}\\ \boldsymbol{b_2}\end{bmatrix}\\
&C\begin{bmatrix}\boldsymbol{b_3}\\ \boldsymbol{b_1}\end{bmatrix} = -C\begin{bmatrix}\tilde{\boldsymbol{S}}\\ \boldsymbol{b_2}\end{bmatrix}C\begin{bmatrix}\tilde{\boldsymbol{S}}\\ \boldsymbol{b_3}\end{bmatrix}C\begin{bmatrix}\boldsymbol{b_1}\\ \boldsymbol{b_2}\end{bmatrix}.
\end{aligned} \tag{6.7}$$

These conditions mean that 9 of the 21 GGSO phases are fixed in order to obtain Type 0 vacua. Hence, the number of possible Type 0 models is reduced to $2^{12} = 4096$.

We can now inspect the projection conditions on the massless bosonic sectors (6.6), subject to these Type 0 conditions (6.7). In particular, taking the sectors $\boldsymbol{b_k}$, for $k = 1, 2, 3$, we get

$$\boldsymbol{b_k} \text{ survives} \iff C\begin{bmatrix}\boldsymbol{b_k}\\ \tilde{\boldsymbol{S}} + \boldsymbol{b_j} + \boldsymbol{b_k}\end{bmatrix} = 1 \quad \text{and} \quad C\begin{bmatrix}\boldsymbol{b_k}\\ \boldsymbol{z_1}\end{bmatrix} = 1 \tag{6.8}$$

these conditions are necessitated by the Type 0 conditions and so these sectors must survive and similarly can easily be found for the other spinorial bosonic sectors: $\boldsymbol{b_k} + \boldsymbol{x} + \boldsymbol{z_1}, \boldsymbol{b_k} + \boldsymbol{x} + \boldsymbol{z_3}$ and $\boldsymbol{b_k} + \boldsymbol{x} + \boldsymbol{z_4}$.

For the bosonic vectorial sectors: $\boldsymbol{b_k} + \boldsymbol{x}$ we have the conditions

$$\{\bar{y}, \bar{w}, \bar{\psi}^{1,\dots,5}, \bar{\eta}^i, \bar{\phi}^{5,6}\} \left|\boldsymbol{b_k} + \boldsymbol{x}\right\rangle \text{ survives } \implies \frac{1}{4}\left(1 + C\begin{bmatrix}\boldsymbol{b_k}+\boldsymbol{x}\\ \boldsymbol{z_3}\end{bmatrix}\right)\left(1 + C\begin{bmatrix}\boldsymbol{b_k}+\boldsymbol{x}\\ \boldsymbol{z_1}\end{bmatrix}\right) = 1 \tag{6.9}$$

$$\{\bar{\phi}^{1,2}\} \left|\boldsymbol{b_k} + \boldsymbol{x}\right\rangle \text{ survives } \implies \frac{1}{4}\left(1 - C\begin{bmatrix}\boldsymbol{b_k}+\boldsymbol{x}\\ \boldsymbol{z_3}\end{bmatrix}\right)\left(1 - C\begin{bmatrix}\boldsymbol{b_k}+\boldsymbol{x}\\ \boldsymbol{z_1}\end{bmatrix}\right) = 1 \tag{6.10}$$

$$\{\bar{\phi}^{3,4}\} \left|\boldsymbol{b_k} + \boldsymbol{x}\right\rangle \text{ survives } \implies \frac{1}{4}\left(1 + C\begin{bmatrix}\boldsymbol{b_k}+\boldsymbol{x}\\ \boldsymbol{z_3}\end{bmatrix}\right)\left(1 - C\begin{bmatrix}\boldsymbol{b_k}+\boldsymbol{x}\\ \boldsymbol{z_1}\end{bmatrix}\right) = 1 \tag{6.11}$$

$$\{\bar{\phi}^{7,8}\} \left|\boldsymbol{b_k} + \boldsymbol{x}\right\rangle \text{ survives } \implies \frac{1}{4}\left(1 - C\begin{bmatrix}\boldsymbol{b_k}+\boldsymbol{x}\\ \boldsymbol{z_3}\end{bmatrix}\right)\left(1 + C\begin{bmatrix}\boldsymbol{b_k}+\boldsymbol{x}\\ \boldsymbol{z_1}\end{bmatrix}\right) = 1 \tag{6.12}$$

the Type 0 conditions (6.7) guarantee that $C\left[\begin{smallmatrix}\boldsymbol{b_k}+\boldsymbol{x}\\ \boldsymbol{z_3}\end{smallmatrix}\right] = 1$ and $C\left[\begin{smallmatrix}\boldsymbol{b_k}+\boldsymbol{x}\\ \boldsymbol{z_1}\end{smallmatrix}\right] = 1$ and thus the first case survives.

Finally, let us show that the bosonic sector $\boldsymbol{x}$ survives. In order to make this sector massless there must be a left moving oscillator, which could make it a gauge boson if this oscillator is ψ^μ. However, since for Type 0 models $C\left[\begin{smallmatrix}\boldsymbol{x}\\ \boldsymbol{S}\end{smallmatrix}\right] = 1$ only the states of the type $\{y^i/w^i\}_{1/2}\left|\boldsymbol{x}\right\rangle$ can survive, which they must do due to $C\left[\begin{smallmatrix}\boldsymbol{x}\\ \boldsymbol{z_1}\end{smallmatrix}\right] = C\left[\begin{smallmatrix}\boldsymbol{x}\\ \boldsymbol{z_3}\end{smallmatrix}\right] = 1$.

For the $\boldsymbol{z_1}$ massless sector the conditions for Type 0 models necessitate that states of the type $\{y/w\}\{\bar{y}/\bar{w}\}\left|\boldsymbol{z_1}\right\rangle$ and extra gauge bosons of the type $\{\psi^\mu\}\{\bar{\phi}^{5,6,7,8}\}\left|\boldsymbol{z_1}\right\rangle$ survive. Similarly for the $\boldsymbol{z_3}$ massless sector Type 0 models must have states of the type $\{y/w\}\{\bar{y}/\bar{w}\}\left|\boldsymbol{z_3}\right\rangle$ and extra gauge bosons of the type $\{\psi^\mu\}\{\bar{\phi}^{3,4,5,6}\}\left|\boldsymbol{z_3}\right\rangle$. Finally, for the $\boldsymbol{z_4}$ massless sector Type 0 models must have states of the type $\{y/w\}\{\bar{y}/\bar{w}\}\left|\boldsymbol{z_4}\right\rangle$ and extra gauge bosons of the type $\{\psi^\mu\}\{\bar{\phi}^{1,2,5,6}\}\left|\boldsymbol{z_4}\right\rangle$. Therefore, all Type 0 models derived from this basis (6.1) have a hidden sector enhancement of $SU(2)^4 \to SO(16)$.

Therefore, this analysis tells us that all 4096 possible Type 0 models contain all bosonic sectors 6.6 with the specific set of oscillators given above. In other words, their massless spectra are identical. Doing the counting of all the bosonic states can be shown to give 4264, which is thus the constant term in the q-expansion of the partition function in all 4096 cases. Having seen how restrictive the Type 0 conditions 6.7 are at the massless level it makes sense to analyse what happens with the tachyonic sectors.

Tachyon analysis for Type 0 vacua

The tachyonic sectors for models derived from the basis (6.1) come from the sectors $\left|\boldsymbol{z_1}\right\rangle$, $\left|\boldsymbol{z_3}\right\rangle$ and $\left|\boldsymbol{z_4}\right\rangle$ as well as the untwisted tachyon of the NS sector. We can immediately see that all vacua in this basis will contain an untwisted tachyon $\{\bar{\phi}^{5,6}\}\left|0\right\rangle_{NS}$. This can be seen as being related to the absence of $\boldsymbol{z_2} = \{\bar{\phi}^{5,6,7,8}\}$ in the basis which

would allow for the projection of this tachyon since we would be equipped with the GGSO projection with the phase $C[^{NS}_{\boldsymbol{z_2}}] = 1$.

In regard to the tachyons from the sectors $|\boldsymbol{z_1}\rangle$, $|\boldsymbol{z_3}\rangle$ and $|\boldsymbol{z_4}\rangle$, we see that the Type 0 conditions (6.7) necessitate their presence. For example, all phases that could project the $\boldsymbol{z_1}$ tachyon: $C[^{\boldsymbol{z_1}}_{\boldsymbol{b_1}}], C[^{\boldsymbol{z_1}}_{\boldsymbol{b_2}}], C[^{\boldsymbol{z_1}}_{\boldsymbol{b_3}}], C[^{\boldsymbol{z_1}}_{\boldsymbol{x}}]$ are all equal to +1 and thus leave it in the Hilbert space. Therefore, we conclude that all Type 0 in this construction contain the tachyons from the sectors $|\boldsymbol{z_1}\rangle$, $|\boldsymbol{z_3}\rangle$ and $|\boldsymbol{z_4}\rangle$, along with the model-independent untwisted tachyon $\bar{\phi}^{5,6}\,|0\rangle_{NS}$.

Equivalence of Type 0 models

Having shown that the massless spectrum and tachyonic sectors are identical for all the 4096 choices of GGSO phases consistent with the Type 0 conditions (6.7), we might wonder whether these models are in fact identical at all mass levels. Calculating the partition function for all 4096 Type 0 models proved that they indeed all have the same partition function

$$Z = 2\bar{q}^{-1} + 16q^{-1/2}\bar{q}^{-1/2} + 4264 + 45056q^{1/4}\bar{q}^{1/4} + \cdots \tag{6.13}$$

and thus there is only one Type 0 model in our construction with degeneracy 4096. This is a good example of the non-uniqueness of models in the free fermionic construction mentioned in Section 3.3. In this case we see that the partition function is invariant under the 12 phases: $C[^{\mathbb{1}}_{\tilde{\boldsymbol{S}}}]$, $C[^{\mathbb{1}}_{\boldsymbol{b_1}}]$, $C[^{\mathbb{1}}_{\boldsymbol{b_2}}]$, $C[^{\mathbb{1}}_{\boldsymbol{b_3}}]$, $C[^{\mathbb{1}}_{\boldsymbol{z_1}}]$, $C[^{\tilde{\boldsymbol{S}}}_{\boldsymbol{b_2}}]$, $C[^{\tilde{\boldsymbol{S}}}_{\boldsymbol{b_3}}]$, $C[^{\tilde{\boldsymbol{S}}}_{\boldsymbol{z_1}}]$, $C[^{\boldsymbol{b_1}}_{\boldsymbol{b_2}}]$, $C[^{\boldsymbol{x}}_{\boldsymbol{b_1}}]$, $C[^{\boldsymbol{x}}_{\boldsymbol{b_2}}]$, $C[^{\boldsymbol{x}}_{\boldsymbol{b_3}}]$. This result will ultimately be related to the many symmetries underlying models defined by the basis (6.1).

6.1.3 Classification of Type 0 $\tilde{S}$-Models

Having found that Type 0, tachyonic models exist for the simple basis (6.1), we can consider a more general basis

$$\begin{aligned}
\mathbb{1} &= \{\psi^{\mu},\ \chi^{1,\ldots,6}, y^{1,\ldots,6}, w^{1,\ldots,6} \mid \overline{y}^{1,\ldots,6}, \overline{w}^{1,\ldots,6}, \overline{\psi}^{1,\ldots,5}, \overline{\eta}^{1,2,3}, \overline{\phi}^{1,\ldots,8}\},\\
\tilde{\boldsymbol{S}} &= \{\psi^{\mu}, \chi^{1,\ldots,6} \mid \overline{\phi}^{3,4,5,6}\},\\
\boldsymbol{T_1} &= \{y^{1,2}, w^{1,2} \mid \overline{y}^{1,2}, \overline{w}^{1,2}\},\\
\boldsymbol{T_2} &= \{y^{3,4}, w^{3,4} \mid \overline{y}^{3,4}, \overline{w}^{3,4}\},\\
\boldsymbol{T_3} &= \{y^{5,6}, w^{5,6} \mid \overline{y}^{5,6}, \overline{w}^{5,6}\},\\
\boldsymbol{b_1} &= \{\chi^{34}, \chi^{56}, y^{34}, y^{56} \mid \overline{y}^{34}, \overline{y}^{56}, \overline{\eta}^{1}, \overline{\psi}^{1,\ldots,5}\},\\
\boldsymbol{b_2} &= \{\chi^{12}, \chi^{56}, y^{12}, w^{56} \mid \overline{y}^{12}, \overline{w}^{56}, \overline{\eta}^{2}, \overline{\psi}^{1,\ldots,5}\},\\
\boldsymbol{b_3} &= \{\chi^{12}, \chi^{34}, w^{12}, w^{34} \mid \overline{w}^{12}, \overline{w}^{34}, \overline{\eta}^{3}, \overline{\psi}^{1,\ldots,5}\},\\
\boldsymbol{z_1} &= \{\overline{\phi}^{1,\ldots,4}\},
\end{aligned} \tag{6.14}$$

where the $\boldsymbol{T_i}$, $i = 1,2,3$ allow for internal symmetric shifts in the compactified coordinates around the 3 tori. The only other difference to the basis (6.1) is that $\boldsymbol{x}$ is now a linear combination:

$$\boldsymbol{x} = \boldsymbol{b_1} + \boldsymbol{b_2} + \boldsymbol{b_3} + \boldsymbol{T_1} + \boldsymbol{T_2} + \boldsymbol{T_3} \tag{6.15}$$

and we have the same combinations $\boldsymbol{z_3} = \mathbb{1} + \tilde{\boldsymbol{S}} + \boldsymbol{b_1} + \boldsymbol{b_2} + \boldsymbol{b_3}$ and $\boldsymbol{z_4} = \boldsymbol{z_3} + \boldsymbol{z_1}$. We can further note that the space of independent GGSO phase configuration is now $2^{36} \sim 6 \times 10^{10}$ for this basis.

The addition of the $\boldsymbol{T_i}$'s has some key consequences in relation to finding tachyon-free Type 0 vacua. It multiplies the number of massless fermionic sectors and also increases the number of ways to project the (fermionic) sectors. Furthermore, we now have 15 tachyonic sectors: $\boldsymbol{z_1}, \boldsymbol{z_3}, \boldsymbol{z_4}, \boldsymbol{T_i}, \boldsymbol{z_1} + \boldsymbol{T_i}, \boldsymbol{z_3} + \boldsymbol{T_i}$ and $\boldsymbol{z_4} + \boldsymbol{T_i}$, $i = 1,2,3$ rather than just the 3 for basis (6.1). We can notice that the model-independent NS tachyon $\{\bar{\phi}^{5,6}\}\,|0\rangle_{NS}$ remains in this construction so the minimal number of tachyons is to only have this tachyon.

Fermionic sector analysis

Using a similar methodology to Section 6.1.2, we wish to analyse the conditions on the projection of all fermionic sectors from these models. Due to the increased size of the space of models from the added complexity of having of $\boldsymbol{T_{i=1,2,3}}$ in the basis, we developed a computer algorithm to scan efficiently over the space of vacua and check for the absence of fermionic massless states. We note that massless fermionic vectorials in these models arise from the sectors

$$\begin{aligned} &\tilde{\boldsymbol{S}};\\ &\tilde{\boldsymbol{S}} + \boldsymbol{z_1};\\ &\tilde{\boldsymbol{S}} + \boldsymbol{z_4} \end{aligned} \tag{6.16}$$

and the massless fermionic spinorial sectors from

$$\begin{aligned} &\tilde{\boldsymbol{S}} + \boldsymbol{b_k} + \boldsymbol{b_j} + \boldsymbol{T_k} + p\boldsymbol{T_i} + q\boldsymbol{T_j};\\ &\tilde{\boldsymbol{S}} + \boldsymbol{b_k} + \boldsymbol{b_j} + \boldsymbol{z_1} + \boldsymbol{T_k} + p\boldsymbol{T_i} + q\boldsymbol{T_j};\\ &\tilde{\boldsymbol{S}} + \boldsymbol{b_{1,2,3}} + \boldsymbol{x} + \boldsymbol{z_4};\\ &\tilde{\boldsymbol{S}} + \boldsymbol{z_3}. \end{aligned} \tag{6.17}$$

Our computer algorithm can then be further applied to analyse the tachyonic sectors arising in Type 0 models. The results of this computerised scan are presented in the following section.

$\tilde{S}$ Classification Results

By implementing the projection conditions on the massless fermionic sectors (6.16) and (6.17) in a computer scan we can collect data for the number of fermionic states remaining in the Hilbert space of a model and see how many are Type 0. The distribution of the number of fermionic states for a scan of 10^7 is displayed in Figure 6.1. In this sample we find a total of 24508 which are free of fermionic states.

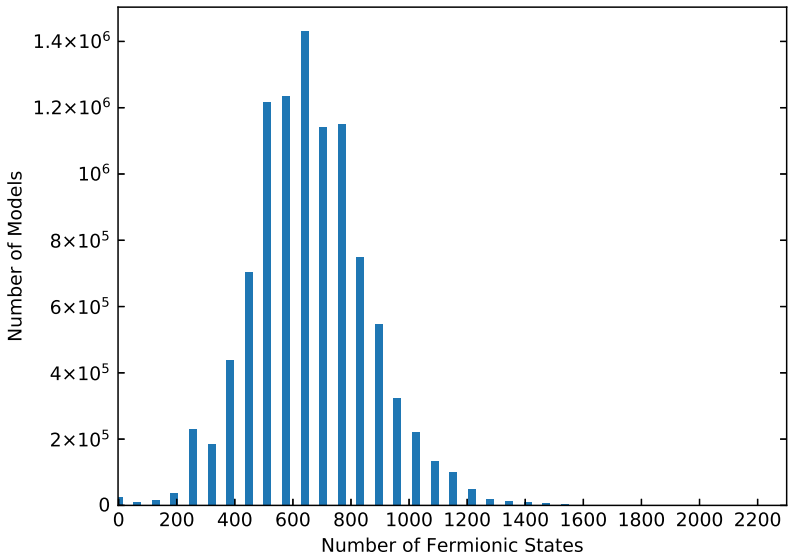

Figure 6.1: *Frequency plot for the number of fermionic states in a model from a sample of* 10^7 *randomly generated GGSO configurations.*

In order to gather a slightly larger sample of Type 0 models in this basis we take a larger sample of 10^8 models which still does not take much computing time. From this sample, we find 245685 Type 0 models which gives a probability $\sim 2.46 \times 10^{-3}$ for Type 0 vacua in the total space. We now wish to classify these Type 0 configurations according to which tachyonic sectors remain in their spectra (along with the model-independent untwisted tachyon), as shown in Table 6.1.

z_k Tachyon	$z_k + T_i$ Tachyon	$\{\bar{\lambda}^a\}\,\|T_i\rangle$ Tachyon	Frequency
0	2	2	42773
1	2	1	33513
1	2	2	19402
1	0	2	17405
1	0	1	17140
1	1	2	12056
0	3	1	11996
3	0	1	7141
0	1	3	6044
3	0	2	5708
1	2	3	5575
1	2	0	5175
1	1	1	5170
1	4	2	5071
0	4	2	5017
0	0	2	4262
0	2	3	4253
1	4	1	4226
3	0	0	3827
0	3	2	3405
0	1	1	3389
1	4	0	3322
1	1	3	2625
1	3	3	2179
0	3	3	1774
0	4	3	1724
3	3	2	1713
1	3	2	1631
3	0	3	1529
3	3	3	1168
1	5	2	913
1	5	3	888
0	4	1	854
1	0	3	840
1	4	3	795
1	6	3	583
0	0	3	308
3	6	3	291

Table 6.1: *Number of tachyonic sectors for 245685 Type 0 $\tilde{\boldsymbol{S}}$-models, where $k = 1, 3, 4$, $i = 1, 2, 3$ and $\bar{\lambda}^a$ is any right-moving oscillator with NS boundary condition.*

These results clearly show that all Type 0 models have both the model-independent untwisted tachyon and some combination of at least 2 twisted tachyonic sectors. One might wonder how general this result is since our sample size of 10^8 only covers about $1 : 687$ models in the total space of GGSO phase configurations. Recalling the 4096 degeneracy factor from the analysis of models in the basis (6.1), we can reasonably suppose that Type 0 models are highly constrained and degenerate also in the current construction where the $T_{i=1,2,3}$ are incorporated in the basis.

To see this, we took 10^4 Type 0 models out from the 245685 total sample and calculated their partition functions and found a total of 109 distinct ones. In Figure 6.2 a comparison between the degeneracy of these 10^4 Type 0 models and those of a random sample of 10^4 models is shown and the number of different Type 0 models are seen to converge fast to just over 100. This shows, just as in the earlier case, that the subspace of Type 0 vacua is highly symmetric. This result strongly justifies the generality of our results from the 10^8 sample for the tachyonic analysis and makes it highly likely that our 245685 Type 0 models from the 10^8 sample captures all such unique models. In Section 6.1.5, we will further discuss the structure of these Type 0 models from the point of view of the partition function and one-loop vacuum energy.

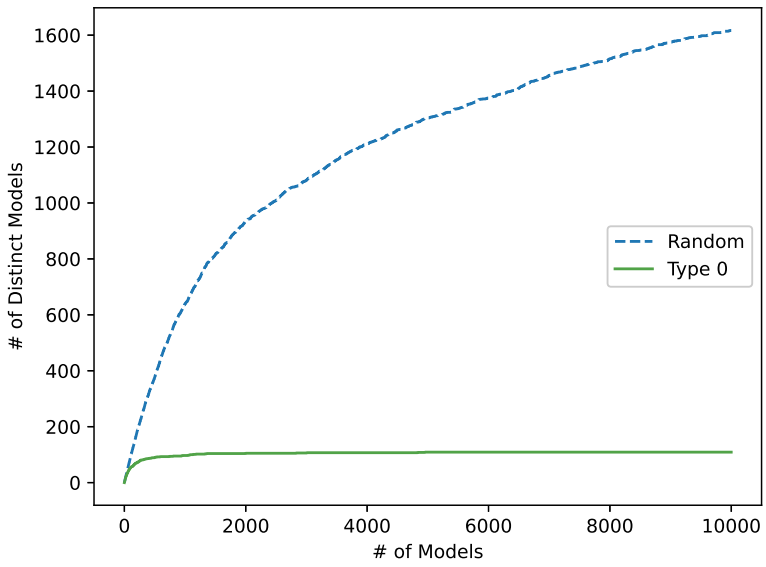

Figure 6.2: *The degeneracy of models for a random sample of models versus Type 0 models for a sample of* 10^4 *models each. We see that the space of Type 0 models is indeed highly degenerate.*

6.1.4 Classification of Type 0 S-Models

Having explored a space of $\tilde{S}$-models in the previous section we now wish to do the same analysis for models deriving from the ten-dimensional $SO(16) \times SO(16)$ non-supersymmetric heterotic string, which we will refer to as S-models since their basis contains the SUSY-generating vector S. The precise basis we use is

$$\begin{aligned}
\mathbb{1} &= \{\psi^\mu,\ \chi^{1,\dots,6}, y^{1,\dots,6}, w^{1,\dots,6} \mid \overline{y}^{1,\dots,6}, \overline{w}^{1,\dots,6}, \overline{\psi}^{1,\dots,5}, \overline{\eta}^{1,2,3}, \overline{\phi}^{1,\dots,8}\},\\
\boldsymbol{S} &= \{\psi^\mu, \chi^{1,\dots,6}\},\\
\boldsymbol{T_1} &= \{y^{1,2}, w^{1,2} \mid \overline{y}^{1,2}, \overline{w}^{1,2}\},\\
\boldsymbol{T_2} &= \{y^{3,4}, w^{3,4} \mid \overline{y}^{3,4}, \overline{w}^{3,4}\},\\
\boldsymbol{T_3} &= \{y^{5,6}, w^{5,6} \mid \overline{y}^{5,6}, \overline{w}^{5,6}\},\\
\boldsymbol{b_1} &= \{\chi^{34}, \chi^{56}, y^{34}, y^{56} \mid \overline{y}^{34}, \overline{y}^{56}, \overline{\eta}^{1}, \overline{\psi}^{1,\dots,5}\},\\
\boldsymbol{b_2} &= \{\chi^{12}, \chi^{56}, y^{12}, y^{56} \mid \overline{y}^{12}, \overline{y}^{56}, \overline{\eta}^{2}, \overline{\psi}^{1,\dots,5}\},\\
\boldsymbol{z_1} &= \{\overline{\phi}^{1,\dots,4}\},\\
\boldsymbol{z_2} &= \{\overline{\phi}^{5,\dots,8}\},
\end{aligned} \tag{6.18}$$

which is in fact identical to that used in ref. [43] and the same as that used in the supersymmetric $SO(10)$ classification of [50, 51] up to the swap $\boldsymbol{T_{1,2,3}} \to \boldsymbol{e_{1,\dots,6}}$. As noted previously, we will make regular use of the important linear combination $\boldsymbol{x}$, which appears as the combination

$$\boldsymbol{x} = \mathbb{1} + \boldsymbol{S} + \sum_{i=1}^{3} \boldsymbol{T_i} + \boldsymbol{z_1} + \boldsymbol{z_2} \tag{6.19}$$

in this basis and we further have the combination $\boldsymbol{b_3} = \boldsymbol{b_1} + \boldsymbol{b_2} + \boldsymbol{x}$ to give the generator of the third orbifold plane.

The untwisted gauge bosons in this construction generate a gauge group of $U(1)^6 \times SO(10) \times U(1)^3 \times SO(8)^2$ and the full space of models is again given by the combinations of modular invariant GGSO phase configurations $2^{36} \sim 6 \times 10^{10}$.

An important difference from the $\tilde{S}$-construction is that we do not have a model-independent tachyon as the NS tachyon is automatically projected. This leaves the door open for possible tachyon-free Type 0 models.

Now we turn to the massless fermionic vectorial sectors which for our S-models arise from

$$\begin{aligned}
&\boldsymbol{S}\\
&\boldsymbol{S} + \boldsymbol{z_1};\\
&\boldsymbol{S} + \boldsymbol{z_2}\\
&\boldsymbol{S} + \boldsymbol{b_k} + \boldsymbol{x} + p\boldsymbol{T_j} + q\boldsymbol{T_k}
\end{aligned} \tag{6.20}$$

and the massless fermionic spinorial sectors from

$$\begin{aligned} &\boldsymbol{S}+\boldsymbol{x}\\ &\boldsymbol{S}+\boldsymbol{z_1}+\boldsymbol{z_2}\\ &\boldsymbol{S}+\boldsymbol{b_k}+p\boldsymbol{T_j}+q\boldsymbol{T_k};\\ &\boldsymbol{S}+\boldsymbol{b_k}+\boldsymbol{z_1}+\boldsymbol{x}+p\boldsymbol{T_j}+q\boldsymbol{T_k};\\ &\boldsymbol{S}+\boldsymbol{b_k}+\boldsymbol{z_2}+\boldsymbol{x}+p\boldsymbol{T_j}+q\boldsymbol{T_k}; \end{aligned} \tag{6.21}$$

where $i \neq j \neq k \in \{1,2,3\}$ and $p,q \in \{0,1\}$. We note that there are more fermionic sectors in this construction than in the $\tilde{\boldsymbol{S}}$ case. In particular, the familiar $\mathbf{16}/\overline{\mathbf{16}}$ of $SO(10)$ from the sectors $\boldsymbol{S}+\boldsymbol{b_k}+p\boldsymbol{T_j}+q\boldsymbol{T_k}$ and vectorial $\mathbf{10}$ of $SO(10)$ from the sectors $(\boldsymbol{S}+)\boldsymbol{b_k}+\boldsymbol{x}+p\boldsymbol{T_j}+q\boldsymbol{T_k}$ appear. However, for the $\tilde{\boldsymbol{S}}$-models they were deliberately chosen to be absent and there are in fact no spinorial fermionic sectors with non-trivial representation under the $SO(10)$ observable gauge group factor.

As in the case of the $\tilde{\boldsymbol{S}}$-models we use a computer algorithm to scan for Type 0 configurations where these fermionic sectors are projected out. The results are presented in the following section.

Results of classification

As in the case of the $\tilde{\boldsymbol{S}}$-models we generate a distribution for the number of fermionic states across a sample of 10^7 randomly generated GGSO phase configurations. This is shown in Figure 6.3. Comparing this to Figure 6.1 for the $\tilde{\boldsymbol{S}}$ case we see a more dense distribution with more possible values for the fermionic states.

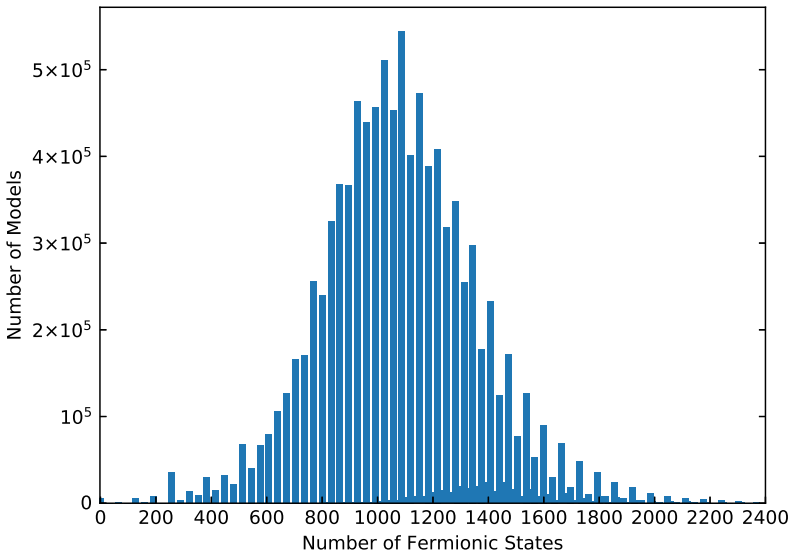

Figure 6.3: *Frequency plot for the number of fermionic states for $\boldsymbol{S}$-models from a random sample of 10^7 GGSO configurations.*

As in the $\tilde{\boldsymbol{S}}$ case we generate a larger sample of Type 0 models by taking a scan of 10^8 GGSO configurations. From this scan we find 54590 Type 0 models which is probability $\sim 5.46 \times 10^{-4}$ which makes them approximately 5 times rarer than in the $\tilde{\boldsymbol{S}}$ case. The likely reason for this and main difference in general between the $\boldsymbol{S}$ case and $\tilde{\boldsymbol{S}}$ case is the already mentioned fact that in the $\boldsymbol{S}$-models we have more fermionic massless sectors to project.

Despite being rarer, we already noted that we do not have any model-independent tachyons for these $\boldsymbol{S}$-models which leaves the possibility of tachyon-free Type 0 vacua open. The data for the numbers of tachyons is shown in Table 6.2 and we see again that no tachyon-free models exist and that the minimal number of tachyonic sectors is 2, which always includes at least 1 vectorial tachyon of the type $\{\bar{\lambda}^a\}\,|\boldsymbol{T_i}\rangle$.

$\boldsymbol{z_k}$ Tachyon	$\boldsymbol{z_k}+\boldsymbol{T_i}$ Tachyon	$\{\bar{\lambda}^a\}\,|\boldsymbol{T_i}\rangle$ Tachyon	Frequency
1	1	2	11605
1	0	2	10471
1	1	1	4431
1	0	3	4388
2	0	2	4066
2	0	1	3749
1	0	1	3363
1	1	3	2384
1	2	2	1870
2	0	3	1509
1	2	3	1318
1	2	1	1080
2	2	1	871
2	2	2	538
0	1	3	488
0	1	2	454
0	2	1	299
1	3	1	291
1	3	2	290
0	0	2	236
1	3	3	189
0	4	3	151
0	2	3	151
0	2	2	135
0	0	3	135
2	4	1	128

Table 6.2: *Number of tachyonic sectors for 54860 Type 0 S-models, where* $k = 1,2$ *and* $i = 1,2,3$.

As in the case of the $\tilde{\boldsymbol{S}}$-models, we observe a degeneracy in the space of Type 0 models and from the sample of 54590 Type 0 $\boldsymbol{S}$-models, we found just 89 independent

partition functions and the same convergence pattern as shown in Figure 6.2, therefore we can confidently claim that the lack of tachyon-free Type 0 models is a generic result in this class of vacua. It is however worth remembering that our models are defined at a free fermionic point in moduli space and so it may be that such tachyonic instabilities may disappear when a model is defined away from the fermionic point.

6.1.5 Misaligned Supersymmetry in Type 0 Models

As discussed in Section 5.5, in non-supersymmetric models, the level-by-level Bose-Fermi cancellation guaranteed from SUSY is not ensured and so such theories in general produce a, often large, non-zero value for the one-loop cosmological constant, Λ. The finiteness of such calculations from the partition function in non-supersymmetric models however traces back to modular invariance and the fascinating phenomenon of misaligned supersymmetry [95, 96, 97, 98, 99]. This mechanism causes the states in the massive tower to oscillate between an excess of bosons and an excess of fermions. This behaviour is referred to as boson-fermion oscillation.

In the case of Type 0 models presented above, due to the presence of on-shell tachyonic states, the partition function diverges. However, this divergence is contained purely in the tachyonic mode, i.e. the degeneracy of states a_{mn} for $m, n > 0$ still behaves in a similar fashion to any other non-tachyonic heterotic theory. This is also emphasised by the presence of misaligned supersymmetry in the massive spectrum of our models. We find that, indeed, both sets of Type 0 models generated by (6.1) and (6.14) exhibit such misalignment of their on-shell massive tower of states. The misalignment pattern appears to have no correlation to whether a specific model has massless fermions or not.

It was proved in [96] that non-SUSY heterotic strings without physical tachyons should always produce such misalignment of their massive spectra. In our case, due to the presence of on-shell tachyons the emergence of misaligned supersymmetry may seem somewhat unexpected and of unknown origin. The analysis presented in the proof of misaligned supersymmetry in [95, 96, 97] relies on modular invariance together with the stated lack of physical tachyons. Since our theory is of course still modular invariant, we can speculate that the emergence of the misalignment should be a consequence of this, however, rigorous analysis is still lacking under these conditions. For the time being, we only present this as an observation for the theories under consideration in this chapter, but further investigation may lead to a deeper understanding of the relationship between on-shell tachyons and misaligned SUSY.

As an example, for the $\tilde{\boldsymbol{S}}$-models of Section 6.1.3 we observe the two general patterns shown in Figure 6.4, or in general a combination of these two.

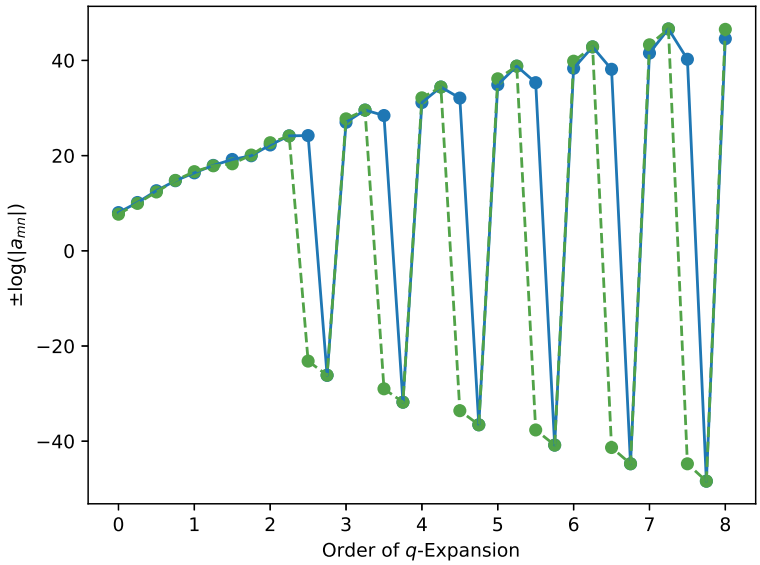

Figure 6.4: *The boson-fermion oscillation of misaligned supersymmetry for the on-shell states of two $\tilde{\boldsymbol{S}}$ models to 8^{th} order in the q-expansion. The overall sign of $\pm\log(|\ a_{mn}\ |)$ is chosen according to the sign of a_{mn}.*

This is true whether or not the choice of GGSO coefficients project all massless fermions. The only observable difference we find for Type 0 models from the partition function point of view is the larger value of a_{00}. This is of course fully expected due to the lack of fermions at the massless level. The misalignment pattern is mostly similar for the $\boldsymbol{S}$-models of Section 6.1.4. It is important to note that, unlike for tachyon-free non-supersymmetric theories, this oscillatory behaviour does not result in a finite value for the cosmological constant due to the presence of the physical tachyons described in Sections 6.1.3 and 6.1.4.

6.2 Type $\overline{\mathbf{0}}$

Having discussed the case of vacua free of massless fermions, we now extend the analysis to the other extreme: tachyon-free heterotic string models that do not contain any twisted bosonic degrees of freedom. In analogy with Type 0 models, we refer to such configurations as Type $\bar{0}$ models. It is apparent that such models contain untwisted bosonic degrees of freedom that correspond to the gravitational, gauge and untwisted scalar fields. However, in the Type $\bar{0}$ configurations that we present all the bosonic degrees of freedom from the twisted sectors of the $\mathbb{Z}_2 \times \mathbb{Z}_2$ orbifold are projected out. As a consequence, one would expect an excess of fermionic over bosonic degrees of freedom at the massless level to potentially generate a positive cosmological constant. Furthermore, in contrast to the Type 0 models that necessarily contains some tachyonic degrees

of freedom, we find that most cases of Type $\bar{0}$ models are free of tachyonic states. We present Type $\bar{0}$ models that belong to the class of $\tilde{\boldsymbol{S}}$-models as well as the class of $\boldsymbol{S}$-models. We also note the existence of a supersymmetric vacuum that does not contain massless twisted bosons that has indeed appeared in previous classifications [50, 51, 59, 67]. In these cases the partition function is vanishing, whereas the Type $\bar{0}$ of interest are those that are not supersymmetric. Though such models are unstable they may still serve as laboratories to explore the possible string dynamics in the early universe. We also remark that in all the Type $\bar{0}$ models that we find there are no spinorial or anti-spinorial representations of the $SO(10)$ GUT group, which is necessarily the case in the supersymmetric $\bar{0}$ configurations.

6.2.1 Type $\mathbb{Z}_2 \times \mathbb{Z}_2$ Heterotic String Orbifold

As in the Type 0 case, the first Type $\bar{0}$ model we found is built off the $\overline{\text{NAHE}}$-set through the basis

$$\begin{aligned}
\mathbb{1} &= \{\psi^\mu,\ \chi^{1,\dots,6}, y^{1,\dots,6}, w^{1,\dots,6} \mid \overline{y}^{1,\dots,6}, \overline{w}^{1,\dots,6}, \overline{\psi}^{1,\dots,5}, \overline{\eta}^{1,2,3}, \overline{\phi}^{1,\dots,8}\},\\
\tilde{\boldsymbol{S}} &= \{\psi^\mu, \chi^{1,\dots,6} \mid \overline{\phi}^{3,4,5,6}\},\\
\boldsymbol{b_1} &= \{\psi^\mu, \chi^{12}, y^{34}, y^{56} \mid \overline{y}^{34}, \overline{y}^{56}, \overline{\eta}^{1}, \overline{\psi}^{1,\dots,5}\},\\
\boldsymbol{b_2} &= \{\psi^\mu, \chi^{34}, y^{12}, w^{56} \mid \overline{y}^{12}, \overline{w}^{56}, \overline{\eta}^{2}, \overline{\psi}^{1,\dots,5}\},\\
\boldsymbol{b_3} &= \{\psi^\mu, \chi^{56}, w^{12}, w^{34} \mid \overline{w}^{12}, \overline{w}^{34}, \overline{\eta}^{3}, \overline{\psi}^{1,\dots,5}\},\\
\boldsymbol{z_1} &= \{\overline{\phi}^{1,\dots,4}\},\\
\boldsymbol{G} &= \{y^{1,\dots,6}, w^{1,\dots,6} \mid \overline{y}^{1,\dots,6}, \overline{w}^{1,\dots,6}\},
\end{aligned} \tag{6.22}$$

and we further define the familiar linear combination

$$\boldsymbol{z_2} = \mathbb{1} + \boldsymbol{b_1} + \boldsymbol{b_2} + \boldsymbol{b_3} + \boldsymbol{z_1} = \{\bar{\phi}^{5,6,7,8}\}. \tag{6.23}$$

A model may then be specified through the assignment of modular invariant GGSO phases $C\binom{v_i}{v_j}$ between the basis vectors. An example Type $\bar{0}$ configuration arises for the GGSO assignment

$$C\begin{bmatrix}\boldsymbol{v_i}\\ \boldsymbol{v_j}\end{bmatrix} = \begin{array}{c} \\ \mathbf{1} \\ \tilde{\boldsymbol{S}} \\ \boldsymbol{b_1} \\ \boldsymbol{b_2} \\ \boldsymbol{b_3} \\ \boldsymbol{z_1} \\ \boldsymbol{G} \end{array} \begin{array}{c} \begin{array}{ccccccc} \mathbf{1} & \tilde{\boldsymbol{S}} & \boldsymbol{b_1} & \boldsymbol{b_2} & \boldsymbol{b_3} & \boldsymbol{z_1} & \boldsymbol{G} \end{array} \\ \begin{pmatrix} 1 & 1 & -1 & -1 & 1 & 1 & 1 \\ 1 & -1 & 1 & -1 & 1 & -1 & -1 \\ -1 & -1 & -1 & 1 & 1 & 1 & -1 \\ -1 & 1 & 1 & -1 & 1 & 1 & -1 \\ 1 & -1 & 1 & 1 & 1 & 1 & 1 \\ 1 & 1 & 1 & 1 & 1 & 1 & -1 \\ 1 & -1 & -1 & -1 & 1 & -1 & -1 \end{pmatrix} \end{array} \tag{6.24}$$

The model is free of (on-shell) tachyons and the gauge group is given by the model-independent contribution from the NS (untwisted) sector giving the vector bosons of $SO(10) \times U(1)^3 \times SO(4)^3 \times SU(2)^8$, as well as additional scalars from the $\{\lambda^a\}\{\bar{\lambda}^b\}\,|\boldsymbol{z_k}\rangle$, $k = 1,2$ and λ^a is some left-moving oscillator not equal to ψ^μ and $\bar{\lambda}^b$ is any right-moving oscillator with NS boundary conditions in $\boldsymbol{z_k}$. These additional scalars arise in the untwisted sector necessarily to give the scalar moduli degrees of freedom. There are additional gauge bosons arising from the presence of $\psi^\mu\,|\boldsymbol{z_1}+\boldsymbol{z_2}\rangle$ in the massless spectrum, which induces a gauge enhancement leaving the full gauge group of the model

$$SO(10) \times U(1)^3 \times SO(4)^3 \times SO(8)^2. \tag{6.25}$$

Apart from these untwisted sector gauge bosons and scalars though, the massless spectrum contains exclusively fermionic states, as advertised for a Type $\bar{0}$ configuration. These fermionic sectors are

$$\begin{aligned}
&\boldsymbol{\tilde{S}},\ \ \boldsymbol{\tilde{S}}+\boldsymbol{z_1},\ \ \boldsymbol{\tilde{S}}+\boldsymbol{z_1}+\boldsymbol{z_2},\ \ \boldsymbol{\tilde{S}}+\boldsymbol{z_2},\\
&\boldsymbol{b_1}+\boldsymbol{b_2}+\boldsymbol{b_3}+\boldsymbol{G},\\
&\boldsymbol{\tilde{S}}+\boldsymbol{b_i}+\boldsymbol{b_j}+\boldsymbol{G},\\
&\boldsymbol{\tilde{S}}+\boldsymbol{b_i}+\boldsymbol{b_j}+\boldsymbol{z_1}+\boldsymbol{G},\\
&\mathbb{1}+\boldsymbol{\tilde{S}}+\boldsymbol{b_i}+\boldsymbol{G},\\
&\mathbb{1}+\boldsymbol{\tilde{S}}+\boldsymbol{b_i}+\boldsymbol{z_1}+\boldsymbol{G},
\end{aligned} \tag{6.26}$$

where $i \neq j \in \{1,2,3\}$. This is notably all the possible fermionic massless sectors except $\boldsymbol{b_{1,2,3}}$ which generate the $\mathbf{16}/\overline{\mathbf{16}}$ of $SO(10)$.

Within the class of models with the minimal basis (6.22), possible twisted bosons may arise from the vectorial sectors

$$\begin{aligned}
\boldsymbol{V}^1 &= \boldsymbol{b_2}+\boldsymbol{b_3}+\boldsymbol{G},\\
\boldsymbol{V}^2 &= \boldsymbol{b_1}+\boldsymbol{b_3}+\boldsymbol{G},\\
\boldsymbol{V}^3 &= \boldsymbol{b_1}+\boldsymbol{b_2}+\boldsymbol{G},
\end{aligned} \tag{6.27}$$

which come with a right-moving oscillator, and the fermionic spinorial sectors

$$\begin{aligned}
\boldsymbol{B}^1 &= \boldsymbol{b_2}+\boldsymbol{b_3}+\boldsymbol{z_1}+\boldsymbol{G},\\
\boldsymbol{B}^2 &= \boldsymbol{b_1}+\boldsymbol{b_3}+\boldsymbol{z_1}+\boldsymbol{G},\\
\boldsymbol{B}^3 &= \boldsymbol{b_1}+\boldsymbol{b_2}+\boldsymbol{z_1}+\boldsymbol{G},\\
\boldsymbol{B}^4 &= \mathbb{1}+\boldsymbol{b_1}+\boldsymbol{z_1}+\boldsymbol{G},\\
\boldsymbol{B}^5 &= \mathbb{1}+\boldsymbol{b_2}+\boldsymbol{z_1}+\boldsymbol{G},\\
\boldsymbol{B}^6 &= \mathbb{1}+\boldsymbol{b_3}+\boldsymbol{z_1}+\boldsymbol{G}.
\end{aligned} \tag{6.28}$$

As we did in the Type 0 case we can use the GGSO projections to derive the conditions on the GGSO phases in order to realise Type $\bar{0}$ configurations. Doing these trivial calculations gives the following conditions for the Type $\bar{0}$ string vacua

$$C\begin{bmatrix}\boldsymbol{z_1}\\ \boldsymbol{b_1}\end{bmatrix} = C\begin{bmatrix}\boldsymbol{z_1}\\ \boldsymbol{b_2}\end{bmatrix} = C\begin{bmatrix}\boldsymbol{z_1}\\ \boldsymbol{b_3}\end{bmatrix} = 1, \quad C\begin{bmatrix}\boldsymbol{z_1}\\ \boldsymbol{G}\end{bmatrix} = -1, \tag{6.29}$$

$$C\begin{bmatrix}\boldsymbol{b_1}\\ \boldsymbol{b_2}\end{bmatrix} = C\begin{bmatrix}\boldsymbol{b_1}\\ \boldsymbol{b_3}\end{bmatrix}, \quad C\begin{bmatrix}\boldsymbol{b_2}\\ \boldsymbol{b_3}\end{bmatrix} = C\begin{bmatrix}\boldsymbol{b_1}\\ \boldsymbol{b_3}\end{bmatrix}, \tag{6.30}$$

$$C\begin{bmatrix}\mathbb{1}\\ \boldsymbol{G}\end{bmatrix} = C\begin{bmatrix}\boldsymbol{b_1}\\ \boldsymbol{G}\end{bmatrix} C\begin{bmatrix}\boldsymbol{b_2}\\ \boldsymbol{G}\end{bmatrix} C\begin{bmatrix}\boldsymbol{b_3}\\ \boldsymbol{G}\end{bmatrix}. \tag{6.31}$$

Therefore we see that 7 GGSO phases are fixed and we have 14 free phases. In the Type 0 case in Section 6.1.2 we saw there were 12 free phases giving $2^{12} = 4096$ versions of a single unique Type 0 partition function. To check whether we have 2^{14} versions of a unique partition function or not in our Type $\bar{0}$ case we can analyse the partition function. Calculating this partition function for the $2^{14} = 16384$ Type $\bar{0}$ configurations we find that they all share the partition function

$$Z = 2\,q^0\bar{q}^{-1} - 728\,q^0\bar{q}^0 + 288\,q^{1/2}\bar{q}^{-1/2} + 1088\,q^{-1/2}\bar{q}^{1/2} + 38400\,q^{1/2}\bar{q}^{1/2} + \cdots, \tag{6.32}$$

and so are, indeed, the same model. We note that there are no on-shell tachyons and the absence of twisted bosons ensures a large negative contribution at the massless level $N_b^0 - N_f^0 = -728$. We can calculate the cosmological constant now for this unique case. Due to the abundance of fermionic states compared to bosonic ones, we expect a positive cosmological constant, and performing the modular integral using standard techniques we, indeed, find

$$\Lambda = 238.38 \times \mathcal{M}^4. \tag{6.33}$$

As we discussed for Type 0 models, all Type $\bar{0}$ models we present exhibit a form of misaligned supersymmetry, meaning that the boson-fermion degeneracies oscillate while ascending through the massive states.

6.2.2 Generalised Type $\bar{0}$ $\tilde{S}$-models

In order to do a more general search for Type $\bar{0}$ models we can generalise from the basis (6.22) to

$$\begin{aligned}
\mathbb{1} &= \{\psi^\mu,\ \chi^{1,\dots,6}, y^{1,\dots,6}, w^{1,\dots,6} \mid \overline{y}^{1,\dots,6}, \overline{w}^{1,\dots,6}, \overline{\psi}^{1,\dots,5}, \overline{\eta}^{1,2,3}, \overline{\phi}^{1,\dots,8}\},\\
\tilde{\boldsymbol{S}} &= \{\psi^\mu, \chi^{1,\dots,6} \mid \overline{\phi}^{3,4,5,6}\},\\
\boldsymbol{T_1} &= \{y^{1,2}, w^{1,2} \mid \overline{y}^{1,2}, \overline{w}^{1,2}\},\\
\boldsymbol{T_2} &= \{y^{3,4}, w^{3,4} \mid \overline{y}^{3,4}, \overline{w}^{3,4}\},\\
\boldsymbol{T_3} &= \{y^{5,6}, w^{5,6} \mid \overline{y}^{5,6}, \overline{w}^{5,6}\},\\
\boldsymbol{b_1} &= \{\psi^\mu, \chi^{12}, y^{34}, y^{56} \mid \overline{y}^{34}, \overline{y}^{56}, \overline{\eta}^1, \overline{\psi}^{1,\dots,5}\},\\
\boldsymbol{b_2} &= \{\psi^\mu, \chi^{34}, y^{12}, w^{56} \mid \overline{y}^{12}, \overline{w}^{56}, \overline{\eta}^2, \overline{\psi}^{1,\dots,5}\},\\
\boldsymbol{b_3} &= \{\psi^\mu, \chi^{56}, w^{12}, w^{34} \mid \overline{w}^{12}, \overline{w}^{34}, \overline{\eta}^3, \overline{\psi}^{1,\dots,5}\},\\
\boldsymbol{z_1} &= \{\overline{\phi}^{1,\dots,4}\},
\end{aligned} \tag{6.34}$$

where introducing $\boldsymbol{T_i}$, $i = 1,2,3$ allows for internal symmetric shifts around the 3 internal T^2 tori. Since we have 9 basis vectors there are $2^{9(9-1)/2} = 2^{36} \sim 6.87 \times 10^{10}$ independent GGSO phase configurations.

The bosonic sectors that need projecting in this basis are similar to (6.27), up to allowing for the shifts induced by $\boldsymbol{T_i}$. Explicitly, there are 15 vectorial bosonic sectors

$$\begin{aligned}
\boldsymbol{V}^1_{pq} &= \boldsymbol{b_2} + \boldsymbol{b_3} + \boldsymbol{T_1} + p\boldsymbol{T_2} + q\boldsymbol{T_3},\\
\boldsymbol{V}^2_{pq} &= \boldsymbol{b_1} + \boldsymbol{b_3} + \boldsymbol{T_2} + p\boldsymbol{T_1} + q\boldsymbol{T_3},\\
\boldsymbol{V}^3_{pq} &= \boldsymbol{b_1} + \boldsymbol{b_2} + \boldsymbol{T_3} + p\boldsymbol{T_1} + q\boldsymbol{T_2},\\
\boldsymbol{V}^4 &= \boldsymbol{T_1} + \boldsymbol{T_2},\\
\boldsymbol{V}^5 &= \boldsymbol{T_1} + \boldsymbol{T_3},\\
\boldsymbol{V}^6 &= \boldsymbol{T_2} + \boldsymbol{T_3},
\end{aligned} \tag{6.35}$$

which come with a right-moving oscillator and $p, q = 0, 1$. Additionally, there are 30 fermionic spinorial sectors

$$\begin{aligned}
\boldsymbol{F}^1_{pq} &= \boldsymbol{b_2} + \boldsymbol{b_3} + \boldsymbol{z_1} + \boldsymbol{T_1} + p\boldsymbol{T_2} + q\boldsymbol{T_3}, \\
\boldsymbol{F}^2_{pq} &= \boldsymbol{b_1} + \boldsymbol{b_3} + \boldsymbol{z_1} + \boldsymbol{T_2} + p\boldsymbol{T_1} + q\boldsymbol{T_3}, \\
\boldsymbol{F}^3_{pq} &= \boldsymbol{b_1} + \boldsymbol{b_2} + \boldsymbol{z_1} + \boldsymbol{T_3} + p\boldsymbol{T_1} + q\boldsymbol{T_2}, \\
\boldsymbol{F}^4_{pq} &= \mathbb{1} + \boldsymbol{b_1} + \boldsymbol{z_1} + \boldsymbol{T_1} + p\boldsymbol{T_2} + q\boldsymbol{T_3}, \\
\boldsymbol{F}^5_{pq} &= \mathbb{1} + \boldsymbol{b_2} + \boldsymbol{z_1} + \boldsymbol{T_2} + p\boldsymbol{T_1} + q\boldsymbol{T_3}, \\
\boldsymbol{F}^6_{pq} &= \mathbb{1} + \boldsymbol{b_3} + \boldsymbol{z_1} + \boldsymbol{T_3} + p\boldsymbol{T_1} + q\boldsymbol{T_2}, \\
\boldsymbol{F}^7 &= \boldsymbol{T_1} + \boldsymbol{T_2} + \boldsymbol{z_1}, \\
\boldsymbol{F}^8 &= \boldsymbol{T_1} + \boldsymbol{T_3} + \boldsymbol{z_1}, \\
\boldsymbol{F}^9 &= \boldsymbol{T_2} + \boldsymbol{T_3} + \boldsymbol{z_1}, \\
\boldsymbol{F}^{10} &= \boldsymbol{T_1} + \boldsymbol{T_2} + \boldsymbol{z_2}, \\
\boldsymbol{F}^{11} &= \boldsymbol{T_1} + \boldsymbol{T_3} + \boldsymbol{z_2}, \\
\boldsymbol{F}^{12} &= \boldsymbol{T_2} + \boldsymbol{T_3} + \boldsymbol{z_2}.
\end{aligned} \tag{6.36}$$

Implementing the GGSO projection conditions on all the sectors and scanning over 10^8 random GGSO phase configurations results in uncovering 5676 Type $\bar{0}$ configurations that correspond to just two distinct tachyon-free models and two distinct tachyonic models. The first tachyon-free model has partition function

$$Z = 2\,q^0\bar{q}^{-1} - 440\,q^0\bar{q}^0 + 32\,q^{1/4}\bar{q}^{-3/4} - 6080\,q^{1/4}\bar{q}^{1/4} + \cdots, \tag{6.37}$$

and cosmological constant

$$\Lambda = 213.27 \times \mathcal{M}^4. \tag{6.38}$$

Whereas the second tachyon-free model has partition function

$$Z = 2\,q^0\bar{q}^{-1} - 504\,q^0\bar{q}^0 + 48\,q^{1/4}\bar{q}^{-3/4} - 12192\,q^{1/4}\bar{q}^{1/4} + \cdots, \tag{6.39}$$

and cosmological constant

$$\Lambda = 278.60 \times \mathcal{M}^4. \tag{6.40}$$

Both models contain the same gauge boson enhancement and additional scalars from the sectors $\boldsymbol{z_1}$, $\boldsymbol{z_2}$ and $\boldsymbol{z_1} + \boldsymbol{z_2}$ as in case with minimal basis (6.22). Other than these untwisted bosons the two models contain only twisted fermionic states in their massless spectra, as required for Type $\bar{0}$ configurations.

Regarding the two tachyonic models, we have one model with partition function

$$Z = 2\,q^0\bar{q}^{-1} + 32q^{-1/4}\bar{q}^{-1/4} - 1016\,q^0\bar{q}^0 + 4096\,q^{1/4}\bar{q}^{1/4} + \cdots, \tag{6.41}$$

which has 32 tachyonic states and one with partition function

$$Z = 2\,q^0\bar{q}^{-1} + 48\,q^{-1/4}\bar{q}^{-1/4} - 1272\,q^0\bar{q}^0 + 5120\,q^{1/4}\bar{q}^{1/4} + \cdots, \tag{6.42}$$

which has 48 tachyonic states.

6.2.3 Generalised Type $\bar{0}$ S-models

We can now do a similar exploration of Type $\bar{0}$ models within a class of models which include the SUSY generating basis vector $\boldsymbol{S}$. We employ a very familiar choice of $SO(10)$ basis

$$\begin{aligned}
\mathbb{1} &= \{\psi^\mu,\ \chi^{1,\ldots,6}, y^{1,\ldots,6}, w^{1,\ldots,6} \mid \overline{y}^{1,\ldots,6}, \overline{w}^{1,\ldots,6}, \overline{\psi}^{1,\ldots,5}, \overline{\eta}^{1,2,3}, \overline{\phi}^{1,\ldots,8}\},\\
\boldsymbol{S} &= \{\psi^\mu, \chi^{1,\ldots,6}\},\\
\boldsymbol{T_1} &= \{y^{1,2}, w^{1,2} \mid \overline{y}^{1,2}, \overline{w}^{1,2}\},\\
\boldsymbol{T_2} &= \{y^{3,4}, w^{3,4} \mid \overline{y}^{3,4}, \overline{w}^{3,4}\},\\
\boldsymbol{T_3} &= \{y^{5,6}, w^{5,6} \mid \overline{y}^{5,6}, \overline{w}^{5,6}\},\\
\boldsymbol{b_1} &= \{\chi^{3,4,5,6}, y^{34}, y^{56} \mid \overline{y}^{34}, \overline{y}^{56}, \overline{\eta}^1, \overline{\psi}^{1,\ldots,5}\},\\
\boldsymbol{b_2} &= \{\chi^{1,2,5,6}, y^{12}, y^{56} \mid \overline{y}^{12}, \overline{y}^{56}, \overline{\eta}^2, \overline{\psi}^{1,\ldots,5}\},\\
\boldsymbol{z_1} &= \{\overline{\phi}^{1,\ldots,4}\},\\
\boldsymbol{z_2} &= \{\overline{\phi}^{5,\ldots,8}\},
\end{aligned} \tag{6.43}$$

which is exactly the same as that used to classify non-SUSY string models in ref. [43]. We will note the important linear combination in this basis

$$\boldsymbol{x} = \mathbb{1} + \boldsymbol{S} + \sum_{i=1,2,3} \boldsymbol{T_i} + \sum_{k=1,2} \boldsymbol{z_k}, \tag{6.44}$$

and then have the combination $\boldsymbol{b_3} = \boldsymbol{b_1} + \boldsymbol{b_2} + \boldsymbol{x}$. As in the $\tilde{\boldsymbol{S}}$-models we have 9 basis vectors and so the number of independent GGSO phase configurations is $2^{9(9-1)/2} = 2^{36} \sim 6.87 \times 10^{10}$.

A key difference between this basis and the basis (6.34) is that there exists a supersymmetric subspace of the full space for certain choices of GGSO phase. In particular, the $\boldsymbol{S}$ sector generates supersymmetry

$$C\begin{bmatrix}\boldsymbol{S}\\ \mathbb{1}\end{bmatrix} = C\begin{bmatrix}\boldsymbol{S}\\ \boldsymbol{T_i}\end{bmatrix} = C\begin{bmatrix}\boldsymbol{S}\\ \boldsymbol{b_j}\end{bmatrix} = C\begin{bmatrix}\boldsymbol{S}\\ \boldsymbol{z_k}\end{bmatrix} = -1, \qquad i = 1,2,3 \text{ and } j,k = 1,2 \tag{6.45}$$

which, furthermore, automatically ensures the projection of tachyonic sectors through the $\boldsymbol{S}$ GGSO projection.

Now we turn to the massless bosonic vectorial sectors that arise from

$$\begin{aligned} &\boldsymbol{b_i} + \boldsymbol{x} + p\boldsymbol{T_j} + q\boldsymbol{T_k}, \\ &\boldsymbol{T_1} + \boldsymbol{T_2}, \\ &\boldsymbol{T_1} + \boldsymbol{T_3}, \\ &\boldsymbol{T_2} + \boldsymbol{T_3}, \end{aligned} \tag{6.46}$$

and the massless bosonic spinorial sectors from

$$\begin{aligned} &\boldsymbol{b_i} + p\boldsymbol{T_j} + q\boldsymbol{T_k}, \\ &\boldsymbol{b_i} + \boldsymbol{x} + \boldsymbol{z_1} + p\boldsymbol{T_j} + q\boldsymbol{T_k}, \\ &\boldsymbol{b_i} + \boldsymbol{x} + \boldsymbol{z_2} + p\boldsymbol{T_j} + q\boldsymbol{T_k}, \\ &\boldsymbol{T_1} + \boldsymbol{T_2} + \boldsymbol{z_1}, \\ &\boldsymbol{T_1} + \boldsymbol{T_3} + \boldsymbol{z_1}, \\ &\boldsymbol{T_2} + \boldsymbol{T_3} + \boldsymbol{z_1}, \\ &\boldsymbol{T_1} + \boldsymbol{T_2} + \boldsymbol{z_2}, \\ &\boldsymbol{T_1} + \boldsymbol{T_3} + \boldsymbol{z_2}, \\ &\boldsymbol{T_2} + \boldsymbol{T_3} + \boldsymbol{z_2}, \end{aligned} \tag{6.47}$$

where $i \neq j \neq k \in \{1,2,3\}$ and $p, q \in \{0,1\}$.

We can now search for Type $\bar{0}$ GGSO configurations by implementing the conditions for the GGSO projection of all these massless twisted bosonic sectors.

In a random scan of 10^8 independent GGSO phase configurations we found one supersymmetric model which contains a very simple massless spectrum containing the untwisted gauge bosons from the NS sector and its gauginos from the $\boldsymbol{S}$ sector, along with gauge enhancements and additional scalars of some form from $\boldsymbol{z_1}, \boldsymbol{z_2}, \boldsymbol{z_1} + \boldsymbol{z_2}$ and $\boldsymbol{x}$ and their superpartners from $\boldsymbol{S} + \boldsymbol{z_1}, \boldsymbol{S} + \boldsymbol{z_2}, \boldsymbol{S} + \boldsymbol{z_1} + \boldsymbol{z_2}$ and $\boldsymbol{S} + \boldsymbol{x}$, respectively. The other Type $\bar{0}$ models arising in our 10^8 scan are non-supersymmetric.

All the Type $\bar{0}$ models are summarised in Table 6.3 with their partition functions, key characteristics and frequency within the sample delineated. We note that the frequency refers to the number of different GGSO phase configurations corresponding to the same partition function. The projected total number is simply how many we expect in the full space of 2^{36} independent GGSO phase configurations. In principle, the exact constraints on the GGSO phases for each model could be derived and the exact number of each model in the total space deduced.

Partition Function	$\Lambda\,[\mathcal{M}^4]$	Tachyons?	SUSY?	# Models in Sample	Total # Projected
$Z = 0$	0	No	Yes	562	3.86×10^5
$Z = 2\bar{q}^{-1} - 632 + 48q^{1/4}\bar{q}^{-3/4} - 8096q^{1/4}\bar{q}^{1/4} + \cdots$	293.8	No	No	389	2.67×10^5
$Z = 2\bar{q}^{-1} - 120 + 32q^{1/4}\bar{q}^{-3/4} - 6080q^{1/4}\bar{q}^{1/4} + \cdots$	125.6	No	No	284	1.95×10^5
$Z = 2\bar{q}^{-1} - 568 + 32q^{1/4}\bar{q}^{-3/4} - 1984q^{1/4}\bar{q}^{1/4} + \cdots$	223.97	No	No	1163	7.99×10^5
$Z = 2\bar{q}^{-1} - 504 + 32q^{1/4}\bar{q}^{-3/4} + 4128q^{1/4}\bar{q}^{1/4} + \cdots$	158.64	No	No	715	3.91×10^5
$Z = 2\bar{q}^{-1} + 32q^{-1/4}\bar{q}^{-1/4} - 664 + 6144q^{1/4}\bar{q}^{1/4} + \cdots$	∞	Yes	No	287	1.97×10^5
$Z = 2\bar{q}^{-1} + 32q^{-1/4}\bar{q}^{-1/4} - 1272 + 5888^{1/4}\bar{q}^{1/4} + \cdots$	∞	Yes	No	290	1.99×10^5
$Z = 2\bar{q}^{-1} + 32q^{-1/4}\bar{q}^{-1/4} - 632 - 512q^{1/4}\bar{q}^{1/4} + \cdots$	∞	Yes	No	301	2.07×10^5
$Z = 2\bar{q}^{-1} + 32q^{-1/4}\bar{q}^{-1/4} - 1528 + 4608q^{1/4}\bar{q}^{1/4} + \cdots$	∞	Yes	No	429	2.95×10^5
$Z = 2\bar{q}^{-1} + 32q^{-1/4}\bar{q}^{-1/4} - 1528 + 11008q^{1/4}\bar{q}^{1/4} + \cdots$	∞	Yes	No	395	2.71×10^5
$Z = 2\bar{q}^{-1} + 48q^{-1/4}\bar{q}^{-1/4} - 1016 - 1792q^{1/4}\bar{q}^{1/4} + \cdots$	∞	Yes	No	155	1.07×10^5
$Z = 2\bar{q}^{-1} + 144q^{-1/4}\bar{q}^{-1/4} - 504 + 9472^{1/4}\bar{q}^{1/4} + \cdots$	∞	Yes	No	153	1.05×10^5

Table 6.3: *Summary of Type $\bar{0}$ models arising from the basis (6.43). The cosmological constant Λ is expressed in units of $\mathcal{M}^4$.*

6.3 Discussion

In this chapter we explored the existence of two contrasting novel vacua. The case of Type 0 models have been of interest in other string theory limits, *e.g.* the issue of tree level stability has been studied in the framework of Type II orientifolds, whereas other authors have advocated that there is holographic duality of the Type 0B string theory and four dimensional non-supersymmetric Yang-Mills theory [117, 118]. In our framework we demonstrated the existence of Type 0 $\mathbb{Z}_2 \times \mathbb{Z}_2$ heterotic string orbifolds with a large degree of redundancy in the space of GGSO projection coefficients. We showed that these Type 0 models all contain physical tachyons at the free fermionic point in the moduli space. These vacua are therefore necessarily unstable. We further demonstrated the existence of misaligned supersymmetry in the Type 0 models that guarantee the finiteness of the one-loop amplitude, aside from the divergence due to the tachyonic states.

The second novel vacua we studied were the Type $\bar{0}$. While our findings at this

stage should be regarded as mere curiosities, it is plausible that they may have some relevance to studying string dynamics in the early universe. We have also found that in all the Type $\bar{0}$ models, there are no spinorial or anti-spinorial representations of the $SO(10)$ GUT group. The non-supersymmetric $\bar{0}$ configurations may therefore be interpreted as supersymmetric $\bar{0}$ models, in which supersymmetry is maximally violated. A feature that may be explored by studying the interpolations between the two cases.

Chapter 7

Satisfiability Modulo Theories and an Application to Free Fermionic Model Building

In this chapter we introduce the powerful SAT/SMT solvers into the analysis of free fermionic string vacua from the $\mathbb{Z}_2 \times \mathbb{Z}_2$ orbifold. The work in this chapter is taken from ref. [10].

We will begin by explaining the background of SAT and SMT solvers and demonstrate how to implement constraints from the free fermionic classification into a form optimised for SAT/SMT methods. To this end, the classes of Type 0 and Type $\bar{0}$ vacua studied in Chapter 6 will be an excellent testing ground for these sophisticated computing methods. Not only were these constructions relatively simple (few basis vectors), we also saw how certain characteristics of models were often correlated or in contradiction. For example, in the Type 0 case we saw how these models necessarily contained tachyons, meanwhile in the Type $\bar{0}$ case we saw how the presence of observable spinorial sectors contradicted the Type $\bar{0}$ condition. In this chapter we will focus on this latter issue and test the efficiency of reducing the problem of finding tachyon-free Type $\bar{0}$ models, of the sort found in Chapter 6, to SAT or SMT. This setting will allow the SAT/SMT solver to essentially produce a no-go theorem for Type $\bar{0}$ models with fermion generations by returning an unsatisfiable constraint system with a proof.

7.1 SMT and SAT

Satisfiability Modulo Theories (SMTs) are powerful algorithms used for deciding whether a set of constraints describing a problem is satisfiable. In other words, SMTs determine whether there exists a 'satisfying assignment' of a set of input variables to a system of constraints. These constraint formulae are constructed by defining operations over, what are referred to as, theory variables, and combining them with logical

connectives. SMT problems are more expressive and powerful than the Boolean Satisfiability (SAT) problems that restrict all variables to be true or false and operators to be logical connectives. This is to say that SMTs allow for operations over non-Boolean types such as integers, reals, bitvectors, and arrays. Both SMT and SAT are canonical NP-complete problems [119, 120], which is a class of computational problems for which checking whether a given variable assignment satisfies the constraints can be done in polynomial time, but finding such an assignment is believed to be hard. Despite a lot of effort, no polynomial time algorithm was shown for any NP-complete problem since the class was defined in 1971. More than that, a widely believed conjecture [121] states that in the worst-case one cannot significantly improve over an exhaustive search of all possible assignments. Nevertheless, there has been tremendous progress over the last decades in efficiency of algorithms solving these problems in practice, solving instances with hundreds and even thousands of variables, which shows that truly hard instances are few and far between.

A key aspect of how SMT-solvers work so effectively is through following the DPLL or conflict-driven clause learning (CDCL) class of algorithms. These algorithms implement a decision procedure for each theory by adding or subtracting constraints and querying for satisfiability as it goes. More detail on DPLL(T) and other decision procedures may be found in ref. [122], for example.

One of the most efficient and easy to use SMT solvers is Z3[1]. Z3 was developed by Microsoft primarily for software verification purposes. It also implements an efficient SAT solver that we use for the Boolean encoding of our problem. It has bindings for most common programming languages and in our case we used the Python front-end as a means of interfacing with Z3.

7.2 SMTs and Free Fermionic Classification

It is a great advantage of the free fermionic construction that phenomenological constraints reduce to elementary algebraic expressions in terms of the GGSO phases $C[^{v_i}_{v_j}]$, which are binary inputs. Therefore the reduction to Boolean expressions is almost immediate but it is worthwhile giving some details on how to perform this reduction before we go on to a specific application.

7.2.1 Boolean Reduction

In the classification program of free fermionic models outlined in Chapter 4, phenomenological criteria are typically constructed through selection rules on certain sectors. Typically these are massless sectors or, for non-supersymmetric models, the on-shell tachyonic sectors when ensuring that the models are tachyon-free. Depending on the mass formulae (3.35), the level-matching condition may necessitate that there are

[1]This can be accessed open source on Github at https://github.com/Z3Prover/Z3

left-moving oscillators, λ, or right-moving oscillators, $\bar{\lambda}$, acting on the ket vector of the sector $\boldsymbol{\alpha}$, which is given by the combined degenerate Ramond vacua of all fermions with $\alpha(f) = 1$ in $\boldsymbol{\alpha}$.

Given a basis, to determine whether a particular sector $\boldsymbol{\alpha}$ survives for a model depends solely on the GGSO phase configuration. In particular, we employ the generalised projectors given through eqs (4.7) and (4.9). The translation of these generalised projector equations that build up to form our phenomenological criteria into a Boolean language ripe for a SAT or SMT solver is immediate. For example, taking a sector with no oscillator with projector of the form (4.7), the condition $\mathbb{P}_{\boldsymbol{\alpha}} = 0$ can be translated into a Boolean constraint by taking the set

$$C = \left\{ \delta_{\boldsymbol{\alpha}} C\begin{bmatrix}\boldsymbol{\alpha}\\ \boldsymbol{\xi}_1\end{bmatrix}, ..., \delta_{\boldsymbol{\alpha}} C\begin{bmatrix}\boldsymbol{\alpha}\\ \boldsymbol{\xi}_n\end{bmatrix} \right\}, \tag{7.1}$$

where $\boldsymbol{\xi} \in \Upsilon(\boldsymbol{\alpha})$ with $n = |\Upsilon(\boldsymbol{\alpha})|$. Using eq. (3.30) we can rewrite the phases $C[^{\boldsymbol{\alpha}}_{\boldsymbol{\xi}_i}]$ in terms of a product of basis GGSO phases $C[^{\boldsymbol{v}_i}_{\boldsymbol{v}_j}]$. We then associate to each of these a Boolean. In the case of a real GGSO phase this can be taken to be

$$B_{ij} = \begin{cases} \texttt{True} \quad \text{if } C[^{\boldsymbol{v}_i}_{\boldsymbol{v}_j}] = -1 \\ \texttt{False} \text{ if } C[^{\boldsymbol{v}_i}_{\boldsymbol{v}_j}] = +1, \end{cases} \tag{7.2}$$

where $i, j = 1, ..., N$ such that $N = |\mathcal{B}|$ is the number of basis vectors. Then the product of such basis GGSO phases can be rewritten in Boolean language as an exclusive or, $\veebar$, that returns `True` if there is an odd number of `True` $C[^{\boldsymbol{v}_i}_{\boldsymbol{v}_j}]$'s in the product, and `False` if even. In this way, each entry $\delta_{\boldsymbol{\alpha}} C[^{\boldsymbol{\alpha}}_{\boldsymbol{\xi}_i}]$ of C can be recast as a Boolean clause constructed through the $\veebar$ of basis GGSO phases. There is then the complication of dealing with any imaginary basis GGSO phases. This is easy to resolve by consistently taking $\pm i$ as the binary to assign Boolean values to. Then the set C can be redefined as a set of Boolean clauses.

Once this reduction to Booleans is complete, the constraint $\mathbb{P}_{\boldsymbol{\alpha}} = 0$ from (4.7) is equivalent to imposing

$$\neg(C_1 \wedge ... \wedge C_n). \tag{7.3}$$

where $C_i \in C$, $i = 1, ..., n$. It is precisely this kind of constraint that can be added to a constraint system for an SAT/SMT solver.

In the application studied in this chapter, we search for the absence of twisted bosons at the massless level, which is just a repeated application of this constraint for all massless bosonic sectors.

We note that a phenomenological constraint such as checking for three generations requires a couple of additional steps that need encoding into SMT language. Once again, sectors giving rise to the fermion generations need checking for survival via

$\mathbb{P}_{\boldsymbol{\alpha}} \neq 0$, then additional GGSO projection determining the chirality of the sectors under the relevant observable gauge factors need encoding. This can be done as a natural extension of the projections done in $\mathbb{P}_{\boldsymbol{\alpha}}$. Then, checking for 3 generations can be handled easily through the implementation of a Boolean adder.

7.3 Minimal Tachyon-free $SO(10)$ $\tilde{S}$-models

We will use the basis explored in Section 6.2.2 given by eq. (6.34). For clarity we rewrite this basis here

$$\begin{aligned}
\mathbb{1} &= \{\psi^{\mu},\ \chi^{1,\ldots,6}, y^{1,\ldots,6}, w^{1,\ldots,6} \mid \overline{y}^{1,\ldots,6}, \overline{w}^{1,\ldots,6}, \overline{\psi}^{1,\ldots,5}, \overline{\eta}^{1,2,3}, \overline{\phi}^{1,\ldots,8}\},\\
\tilde{\boldsymbol{S}} &= \{\psi^{\mu}, \chi^{1,\ldots,6} \mid \overline{\phi}^{3,4,5,6}\},\\
\boldsymbol{T_1} &= \{y^{1,2}, w^{1,2} \mid \overline{y}^{1,2}, \overline{w}^{1,2}\},\\
\boldsymbol{T_2} &= \{y^{3,4}, w^{3,4} \mid \overline{y}^{3,4}, \overline{w}^{3,4}\},\\
\boldsymbol{T_3} &= \{y^{5,6}, w^{5,6} \mid \overline{y}^{5,6}, \overline{w}^{5,6}\},\\
\boldsymbol{b_1} &= \{\psi^{\mu}, \chi^{12}, y^{34}, y^{56} \mid \overline{y}^{34}, \overline{y}^{56}, \overline{\eta}^{1}, \overline{\psi}^{1,\ldots,5}\},\\
\boldsymbol{b_2} &= \{\psi^{\mu}, \chi^{34}, y^{12}, w^{56} \mid \overline{y}^{12}, \overline{w}^{56}, \overline{\eta}^{2}, \overline{\psi}^{1,\ldots,5}\},\\
\boldsymbol{b_3} &= \{\psi^{\mu}, \chi^{56}, w^{12}, w^{34} \mid \overline{w}^{12}, \overline{w}^{34}, \overline{\eta}^{3}, \overline{\psi}^{1,\ldots,5}\},\\
\boldsymbol{z_1} &= \{\overline{\phi}^{1,\ldots,4}\}.
\end{aligned} \tag{7.4}$$

We recall that the NS sector vector gauge bosons in these models give rise to a gauge group

$$SO(10) \times U(1)^3 \times SO(4)^3 \times SU(2)^8, \tag{7.5}$$

and may receive additional vector boson enhancements from the sectors

$$\left\{ \begin{array}{c} \psi^{\mu} \left|\boldsymbol{z_1}\right\rangle_L \otimes \{\bar{\lambda}^i\} \left|\boldsymbol{z_1}\right\rangle_R \\ \psi^{\mu} \left|\boldsymbol{z_2}\right\rangle_L \otimes \{\bar{\lambda}^i\} \left|\boldsymbol{z_2}\right\rangle_R \\ \psi^{\mu} \left|\boldsymbol{z_1}+\boldsymbol{z_2}\right\rangle_L \otimes \left|\boldsymbol{z_1}+\boldsymbol{z_2}\right\rangle_R \end{array} \right\}, \tag{7.6}$$

where $\bar{\lambda}^i$ are all possible right moving Neveu-Schwarz oscillators and $\boldsymbol{z_2}$ is the important linear combination

$$\boldsymbol{z_2} = \mathbb{1} + \boldsymbol{b_1} + \boldsymbol{b_2} + \boldsymbol{b_3} + \boldsymbol{z_1} = \{\bar{\phi}^{5,6,7,8}\}. \tag{7.7}$$

In order to impose the Type $\bar{0}$ conditions into the SAT/SMT solver we remind ourselves of the bosonic sectors in this set-up given in Section 6.2.2. There are the 15

vectorial bosonic sectors of the form

$$\begin{aligned}
\boldsymbol{V}^1_{pq} &= \boldsymbol{b_2} + \boldsymbol{b_3} + \boldsymbol{T_1} + p\boldsymbol{T_2} + q\boldsymbol{T_3} \\
\boldsymbol{V}^2_{pq} &= \boldsymbol{b_1} + \boldsymbol{b_3} + \boldsymbol{T_2} + p\boldsymbol{T_1} + q\boldsymbol{T_3} \\
\boldsymbol{V}^3_{pq} &= \boldsymbol{b_1} + \boldsymbol{b_2} + \boldsymbol{T_3} + p\boldsymbol{T_1} + q\boldsymbol{T_2} \\
\boldsymbol{V}^4 &= \boldsymbol{T_1} + \boldsymbol{T_2} \\
\boldsymbol{V}^5 &= \boldsymbol{T_1} + \boldsymbol{T_3} \\
\boldsymbol{V}^6 &= \boldsymbol{T_2} + \boldsymbol{T_3}
\end{aligned} \tag{7.8}$$

where $p, q = 0, 1$ and these sectors all come with a right-moving NS oscillator. Additionally, there are 30 sectors with no oscillators

$$\begin{aligned}
\boldsymbol{B}^1_{pq} &= \boldsymbol{b_2} + \boldsymbol{b_3} + \boldsymbol{z_1} + \boldsymbol{T_1} + p\boldsymbol{T_2} + q\boldsymbol{T_3} \\
\boldsymbol{B}^2_{pq} &= \boldsymbol{b_1} + \boldsymbol{b_3} + \boldsymbol{z_1} + \boldsymbol{T_2} + p\boldsymbol{T_1} + q\boldsymbol{T_3} \\
\boldsymbol{B}^3_{pq} &= \boldsymbol{b_1} + \boldsymbol{b_2} + \boldsymbol{z_1} + \boldsymbol{T_3} + p\boldsymbol{T_1} + q\boldsymbol{T_2} \\
\boldsymbol{B}^4_{pq} &= \mathbb{1} + \boldsymbol{b_1} + \boldsymbol{z_1} + \boldsymbol{T_1} + p\boldsymbol{T_2} + q\boldsymbol{T_3} \\
\boldsymbol{B}^5_{pq} &= \mathbb{1} + \boldsymbol{b_2} + \boldsymbol{z_1} + \boldsymbol{T_2} + p\boldsymbol{T_1} + q\boldsymbol{T_3} \\
\boldsymbol{B}^6_{pq} &= \mathbb{1} + \boldsymbol{b_3} + \boldsymbol{z_1} + \boldsymbol{T_3} + p\boldsymbol{T_1} + q\boldsymbol{T_2}. \\
\boldsymbol{B}^7 &= \boldsymbol{T_1} + \boldsymbol{T_2} + \boldsymbol{z_1} \\
\boldsymbol{B}^8 &= \boldsymbol{T_1} + \boldsymbol{T_3} + \boldsymbol{z_1} \\
\boldsymbol{B}^9 &= \boldsymbol{T_2} + \boldsymbol{T_3} + \boldsymbol{z_1} \\
\boldsymbol{B}^{10} &= \boldsymbol{T_1} + \boldsymbol{T_2} + \boldsymbol{z_2} \\
\boldsymbol{B}^{11} &= \boldsymbol{T_1} + \boldsymbol{T_3} + \boldsymbol{z_2} \\
\boldsymbol{B}^{12} &= \boldsymbol{T_2} + \boldsymbol{T_3} + \boldsymbol{z_2}
\end{aligned} \tag{7.9}$$

A Type $\bar{0}$ model then requires that all these sectors are projected for an assignment of GGSO phases.

Tachyon Sector Analysis

The next constraint to impose after the projection of massless bosonic sectors, is the absence of tachyonic sectors. Since our models are non-supersymmetric this is an important check for determining the stability of our models for a 4D Minkowski background. The same procedure of encoding the GGSO projections applies to the tachyonic sectors. The tachyonic sectors in this construction are: $\{\bar{\lambda}\}\boldsymbol{T_i}, \boldsymbol{z_1}, \boldsymbol{z_2}, \boldsymbol{z_1} + \boldsymbol{T_i}$ and $\boldsymbol{z_2} + \boldsymbol{T_i}$, $i = 1, 2, 3$, where $i = 1, 2, 3$ and $\bar{\lambda}$ is some right-moving NS oscillator and we note that the untwisted tachyon from $|0\rangle_L \otimes \{\bar{\lambda}\}\,|0\rangle_R$ is projected regardless of the GGSO phase choices in this basis.

As an example, we can delineate the condition for the projection of the $\{\bar{\lambda}\}\boldsymbol{T_1}$ tachyonic sector

$$\forall\bar{\lambda}: \quad \mathbb{P}_{\{\bar{\lambda}\}\boldsymbol{T_1}} = \prod_{\boldsymbol{\xi}\in \mathrm{Y}(\boldsymbol{T_1})} \frac{1}{2}\left(1 + C\begin{bmatrix}\boldsymbol{T_1}\\ \boldsymbol{\xi}\end{bmatrix}\right) = 0 \tag{7.10}$$

where

$$\mathrm{Y}(\boldsymbol{T_1}) = \{\boldsymbol{T_2}, \boldsymbol{T_3}, \boldsymbol{z_1}, \boldsymbol{z_2}, \boldsymbol{x}\}. \tag{7.11}$$

Spinorial $\mathbf{16}/\overline{\mathbf{16}}$ Sectors

The fermion generations transforming in the spinorial $\mathbf{16}/\overline{\mathbf{16}}$ of $SO(10)$ arise from the twisted sectors

$$\begin{aligned}\boldsymbol{F}^1_{pq} &= \boldsymbol{b_1} + p\boldsymbol{T_2} + q\boldsymbol{T_3}\\ \boldsymbol{F}^2_{pq} &= \boldsymbol{b_2} + p\boldsymbol{T_1} + q\boldsymbol{T_3}\\ \boldsymbol{F}^3_{pq} &= \boldsymbol{b_3} + p\boldsymbol{T_1} + q\boldsymbol{T_2}.\end{aligned} \tag{7.12}$$

The projectors of which can be used to tell us $\#(\mathbf{16} + \overline{\mathbf{16}})$ for any model. Knowing this is sufficient for our purposes here with the SMT solver analysis, we will not implement the chirality projection distinguishing the $\mathbf{16}$ and $\overline{\mathbf{16}}$.

7.4 Application of SMT

Now we turn our attention to the analysis of these model characteristics with an SMT written using Z3 in Python. We recall eq. (7.2) defines a Boolean encoding of the GGSO phase inputs. For reasons of comparison and to make use of SMT solver expressibility we also define the integer encoding through

$$C\begin{bmatrix}\boldsymbol{v_i}\\ \boldsymbol{v_j}\end{bmatrix} = \exp\{i\pi(\boldsymbol{v_i}|\boldsymbol{v_j})\} \tag{7.13}$$

and use the 36 independent phases $(\boldsymbol{v_i}|\boldsymbol{v_j}) \in \{0, 1\}$ as the input variables for our SMT solver. We will see this integer encoding comes at the expense of performance compared with the Boolean case because the SMT solver needs to include reasoning for mathematical theories (such as integer arithmetic).

It turns out that the conditions for the projection of massless twisted bosons and tachyonic sectors do not involve the following 9 of the 36 $(\boldsymbol{v_i}|\boldsymbol{v_j})$ phases:

$$(\mathbb{1}|\tilde{\boldsymbol{S}}), (\mathbb{1}|\boldsymbol{b_1}), (\mathbb{1}|\boldsymbol{b_2}), (\mathbb{1}|\boldsymbol{b_3}), (\mathbb{1}|\boldsymbol{z_1}), (\tilde{\boldsymbol{S}}|\boldsymbol{b_1}), (\tilde{\boldsymbol{S}}|\boldsymbol{b_2}), (\tilde{\boldsymbol{S}}|\boldsymbol{b_3}), (\tilde{\boldsymbol{S}}|\boldsymbol{z_1}) \tag{7.14}$$

and so our space of models to explore is reduced to 2^{27} (ca. 1.34×10^8). This is well within the reach of a complete enumeration of possible GGSO configurations but our purpose here is testing the features and efficiency of the SMT solver within this simple

class of models. Moreover, as it does not adversely effect performance, we have re-introduced these 9 variables as input to our Boolean encoding with the expectation that it will not significantly impact the running time (in fact, it actually cuts the running time by 4%).

For both representations we can schematically write the steps for the construction of the Z3 solver in the case of finding tachyon-free Type $\bar{0}$ string models[2]

1: Define the 27 input variables $c_0, ..., c_{26}$
2: Add constraints on input variable domain $(c_i = 0 \vee c_i = 1)\ \forall i = 0, ..., 26$.
3: Add constraints for GGSO projection of all twisted massless bosons: $\forall \boldsymbol{B} :\ \mathbb{P}_{\boldsymbol{B}} = 0$.
4: Add constraints for GGSO projection of all tachyonic sectors, $\boldsymbol{T}$: $\forall \boldsymbol{t} \in \boldsymbol{T} :\ \mathbb{P}_t = 0$.
5: Check satisfiability
6: if `unsat` print proof
7: if `sat` find satisfying assignments (print all solutions)

7.5 Results of SMT search for tachyon-free Type $\bar{0}$ models

Enumerating all tachyon-free Type $\bar{0}$ models within the class of models under consideration is a good testing ground for the efficiency of the SMT/SAT solver. As mentioned earlier, the space of models is 2^{27} (ca. 1.34×10^8), which is within the grasp of a complete enumeration approach. We have run a random search in comparison, which is able to analyse ca. 16,000 sample points per second. An exhaustive enumeration of the model space thus takes around 2 hours 20 minutes, and a random search (with repetitions) needs on average around 19 hours to find all solutions and 4 seconds to find the first model.

Within the integer representation, Z3's SMT solver determines satisfiability in 12 seconds and finds all 2048 solutions in the full 2^{27} space in 2405 seconds (ca. 40 minutes). A random search found just under a quarter of these models in the same amount of time (500 models). While this is a useful speed up, it is not that impressive. This is expected since, in this representation, the SMT solver deals with mathematical theories that create a significant overhead. Figure 7.1 depicts the accumulation of solutions over time for the SMT solver within the integer representation.

The performance is significantly improved when implementing a Boolean encoding. In this case, Z3's SAT solver determines satisfiablitiy in 0.04 seconds. It can find and print all 2048 solutions in 19 seconds. This is 126 times faster than for the integer representation, and 450 times faster than exhaustively enumerating and checking the statespace. Figure 7.2 depicts the accumulation of solutions over time for the SAT

[2]Both the integer and Boolean Z3 codes are available at https://github.com/BenjaminPercival/SMTsTypeObar.

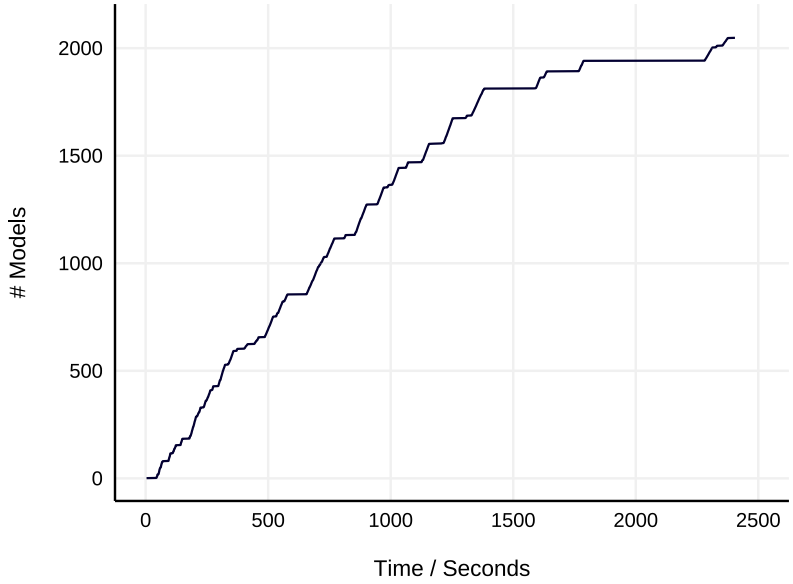

Figure 7.1: *Rate at which the Integer representation finds all tachyon-free Type* $\bar{0}$ *models.*

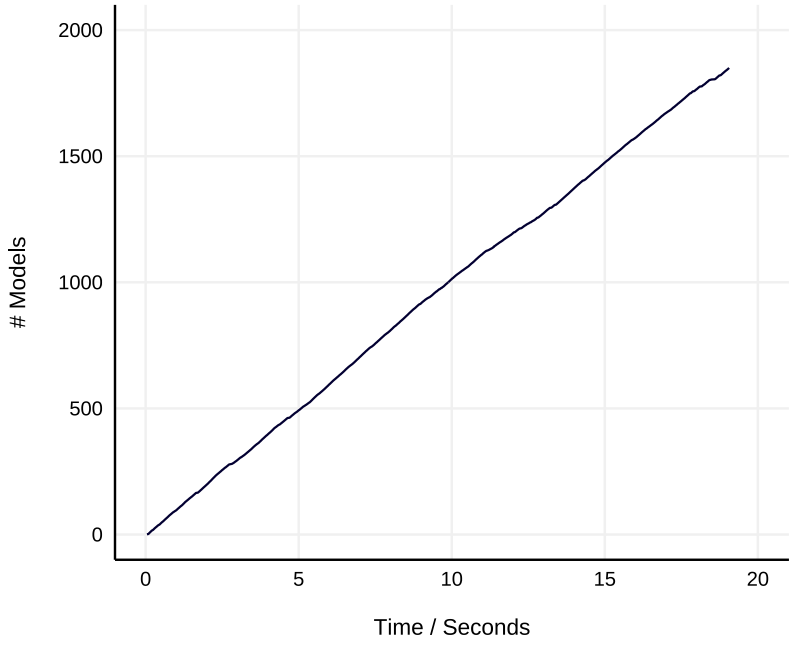

Figure 7.2: *Rate at which the Boolean representation finds all tachyon-free Type* $\bar{0}$ *models, depicting the number of compact solutions found; the 1850 compact solutions contain all 2048 explicit solutions (exactly once).*

solver, where we see that the solver is not slowed down by the creation of new lemmas as solutions are enumerated. It can be seen that only 1850 compact solutions are recorded on the graph in Figure 7.2. This is because some of the compact solutions

include variables labelled with `None`, meaning that these variables can be set to `True` or `False`; they can be trivially expanded to the 2048 solutions (without omissions and without multiple occurrences of individual solutions).

We have repeated the experiment using all 36 original input variables. Our expectation was that the SAT solver would essentially ignore them, as they do not enter into the reasoning at any point, though it will need to output a few additional `None` in the compact representation. We expected an insignificant increase in the overall running time. We found that the solver worked 4% faster, which is likely due to different decisions made by the heuristics. But it shows an interesting effect: overlooking the variables that do not matter did not slow the SAT solver down, whereas an exhaustive search would have taken 6 orders of magnitude longer.

7.5.1 Identifying Chiral, Tachyon-free Type $\bar{0}$ Vacua

In the analysis from Chapter 6 it was found that no Type $\bar{0}$ vacua include the fermion generations from the spinorial $\mathbf{16}/\overline{\mathbf{16}}$ sectors (7.12). Since these sectors are phenomenologically desirable, we aim to ensure at least one remains in the Hilbert space after GGSO projections.

With the addition of this condition the SMT structure summary can be updated to

1: Define the 27 input variables $c_0, ..., c_{26}$
2: Add constraint on input variable domain $(c_i = 0 \vee c_i = 1)\ \forall i = 0, ..., 26$.
3: Add constraints for GGSO projection of all twisted massless bosons
4: Add constraints for GGSO projection of all tachyonic sectors.
5: Add constraint on presence of at least 1 $\mathbf{16}/\overline{\mathbf{16}}$ sector
6: Check satisfiability
7: if `unsat` print proof
8: if `sat` find satisfying assignments (print all solutions)

As expected from the findings of ref. [9], with this added constraint on the spinorial $\mathbf{16}/\overline{\mathbf{16}}$ the Z3 solver returns `unsat`. This takes only 0.06 seconds in the Boolean encoding (163 seconds in the integer encoding), underlining the feasibility of combing large parameter spaces.

In such cases where constraint systems are unsatisfiable, there are several tools within Z3 that are helpful to understand and isolate where the inconsistency arises from. Using its `proof()` method, Z3 will output a proof of inconsistency. Unsatisfiability proofs can be long and tedious because, while satisfiability can be shown by providing a model, unsatisfiability needs to make a mathematical argument that establishes the contradiction. Such proofs thus do not provide much accessible further insight but are certainly preferable than trying to distill the contradiction by hand.

There are, however, several other helpful tools that can be used to isolate inconsistencies. In particular, a minimal 'unsatisfiable core' of constraints can be returned by most SMT solvers [123], which isolates where the contradiction arises by giving a (locally) minimal subset of constraints such that dropping either of them results in a satisfiable constraint system. From this, it is straightforward to apply Optimisation Modulo Theory (OMT), offered by many SMT solvers. Additionally, a more manual approach of using push and pop methods on constraints allows for pinning down the source of an inconsistency. Using this approach, the presence of the spinorial $\mathbf{16}/\overline{\mathbf{16}}$'s from $\boldsymbol{F}^i_{pq}$ is found to contradict the projection of the vectorial $\boldsymbol{V}^i_{pq}$ (under the presence of the remaining constraints). Since the Higgs bidoublet representation would reside within the vectorial $\mathbf{10}$ of $SO(10)$ coming from the $\boldsymbol{V}^i_{pq}$, $i = 1,2,3$, there is physical motivation to keep at least one of these twisted bosonic sectors in the Hilbert space. Demanding that at least one sector from $\boldsymbol{F}^1_{pq}$ remains, and at least one of $\boldsymbol{V}^1_{pq}$ makes the SMT return `sat`, takes 0.03 seconds for the Boolean constraint system and 8.4 seconds for the integer encoding. Creating all 640 satisfying assignments takes 7.5 seconds for the Boolean constraint system (1661 seconds for the integer encoding) of the 27 input variables with these conditions. One such model is defined by

$$C\begin{bmatrix}\boldsymbol{v_i}\\ \boldsymbol{v_j}\end{bmatrix} = \begin{array}{c} \\ \mathbb{1} \\ \tilde{\boldsymbol{S}} \\ \boldsymbol{T_1} \\ \boldsymbol{T_2} \\ \boldsymbol{T_3} \\ \boldsymbol{b_1} \\ \boldsymbol{b_2} \\ \boldsymbol{b_3} \\ \boldsymbol{z_1} \end{array} \begin{array}{c} \begin{array}{ccccccccc} \mathbb{1} & \tilde{\boldsymbol{S}} & \boldsymbol{T_1} & \boldsymbol{T_2} & \boldsymbol{T_3} & \boldsymbol{b_1} & \boldsymbol{b_2} & \boldsymbol{b_3} & \boldsymbol{z_1} \end{array} \\ \begin{pmatrix} 1 & 1 & 1 & -1 & 1 & 1 & -1 & -1 & 1 \\ 1 & -1 & -1 & -1 & -1 & 1 & 1 & 1 & 1 \\ 1 & -1 & -1 & 1 & 1 & -1 & 1 & -1 & 1 \\ -1 & -1 & 1 & 1 & 1 & -1 & 1 & 1 & 1 \\ 1 & -1 & 1 & 1 & -1 & 1 & 1 & 1 & 1 \\ 1 & -1 & -1 & -1 & 1 & 1 & -1 & -1 & -1 \\ -1 & -1 & 1 & 1 & 1 & -1 & -1 & -1 & 1 \\ -1 & -1 & -1 & 1 & 1 & -1 & -1 & -1 & 1 \\ 1 & -1 & 1 & 1 & 1 & -1 & 1 & 1 & 1 \end{pmatrix} \end{array} \tag{7.15}$$

which has partition function

$$Z = 2\bar{q}^{-1} + 1280q^{-1/2}\bar{q}^{1/4} + 48q^{1/4}\bar{q}^{-3/4} - 1016 - 16288q^{1/4}\bar{q}^{1/4} + \cdots \tag{7.16}$$

where we can see that $N^0_b - N^0_f = -1016$, which is a large abundance of massless fermions as expected. This model generates a worldsheet cosmological constant of $\Lambda = -886.43$ which corresponds to a large positive cosmological constant, λ, via the rescaling $\lambda = -\frac{1}{2}\mathcal{M}^4\Lambda$, where $\mathcal{M} = M_{String}/2\pi$.

7.6 Discussion

The application of Machine Learning techniques within the string landscape is already a burgeoning field [4]. In this chapter, we open the door to the application of SAT and SMT solvers within this context and have demonstrated their power and efficiency

within a simplified class of string models and expect their benefits to only increase as more generalised and (quasi-)realistic classes of vacua are studied.

We have demonstrated how SAT and SMT solvers can be used to help isolate inconsistent constraints and be used to optimise desired characteristics. This method was then employed to find string vacua with positive cosmological constant and desirable $SO(10)$ representations. Furthermore, this approach essentially meant minimising the number of massless twisted bosons, which is generally enough to ensure a large abundance of massless fermions resulting in the largest contribution to cosmological constant (the massless level) being positive. Although the massive and off-shell contributions also need accounting for, a large abundance of massless fermions can effectively guarantee a positive cosmological constant. Such vacua are then ripe for analysis away from the free fermionic point in the moduli space by exploring the one-loop potential in terms of the moduli fields as was pursued in [43, 44], where models with $N_f > N_b$ at the free fermionic point and $N_b = N_f$ at a generic point in the moduli space resulted in guaranteeing a positivity of the one-loop potential. Using the SAT and SMT solvers described in the current work makes it very quick and easy to find string models at the free fermionic point with desired properties at the massless level, even when the models are rare in the full space.

There are a couple of obvious limitations, from a phenomenological perspective, in the class of models that we have examined in this chapter. First of all, a $\boldsymbol{F}^1_{pq}$ and $\boldsymbol{V}^1_{pq}$ could not give rise to desired coupling as they reside on the same orbifold plane. Secondly, due to only employing the $\boldsymbol{T_i}$, $i = 1, 2, 3$, in the basis we do not allow for shifts around the 6 circles of the internal T^6 and there is a multiplicity factor of 4 attached to each sector, making 3 generation models impossible. However, our focus here is on the introduction of SAT and SMT solving and the illustration of its application. An application of SAT and SMT solving to the more realistic constructions of asymmetric orbifolds is presented in the following chapter.

It is already evident however, even at this stage, that as we seek to construct satisfiability criteria for more detailed phenomenological string models, these algorithmic approaches are of immense interest and utility.

Chapter 8

Towards the Classification of Asymmetric Orbifolds

In this chapter we explore some asymmetric orbifold constructions with Flipped $SU(5)$ (FSU5) subgroup with help from our SAT/SMT solver. This work is based on that of ref. [11]. The classification methodology so far discussed has solely been developed for models with symmetric boundary conditions. The heterotic string in general, and the free fermionic models in particular, allow for more general assignments of boundary conditions, which are asymmetric between the left and the right-moving world-sheet fermions. These can be complicated assignments that realise the non-Abelian gauge symmetries at higher level Kac-Moody algebra [83, 84, 85], or more mundane assignments that leave the gauge symmetries at level $k = 1$. Although symmetric in the $\mathbb{Z}_2 \times \mathbb{Z}_2$ twists, these asymmetric assignments produce asymmetric shift orbifold models, which amount to non-geometric compactifications, a review of which is given in ref. [86]. Completing a first step towards the extension of the classification methodology to such asymmetric orbifolds is our objective here. We choose to study models with Flipped $SU(5)$ (FSU5) gauge symmetry for both the $\mathcal{N} = 0$ and $\mathcal{N} = 1$ cases.

There are several profound phenomenological implications of choosing such asymmetric boundary condition assignments rather than symmetric ones. Of crucial importance to us is how they help to realise moduli fixing [124], top-quark Yukawa couplings from the untwisted sector [125] and doublet-triplet splitting [126]. Furthermore, we note that the early free fermionic constructions [127, 128] do utilise asymmetric boundary conditions, which gave rise to a stringy explanation of the hierarchical top-bottom quark mass splitting [129, 130].

The fixing of some of the three complex and Kähler structures that comprise the moduli space of the $\mathbb{Z}_2 \times \mathbb{Z}_2$ orbifold is of particular significance in the context of investigating the one-loop potential generating the (leading order) vacuum energy of a string model. This is of key interest in this work since we classify non-supersymmetric configurations. Various works on non-supersymmetric string vacua have attempted to use Scherk-Schwarz supersymmetry breaking [75, 80, 81, 77, 79] and a so-called 'super

no-scale' condition [73, 74, 101] to argue for a suppression of the one-loop cosmological constant. Florakis and Rizos demonstrated the existence of free fermion models with positive vacuum energy at the minimum of the potential for one of the radii [43, 44]. However, in order to argue for stability of the vacua one needs to incorporate all moduli into the analysis, which is far too cumbersome in the symmetric orbifold case to be performed. This is where asymmetric orbifolds come into their own, as they give some control over the fixing of certain moduli. To this end, we will classify different asymmetric pairings according to their moduli fixing and then explore two classes of FSU5 models, one of which has no fixed moduli and the other in which only the moduli of the 1st internal torus are unfixed.

The fermionisation of the worldsheet degrees of freedom employed in the free fermionic construction demands that the heterotic string is constructed at the self-dual point in the moduli space where the radii are fixed to $R = \sqrt{\alpha'/2}$. At this point the theory is consistent and, as was shown in [29, 30, 31], the modular invariance constraints for one-loop and higher-loop amplitudes can be completely solved. A key advantage of the free fermionic formulation is that non-geometric constructions [86], such as the asymmetric orbifolds studied in this chapter, may be realised naturally. However, as mentioned in Section 3.5, being fixed at the self-dual point in the moduli space becomes restrictive when we wish to study stability issues that arise for non-supersymmetric string models. For example, it becomes essential to introduce moduli dependence when investigating the non-trivial one-loop potential arising in the absence of supersymmetry or to understand the type of supersymmetry breaking within the string model. One approach to tackling these issues is a translation of the free fermionic theory into a bosonic orbifold construction using the tools reviewed in [42] and employed in [43, 44].

However, for the purposes of initiating a systematic classification of asymmetric orbifolds, the free fermionic construction is the perfect starting point since it provides great computational power through the simplicity of representation for worldsheet boundary conditions. As explained in Chapter 7, the sophisticated SAT/SMT solvers can easily be employed to aid in our classification and will be used throughout our analysis.

8.1 Asymmetric Orbifold Classification Set-up

We can take the NAHE-set [131, 132] as the starting point for classifying large spaces of asymmetric orbifolds, which is the set:

$$\begin{aligned}
\mathbb{1} &= \{\psi^\mu,\ \chi^{1,\dots,6}, y^{1,\dots,6}, w^{1,\dots,6} \mid \overline{y}^{1,\dots,6}, \overline{w}^{1,\dots,6}, \overline{\psi}^{1,\dots,5}, \overline{\eta}^{1,2,3}, \overline{\phi}^{1,\dots,8}\},\\
\boldsymbol{S} &= \{\psi^\mu, \chi^{1,\dots,6}\ \}\\
\boldsymbol{b_1} &= \{\psi^\mu, \chi^{12}, y^{34}, y^{56} \mid \overline{y}^{34}, \overline{y}^{56}, \overline{\psi}^{1,\dots,5}, \overline{\eta}^{1}\},\\
\boldsymbol{b_2} &= \{\psi^\mu, \chi^{34}, y^{12}, w^{56} \mid \overline{y}^{12}, \overline{w}^{56}, \overline{\psi}^{1,\dots,5}, \overline{\eta}^{2}\},\\
\boldsymbol{b_3} &= \{\psi^\mu, \chi^{56}, w^{12}, w^{34} \mid \overline{w}^{12}, \overline{w}^{34}, \overline{\psi}^{1,\dots,5}, \overline{\eta}^{3}\},
\end{aligned} \tag{8.1}$$

which gives rise to an $SO(10)$ symmetric GUT and, due to the $\boldsymbol{S}$ vector, can realise $\mathcal{N}=1$ supersymmetry for appropriate choices of GGSO phases. We will then choose to add the additional basis vectors:

$$\begin{aligned}
\boldsymbol{x} &= \{\bar{\psi}^{1,\dots,5}, \bar{\eta}^{1,2,3}\}\\
\boldsymbol{z_1} &= \{\bar{\phi}^{1,\dots,4}\},
\end{aligned} \tag{8.2}$$

such that $\boldsymbol{z_1}$ reduces the dimension of the hidden gauge group and the $\boldsymbol{x}$ vector induces the enhancement $SO(10)\times U(1)\to E_6$ for certain choices of GGSO phases. This enhancement can be seen as taking us from the space of vacua with $(2,0)$ worldsheet supersymmetry to those with $(2,2)$.

The untwisted gauge group is

$$SO(10)\times SO(4)^3\times U(1)^3\times SO(8)\times SO(8), \tag{8.3}$$

at this level, with the three $SO(4)$ factors arising from the three groups of internal fermions in $\boldsymbol{b_k}$, $k=1,2,3$, such that the NS sector gauge bosons can be written

$$\begin{aligned}
&\psi^\mu\{\bar{y}^{3,4,5,6}\}\{\bar{y}^{3,4,5,6}\}\,|0\rangle_{NS}\,,\\
&\psi^\mu\{\bar{y}^{1,2},\bar{w}^{5,6}\}\{\bar{y}^{1,2},\bar{w}^{5,6}\}\,|0\rangle_{NS}\,,\\
&\psi^\mu\{\bar{w}^{1,2,3,4}\}\{\bar{w}^{1,2,3,4}\}\,|0\rangle_{NS}\,.
\end{aligned} \tag{8.4}$$

The NAHE-set naturally implements a $\mathbb{Z}_2\times\mathbb{Z}_2$ orbifolding through the twist vectors $\boldsymbol{b_k}$ that leave an untwisted moduli space of

$$\left(\frac{SO(2,2)}{SO(2)\times SO(2)}\right)^3, \tag{8.5}$$

where each of the three factors is parameterised by the moduli scalar fields from the NS sector

$$h_{ij} = \left|\chi^i\right\rangle_L \otimes \left|\bar{y}^j\bar{w}^j\right\rangle_R = \begin{cases} (i,j=1,2) \\ (i,j=3,4) \\ (i,j=5,6) \end{cases} . \tag{8.6}$$

In free fermionic models these untwisted moduli are in one to one correspondence with marginal operators that generate Abelian Thirring Interactions. For the NAHE-set the only such marginal operators left invariant are

$$J_L^i(z)\bar{J}_R^j(\bar{z}) =: y^i w^i :: \bar{y}^j\bar{w}^j := \begin{cases} (i,j=1,2) \\ (i,j=3,4) \\ (i,j=5,6) \end{cases} . \tag{8.7}$$

From this, it is straightforward to observe that the projection or retention of moduli is governed by the boundary conditions of the set of 12 internal real fermions $\{y^I, w^I \mid \bar{y}^I, \bar{w}^I\}$. In particular, we note that if the basis remains left-right symmetric in these internal fermions then all the untwisted moduli of the NAHE-set are retained. This is a central reason for attempting to classify asymmetric orbifolds models where the internal real fermions $\{y^I, w^I \mid \bar{y}^I, \bar{w}^I\}$ are not left-right symmetric.

In order to make the connection between the fields h_{ij} and the familiar three Kähler and three complex structure moduli of the $\mathbb{Z}_2 \times \mathbb{Z}_2$ orbifold, we can construct six complex moduli from the six real ones of eq. (8.6). For the first complex plane we can write

$$\begin{aligned} H_1^{(1)} &= \frac{1}{\sqrt{2}}(h_{11} + ih_{21}) = \frac{1}{\sqrt{2}}\left|\chi^1 + i\chi^2\right\rangle_L \otimes \left|\bar{y}^1\bar{w}^1\right\rangle_R , \\ H_2^{(1)} &= \frac{1}{\sqrt{2}}(h_{12} + ih_{22}) = \frac{1}{\sqrt{2}}\left|\chi^1 + i\chi^2\right\rangle_L \otimes \left|\bar{y}^2\bar{w}^2\right\rangle_R , \end{aligned} \tag{8.8}$$

which can then be combined to define the Kähler and complex structure moduli for the first complex plane

$$\begin{aligned} T_1 &= \frac{1}{\sqrt{2}}(H_1^{(1)} - iH_2^{(1)}) = \frac{1}{\sqrt{2}}\left|\chi^1 + i\chi^2\right\rangle_L \otimes \left|\bar{y}^1\bar{w}^1 - i\bar{y}^2\bar{w}^2\right\rangle_R , \\ U_1 &= \frac{1}{\sqrt{2}}(H_1^{(1)} + iH_2^{(1)}) = \frac{1}{\sqrt{2}}\left|\chi^1 + i\chi^2\right\rangle_L \otimes \left|\bar{y}^1\bar{w}^1 + i\bar{y}^2\bar{w}^2\right\rangle_R , \end{aligned} \tag{8.9}$$

and similarly for $T_{2,3}$ and $U_{2,3}$.

We choose to classify Flipped SU(5) models such that a single basis vector both breaks the $SO(10)$ GUT and assigns asymmetric pairings to the internal fermions. This

vector can be taken to be of the general form

$$\boldsymbol{\gamma} = \boldsymbol{A} + \left\{ \bar{\psi}^{1,\ldots,5} = \bar{\eta}^{1,2,3} = \bar{\phi}^{1,2,6,7} = \frac{1}{2} \right\} + \boldsymbol{B}, \tag{8.10}$$

where $\boldsymbol{A}$ ensures that the internal fermions are not symmetrically paired and $\boldsymbol{B}$ assigns appropriate boundary conditions to the hidden complex fermions

$$\boldsymbol{B} = \{B(\bar{\phi}^3), B(\bar{\phi}^4), B(\bar{\phi}^5), B(\bar{\phi}^8)\} \tag{8.11}$$

where we choose real boundary conditions $B(\bar{\phi}^{3,4,5,8}) = 0, 1$, so as to be consistent with the modular invariance rules

$$N_\gamma \boldsymbol{\gamma} \cdot \boldsymbol{\gamma} = 0 \bmod 8. \tag{8.12}$$

$$N_{z_1\gamma} \boldsymbol{z_1} \cdot \boldsymbol{\gamma} = 0 \bmod 4, \tag{8.13}$$

where N_γ is the smallest positive integer for which $N_\gamma \boldsymbol{\gamma} = 0$ and $N_{z_1\gamma}$ is the least common multiple of N_{z_1} and N_γ.

The supercurrent constraint (3.72) imposes a different constraint on these boundary conditions depending on whether $\boldsymbol{\gamma}$ is fermionic or bosonic. In the bosonic case we can write $\boldsymbol{A}$ as

$$\boldsymbol{A} = \{A(y^1), ..., A(y^6), A(w^1), ..., A(w^6) \mid A(\bar{y}^1), ..., A(\bar{y}^6), A(\bar{w}^1), ..., A(\bar{w}^6)\} \tag{8.14}$$

and (3.72) thus imposes that the boundary conditions of the holomorphic internal fermions are

$$(y^I, w^I) = (1,1) \text{ or } (0,0), \quad I = 1, ..., 6, \tag{8.15}$$

to ensure a consistent supercurrent. On the other hand, if $\boldsymbol{\gamma}$ is fermionic then we choose $\boldsymbol{A}$ to be of the form

$$\boldsymbol{A} = \{\psi^\mu, \chi^{12}, A(y^1), ..., A(y^6), A(w^1), ..., A(w^6) \mid A(\bar{y}^1), ..., A(\bar{y}^6), A(\bar{w}^1), ..., A(\bar{w}^6)\} \tag{8.16}$$

and the supercurrent consistency imposes that

$$(y^I, w^I) = \begin{cases} (0,0) \text{ or } (1,1), & I = 1,2 \\ (1,0) \text{ or } (0,1), & I = 3, ..., 6, \end{cases} \tag{8.17}$$

and similar for the cases where $A(\chi^{34}) = 1$ or $A(\chi^{56}) = 1$ and $A(\chi^{12}) = 0$.

The next step towards classifying Flipped SU(5) asymmetric orbifolds is the addition of the symmetric shift vectors:

$$\boldsymbol{e_i} = \{y^i, w^i \mid \bar{y}^i, \bar{w}^i\}, \quad i = 1, ..., 6, \tag{8.18}$$

so long as they are consistent with the choice of $\boldsymbol{\gamma}$, in the sense that they satisfy the modular invariance rule

$$N_{\gamma e_i}\boldsymbol{\gamma}\cdot\boldsymbol{e_i} = 0 \mod 4. \tag{8.19}$$

In the previous classifications of symmetric orbifolds, all six $\boldsymbol{e_i}$'s are present in the basis to impose the 12 symmetric pairings between $\{y^I, w^I\}$ and $\{\bar{y}^I, \bar{w}^I\}$ to form 12 Ising model operators. One corollary of this symmetric pairing is that the rank of the untwisted gauge group from the holomorphic sector takes its minimal value of 16. However, asymmetric pairings will generate up to six additional $U(1)$'s from the pairing of two antiholomophic internal fermions $\{\bar{y}^I, \bar{w}^I\}$.

Putting this all together, we can write the basis we take as a starting point for exploring the space of asymmetric orbifolds as

$$\begin{aligned}
\mathbb{1} &= \{\psi^\mu,\ \chi^{1,\dots,6}, y^{1,\dots,6}, w^{1,\dots,6} \mid \overline{y}^{1,\dots,6}, \overline{w}^{1,\dots,6}, \overline{\psi}^{1,\dots,5}, \overline{\eta}^{1,2,3}, \overline{\phi}^{1,\dots,8}\},\\
\boldsymbol{S} &= \{\psi^\mu, \chi^{1,\dots,6}\}\\
\boldsymbol{e_i} &= \{y^i, w^i \mid \bar{y}^i, \bar{w}^i\}, \quad i \subset \{1,2,3,4,5,6\}\\
\boldsymbol{b_1} &= \{\psi^\mu, \chi^{12}, y^{34}, y^{56} \mid \overline{y}^{34}, \overline{y}^{56}, \overline{\psi}^{1,\dots,5}, \overline{\eta}^1\},\\
\boldsymbol{b_2} &= \{\psi^\mu, \chi^{34}, y^{12}, w^{56} \mid \overline{y}^{12}, \overline{w}^{56}, \overline{\psi}^{1,\dots,5}, \overline{\eta}^2\},\\
\boldsymbol{b_3} &= \{\psi^\mu, \chi^{56}, w^{12}, w^{34} \mid \overline{w}^{12}, \overline{w}^{34}, \overline{\psi}^{1,\dots,5}, \overline{\eta}^3\}\\
\boldsymbol{z_1} &= \{\bar{\phi}^{1,2,3,4}\}\\
\boldsymbol{x} &= \{\bar{\psi}^{1,\dots,5}, \bar{\eta}^{1,2,3}\}\\
\boldsymbol{\gamma} &= \boldsymbol{A} + \{\bar{\psi}^{1,\dots,5} = \bar{\eta}^{1,2,3} = \bar{\phi}^{1,2,5,6} = \frac{1}{2}\} + \boldsymbol{B}.
\end{aligned} \tag{8.20}$$

We furthermore note the existence of the following important linear combination of hidden fermions

$$\boldsymbol{z_2} = \mathbb{1} + \sum_{k=1}^{3}\boldsymbol{b_k} + \boldsymbol{z_1} = \{\bar{\phi}^{5,6,7,8}\} \tag{8.21}$$

and the combination generating the internal fermions

$$\boldsymbol{G} = \boldsymbol{S} + \sum_{k=1}^{3}\boldsymbol{b_k} + \boldsymbol{x} = \{y^I, w^I \mid \bar{y}^I, \bar{w}^I\}, \quad I = 1,2,3,4,5,6. \tag{8.22}$$

Our approach towards this classification will be two-fold. The first step is to classify the asymmetric pairings within $\boldsymbol{\gamma}$ given through the $\boldsymbol{A}$ vector in both the bosonic case (8.14) and fermionic case (8.16), with respect to their impact on important characteristics of the resultant models, such as the number of retained moduli. The details are presented in the next section. This step is new to the classification program due to the asymmetric shifts. The second step is to pick a particular pairing and perform a classification of the resultant space of vacua according to their phenomenological features, such as the number of particle generations at the Flipped $SU(5)$ level.

8.2 Classification of Asymmetric Pairings

Due to the centrality of the pairings of the internal fermions $\{y^I, w^I \mid \bar{y}^I, \bar{w}^I\}$ in determining important features of the class of asymmetric orbifold models, a useful first step towards classifying the asymmetric orbifolds is to classify their possible pairings defined through the vector $\boldsymbol{A}$. The key criteria we can classify these pairings according to will be the untwisted moduli they retain and their number of possible chiral generations.

A convenient tool for classifying these pairings is to use an SAT/SMT solver such as Z3, as discussed in Section 7.2, where the input is a list of 24 Boolean variables determining the boundary conditions $\{A(y^{1,\dots,6}, w^{1,\dots,6}) | A(\bar{y}^{1,\dots,6}, \bar{w}^{1,\dots,6})\}$ within $\boldsymbol{A}$. This is sufficient for both the bosonic case (8.14) and the fermionic case (8.16) with the respective boundary conditions (8.15) and (8.17) from the supercurrent condition. Imposing the relevant supercurrent constraint, as well as ensuring the pairing is asymmetric and consistent with the NAHE set allows us to generate all possible pairings as output from the SAT/SMT solver.

8.2.1 Asymmetric Pairings and Three Generations

One key phenomenological feature impacted by the choice of pairings in $\boldsymbol{A}$ is on the number of observable spinorial sectors that are required to give rise to the particle generations. In order to explore this further, it will be helpful to define two quantities which result from a choice of pairings $\boldsymbol{A}$. Firstly we have

$$\boldsymbol{E} = (E_1, E_2, E_3, E_4, E_5, E_6) \text{ s.t. } \begin{cases} E_i = 1 \text{ if } A(y^i) = A(w^i) = A(\bar{y}^i) = A(\bar{w}^i) = 0 \\ E_i = 0 \text{ else,} \end{cases} \tag{8.23}$$

for $i = 1, \dots, 6$. This simply quantifies which of the $\boldsymbol{e_i}$ symmetric shift vectors remain in the basis. We can note that any asymmetric pairing automatically makes two $\boldsymbol{e_i}$ incompatible with modular invariance constraints and therefore

$$\max\left(\sum_i E_i\right) = 4. \tag{8.24}$$

The second quantity we can define is

$$\boldsymbol{\Delta} = (\Delta_1, \Delta_2, \Delta_3) \text{ s.t. } \begin{cases} \Delta_1 = 0 \text{ if } A(y^{3456}) = A(\bar{y}^{3456}) \\ \Delta_1 = 1 \text{ else} \end{cases} \tag{8.25}$$

and similarly for Δ_2 and Δ_3. This notation has been employed, for example, in [124] and [133]. With this notation defined, we can now consider the fermion generations.

At the level of the NAHE-set $\{\mathbb{1}, \boldsymbol{S}, \boldsymbol{b_1}, \boldsymbol{b_2}, \boldsymbol{b_3}\}$, the sectors $\boldsymbol{b_1}$, $\boldsymbol{b_2}$ and $\boldsymbol{b_3}$, if present in the massless spectrum, give rise to sixteen copies of the **16** or $\overline{\mathbf{16}}$ of $SO(10)$ due to the degeneracy of the sets of internal fermions $\{y^{3,4,5,6} \mid \bar{y}^{3,4,5,6}, \bar{\eta}^1\}$, $\{y^{1,2}, w^{5,6} \mid \bar{y}^{1,2}, \bar{w}^{5,6}, \bar{\eta}^2\}$ and $\{w^{1,2,3,4} \mid \bar{w}^{1,2,3,4}, \bar{\eta}^3\}$, respectively. The addition of $\boldsymbol{x}$ reduces the degeneracy to eight copies of **16** or $\overline{\mathbf{16}}$ by separating out the $\bar{\eta}^k$ for each plane.

In the classification program for symmetric orbifolds, the basis contains all six symmetric shift $\boldsymbol{e_i}$ vectors. These symmetric shifts completely remove the degeneracy on the three orbifold planes and the sectors giving rise to observable spinorial states from the $\mathbf{16}/\overline{\mathbf{16}}$ of $SO(10)$ are

$$\begin{aligned} \boldsymbol{F}^1_{pqrs} &= \boldsymbol{b_1} + p\boldsymbol{e_3} + q\boldsymbol{e_4} + r\boldsymbol{e_5} + s\boldsymbol{e_6} \\ \boldsymbol{F}^2_{pqrs} &= \boldsymbol{b_2} + p\boldsymbol{e_1} + q\boldsymbol{e_2} + r\boldsymbol{e_5} + s\boldsymbol{e_6} \\ \boldsymbol{F}^3_{pqrs} &= \boldsymbol{b_3} + p\boldsymbol{e_1} + q\boldsymbol{e_2} + r\boldsymbol{e_3} + s\boldsymbol{e_4}, \end{aligned} \tag{8.26}$$

such that any sector $\boldsymbol{F}^k_{pqrs}$, $k = 1, 2, 3$, in the massless spectrum produces exactly one **16** or $\overline{\mathbf{16}}$.

This picture requires adjustment for the case of the Flipped $SU(5)$ asymmetric orbifolds generated by the basis of eq. (8.20). In particular, the number and degeneracy of each group of sectors $\boldsymbol{F}^k_{pqrs}$ will vary according to the pairing choice $\boldsymbol{A}$. More specifically, we will see that the degeneracies of each plane can be written as a function of $\boldsymbol{E}$ and $\boldsymbol{\Delta}$.

The impact of the inclusion of an $\boldsymbol{e_i}$ vector in the basis (8.20) on the degeneracy of each orbifold plane can be seen to reduce the degeneracy of the orbifold plane $k = 1, 2, 3$ by a factor two if $\boldsymbol{e_i} \cap \boldsymbol{b_k} \neq \emptyset$. Similarly, an asymmetric pairing in one of the three planes, *i.e.* $\Delta_k = 1$, will also reduce the degeneracy by a factor 2.

We can now write the degeneracies as a vector

$$\boldsymbol{D} = (D_1, D_2, D_3) \tag{8.27}$$

for each orbifold plane such that

$$\begin{aligned} D_1 &= \frac{8}{2^{\Delta_1 + E_3 + E_4 + E_5 + E_6}} \\ D_2 &= \frac{8}{2^{\Delta_2 + E_1 + E_2 + E_5 + E_6}} \\ D_3 &= \frac{8}{2^{\Delta_3 + E_1 + E_2 + E_3 + E_4}}, \end{aligned} \tag{8.28}$$

and we note that

$$\min\left(D_k\right) = \frac{1}{2}, \tag{8.29}$$

which, when true, tells us that the sectors $\boldsymbol{F}^k_{pqrs}$ will give rise to one component of the FSU5 representations of the **16** or $\overline{\mathbf{16}}$ and not the whole $SO(10)$ representation. In particular, since the decomposition under $SU(5) \times U(1)$ is

$$\mathbf{16} = \left(\mathbf{10}, +\frac{1}{2}\right) + \left(\bar{\mathbf{5}}, -\frac{3}{2}\right) + \left(\mathbf{1}, \frac{5}{2}\right) \tag{8.30}$$

$$\overline{\mathbf{16}} = \left(\overline{\mathbf{10}}, -\frac{1}{2}\right) + \left(\mathbf{5}, +\frac{3}{2}\right) + \left(\mathbf{1}, -\frac{5}{2}\right) \tag{8.31}$$

sectors $\boldsymbol{F}^k_{pqrs}$ with $D_k = \frac{1}{2}$ will generate either the states with representation $\left(\mathbf{10}, +\frac{1}{2}\right)$ or those transforming under $\left(\bar{\mathbf{5}}, -\frac{3}{2}\right) + \left(\mathbf{1}, \frac{5}{2}\right)$, in the case of the sector being from **16**.

Once we calculate the degeneracies (D_1, D_2, D_3) from $\boldsymbol{A}$ we can immediately check a necessary, but certainly not sufficient, condition for the presence of odd and, in particular, three generations, which is simply

$$\exists\, k \in \{1, 2, 3\} : \; D_k \leq 1. \tag{8.32}$$

A sufficient condition for the presence of three generations is presented in Section 8.3 but the condition (8.32) can be checked immediately from the pairing choice $\boldsymbol{A}$ so will be tested for in this section.

8.2.2 Asymmetric Pairings and Retained Moduli

As mentioned in Section 8.1, the moduli scalar fields (8.6) are in one to one correspondence with the marginal operators (8.7). From the form of these operators we can immediately derive conditions on their retention/projection depending on the boundary condition assignments from $\boldsymbol{A}$. The result is

$$J^i_L(z)\bar{J}^j_R(\bar{z}) \begin{cases} \text{retained if} & \left[A(y^i) + A(w^i) + A(\bar{y}^j) + A(\bar{w}^j)\right] \mod 2 = 0 \\ \text{projected if} & \left[A(y^i) + A(w^i) + A(\bar{y}^j) + A(\bar{w}^j)\right] \mod 2 = 1. \end{cases} \tag{8.33}$$

It will be useful when constructing the pairing classification Tables 8.1 and 8.2 to write the number of retained moduli in each orbifold plane as a triple

$$\boldsymbol{M} = (M_1, M_2, M_3). \tag{8.34}$$

8.2.3 Results for Classification of Pairings

The result of the classification of asymmetric pairings with a bosonic $\boldsymbol{A}$ are summarised in Table 8.1 and with fermionic $\boldsymbol{A}$ in Table 8.2. The data most important to consider is the number of untwisted moduli retained in each plane (8.34) and whether odd number generations are possible through checking (8.32). The Z3 SMT classifies all the asymmetric pairings in each case, bosonic and fermionic, in approximately 20 seconds.

Untwisted Moduli in each Torus	Odd Number Generations Possible	Frequency
(2, 2, 0)	No	992
(2, 0, 2)	No	992
(0, 2, 2)	No	992
(4, 2, 2)	No	824
(2, 4, 2)	No	824
(2, 2, 4)	No	824
(0, 0, 0)	No	256
(4, 0, 0)	No	244
(0, 4, 0)	No	244
(0, 0, 4)	No	244
(4, 4, 0)	No	200
(4, 2, 2)	Yes	200
(4, 0, 4)	No	200
(2, 4, 2)	Yes	200
(2, 2, 4)	Yes	200
(0, 4, 4)	No	200
(4, 4, 4)	No	146
(4, 4, 4)	Yes	94
(4, 4, 0)	Yes	56
(4, 0, 4)	Yes	56
(0, 4, 4)	Yes	56
(2, 2, 0)	Yes	32
(2, 0, 2)	Yes	32
(0, 2, 2)	Yes	32
(4, 0, 0)	Yes	12
(0, 4, 0)	Yes	12
(0, 0, 4)	Yes	12

Table 8.1: *Possible moduli and whether odd number generations are possible for all bosonic type asymmetric pairings of internal fermions.*

Untwisted Moduli in each Torus	Odd Number Generations Possible	Frequency
(2, 4, 2)	No	1024
(2, 2, 4)	No	1024
(2, 2, 0)	No	1024
(2, 0, 2)	No	1024
(0, 2, 2)	No	1024
(4, 2, 2)	No	976
(0, 4, 4)	No	256
(0, 4, 0)	No	256
(0, 0, 4)	No	256
(0, 0, 0)	No	256
(4, 4, 0)	No	244
(4, 0, 4)	No	244
(4, 0, 0)	No	244
(4, 4, 4)	No	228
(4, 2, 2)	Yes	48
(4, 4, 4)	Yes	12
(4, 4, 0)	Yes	12
(4, 0, 4)	Yes	12
(4, 0, 0)	Yes	12

Table 8.2: *Possible moduli and whether odd number generations are possible for all fermionic type asymmetric pairings of internal fermions.*

Having classified the possible FSU5 pairings we can now move to the second step of the asymmetric orbifold classification where we fix the pairing and, therefore, the basis vectors and then classify the space of asymmetric orbifold models in reference to

phenomenological characteristics.

8.3 Class-Independent Analysis

A class of Flipped $SU(5)$ models is defined through the basis (8.20) with a specific choice of $\boldsymbol{A}$. This choice of $\boldsymbol{A}$ tells us a concomitant consistent $\boldsymbol{B}$ and number of $\boldsymbol{e_i}$ vectors quantified by $\boldsymbol{E}$. Two such classes will be investigated in Section 8.4 and Section 8.5. Before inspecting a specific class, it is worth seeing what we can say about all classes of models derived from the generic basis (8.20) since several features will be the same for all models.

8.3.1 Supersymmetry Constraints and Class Parameter Space

We seek to classify both $\mathcal{N} = 0$ and $\mathcal{N} = 1$ models and so it is important to define a necessary and sufficient condition for the presence of $\mathcal{N} = 1$ supersymmetry. The analysis is a simple extension of the symmetric $SO(10)$ case delineated in Section 4.1.

We first note that the gravitini and gaugini arise from

$$\partial\overline{X}^{\mu}\,|\boldsymbol{S}\rangle \tag{8.35}$$

$$\{\bar{\lambda}^{a}\}\{\bar{\lambda}^{b}\}\,|\boldsymbol{S}\rangle, \tag{8.36}$$

respectively. Therefore the following GGSO phases are fixed as follows

$$C\begin{bmatrix}\boldsymbol{S}\\ \boldsymbol{e_i}\end{bmatrix} = C\begin{bmatrix}\boldsymbol{S}\\ \boldsymbol{z_1}\end{bmatrix} = C\begin{bmatrix}\boldsymbol{S}\\ \boldsymbol{x}\end{bmatrix} = C\begin{bmatrix}\boldsymbol{S}\\ \boldsymbol{\gamma}\end{bmatrix} = -1, \tag{8.37}$$

in order to preserve one gravitino. Furthermore we note that the phases $C[\frac{\mathbb{1}}{\boldsymbol{S}}]$ and $C[\frac{\boldsymbol{S}}{\boldsymbol{b_k}}]$, $k = 1,2,3$, determine the chirality of the degenerate Ramond vacuum $|\boldsymbol{S}\rangle$ and the gravitino is retained so long as

$$C\begin{bmatrix}\mathbb{1}\\ \boldsymbol{S}\end{bmatrix} = C\begin{bmatrix}\boldsymbol{S}\\ \boldsymbol{b_1}\end{bmatrix}C\begin{bmatrix}\boldsymbol{S}\\ \boldsymbol{b_2}\end{bmatrix}C\begin{bmatrix}\boldsymbol{S}\\ \boldsymbol{b_3}\end{bmatrix}, \tag{8.38}$$

which can, without loss of generality, be fixed to

$$C\begin{bmatrix}\mathbb{1}\\ \boldsymbol{S}\end{bmatrix} = C\begin{bmatrix}\boldsymbol{S}\\ \boldsymbol{b_1}\end{bmatrix} = C\begin{bmatrix}\boldsymbol{S}\\ \boldsymbol{b_2}\end{bmatrix} = C\begin{bmatrix}\boldsymbol{S}\\ \boldsymbol{b_3}\end{bmatrix} = -1, \tag{8.39}$$

for a scan of $\mathcal{N} = 1$ vacua.

The number of independent GGSO phases for a class of models will be determined from the number of basis vectors, N, which can be written as

$$N = 8 + \sum_i E_i. \tag{8.40}$$

Taking into account the constraints (8.37) and (8.38) for $\mathcal{N}=1$ models there are

$$\frac{N(N-1)}{2}-7-\sum_i E_i, \tag{8.41}$$

independent GGSO phases[1]. The space of $\mathcal{N}=0$ vacua can be defined as the space of models violating condition (8.37) or (8.38). In ref. [94] breaking supersymmetry with different phases is discussed and it is noted how different breakings affect the spectra. If desired, we can restrict the breaking to just shifts beyond the $\mathbb{Z}_2\times\mathbb{Z}_2$ orbifold sectors by preserving condition (8.38), such that $\boldsymbol{b_1}$, $\boldsymbol{b_2}$ and $\boldsymbol{b_3}$ still preserve supersymmetry, then breaking would originate from the vectors beyond the NAHE-set through violating condition (8.37).

8.3.2 Phenomenological Features

Observable Spinorial Representations

As discussed in Section 8.2.1, the twisted sectors such as those giving rise to the spinorial $\mathbf{16}/\overline{\mathbf{16}}$ representations of $SO(10)$ are impacted by the choice of $\boldsymbol{A}$. To write these $\boldsymbol{F}^k_{pqrs}$ for a particular $\boldsymbol{A}$ we must first note the presence of the following possible linear combinations of the vector (8.22), arising for certain $\boldsymbol{E}$

$$\begin{cases} \boldsymbol{e_{3456}}=\boldsymbol{G}+\boldsymbol{e_1}+\boldsymbol{e_2}=\{y^{3456},w^{3456}\mid\bar{y}^{3456},\bar{w}^{3456}\} \text{ for } \boldsymbol{E}=(1,1,0,0,0,0)\\ \boldsymbol{e_{1256}}=\boldsymbol{G}+\boldsymbol{e_3}+\boldsymbol{e_4}=\{y^{1256},w^{1256}\mid\bar{y}^{1256},\bar{w}^{1256}\} \text{ for } \boldsymbol{E}=(0,0,1,1,0,0)\\ \boldsymbol{e_{1234}}=\boldsymbol{G}+\boldsymbol{e_5}+\boldsymbol{e_6}=\{y^{1234},w^{1234}\mid\bar{y}^{1234},\bar{w}^{1234}\} \text{ for } \boldsymbol{E}=(0,0,0,0,1,1). \end{cases} \tag{8.42}$$

Then we can write the sectors giving rise to the fermion generations as

$$\begin{aligned} \boldsymbol{F}^1_{pqrst} =&\boldsymbol{b_1}+pE_3\boldsymbol{e_3}+qE_4\boldsymbol{e_4}+rE_5\boldsymbol{e_5}+sE_6\boldsymbol{e_6}\\ &+tE_1E_2(1-E_3)(1-E_4)(1-E_5)(1-E_6)\boldsymbol{e_{3456}}\\ \boldsymbol{F}^2_{pqrst} =&\boldsymbol{b_2}+pE_1\boldsymbol{e_1}+qE_2\boldsymbol{e_2}+rE_5\boldsymbol{e_5}+sE_6\boldsymbol{e_6}\\ &+tE_3E_4(1-E_1)(1-E_2)(1-E_5)(1-E_6)\boldsymbol{e_{1256}}\\ \boldsymbol{F}^3_{pqrst} =&\boldsymbol{b_3}+pE_1\boldsymbol{e_1}+qE_2\boldsymbol{e_2}+rE_3\boldsymbol{e_3}+sE_4\boldsymbol{e_4}\\ &+tE_5E_6(1-E_1)(1-E_2)(1-E_3)(1-E_4)\boldsymbol{e_{1234}}, \end{aligned} \tag{8.43}$$

where $p,q,r,s,t\in\{0,1\}$.

In order to write down the number of $\mathbf{16}$ and $\overline{\mathbf{16}}$, N_{16} and $N_{\overline{16}}$, as a function of the GGSO coefficients we can construct the generalised projectors for these sectors $\mathbb{P}_{\boldsymbol{F}^k_{pqrst}}$,

[1] We can fix $C\binom{\mathbb{1}}{\mathbb{1}}=+1$ without loss of generality and all other phases are determined from modular invariance rules.

$k = 1, 2, 3$, such that

$$\begin{aligned}
\Upsilon(\boldsymbol{F}^1_{pqrst}) &= \{\boldsymbol{x} + 2\boldsymbol{\gamma}, \boldsymbol{z_1}, \boldsymbol{z_2}, E_1\boldsymbol{e_1}, E_2\boldsymbol{e_2}\} \\
\Upsilon(\boldsymbol{F}^2_{pqrst}) &= \{\boldsymbol{x} + 2\boldsymbol{\gamma}, \boldsymbol{z_1}, \boldsymbol{z_2}, E_3\boldsymbol{e_3}, E_4\boldsymbol{e_4}\} \\
\Upsilon(\boldsymbol{F}^3_{pqrst}) &= \{\boldsymbol{x} + 2\boldsymbol{\gamma}, \boldsymbol{z_1}, \boldsymbol{z_2}, E_5\boldsymbol{e_5}, E_6\boldsymbol{e_6}\},
\end{aligned} \tag{8.44}$$

where we recall that the vector $\boldsymbol{z_2} = \{\overline{\phi}^{5,6,7,8}\}$ is the combination defined in eq. (8.21).

In order to determine whether a sector will give rise to a **16** or a $\overline{\mathbf{16}}$ we can first define the chirality phases

$$\begin{aligned}
\boldsymbol{X}^1_{pqrs0} &= -\mathrm{ch}(\psi^\mu)C\begin{bmatrix} \boldsymbol{F}^1_{pqrs0} \\ \boldsymbol{b_2} + rE_5\boldsymbol{e_5} + sE_6\boldsymbol{e_6} \end{bmatrix}^* \\
\boldsymbol{X}^2_{pqrs0} &= -\mathrm{ch}(\psi^\mu)C\begin{bmatrix} \boldsymbol{F}^2_{pqrs0} \\ \boldsymbol{b_1} + rE_5\boldsymbol{e_5} + sE_6\boldsymbol{e_6} \end{bmatrix}^* \\
\boldsymbol{X}^3_{pqrs0} &= -\mathrm{ch}(\psi^\mu)C\begin{bmatrix} \boldsymbol{F}^3_{pqrs0} \\ \boldsymbol{b_1} + pE_3\boldsymbol{e_3} + qE_4\boldsymbol{e_4} \end{bmatrix}^*,
\end{aligned} \tag{8.45}$$

where $\mathrm{ch}(\psi^\mu)$ is the spacetime fermion chirality and we note that the sectors $\boldsymbol{F}^k_{00001}$ do not have a chirality and, instead, give rise to $D_k/2$ copies of both the **16** and the $\overline{\mathbf{16}}$.

With these definitions we can write compact expressions for N_{16} and $N_{\overline{16}}$

$$\begin{aligned}
N_{16} &= \frac{1}{2}\sum_{\substack{k=1,2,3 \\ p,q,r,s=0,1}} D_k \mathbb{P}_{\boldsymbol{F}^k_{pqrs0}}\left(1 + \boldsymbol{X}^k_{pqrs0}\right) + \frac{D_k}{2}\mathbb{P}_{F^k_{00001}} \\
N_{\overline{16}} &= \frac{1}{2}\sum_{\substack{k=1,2,3 \\ p,q,r,s=0,1}} D_k \mathbb{P}_{\boldsymbol{F}^k_{pqrs0}}\left(1 - \boldsymbol{X}^k_{pqrs0}\right) + \frac{D_k}{2}\mathbb{P}_{F^k_{00001}}.
\end{aligned} \tag{8.46}$$

Since the $SO(10)$ breaking projection $\boldsymbol{\gamma}$ decomposes the $\mathbf{16}/\overline{\mathbf{16}}$ representations into those of $SU(5) \times U(1)$ according to eq. (8.30), we can write a compact expression for each of the FSU5 quantum numbers. These of course depend on the degeneracies (8.28)

and can be written

$$
\begin{aligned}
n_{10} &= \sum_{\substack{k=1,2,3\\ p,q,r,s=0,1}} \frac{1}{2^{2-\Delta_k}} D_k \mathbb{P}_{\boldsymbol{F}^k_{pqrs0}} \left(1+\boldsymbol{X}^k_{pqrs0}\right)\left(1+(1-\Delta_k)C\begin{bmatrix}\boldsymbol{F}^k_{pqrs0}\\ \boldsymbol{\gamma}\end{bmatrix}\right)+\frac{D_k}{2}\mathbb{P}_{F^k_{00001}}\\
n_{\bar{5}} &= \sum_{\substack{k=1,2,3\\ p,q,r,s=0,1}} \frac{1}{2^{2-\Delta_k}} D_k \mathbb{P}_{\boldsymbol{F}^k_{pqrs0}} \left(1+\boldsymbol{X}^k_{pqrs0}\right)\left(1-(1-\Delta_k)C\begin{bmatrix}\boldsymbol{F}^k_{pqrs0}\\ \boldsymbol{\gamma}\end{bmatrix}\right)+\frac{D_k}{2}\mathbb{P}_{F^k_{00001}}\\
n_{\overline{10}} &= \sum_{\substack{k=1,2,3\\ p,q,r,s=0,1}} \frac{1}{2^{2-\Delta_k}} \mathbb{P}_{\boldsymbol{F}^k_{pqrs0}} \left(1-\boldsymbol{X}^k_{pqrs0}\right)\left(1+(1-\Delta_k)C\begin{bmatrix}\boldsymbol{F}^k_{pqrs0}\\ \boldsymbol{\gamma}\end{bmatrix}\right)+\frac{D_k}{2}\mathbb{P}_{F^k_{00001}}\\
n_{5} &= \sum_{\substack{k=1,2,3\\ p,q,r,s=0,1}} \frac{1}{2^{2-\Delta_k}} D_k \mathbb{P}_{\boldsymbol{F}^k_{pqrs0}} \left(1-\boldsymbol{X}^k_{pqrs0}\right)\left(1-(1-\Delta_k)C\begin{bmatrix}\boldsymbol{F}^k_{pqrs0}\\ \boldsymbol{\gamma}\end{bmatrix}\right)+\frac{D_k}{2}\mathbb{P}_{F^k_{00001}}.
\end{aligned}
\tag{8.47}
$$

The number of generations for a model is then

$$
n_g = n_{10} - n_{\overline{10}} = n_{\bar{5}} - n_5. \tag{8.48}
$$

From this we can construct a necessary condition for three generation models to exist once $\boldsymbol{A}$ is specified

$$
\exists\, C\begin{bmatrix}\boldsymbol{v_i}\\ \boldsymbol{v_j}\end{bmatrix}: \quad \sum_{\substack{k=1,2,3\\ p,q,r,s=0,1}} \frac{1}{2^{1-\Delta_k}} D_k \mathbb{P}_{\boldsymbol{F}^k_{pqrs0}} \boldsymbol{X}^k_{pqrs0}\left(1+(1-\Delta_k)C\begin{bmatrix}\boldsymbol{F}^k_{pqrs0}\\ \boldsymbol{\gamma}\end{bmatrix}\right) = 3 \tag{8.49}
$$

$$
\text{and} \quad \sum_{\substack{k=1,2,3\\ p,q,r,s=0,1}} 2^{\Delta_k} D_k \mathbb{P}_{\boldsymbol{F}^k_{pqrs0}} \boldsymbol{X}^k_{pqrs0}(1-\Delta_k)C\begin{bmatrix}\boldsymbol{F}^k_{pqrs0}\\ \boldsymbol{\gamma}\end{bmatrix} = 0. \tag{8.50}
$$

Checking that there exists a solution to this equation for a class of models and enumerating such solutions can be done easily by inputting this constraint into an SMT solver, such as Z3.

Heavy Higgs

Another key representation for phenomenology is the presence of a Higgs breaking the $SU(5)\times U(1)$ that we call the Heavy Higgs. This arises from the representation $\left(\mathbf{10},+\frac{1}{2}\right)+\left(\overline{\mathbf{10}},-\frac{1}{2}\right)$. The relevant sectors are

$$
\boldsymbol{B}^k_{pqrst} = \boldsymbol{S} + \boldsymbol{F}^k_{pqrst}, \quad k=1,2,3, \tag{8.51}
$$

which in the case of $\mathcal{N}=1$ supersymmetric models are the (bosonic) superpartners of the spinorials $\mathbf{16}/\overline{\mathbf{16}}$ sectors (8.43). We note that the generalised projectors for these sectors $\mathbb{P}_{\boldsymbol{B}^k_{pqrst}}$, $k=1,2,3$, can be constructed such that $\mathrm{Y}(\boldsymbol{B}^k_{pqrst})$ equals $\mathrm{Y}(\boldsymbol{F}^k_{pqrst})$ from

eq. (8.44).

We note that with a Heavy Higgs the FSU5 GUT can be broken and the particles of Standard Model arise from the decomposition of the FSU5 representations (8.30) under $SU(3) \times SU(2) \times U(1)$. From the **16** we have

$$\begin{aligned}
\left(\bar{\mathbf{5}}, -\frac{3}{2}\right) &= \left(\bar{\mathbf{3}}, \mathbf{1}, -\frac{2}{3}\right)_{u^c} + \left(\mathbf{1}, \mathbf{2}, -\frac{1}{2}\right)_{L}, \\
\left(\mathbf{10}, +\frac{1}{2}\right) &= \left(\mathbf{3}, \mathbf{2}, +\frac{1}{6}\right)_{Q} + \left(\bar{\mathbf{3}}, \mathbf{1}, +\frac{1}{3}\right)_{d^c} + (\mathbf{1}, \mathbf{1}, 0)_{\nu^c}, \\
\left(\mathbf{1}, +\frac{5}{2}\right) &= (\mathbf{1}, \mathbf{1}, +1)_{e^c},
\end{aligned} \tag{8.52}$$

where L is the lepton–doublet; Q is the quark–doublet; d^c, u^c, e^c and ν^c are the quark and lepton singlets.

Light Higgs

The light Higgs representations are electroweak Higgs doublets. In $\mathcal{N} = 1$ supersymmetric models, a pair is required to give masses to up and down-quark, respectively. In models in which spacetime supersymmetry is broken entirely at the string level, this may be relaxed. However, as the models descend from $\mathcal{N} = 1$ supersymmetric models, they retain some of this underlying structure and mass terms at leading order are generated for the respective Higgs doublets pairs. We therefore require the existence of a pair of light Higgs multiplets also in $\mathcal{N} = 0$ models. We further note the existence of a doublet-triplet splitting mechanism in the untwisted sector of the asymmetric models [126]. This mechanism is operational in asymmetric models with the breaking pattern $SO(10) \to SO(6) \times SO(4)$ and is therefore not relevant in the Flipped $SU(5)$ models that are of interest here. We note, however, that in Flipped $SU(5)$ models the untwisted sector produces three pairs in the $\mathbf{5} + \bar{\mathbf{5}}$ representation of $SU(5)$, which contain electroweak Higgs doublets that may serve as light Higgs multiplets. However, we note that the generation of hierarchical fermion masses typically necessitates utilisation of Higgs doublets that arise from twisted sectors [134, 135]. We therefore examine here the conditions for obtaining vectorial representations in the twisted sectors.

Sectors giving rise to vectorial **10** representations, that include the twisted Light Higgs, can be written

$$\boldsymbol{V}^k_{pqrst} = \boldsymbol{S} + \boldsymbol{F}^k_{pqrst} + \boldsymbol{x}, \tag{8.53}$$

where the states are of the form $\{\bar{\lambda}\}_{\frac{1}{2}} \left|\boldsymbol{V}^k_{pqrst}\right\rangle$, $k = 1, 2, 3$, meaning that they have a single antiholomorphic oscillator of frequency $\frac{1}{2}$, as defined in eq. (3.39), accompanying the degenerate Ramond vacuum. The SM Higgs will arise when this sector, with $\bar{\lambda} = \bar{\psi}^a$, $a \in \{1, 2, 3, 4, 5\}$, is retained in the massless spectrum of a model. For these sectors

the generalised projector $\mathbb{P}_{\{\bar{\psi}^a\}\boldsymbol{V}^k_{pqrst}}$ takes the general form of eq. (4.9) and $\Upsilon(\boldsymbol{V}^k_{pqrst})$ will be the same as $\Upsilon(\boldsymbol{F}^k_{pqrst})$ from eq. (8.44).

We note that any surviving sector gives rise to a vectorial **10** decomposing under $SU(5) \times U(1)$ according to

$$\mathbf{10} = (\mathbf{5}, -1) + (\bar{\mathbf{5}}, +1). \tag{8.54}$$

These two representations taken together can be identified as the SM Higgs breaking the electroweak gauge group. Therefore the number of Light Higgses from the twisted sectors is given by

$$n_{5h} = \#\left[(\mathbf{5}, -1) + (\bar{\mathbf{5}}, +1)\right]. \tag{8.55}$$

Tachyonic Sectors

Since we include non-supersymmetric models in our classification it is vital we check for the absence of on-shell tachyons, in order to ensure the stability of our models for a 4D Minkowski background. To do this, we encode the GGSO projections for all on-shell tachyonic sectors. Many tachyonic sectors can arise due to $\boldsymbol{e_i}$ vectors, certain $\boldsymbol{\gamma}$ combinations and other class-dependent combinations and therefore depend on the choice of $\boldsymbol{A}$ and require class-by-class analysis. However, we will always have the untwisted tachyon

$$\{\bar{\lambda}\}\,|0\rangle_{NS}\,, \tag{8.56}$$

that is projected for all models through the $\boldsymbol{S}$ projection. In addition, the following on-shell tachyonic sectors arise for all classes of models

$$T = \begin{Bmatrix} |\boldsymbol{z_1}\rangle & |\boldsymbol{z_2}\rangle & |\boldsymbol{x}+2\boldsymbol{\gamma}\rangle \\ |\boldsymbol{z_1}+\boldsymbol{x}+2\boldsymbol{\gamma}\rangle & |\boldsymbol{z_2}+\boldsymbol{x}+2\boldsymbol{\gamma}\rangle & |\boldsymbol{z_1}+\boldsymbol{z_2}+\boldsymbol{x}+2\boldsymbol{\gamma}\rangle \end{Bmatrix}. \tag{8.57}$$

All of these sectors, $\boldsymbol{t} \in T$, must be projected from the spectrum through appropriate definitions of their generalised projectors $\mathbb{P}_{\boldsymbol{t}} = 0$. Once we specify the vector $\boldsymbol{A}$ we can then determine the further class-dependent tachyonic sectors and ensure their projection.

Enhancements

Additional space-time vector bosons may arise in all models derived from the basis (8.20). The following enhancements arise independent of the class

$$\begin{Bmatrix} \psi^\mu\{\bar{\lambda}\}_{\frac{1}{2}}: & |\boldsymbol{z_1}\rangle & |\boldsymbol{z_2}\rangle & |\boldsymbol{x}+2\boldsymbol{\gamma}\rangle & |\boldsymbol{z_1}+\boldsymbol{x}+2\boldsymbol{\gamma}\rangle & |\boldsymbol{z_2}+\boldsymbol{x}+2\boldsymbol{\gamma}\rangle \\ \psi^\mu: & |\boldsymbol{x}\rangle & |\boldsymbol{z_1}+\boldsymbol{z_2}\rangle & & & \end{Bmatrix}, \tag{8.58}$$

with the following subset being enhancements to the observable gauge factors

$$H = \begin{Bmatrix} \psi^\mu\{\bar{\psi}^a\}: & |\boldsymbol{z_1}\rangle & |\boldsymbol{z_2}\rangle & |\boldsymbol{x}+2\boldsymbol{\gamma}\rangle \\ \psi^\mu\{\bar{\psi}^a\}: & |\boldsymbol{z_1}+\boldsymbol{x}+2\boldsymbol{\gamma}\rangle & |\boldsymbol{z_2}+\boldsymbol{x}+2\boldsymbol{\gamma}\rangle & |\boldsymbol{x}+2\boldsymbol{\gamma}+\boldsymbol{z_1}+\boldsymbol{z_2}\rangle \\ \psi^\mu: & |\boldsymbol{x}\rangle & & \end{Bmatrix}, \tag{8.59}$$

with $a = 1,2,3,4,5$. Therefore, from these sectors we can restrict our analysis to models with observable gauge group $SU(5) \times U(1) \times U(1)_{i=1,2,3}$ by imposing

$$\forall\, \boldsymbol{h} \in H:\ \mathbb{P}_{\boldsymbol{h}} = 0. \tag{8.60}$$

In this case, for these generalised projectors we have

$$\begin{aligned}
\Upsilon(\boldsymbol{z_1}) &= \{\boldsymbol{S}, E_1\boldsymbol{e_1}, E_2\boldsymbol{e_2}, E_3\boldsymbol{e_3}, E_4\boldsymbol{e_4}, E_5\boldsymbol{e_5}, E_6\boldsymbol{e_6}, \boldsymbol{x}, \boldsymbol{b_1}, \boldsymbol{b_2}, \boldsymbol{z_2}\}\\
\Upsilon(\boldsymbol{z_2}) &= \{\boldsymbol{S}, E_1\boldsymbol{e_1}, E_2\boldsymbol{e_2}, E_3\boldsymbol{e_3}, E_4\boldsymbol{e_4}, E_5\boldsymbol{e_5}, E_6\boldsymbol{e_6}, \boldsymbol{x}, \boldsymbol{b_1}, \boldsymbol{b_2}, \boldsymbol{z_1}\}\\
\Upsilon(\boldsymbol{x}+2\boldsymbol{\gamma}) &= \{\boldsymbol{S}, E_1\boldsymbol{e_1}, E_2\boldsymbol{e_2}, E_3\boldsymbol{e_3}, E_4\boldsymbol{e_4}, E_5\boldsymbol{e_5}, E_6\boldsymbol{e_6}, \boldsymbol{x}, \boldsymbol{x}+2\boldsymbol{\gamma}+\boldsymbol{z_1}+\boldsymbol{z_2}\}\\
\Upsilon(\boldsymbol{x}+2\boldsymbol{\gamma}+\boldsymbol{z_1}) &= \{\boldsymbol{S}, E_1\boldsymbol{e_1}, E_2\boldsymbol{e_2}, E_3\boldsymbol{e_3}, E_4\boldsymbol{e_4}, E_5\boldsymbol{e_5}, E_6\boldsymbol{e_6}, \boldsymbol{x}, \boldsymbol{x}+2\boldsymbol{\gamma}+\boldsymbol{z_2}\}\\
\Upsilon(\boldsymbol{x}+2\boldsymbol{\gamma}+\boldsymbol{z_2}) &= \{\boldsymbol{S}, E_1\boldsymbol{e_1}, E_2\boldsymbol{e_2}, E_3\boldsymbol{e_3}, E_4\boldsymbol{e_4}, E_5\boldsymbol{e_5}, E_6\boldsymbol{e_6}, \boldsymbol{x}, \boldsymbol{x}+2\boldsymbol{\gamma}+\boldsymbol{z_1}\}\\
\Upsilon(\boldsymbol{x}+2\boldsymbol{\gamma}+\boldsymbol{z_1}+\boldsymbol{z_2}) &= \{\boldsymbol{S}, E_1\boldsymbol{e_1}, E_2\boldsymbol{e_2}, E_3\boldsymbol{e_3}, E_4\boldsymbol{e_4}, E_5\boldsymbol{e_5}, E_6\boldsymbol{e_6}, \boldsymbol{x}, \boldsymbol{x}+2\boldsymbol{\gamma}\}\\
\Upsilon(\boldsymbol{x}) &= \{\boldsymbol{S}, E_1\boldsymbol{e_1}, E_2\boldsymbol{e_2}, E_3\boldsymbol{e_3}, E_4\boldsymbol{e_4}, E_5\boldsymbol{e_5}, E_6\boldsymbol{e_6}, \boldsymbol{z_1}, \boldsymbol{z_2}\}.
\end{aligned} \tag{8.61}$$

Additional enhancements may arise depending on the specific form of $\boldsymbol{\gamma}$ which can be analysed class-by-class.

Exotics

Another important consideration for ensuring reasonable phenomenology is the absence of chiral exotics. The exotics sectors in general depend on the class, in particular on the exact form of $\boldsymbol{\gamma}$ since combinations of $\boldsymbol{\gamma}$ will be those that can generate exotics.

However, we can note here the following exotic sectors with $(\boldsymbol{\alpha}_L \cdot \boldsymbol{\alpha}_L, \boldsymbol{\alpha}_R \cdot \boldsymbol{\alpha}_R) = (4,4)$

$$\{\bar{\psi}^a\}_{\frac{1}{2}} : \Big\{|\boldsymbol{S}+\boldsymbol{z_1}\rangle \quad |\boldsymbol{S}+\boldsymbol{z_2}\rangle \quad |\boldsymbol{S}+\boldsymbol{x}+2\boldsymbol{\gamma}\rangle \quad |\boldsymbol{S}+\boldsymbol{z_1}+\boldsymbol{x}+2\boldsymbol{\gamma}\rangle \quad |\boldsymbol{S}+\boldsymbol{z_2}+\boldsymbol{x}+2\boldsymbol{\gamma}\rangle\Big\} \tag{8.62}$$

where $a \in \{1,...,5\}$. We note that these are the would-be gaugini of the enhancements (8.58). These sectors will not contribute to a chiral anomaly as they are automatically vector-like. It will then be necessary to analyse the other exotics at the level of a particular class of vacua.

8.3.3 Asymmetric Pairings, Up-Type Yukawa Couplings and Higgs Doublet-Triplet Splitting

Top quark Yukawa couplings in the string models derived from the $\mathbb{Z}_2 \times \mathbb{Z}_2$ heterotic orbifold take the general form

$$\lambda_t \mathbf{S}^{Q_L} \mathbf{S}^{u_R} \mathbf{V}^{H_u}. \tag{8.63}$$

It can be demonstrated that this coupling can come either from a coupling of the type $T_k T_k U_k$, $k = 1,2,3$, or of the type $T_k T_l T_m$, $k \neq l \neq m = 1,2,3$, where T indicates a

twisted sector and U indicates the (untwisted) Neveu-Schwarz sector. The assignment of asymmetric boundary conditions determines which of the two couplings can appear at leading order in the string vacua [130].

The asymmetric boundary conditions for the internal worldsheet fermions $\{y^I, w^I \mid \bar{y}^I, \bar{w}^I\}$ induce a doublet–triplet splitting mechanism of the untwisted $\mathbf{5}$ and $\bar{\mathbf{5}}$ representations [126]. The mechanism is induced by the basis vectors that break the $SO(10)$ symmetry to the Pati–Salam subgroup, with respect to the three pairs of untwisted vectorial $\mathbf{5}$ and $\bar{\mathbf{5}}$ multiplets, where symmetric boundary conditions retain the colour triplet pairs, and project the electroweak doublets, whereas asymmetric boundary conditions project the triplets and retain the doublets. Thus, in the case of models with solely symmetric boundary conditions, only Flipped $SU(5)$ models can produce cubic level couplings of the type $T_kT_kU_k$, utilising the Higgs doublets from the NS sector.

Similar to the stringy doublet-triplet splitting mechanism that is determined by the assignment of asymmetric versus symmetric boundary conditions, the asymmetric/symmetric assignment selects between up/down-quark Yukawa couplings at leading order [125, 130, 133]. This Yukawa coupling selection mechanism operates in the basis vector that breaks the $SO(10)$ symmetry to the $SU(5) \times U(1)$ subgroup, where symmetric boundary conditions select a down-quark type Yukawa coupling, whereas asymmetric boundary conditions select an up-quark type Yukawa coupling. Hence, this Yukawa coupling selection mechanism can be utilised in Flipped $SU(5)$ and standard-like string models.

Given that we consider Flipped $SU(5)$ models, representations in the $\mathbf{5}$ and $\bar{\mathbf{5}}$ of $SU(5)$ arise from the NS sector generically. These representations yield the electroweak Higgs doublets and color Higgs triplets. Through asymmetric boundary condition assignments of the internal fermions under an extra Pati-Salam type breaking vector, the doublets and triplets may be distinguished. However, in our case, we will get both regardless of the GGSO configuration and boundary condition assignment from $\boldsymbol{A}$. Therefore top mass couplings of the form $T_kT_kU_k$ can arise in our models.

As is familiar from the symmetric orbifold classification, couplings $T_kT_lT_m$ can also arise. In this case the Higgs doublet arises from the twisted sectors (8.53). Therefore, both types of couplings can give rise to a realistic up-Type Yukawa coupling and both will be analysed. Similar to the case of the couplings to the untwisted Higgs doublets, selection conditions of up-type versus down-type quark Yukawa couplings can be formulated [136].

8.3.4 Partition Function and Cosmological Constant for Asymmetric Orbifolds

The analysis of the partition function for our asymmetric orbifolds is largely similar to the symmetric case presented in Section 5.5. However, there are some key differences and subtleties which are important to explicitly discuss. These arise for two main reasons, namely the asymmetric pairings introduced by the basis vector $\boldsymbol{\gamma}$ and the appearance of half boundary conditions in the basis set (8.20).

From the point of view of the partition function, the asymmetric pairings introduce imaginary GGSO phases, meaning that the fermionic partition function

$$Z = \sum_{\boldsymbol{\alpha},\boldsymbol{\beta}} C\begin{bmatrix}\boldsymbol{\alpha}\\ \boldsymbol{\beta}\end{bmatrix} \prod_f Z\begin{bmatrix}\boldsymbol{\alpha}(f)\\ \boldsymbol{\beta}(f)\end{bmatrix}, \tag{8.64}$$

will have imaginary terms which have to cancel. This cancellation is, however, ensured by modular invariance. In the case of symmetric orbifolds, since $Z\left[\begin{smallmatrix}a\\ b\end{smallmatrix}\right] = \sqrt{\vartheta\left[\begin{smallmatrix}a\\ b\end{smallmatrix}\right]}$, the fermionic part of the partition function can be expressed using the four standard Jacobi theta functions of eq. (2.120). In the presence of half boundary conditions there will be sixteen such theta functions with a and b now taking values in the set $a, b \in \{-1/2, 0, 1/2, 1\}$.

To express the partition function of the models under consideration in the classification setup, it is beneficial to use the notation utilised in [42, 43, 44]. This makes many properties immediately readable from the form of the partition function and allows us to economically express all models used in this chapter in one compact form. Since the classification of asymmetric shifts depends on the exact form of the vector $\boldsymbol{\gamma}$ it is instructive to first write down the partition function of the subset $\{\mathbb{1}, \boldsymbol{e_i}, \boldsymbol{S}, \boldsymbol{b_1}, \boldsymbol{b_2}, \boldsymbol{b_3}, \boldsymbol{z_1}, \boldsymbol{x}\}$, without $\boldsymbol{\gamma}$. In this case, all $\boldsymbol{e_i}$ are compatible and so we have 13 basis vectors giving

$$\begin{aligned} Z =& \frac{1}{\eta^{10}\bar{\eta}^{22}} \frac{1}{2^4} \sum_{\substack{a,k,r,\rho\\ b,l,s,\sigma}} \frac{1}{2^6} \sum_{\substack{H_i\\ G_i}} \frac{1}{2^3} \sum_{\substack{h_1,h_2,H\\ g_1,g_2,G}} (-1)^{\Phi\left[\begin{smallmatrix} a & k & \rho & r & H_i & h_1 & h_2 & H\\ b & l & s & \sigma & G_i & g_1 & g_2 & G\end{smallmatrix}\right]} \\ &\times \vartheta\left[\begin{smallmatrix}a\\ b\end{smallmatrix}\right] \vartheta\left[\begin{smallmatrix}a+h_1\\ b+g_1\end{smallmatrix}\right] \vartheta\left[\begin{smallmatrix}a+h_2\\ b+g_2\end{smallmatrix}\right] \vartheta\left[\begin{smallmatrix}a-h_1-h_2\\ b-g_1-g_2\end{smallmatrix}\right] \\ &\times \Gamma_{(6,6)}\left[\begin{smallmatrix} r & H_i & h_1 & h_2\\ s & G_i & g_1 & g_2\end{smallmatrix}\right] \\ &\times \bar{\vartheta}\left[\begin{smallmatrix}k\\ l\end{smallmatrix}\right]^5 \bar{\vartheta}\left[\begin{smallmatrix}k+h_1\\ l+g_1\end{smallmatrix}\right] \bar{\vartheta}\left[\begin{smallmatrix}k+h_2\\ l+g_2\end{smallmatrix}\right] \bar{\vartheta}\left[\begin{smallmatrix}k-h_1-h_2\\ l-g_1-g_2\end{smallmatrix}\right] \bar{\vartheta}\left[\begin{smallmatrix}\rho\\ \sigma\end{smallmatrix}\right]^4 \bar{\vartheta}\left[\begin{smallmatrix}\rho+H\\ \sigma+G\end{smallmatrix}\right]^4, \end{aligned} \tag{8.65}$$

where all indices are summed over the set $\{0, 1\}$. The phase Φ, which is a polynomial in the summation indices, is chosen such that the entire partition function is modular invariant. The choice of this phase translates to a choice of GGSO matrix in the classification setup. Indices k, l and ρ, σ represent the sixteen complex right-moving fermions

giving the fermionic representation of the $E_8 \times E_8$ lattice of the underlying 10D heterotic theory. The non-freely acting $\mathbb{Z}_2 \times \mathbb{Z}_2$ orbifold is represented by the parameters h_i and g_i, where the h_i give the various twists, while the g_i implement the orbifold projections. The H_i and G_i correspond to the basis vectors $\mathbf{e_i}$ and, hence, are responsible for orbifold shifts along the six internal dimensions of the T^6. Finally, H and G break one of the E_8 factors in the hidden sector by a $\mathbb{Z}_2$ twist.

The internal lattice, $\Gamma_{(6,6)}$, which corresponds to the T^6 is given by

$$\begin{aligned}\Gamma_{(6,6)}\begin{bmatrix} r & H_i & h_1 & h_2 \\ s & G_i & g_1 & g_2 \end{bmatrix} = \Big| & \vartheta_{y\bar{y}^1}\begin{bmatrix} r+h_1+H_1 \\ s+g_1+G_1 \end{bmatrix}\vartheta_{y\bar{y}^2}\begin{bmatrix} r+h_1+H_2 \\ s+g_1+G_2 \end{bmatrix}\vartheta_{y\bar{y}^3}\begin{bmatrix} r+h_2+H_3 \\ s+g_2+G_3 \end{bmatrix} \\ & \times \vartheta_{y\bar{y}^4}\begin{bmatrix} r+h_2+H_4 \\ s+g_2+G_4 \end{bmatrix}\vartheta_{y\bar{y}^5}\begin{bmatrix} r+h_2+H_5 \\ s+g_2+G_5 \end{bmatrix}\vartheta_{y\bar{y}^6}\begin{bmatrix} r+h_2+H_6 \\ s+g_2+G_6 \end{bmatrix} \\ & \times \vartheta_{w\bar{w}^1}\begin{bmatrix} r-h_1-h_2+H_1 \\ s-g_1-g_2+G_1 \end{bmatrix}\vartheta_{w\bar{w}^2}\begin{bmatrix} r-h_1-h_2+H_2 \\ s-g_1-g_2+G_2 \end{bmatrix}\vartheta_{w\bar{w}^3}\begin{bmatrix} r-h_1-h_2+H_3 \\ s-g_1-g_2+G_3 \end{bmatrix} \\ & \times \vartheta_{w\bar{w}^4}\begin{bmatrix} r-h_1-h_2+H_4 \\ s-g_1-g_2+G_4 \end{bmatrix}\vartheta_{w\bar{w}^5}\begin{bmatrix} r+h_1+H_5 \\ s+g_1+G_5 \end{bmatrix}\vartheta_{w\bar{w}^6}\begin{bmatrix} r+h_1+H_6 \\ s+g_1+G_6 \end{bmatrix}\Big|,\end{aligned} \tag{8.66}$$

where $|\vartheta\left[\begin{smallmatrix} a \\ b \end{smallmatrix}\right]| = \sqrt{\vartheta\left[\begin{smallmatrix} a \\ b \end{smallmatrix}\right]\bar{\vartheta}\left[\begin{smallmatrix} a \\ b \end{smallmatrix}\right]}$. The subscript on the ϑ's denotes which worldsheet fermions the terms correspond to. We see that with this basis the internal lattice is left-right symmetric.This is why the internal lattice can be written as a magnitude.

The introduction of asymmetric pairings via the vector $\boldsymbol{\gamma}$ introduces further complexity to the above partition function. Recall the notation introduced in Section 8.1, where the most general consistent form of $\boldsymbol{\gamma}$ is written as in (8.10)

$$\boldsymbol{\gamma} = \boldsymbol{A} + \{\bar{\psi}^{1,\dots,5} = \bar{\eta}^{1,2,3} = \bar{\phi}^{1,2,6,7} = \frac{1}{2}\} + \boldsymbol{B}, \tag{8.67}$$

where

$$\begin{aligned}\boldsymbol{B} &= \{B(\bar{\phi}^3), B(\bar{\phi}^4), B(\bar{\phi}^5), B(\bar{\phi}^8)\}, \\ \boldsymbol{A} &= \begin{cases} \{A(y^1), \cdots, A(w^6)\,|A(\bar{y}^1), \cdots, A(\bar{w}^6)\} & \text{if } \boldsymbol{\gamma} \text{ bosonic;} \\ \{\psi^\mu, \chi^{12}, A(y^1), \cdots, A(w^6) \mid A(\bar{y}^1), \cdots, A(\bar{w}^6)\} & \text{if } \boldsymbol{\gamma} \text{ fermionic.} \end{cases}\end{aligned} \tag{8.68}$$

Also recall the vector $\boldsymbol{E} = (E_1, E_2, E_3, E_4, E_5, E_6)$ of (8.23), which qualifies which of the $\boldsymbol{e_i}$ are compatible with a specific choice of $\boldsymbol{\gamma}$ and hence appears in the basis set. That is, if $E_i = 0$ then $\boldsymbol{e_i} \notin \mathcal{B}$ and vice-versa.

In terms of the above quantities, we can now examine the effect of $\boldsymbol{\gamma}$ on the partition function (8.65) within the frame of the general classification setup. For simplicity, we consider the case where $\boldsymbol{\gamma}$ is bosonic and hence has no action on ψ^μ and $\chi^{1,\dots,6}$. The antiholomorphic hidden worldsheet fermions are affected by the choice of $\boldsymbol{B}$, while the specific choice of $\boldsymbol{A}$ will only change how the internal lattice is structured. Thus the

partition function takes the form

$$
\begin{aligned}
Z =& \frac{1}{\eta^{10}\bar{\eta}^{22}}\,\frac{1}{2^4}\sum_{\substack{a,k,r,\rho\\ b,l,s,\sigma}}\frac{1}{2^{\sum_i E_i}}\sum_{\substack{H_i\\ G_i}}\frac{1}{2^3}\sum_{\substack{h_1,h_2,H\\ g_1,g_2,G}}\frac{1}{4}\sum_{\substack{H'\\ G'}}(-1)^{\Phi\left[\begin{smallmatrix} a & k & \rho & r & H_i & h_1 & h_2 & H & H'\\ b & l & s & \sigma & G_i & g_1 & g_2 & G & G'\end{smallmatrix}\right]}\\
&\times\vartheta\left[\begin{smallmatrix}a\\ b\end{smallmatrix}\right]\vartheta\left[\begin{smallmatrix}a+h_1\\ b+g_1\end{smallmatrix}\right]\vartheta\left[\begin{smallmatrix}a+h_2\\ b+g_2\end{smallmatrix}\right]\vartheta\left[\begin{smallmatrix}a-h_1-h_2\\ b-g_1-g_2\end{smallmatrix}\right]\\
&\times\Gamma^{\gamma}_{(6,6)}\left[\begin{smallmatrix} r & H_i & h_1 & h_2 & H'\\ s & G_i & g_1 & g_2 & G'\end{smallmatrix}\right]\\
&\times\bar{\vartheta}\left[\begin{smallmatrix}k+H'\\ l+G'\end{smallmatrix}\right]^5\bar{\vartheta}\left[\begin{smallmatrix}k+h_1+H'\\ l+g_1+G'\end{smallmatrix}\right]\bar{\vartheta}\left[\begin{smallmatrix}k+h_2+H'\\ l+g_2+G'\end{smallmatrix}\right]\bar{\vartheta}\left[\begin{smallmatrix}k-h_1-h_2+H'\\ l-g_1-g_2+G'\end{smallmatrix}\right]\\
&\times\bar{\vartheta}\left[\begin{smallmatrix}\rho+H'\\ \sigma+G'\end{smallmatrix}\right]^2\bar{\vartheta}\left[\begin{smallmatrix}\rho+H+H'\\ \sigma+G+G'\end{smallmatrix}\right]^2\bar{\vartheta}\left[\begin{smallmatrix}\rho+2B(\bar{\phi}^3)H'\\ \sigma+2B(\bar{\phi}^3)G'\end{smallmatrix}\right]\bar{\vartheta}\left[\begin{smallmatrix}\rho+2B(\bar{\phi}^4)H'\\ \sigma+2B(\bar{\phi}^4)G'\end{smallmatrix}\right]\\
&\times\bar{\vartheta}\left[\begin{smallmatrix}\rho+H+2B(\bar{\phi}^5)H'\\ \sigma+G+2B(\bar{\phi}^5)G'\end{smallmatrix}\right]\bar{\vartheta}\left[\begin{smallmatrix}\rho+H+2B(\bar{\phi}^8)H'\\ \sigma+G+2B(\bar{\phi}^8)G'\end{smallmatrix}\right],
\end{aligned}
\tag{8.69}
$$

where the sum in the new indices H' and G' run over $\{-1/2, 0, 1/2, 1\}$, as opposed to the other indices, which still take values in $\{0, 1\}$. This is because the half boundary conditions in $\boldsymbol{\gamma}$ introduce a new $\mathbb{Z}_4$ orbifold to the picture. The factor of two in front of some indices is a result of having both half and integer boundary conditions within the same basis vector, and hence this factor ensures that integer boundary conditions are correctly accounted for.

The form of the internal lattice $\Gamma^{\gamma}_{(6,6)}$ depends on the choice of asymmetric shifts in the internal degrees of freedom, *i.e.* $\boldsymbol{A}$. Consequently, this determines which of the symmetric $\mathbb{Z}_2$ shifts, $\boldsymbol{e_i}$, are compatible with this choice, which fixes $\boldsymbol{E}$. The asymmetric shifts introduced by $\boldsymbol{\gamma}$ break the left-right symmetry of the lattice (8.66). To examine this further, we have to look at what happens to a set of internal fermions corresponding to one of the orbifold planes. If we take the fist plane, *i.e.* the fermions $\{y^{3,4,5,6} \mid \bar{y}^{3,4,5,6}\}$, the corresponding part of the lattice is

$$
\begin{aligned}
\Gamma_1 =\ & \vartheta_{y^3}\left[\begin{smallmatrix}r+h_2+H_3\\ s+g_2+G_3\end{smallmatrix}\right]^{1/2}\vartheta_{y^4}\left[\begin{smallmatrix}r+h_2+H_4\\ s+g_2+G_4\end{smallmatrix}\right]^{1/2}\vartheta_{y^5}\left[\begin{smallmatrix}r+h_2+H_5\\ s+g_2+G_5\end{smallmatrix}\right]^{1/2}\vartheta_{y^6}\left[\begin{smallmatrix}r+h_2+H_6\\ s+g_2+G_6\end{smallmatrix}\right]^{1/2}\\
&\times\vartheta_{\bar{y}^3}\left[\begin{smallmatrix}r+h_2+H_3\\ s+g_2+G_3\end{smallmatrix}\right]^{1/2}\bar{\vartheta}_{\bar{y}^4}\left[\begin{smallmatrix}r+h_2+H_4\\ s+g_2+G_4\end{smallmatrix}\right]^{1/2}\bar{\vartheta}_{\bar{y}^5}\left[\begin{smallmatrix}r+h_2+H_5\\ s+g_2+G_5\end{smallmatrix}\right]^{1/2}\bar{\vartheta}_{\bar{y}^6}\left[\begin{smallmatrix}r+h_2+H_6\\ s+g_2+G_6\end{smallmatrix}\right]^{1/2}.
\end{aligned}
\tag{8.70}
$$

Since the asymmetric shifts cannot mix the orbifold planes, we either have 0, 1 or 2 such shifts affecting these fermions. As an example, we consider what happens when $\boldsymbol{A}$ contains one such pairing, say y^5y^6. Firstly, this imposes that $\boldsymbol{E} = (1,1,1,1,0,0)$, *i.e.* $\boldsymbol{e_{5,6}}$ are no longer in the basis, so that $H_{5,6}$ and $G_{5,6}$ are not present. Secondly, it breaks the left-right symmetry of the $(y^5\bar{y}^5)$ and $(y^6\bar{y}^6)$ pairings, which become $(y^5\bar{y}^5)(y^6\bar{y}^6) \to (y^5y^6)(\bar{y}^5\bar{y}^6)$. Given the above factors, the internal lattice of the first

orbifold plane becomes

$$\begin{aligned}\Gamma_1^{\gamma} = \; & \vartheta_{y^3}\begin{bmatrix} r+h_2+H_3 \\ s+g_2+G_3 \end{bmatrix}^{1/2} \vartheta_{y^4}\begin{bmatrix} r+h_2+H_4 \\ s+g_2+G_4 \end{bmatrix}^{1/2} \vartheta_{y^{5,6}}\begin{bmatrix} r+h_2+2H' \\ s+g_2+2G' \end{bmatrix} \\ & \times \vartheta_{\bar{y}^3}\begin{bmatrix} r+h_2+H_3 \\ s+g_2+G_3 \end{bmatrix}^{1/2} \bar{\vartheta}_{\bar{y}^4}\begin{bmatrix} r+h_2+H_4 \\ s+g_2+G_4 \end{bmatrix}^{1/2} \bar{\vartheta}_{\bar{y}^{5,6}}\begin{bmatrix} r+h_2 \\ s+g_2 \end{bmatrix}. \end{aligned} \tag{8.71}$$

If there are two such asymmetric holomorphic pairings in the first plane then, regardless of the specific pairing, the lattice simply becomes

$$\Gamma_1^{\gamma} = \; \vartheta_{y^{3,4,5,6}}\begin{bmatrix} r+h_2+2H' \\ s+g_2+2G' \end{bmatrix}^2 \bar{\vartheta}_{\bar{y}^{3,4,5,6}}\begin{bmatrix} r+h_2 \\ s+g_2 \end{bmatrix}^2. \tag{8.72}$$

The construction of the partition function for the remaining two planes is equivalent and can be straightforwardly done once a specific basis is taken.

Once a model is chosen and the partition function is fixed according to the above considerations, the one-loop cosmological constant can be calculated according to methods outlined in Section 5.5. Since we seek models free of physical tachyons, the series expansion contains only finite terms and converges exponentially fast. It is also interesting to note that all of the above models considered in the classification exhibit a form of misaligned supersymmetry discovered in [95, 96]. This is not unexpected as this phenomenon is a direct consequence of modular invariance [95, 96, 97], or a smaller subgroup of the modular group in some cases [98, 99], and so heterotic asymmetric orbifolds should also respect this mechanism.

8.4 Asymmetric Orbifold Class A

The first class of models we will choose is a pairing choice where all untwisted moduli are retained, *i.e.* $\boldsymbol{M} = (4,4,4)$. The pairing we choose is inspired by that used in the model of [127] and is given by $\boldsymbol{A} = \{y^3y^6, y^1w^6, w^1w^3\}$. The basis for this class of

models is then

$$\begin{aligned}
\mathbb{1} &= \{\psi^\mu, \chi^{1,\dots,6}, y^{1,\dots,6}, w^{1,\dots,6} \mid \overline{y}^{1,\dots,6}, \overline{w}^{1,\dots,6}, \overline{\psi}^{1,\dots,5}, \overline{\eta}^{1,2,3}, \overline{\phi}^{1,\dots,8}\},\\
\boldsymbol{S} &= \{\psi^\mu, \chi^{1,\dots,6}\},\\
\boldsymbol{e_2} &= \{y^2, w^2 \mid \overline{y}^2, \overline{w}^2\},\\
\boldsymbol{e_4} &= \{y^4, w^4 \mid \overline{y}^4, \overline{w}^4\},\\
\boldsymbol{e_5} &= \{y^5, w^5 \mid \overline{y}^5, \overline{w}^5\},\\
\boldsymbol{b_1} &= \{\psi^\mu, \chi^{12}, y^{34}, y^{56} \mid \overline{y}^{34}, \overline{y}^{56}, \overline{\eta}^1, \overline{\psi}^{1,\dots,5}\},\\
\boldsymbol{b_2} &= \{\psi^\mu, \chi^{34}, y^{12}, w^{56} \mid \overline{y}^{12}, \overline{w}^{56}, \overline{\eta}^2, \overline{\psi}^{1,\dots,5}\},\\
\boldsymbol{b_3} &= \{\psi^\mu, \chi^{56}, w^{1234} \mid \overline{w}^{1234}, \overline{\eta}^3, \overline{\psi}^{1,\dots,5}\},\\
\boldsymbol{z_1} &= \{\overline{\phi}^{1,\dots,4}\},\\
\boldsymbol{x} &= \{\overline{\psi}^{1,\dots,5}, \overline{\eta}^{1,2,3}\},\\
\gamma &= \{y^3y^6, y^1w^6, w^1w^3 \mid \bar{\psi}^{1,2,3,4,5} = \bar{\eta}^{1,2,3} = \frac{1}{2}, \bar{\phi}^{1,2,6,7} = \frac{1}{2}\}.
\end{aligned} \tag{8.73}$$

We can immediately note the following for this class

$$\begin{aligned}
\boldsymbol{E} &= (0,1,0,1,1,0)\\
\boldsymbol{\Delta} &= (1,1,1)\\
\boldsymbol{D} &= (1,1,1),
\end{aligned} \tag{8.74}$$

which will help us easily determine the key characteristics of the models in this class.

The vector bosons from the untwisted sector of these models generate the gauge symmetry group

$$\text{Observable: } SU(5) \times U(1) \times U(1)_{k=1,2,3} \times U(1)_{l=4,5,6} \tag{8.75}$$

$$\text{Hidden: } SU(2) \times U(1)_{H_1} \times SO(4)^2 \times SU(2) \times U(1)_{H_2}. \tag{8.76}$$

where we note that $U(1)_{k=1,2,3}$ are generated by the antiholomorphic currents $\bar{\eta}^k\bar{\eta}^{k*}$ and the $U(1)_{l=4,5,6}$ are horizontal symmetries arising from the asymmetric pairings: $\bar{y}^3\bar{y}^6, \bar{y}^1\bar{w}^6$ and $\bar{w}^1\bar{w}^3$. Another important note is that for this class of models we can apply eq. (8.7) and see that all the untwisted moduli are, indeed, retained.

From the discussion in Section 8.3.1, we note that the space of $\mathcal{N} = 1$ vacua is $2^{45} \sim 3.52 \times 10^{13}$. It is important to observe that there are two imaginary phases $C\binom{\mathbb{1}}{\gamma} = \pm i$ and $C\binom{\boldsymbol{z_1}}{\gamma} = \pm i$, consistent with modular invariance, and all other phases are real. Furthermore, we note that the latter of these, $C\binom{\boldsymbol{z_1}}{\gamma}$, and the following four phases do not play a role in the phenomenological constraints

$$C\begin{bmatrix}\mathbb{1}\\ \boldsymbol{b_1}\end{bmatrix}, C\begin{bmatrix}\mathbb{1}\\ \boldsymbol{b_2}\end{bmatrix}, C\begin{bmatrix}\mathbb{1}\\ \boldsymbol{b_3}\end{bmatrix}, C\begin{bmatrix}\mathbb{1}\\ \boldsymbol{z_1}\end{bmatrix}. \tag{8.77}$$

This leaves a space of $2^{40} \sim 1.1 \times 10^{12}$ $\mathcal{N} = 1$ GGSO phase configurations.

8.4.1 Class A Phenomenological Features

Observable Spinorial Representations

From eq. (8.43) we can write the sectors producing fermions generations

$$\begin{aligned} \boldsymbol{F}^1_{qr} &= \boldsymbol{b_1} + q\boldsymbol{e_4} + r\boldsymbol{e_5} \\ \boldsymbol{F}^2_{qr} &= \boldsymbol{b_2} + q\boldsymbol{e_2} + r\boldsymbol{e_5} \\ \boldsymbol{F}^3_{qs} &= \boldsymbol{b_3} + q\boldsymbol{e_2} + s\boldsymbol{e_4} \end{aligned} \tag{8.78}$$

and $\boldsymbol{D} = (1,1,1)$ means that any of these sectors will produce one copy of all states in the **16** or $\overline{\mathbf{16}}$ when present in the massless spectrum. Therefore, the number of generations (8.48) simplifies to

$$n_g = N_{16} - N_{\overline{16}}. \tag{8.79}$$

Encoding the condition for 3 generations (8.49) for this class of models into Z3 returns `sat` to confirm 3 generation models are present for this class. In order to see the spread of generation number, n_g, we can generate a bar graph of generations for a random scan of Class A models. This graph is shown in Figure 8.1 for a sample of 10^7 vacua with $N_{16} \geq N_{\overline{16}}$ so that models with $n_g \geq 0$ are plotted. From this sample we find 3 generations models with probability of approximately 6×10^{-3}.

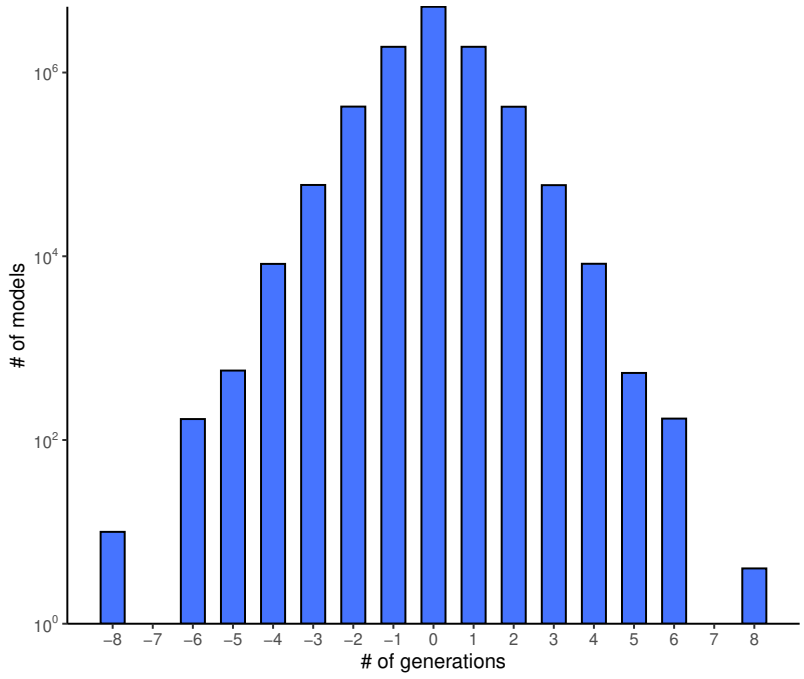

Figure 8.1: *Frequency plot for number of generations from a sample of* 10^7 *Class A vacua.*

Heavy Higgs

From eq. (8.51) we can write the Heavy Higgs producing sectors for the Class A models as

$$\begin{aligned} \boldsymbol{B}^1_{qr} &= \boldsymbol{S} + \boldsymbol{b_1} + q\boldsymbol{e_4} + r\boldsymbol{e_5} \\ \boldsymbol{B}^2_{qr} &= \boldsymbol{S} + \boldsymbol{b_2} + q\boldsymbol{e_2} + r\boldsymbol{e_5} \\ \boldsymbol{B}^3_{qs} &= \boldsymbol{S} + \boldsymbol{b_3} + q\boldsymbol{e_2} + s\boldsymbol{e_4} \end{aligned} \tag{8.80}$$

and note that each sector $\boldsymbol{B}^k_{pqrs}$, $k = 1,2,3$, generates a $\mathbf{16} + \overline{\mathbf{16}}$, which correspond to the would-be superpartners of the fermionic states in the $\mathbf{16}/\overline{\mathbf{16}}$ and their CPT conjugates. Therefore, any sector $\boldsymbol{B}^k_{pq}$ that survives generates one Heavy Higgs $\left(\mathbf{10}, +\frac{1}{2}\right) + \left(\overline{\mathbf{10}}, -\frac{1}{2}\right)$, along with a further vector-like pair $\left(\bar{\mathbf{5}}, +\frac{3}{2}\right) + \left(\mathbf{1}, \frac{5}{2}\right) + \left(\mathbf{5}, -\frac{3}{2}\right) + \left(\mathbf{1}, -\frac{5}{2}\right)$. We can thus write the number of Heavy Higgs for a specific model as equal to the number of surviving sectors $\boldsymbol{B}^k_{pqrs}$

$$n_{10H} = \sum_{\substack{k=1,2,3 \\ q,r,s=0,1}} \mathbb{P}_{\boldsymbol{B}^k_{qrs}}. \tag{8.81}$$

Top Quark Mass Couplings

We note that we have possible TQMC from untwisted type couplings of the general form

$$\boldsymbol{F}^1\boldsymbol{F}^1\bar{h}_1, \quad \boldsymbol{F}^2\boldsymbol{F}^2\bar{h}_2, \quad \boldsymbol{F}^3\boldsymbol{F}^3\bar{h}_3 \tag{8.82}$$

where $\bar{h}_k$, $k = 1,2,3$, are the Higgs representations from the Neveu-Schwarz sector. In addition, there is also the possibility of twisted type couplings of the general form

$$\boldsymbol{F}^1\boldsymbol{F}^2\boldsymbol{V}^3_{\{\bar{\psi}^a\}}, \quad \boldsymbol{F}^1\boldsymbol{V}^2_{\{\bar{\psi}^a\}}\boldsymbol{F}^3, \quad \boldsymbol{V}^1_{\{\bar{\psi}^a\}}\boldsymbol{F}^2\boldsymbol{F}^3 \tag{8.83}$$

In classifying vacua from Class A we will account for all 6 possibilities to check for any potentially viable TQMCs for a model.

In particular, the presence of twisted Light Higgs is not a necessary condition for viable phenomenology in the FSU5 asymmetric models since with untwisted Higgs doublets generating a TQMC of untwisted type (8.82) they are not necessary. However, the presence of such a coupling is not automatic *a priori* and so for the analysis of whether a model contains a viable TQMC we will also have to check for TQMC from twisted-type coupling (8.83).

Applying eq. (8.53) we can write the sectors generating the Light Higgs representations as

$$\begin{aligned} \boldsymbol{V}^1_{qr} &= \boldsymbol{S} + \boldsymbol{b_1} + \boldsymbol{x} + q\boldsymbol{e_4} + r\boldsymbol{e_5} \\ \boldsymbol{V}^2_{qr} &= \boldsymbol{S} + \boldsymbol{b_2} + \boldsymbol{x} + q\boldsymbol{e_2} + r\boldsymbol{e_5} \\ \boldsymbol{V}^3_{qs} &= \boldsymbol{S} + \boldsymbol{b_3} + \boldsymbol{x} + q\boldsymbol{e_2} + s\boldsymbol{e_4}, \end{aligned} \tag{8.84}$$

when accompanied by an antiholomorphic oscillator $\{\bar{\psi}^a\}$, $a \in \{1,2,3,4,5\}$.

The projectors can be written as follows for these sectors

$$\begin{aligned} \mathbb{P}_{\{\bar{\psi}^a\}\boldsymbol{V}^1_{qr}} &= \frac{1}{2^4}\left(1+C\begin{bmatrix}\boldsymbol{e_2}\\ \boldsymbol{V}^{(1)}_{qr}\end{bmatrix}\right)\left(1+C\begin{bmatrix}\boldsymbol{2\gamma}+\boldsymbol{x}\\ \boldsymbol{V}^{(1)}_{qr}\end{bmatrix}\right)\prod_{a=1,2}\left(1+C\begin{bmatrix}\boldsymbol{z_a}\\ \boldsymbol{V}^{(1)}_{qr}\end{bmatrix}\right) \\ \mathbb{P}_{\{\bar{\psi}^a\}\boldsymbol{V}^2_{qr}} &= \frac{1}{2^4}\left(1+C\begin{bmatrix}\boldsymbol{e_4}\\ \boldsymbol{V}^{(2)}_{qr}\end{bmatrix}\right)\left(1+C\begin{bmatrix}\boldsymbol{2\gamma}+\boldsymbol{x}\\ \boldsymbol{V}^{(2)}_{qr}\end{bmatrix}\right)\prod_{a=1,2}\left(1+C\begin{bmatrix}\boldsymbol{z_a}\\ \boldsymbol{V}^{(2)}_{qr}\end{bmatrix}\right) \\ \mathbb{P}_{\{\bar{\psi}^a\}\boldsymbol{V}^3_{qs}} &= \frac{1}{2^4}\left(1+C\begin{bmatrix}\boldsymbol{e_5}\\ \boldsymbol{V}^{(3)}_{qs}\end{bmatrix}\right)\left(1+C\begin{bmatrix}\boldsymbol{2\gamma}+\boldsymbol{x}\\ \boldsymbol{V}^{(3)}_{qs}\end{bmatrix}\right)\prod_{a=1,2}\left(1+C\begin{bmatrix}\boldsymbol{z_a}\\ \boldsymbol{V}^{(3)}_{qs}\end{bmatrix}\right). \end{aligned} \tag{8.85}$$

Using these we can write the number of Light Higgs states for a specific model as equal to the number of $\{\bar{\psi}^a\}\left|\boldsymbol{V}^k_{qrs}\right\rangle$ in the massless spectrum

$$n_{5h} = \sum_{\substack{k=1,2,3\\ q,r,s=0,1}} \mathbb{P}_{\boldsymbol{V}^k_{qrs}}. \tag{8.86}$$

Tachyonic Sector Analysis

When classifying the $\mathcal{N}=0$ models we must ensure the projection of all on-shell tachyonic sectors. In addition to the model-independent tachyonic sectors (8.57), we have the following on-shell tachyonic sectors for Class A models that require an antiholomorphic oscillator

$$T_1 = \left\{\begin{array}{llllll} \{\bar{\lambda}\}_{\frac{1}{2}}: & |\boldsymbol{e_2}\rangle & |\boldsymbol{e_4}\rangle & |\boldsymbol{e_5}\rangle & & \\ \{\bar{\lambda}\}_{\frac{1}{2}}: & |\boldsymbol{e_2}+\boldsymbol{e_4}\rangle & |\boldsymbol{e_2}+\boldsymbol{e_5}\rangle & |\boldsymbol{e_4}+\boldsymbol{e_5}\rangle & & \\ \{\bar{\lambda}\}_{\frac{1}{2}}: & |\boldsymbol{e_2}+\boldsymbol{e_4}+\boldsymbol{e_5}\rangle & |\boldsymbol{G}+\boldsymbol{e_2}+\boldsymbol{e_4}+\boldsymbol{e_5}\rangle & & & \\ \{\bar{\lambda}\}_{\frac{1}{2}}: & |(3)\boldsymbol{\gamma}\rangle & |\boldsymbol{x}+(3)\boldsymbol{\gamma}\rangle & & & \\ \{\bar{\lambda}\}_{\frac{1}{4}}: & |\boldsymbol{z_1}+(3)\boldsymbol{\gamma}\rangle & |\boldsymbol{z_2}+(3)\boldsymbol{\gamma}\rangle & |\boldsymbol{z_1}+\boldsymbol{x}+(3)\boldsymbol{\gamma}\rangle & |\boldsymbol{z_2}+\boldsymbol{x}+(3)\boldsymbol{\gamma}\rangle\,. \end{array}\right\} \tag{8.87}$$

As well as the following on-shell tachyonic sectors which arise with no oscillator

$$T_2 = \left\{ \begin{array}{cc} |\boldsymbol{z_1}\rangle & |\boldsymbol{z_2}\rangle \\ |\boldsymbol{e_i}+\boldsymbol{z_1}\rangle & |\boldsymbol{e_i}+\boldsymbol{z_2}\rangle \\ |\boldsymbol{e_i}+\boldsymbol{e_j}+\boldsymbol{z_1}\rangle & |\boldsymbol{e_i}+\boldsymbol{e_j}+\boldsymbol{z_2}\rangle \\ |\boldsymbol{e_i}+\boldsymbol{e_j}+\boldsymbol{e_k}+\boldsymbol{z_1}\rangle & |\boldsymbol{e_i}+\boldsymbol{e_j}+\boldsymbol{e_k}+\boldsymbol{z_2}\rangle \\ |\boldsymbol{G}+\boldsymbol{e_2}+\boldsymbol{e_4}+\boldsymbol{e_5}+\boldsymbol{z_1}\rangle & |\boldsymbol{G}+\boldsymbol{e_2}+\boldsymbol{e_4}+\boldsymbol{e_5}+\boldsymbol{z_2}\rangle \\ \\ |\boldsymbol{x}+2\gamma\rangle & |\boldsymbol{z_1}+\boldsymbol{x}+2\gamma\rangle \\ |\boldsymbol{e_i}+\boldsymbol{x}+2\gamma\rangle & |\boldsymbol{e_i}+\boldsymbol{z_1}+\boldsymbol{x}+2\gamma\rangle \\ |\boldsymbol{e_i}+\boldsymbol{e_j}+\boldsymbol{x}+2\gamma\rangle & |\boldsymbol{e_i}+\boldsymbol{e_j}+\boldsymbol{z_1}+\boldsymbol{x}+2\gamma\rangle \\ |\boldsymbol{e_2}+\boldsymbol{e_4}+\boldsymbol{e_5}+\boldsymbol{x}+2\gamma\rangle & |\boldsymbol{e_2}+\boldsymbol{e_4}+\boldsymbol{e_5}+\boldsymbol{z_1}+\boldsymbol{x}+2\gamma\rangle \\ |\boldsymbol{G}+\boldsymbol{e_2}+\boldsymbol{e_4}+\boldsymbol{e_5}+\boldsymbol{x}+2\gamma\rangle & |\boldsymbol{G}+\boldsymbol{e_2}+\boldsymbol{e_4}+\boldsymbol{e_5}+\boldsymbol{z_1}+\boldsymbol{x}+2\gamma\rangle \\ \\ |\boldsymbol{z_2}+\boldsymbol{x}+2\gamma\rangle & |\boldsymbol{z_1}+\boldsymbol{z_2}+\boldsymbol{x}+2\gamma\rangle \\ |\boldsymbol{e_i}+\boldsymbol{z_2}+\boldsymbol{x}+2\gamma\rangle & |\boldsymbol{e_i}+\boldsymbol{z_1}+\boldsymbol{z_2}+\boldsymbol{x}+2\gamma\rangle \\ |\boldsymbol{e_i}+\boldsymbol{e_j}+\boldsymbol{z_2}+\boldsymbol{x}+2\gamma\rangle & |\boldsymbol{e_i}+\boldsymbol{e_j}+\boldsymbol{z_1}+\boldsymbol{z_2}+\boldsymbol{x}+2\gamma\rangle \\ |\boldsymbol{e_2}+\boldsymbol{e_4}+\boldsymbol{e_5}+\boldsymbol{z_2}+\boldsymbol{x}+2\gamma\rangle & |\boldsymbol{e_2}+\boldsymbol{e_4}+\boldsymbol{e_5}+\boldsymbol{z_1}+\boldsymbol{z_2}+\boldsymbol{x}+2\gamma\rangle \\ |\boldsymbol{G}+\boldsymbol{e_2}+\boldsymbol{e_4}+\boldsymbol{e_5}+\boldsymbol{z_2}+\boldsymbol{x}+2\gamma\rangle & |\boldsymbol{G}+\boldsymbol{e_2}+\boldsymbol{e_4}+\boldsymbol{e_5}+\boldsymbol{z_1}+\boldsymbol{z_2}+\boldsymbol{x}+2\gamma\rangle \\ \\ |\boldsymbol{z_1}+\boldsymbol{z_2}+(3)\gamma\rangle & |\boldsymbol{z_1}+\boldsymbol{z_2}+\boldsymbol{x}+(3)\gamma\rangle \end{array} \right\}, \tag{8.88}$$

where $i \neq j \in \{2,4,5\}$.

All of these sectors, $\boldsymbol{t} \in T_1$ and $\boldsymbol{t} \in T_2$, must be projected from the spectrum through appropriate definitions of their generalised projectors $\mathbb{P}_{\boldsymbol{t}} = 0$. Since there are so many sectors this is generally the most computationally expensive aspect of the classification methodology and is a key reason for introducing SMT methods into the program.

For reasons of efficiency in projecting the tachyonic sectors we can split the projection into two steps. Firstly, since the SUSY generating vector $\boldsymbol{S}$ acts as a projector on all tachyonic sectors, we can implement this projection on all tachyonic sectors and see which sectors remain. Then we can construct and perform the projectors for the remaining sectors.

Enhancements

In classifying the Class A models we should ensure the absence of enhancements to the observable gauge factors coming from the class-Independent sectors given in eq. (8.59) using the generalised projectors discussed in Section 8.3. We have further sectors giving possible observable enhancements through combinations with γ. At the level $(\boldsymbol{\alpha}_L \cdot \boldsymbol{\alpha}_L, \boldsymbol{\alpha}_R \cdot \boldsymbol{\alpha}_R) = (0,6)$ we have the following sectors

$$\psi^\mu\{\bar{\lambda}\}_{\frac{1}{4}} \begin{cases} |\boldsymbol{e_{136}}+(3)\gamma\rangle =: \boldsymbol{O_1} \\ |\boldsymbol{e_{136}}+\boldsymbol{x}+(3)\gamma\rangle =: \boldsymbol{O_2} \end{cases} \tag{8.89}$$

and at level $(0,8)$ there are the sectors

$$\psi^{\mu}\begin{cases}|\boldsymbol{e_{136}}+\boldsymbol{z_1}+(3)\boldsymbol{\gamma}\rangle =: \boldsymbol{O_3}\\ |\boldsymbol{e_{136}}+\boldsymbol{z_1}+\boldsymbol{x}+(3)\boldsymbol{\gamma}\rangle =: \boldsymbol{O_4}\\ |\boldsymbol{e_{136}}+\boldsymbol{z_2}+(3)\boldsymbol{\gamma}\rangle =: \boldsymbol{O_5}\\ |\boldsymbol{e_{136}}+\boldsymbol{z_2}+\boldsymbol{x}+(3)\boldsymbol{\gamma}\rangle =: \boldsymbol{O_6},\end{cases} \tag{8.90}$$

which should be projected to ensure the absence of observable enhancements. In order to construct the projectors we note that

$$\begin{aligned}\Upsilon(\boldsymbol{O_{1,2}}) =&\{\boldsymbol{S},\boldsymbol{e_2},\boldsymbol{e_4},\boldsymbol{e_5},\boldsymbol{z_1}+\boldsymbol{z_2}+\boldsymbol{x}+2\boldsymbol{\gamma}\}\\ \Upsilon(\boldsymbol{O_{3,4}}) =&\{\boldsymbol{S},\boldsymbol{e_2},\boldsymbol{e_4},\boldsymbol{e_5},\boldsymbol{z_2}+\boldsymbol{x}+2\boldsymbol{\gamma}\}\\ \Upsilon(\boldsymbol{O_{5,6}}) =&\{\boldsymbol{S},\boldsymbol{e_2},\boldsymbol{e_4},\boldsymbol{e_5},\boldsymbol{z_1}+\boldsymbol{x}+2\boldsymbol{\gamma}\}\end{aligned} \tag{8.91}$$

and the projectors have the form

$$\mathbb{P}_{\boldsymbol{O}_{1,2}} = \prod_{\boldsymbol{\xi}\in\Upsilon(\boldsymbol{O}_{1,2})}\frac{1}{2}\left(1+\delta_{\boldsymbol{O}_{1,2}}\delta^{\psi^{\mu}}_{\boldsymbol{\xi}}\delta^{\bar{\lambda}}_{\boldsymbol{\xi}}C\begin{bmatrix}\boldsymbol{O}_{1,2}\\ \boldsymbol{\xi}\end{bmatrix}\right) \tag{8.92}$$

$$\mathbb{P}_{\boldsymbol{O}_{3,4,5,6}} = \prod_{\boldsymbol{\xi}\in\Upsilon(\boldsymbol{O}_{3,4,5,6})}\frac{1}{2}\left(1+\delta_{\boldsymbol{O}_{3,4,5,6}}\delta^{\psi^{\mu}}_{\boldsymbol{\xi}}C\begin{bmatrix}\boldsymbol{O}_{3,4,5,6}\\ \boldsymbol{\xi}\end{bmatrix}\right), \tag{8.93}$$

which gives three unique projectors from (8.91), on which we impose

$$\forall\,\bar{\lambda},\ \forall\, i\in[1,6]:\ \ \mathbb{P}_{\boldsymbol{O_i}}=0. \tag{8.94}$$

Exotic Sectors

Another important consideration for ensuring reasonable phenomenology is the absence of chiral exotics.

Along with the sectors (8.62) there are 124 sectors at the level $(4,6)$ that can produce exotic massless states with a right moving oscillator such that $\nu_f=\frac{1}{2}$ or $\nu_{f^*}=-\frac{1}{2}$. These all arise in pairs with $+\boldsymbol{\gamma}$ and $+3\boldsymbol{\gamma}$ which contribute equal and opposite gauge charges and therefore do not contribute to any chiral anomaly. Similarly for the 212 exotic sectors at level $(4,8)$. Therefore we conveniently do not need to implement a condition on chiral exotics in the classification for this class of models.

8.4.2 Class A Results

Having defined the key phenomenological characteristics for models in Class A we now seek to classify a large space of both $\mathcal{N}=0$ and $\mathcal{N}=1$ vacua with reference to the following key classification criteria

(1) No On-Shell Tachyons as discussed in Section 8.3.2 and 8.4.1

(2) No Observable Enhancements as given by eq. (8.60) and (8.94)

(3) Complete Generations: $n_g \neq 0$ and $n_{10} - n_{\overline{10}} = n_{\bar{5}} - n_5$

(4) Three generations: $n_g = 3$: (8.95)

(5) Presence of Heavy Higgs: $n_{10H} \geq 1$

(6) Presence of viable TQMC as discussed in Section 8.3.3 and 8.83

(7) Super No-Scale Condition: $a_{00} = N_b^0 - N_f^0 = 0$.

We note again that determining whether a viable TQMC is present requires checking for either an untwisted or twisted type coupling.

The results of a classification of 10^9 Class A models created through random generation is presented in Table 8.3.

	Total models in sample: 10^9				
	SUSY or Non-SUSY:	$\mathcal{N} = 1$	Probability	$\mathcal{N} = 0$	Probability
	Total	15624051	1.56×10^{-2}	984375949	0.984
(1)	+ Tachyon-Free			30779240	3.08×10^{-2}
(2)	+ No Observable Enhancements	15135704	1.51×10^{-2}	28581301	2.86×10^{-2}
(3)	+ Complete Generations	15135704	1.51×10^{-2}	28581301	2.86×10^{-2}
(4)	+ Three Generations	89930	8.99×10^{-5}	195716	1.96×10^{-4}
(5)	+ Heavy Higgs	89820	8.98×10^{-5}	129233	1.29×10^{-4}
(7)	+ TQMC	89820	8.98×10^{-5}	129233	1.29×10^{-4}
(8)	+ $a_{00} = N_b^0 - N_f^0 = 0$			388	3.88×10^{-7}

Table 8.3: *Phenomenological statistics from sample of* 10^8 *Class A models. Note that the number of* $a_{00} = 0$ *models is an estimate based on extrapolating from a sample of* 2×10^3 *of the 129233* $\mathcal{N} = 0$ *models satisfying (1)-(7).*

As mentioned in Section 7.2 we can employ our Z3 SMT Solver to efficiently find models satisfying the phenomenological criteria as well as to inform us of when criteria are in contradiction and no solutions can be found. As a test of efficiency we ran the SMT for 1 hour to see how many models it finds satisfying the criteria (1)-(7) in Table 8.3 and compared it with the random generation method over the same time. The result of this comparison is displayed in Figure 8.2. We find that the SMT is approximately 322 times faster than the random scan after 3 minutes but after 1 hour it levels out at approximately 93 times faster. This demonstrates that the Z3 SMT tool is especially effective as a fishing algorithm in finding pools of solutions very quickly, whereas its efficiency in complete enumeration of solutions reduces. If we are interested in more complete enumeration it may be instrumental to employ another SAT/SMT solver such

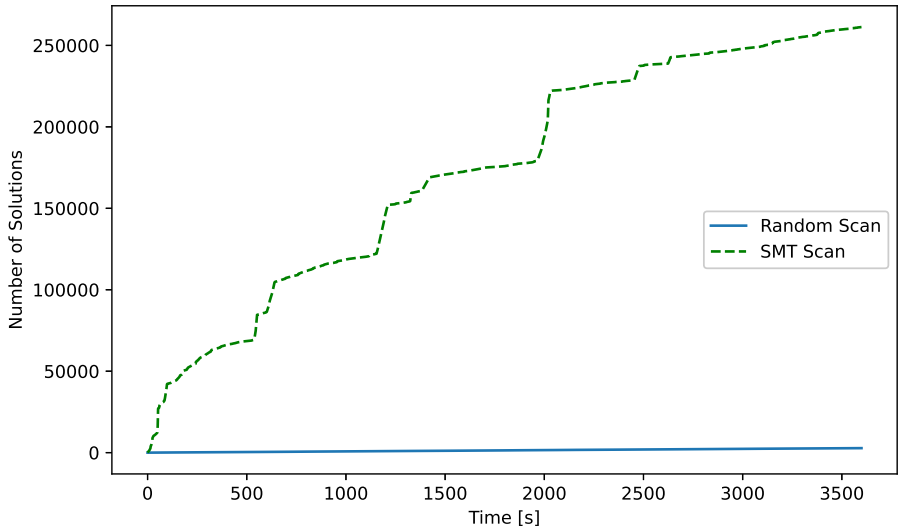

Figure 8.2: *Rate at which the Z3 SMT finds solutions satisfying constraints (1)-(7) compared with a random generation approach over a 1 hour period.*

as PicoSAT[2], which is optimised for such complete enumeration.

We can also perform a statistical analysis at the level of the partition function. This includes the calculation of the q-expanded partition function and the evaluation of the one-loop cosmological constant. In Figure 8.3, we present the distribution of the cosmological constant for a sample of Class A models evaluated at the free fermionic point. This shows that there is a tendency towards negative values, even though positive values are not excluded. It is important to note that this is not guaranteed to be a stable point in moduli space as there may be flat directions, however, the analysis of the potential is outside the scope of this chapter and is left for future work. It is also interesting to compare the effectiveness of the SMT and random scan algorithms in finding unique models from the point of view of the partition function. From Figure 8.4, we see that the SMT algorithm has a tendency to find more degenerate solutions as compared to a random scan. However, this does not conclude that random scans are more efficient. Indeed, comparing this to Figure 8.2, we see that SMT algorithms still vastly outperform random scans by more than 2 orders of magnitude.

[2]Program available on Github via: `https://github.com/zimmski/picosat`

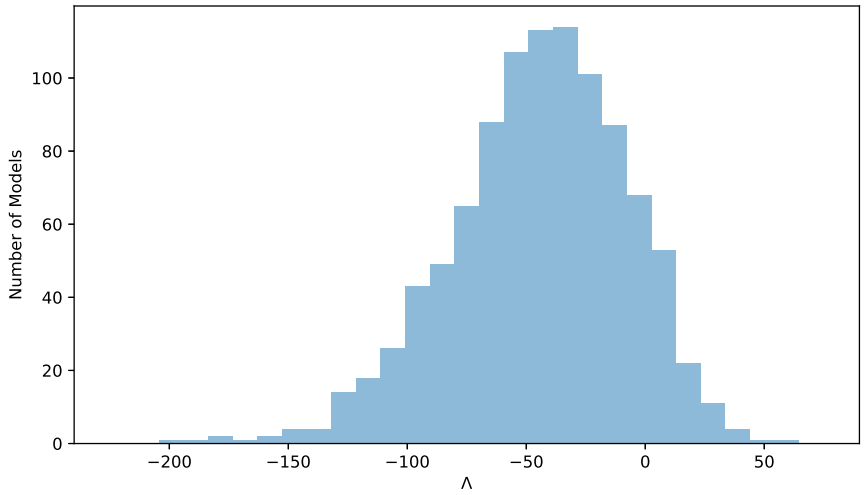

Figure 8.3: *The distribution of the cosmological constant Λ_{ST} for a sample off 10^3 Class A models satisfying conditions (1)-(7) of Table 8.3. To gain the physical value, a factor of $\mathcal{M}^4$ must be reinstated. These values are evaluated at the free fermionic point using methods discussed in Section 8.3.4.*

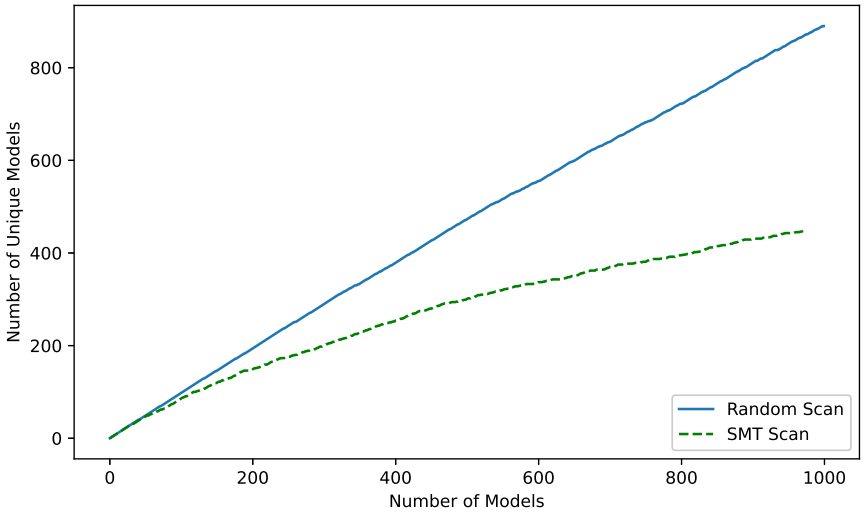

Figure 8.4: *The degeneracy of models in a Random versus an SMT scan for Class A as seen from the partition function.*

8.4.3 Example Model Class A

Having classified a random sample of Class A vacua, we can provide an example model satisfying criteria (1)-(7) of (8.95). Consider a model defined by the basis set (8.73) and

choice of GGSO phases given by

$$C\begin{bmatrix} v_i \\ v_j \end{bmatrix} = \begin{array}{c} \\ \mathbf{1} \\ \boldsymbol{S} \\ \boldsymbol{e_2} \\ \boldsymbol{e_4} \\ \boldsymbol{e_5} \\ \boldsymbol{b_1} \\ \boldsymbol{b_2} \\ \boldsymbol{b_3} \\ \boldsymbol{z_1} \\ \boldsymbol{x} \\ \boldsymbol{\gamma} \end{array} \begin{array}{c} \begin{array}{ccccccccccc} \mathbf{1} & \boldsymbol{S} & \boldsymbol{e_2} & \boldsymbol{e_4} & \boldsymbol{e_5} & \boldsymbol{b_1} & \boldsymbol{b_2} & \boldsymbol{b_3} & \boldsymbol{z_1} & \boldsymbol{x} & \boldsymbol{\gamma} \end{array} \\ \begin{pmatrix} 1 & 1 & -1 & -1 & -1 & 1 & -1 & 1 & 1 & 1 & i \\ 1 & 1 & -1 & 1 & 1 & 1 & 1 & 1 & 1 & -1 & 1 \\ -1 & -1 & 1 & 1 & -1 & -1 & -1 & -1 & 1 & -1 & -1 \\ -1 & 1 & 1 & 1 & -1 & 1 & -1 & 1 & -1 & -1 & -1 \\ -1 & 1 & -1 & -1 & 1 & -1 & -1 & -1 & -1 & -1 & 1 \\ 1 & -1 & -1 & 1 & -1 & 1 & -1 & -1 & 1 & 1 & 1 \\ -1 & -1 & -1 & -1 & -1 & -1 & -1 & -1 & -1 & 1 & -1 \\ 1 & -1 & -1 & 1 & -1 & -1 & -1 & 1 & 1 & -1 & -1 \\ 1 & 1 & 1 & -1 & -1 & 1 & -1 & 1 & 1 & -1 & i \\ 1 & -1 & -1 & -1 & -1 & -1 & -1 & 1 & -1 & -1 & -1 \\ 1 & 1 & -1 & -1 & 1 & -1 & 1 & 1 & -1 & -1 & -1 \end{pmatrix} \end{array} \tag{8.96}$$

This model has 3 fermion generations arising from $\boldsymbol{b_1}+\boldsymbol{e_4}$, $\boldsymbol{b_2}+\boldsymbol{e_2}$ and $\boldsymbol{b_3}+\boldsymbol{e_2}+\boldsymbol{e_4}$. As for all models in this class, there are untwisted Higgs states from all 3 orbifold planes. The top quark mass coupling arises on each plane from a coupling of the type $U_kF_kF_k$ discussed in Section 8.3.3. The Heavy Higgs is provided by the sector $\boldsymbol{S}+\boldsymbol{b_2}+\boldsymbol{e_5}$ to ensure that the $SU(5)\times U(1)$ can be broken to the SM.

The partition function for Class A models can be found using the methods discussed in Section 8.3.4. Specifically, the internal lattice can be constructed by noting that the form of $\boldsymbol{A}$ introduces exactly one asymmetric pairing in each of the three orbifold planes. Thus the internal lattice takes the form

$$\begin{aligned}
\Gamma^{\gamma}_{(6,6)} &= \Gamma^{\gamma}_1 \times \Gamma^{\gamma}_2 \times \Gamma^{\gamma}_3 \\
&= \vartheta_{y^4}\begin{bmatrix} r+h_2+H_4 \\ s+g_2+G_4 \end{bmatrix}^{1/2} \vartheta_{y^5}\begin{bmatrix} r+h_2+H_5 \\ s+g_2+G_5 \end{bmatrix}^{1/2} \vartheta_{y^{3,6}}\begin{bmatrix} r+h_2+2H' \\ s+g_2+2G' \end{bmatrix} \\
&\quad \times \vartheta_{\bar{y}^4}\begin{bmatrix} r+h_2+H_4 \\ s+g_2+G_4 \end{bmatrix}^{1/2} \bar{\vartheta}_{\bar{y}^5}\begin{bmatrix} r+h_2+H_5 \\ s+g_2+G_5 \end{bmatrix}^{1/2} \bar{\vartheta}_{\bar{y}^{3,6}}\begin{bmatrix} r+h_2 \\ s+g_2 \end{bmatrix} \\
&\quad \times \vartheta_{y^2}\begin{bmatrix} r+h_2+H_2 \\ s+g_2+G_2 \end{bmatrix}^{1/2} \vartheta_{w^5}\begin{bmatrix} r+h_2+H_5 \\ s+g_2+G_5 \end{bmatrix}^{1/2} \vartheta_{y^1w^6}\begin{bmatrix} r+h_2+2H' \\ s+g_2+2G' \end{bmatrix} \\
&\quad \times \vartheta_{\bar{y}^2}\begin{bmatrix} r+h_1+H_2 \\ s+g_1+G_2 \end{bmatrix}^{1/2} \bar{\vartheta}_{\bar{w}^5}\begin{bmatrix} r+h_1+H_5 \\ s+g_1+G_5 \end{bmatrix}^{1/2} \bar{\vartheta}_{\bar{y}^1\bar{w}^6}\begin{bmatrix} r+h_1 \\ s+g_1 \end{bmatrix} \\
&\quad \times \vartheta_{w^2}\begin{bmatrix} r-h_1-h_2+H_2 \\ s-g_1-g_2+G_2 \end{bmatrix}^{1/2} \vartheta_{w^4}\begin{bmatrix} r-h_1-h_2+H_4 \\ s-g_1-g_2+G_4 \end{bmatrix}^{1/2} \vartheta_{w^{1,3}}\begin{bmatrix} r-h_1-h_2+2H' \\ s-g_1-g_2+2G' \end{bmatrix} \\
&\quad \times \vartheta_{\bar{w}^2}\begin{bmatrix} r-h_1-h_2+H_2 \\ s-g_1-g_2+G_2 \end{bmatrix}^{1/2} \bar{\vartheta}_{\bar{w}^4}\begin{bmatrix} r-h_1-h_2+H_4 \\ s-g_1-g_2+G_4 \end{bmatrix}^{1/2} \bar{\vartheta}_{\bar{w}^{1,3}}\begin{bmatrix} r-h_1-h_2 \\ s-g_1-g_2 \end{bmatrix},
\end{aligned} \tag{8.97}$$

where Γ^{γ}_i denotes the part corresponding to the i^{th} orbifold plane. We can then use this expression to obtain the q-expanded partition function of this model

$$\begin{aligned}
Z = {} & 2\,q^0\bar{q}^{-1} - 8\,q^{1/4}\bar{q}^{-3/4} - 16\,q^{1/2}\bar{q}^{-1/2} + 8\,q^{-1/2}\bar{q}^{1/2} \\
& + 176\,q^{1/8}\bar{q}^{1/8} + 976\,q^{1/4}\bar{q}^{1/4} + 2048\,q^{3/8}\bar{q}^{3/8} + 2560\,q^{1/2}\bar{q}^{1/2},
\end{aligned} \tag{8.98}$$

including all terms up to at most $\mathcal{O}(q^{1/2})$ and $\mathcal{O}(\bar{q}^{1/2})$. The top line gives the off-shell tachyonic states required by modular invariance, while the bottom line gives all on-shell states. Note the presence of the off-shell model-independent term $2\,q^0\bar{q}^{-1}$ obtained from the so-called 'proto-graviton' resulting from the state $\psi^\mu\,|0\rangle_L \otimes |0\rangle_R$. This provides a neat check to confirm correct normalisation of the partition function. We also see that this model is indeed Bose-Fermi degenerate at the massless level, *i.e.* $a_{00} = N_b^0 - N_f^0 = 0$. Integrating this expansion over the fundamental domain of the modular group yields the spacetime cosmological constant

$$\Lambda_{\rm ST} = 13.34 \times \mathcal{M}^4, \tag{8.99}$$

which was calculated to $4^{\rm th}$ order q and $\bar{q}$.

Whether the cosmological constant can indeed be suppressed requires more in-depth analysis and in these Class A models all untwisted moduli being retained complicates this analysis, which motivates the study of a different class of models where some moduli are projected that we turn to in the next section. Through a translation to an orbifold in the bosonic formulation, the dependence on some of these geometric moduli can be reinstated and a systematic investigation of the one-loop potential can be attempted as done in [43, 44] for symmetric orbifolds, however its implementation for asymmetric models is left for future work.

8.5 Asymmetric Orbifold Class B

The second class of models we study is an example where all untwisted moduli on the second and third tori are projected and only h_{11}, h_{12}, h_{21} and h_{22} are retained. From Table 8.1 and 8.2 we can see there are 12 possible pairings in both the bosonic and fermionic cases that give rise to just h_{11}, h_{12}, h_{21} and h_{22}, whilst allowing for odd number generations. These all have $\boldsymbol{E} = (1,1,0,0,0,0)$. The possible pairings can be grouped into 3 types according to their $\boldsymbol{\Delta} = (\Delta_1, \Delta_2, \Delta_3)$ and degeneracies $\boldsymbol{D} = (D_1, D_2, D_3)$, which for the bosonic case are

$$\boldsymbol{A} = \begin{cases} \{\bar{w}^{3456}\}, \{y^{34}, w^{34}, \bar{y}^{34}, \bar{w}^{56}\}, & \boldsymbol{\Delta} = (0,1,1), \;\; \boldsymbol{D} = (8,1,1) \\ \{y^{3456}, w^{3456}, \bar{y}^{3456}\}, \{y^{56}, w^{56}, \bar{y}^{56}, \bar{w}^{34}\} & \\ \{\bar{y}^{56}, \bar{w}^{34}\}, \{y^{56}, w^{56}, \bar{w}^{3456}\}, & \boldsymbol{\Delta} = (1,0,1), \;\; \boldsymbol{D} = (4,2,1) \\ \{y^{34}, w^{34}, \bar{y}^{3456}\}, \{y^{3456}, w^{3456}, \bar{y}^{34}, \bar{y}^{56}\} & \\ \{\bar{y}^{34}, \bar{w}^{56}\}, \{y^{34}, w^{34}, \bar{y}^{34}\bar{w}^{56}\}, & \boldsymbol{\Delta} = (1,1,0), \;\; \boldsymbol{D} = (4,1,2) \\ \{y^{3456}, w^{3456}, \bar{y}^{3456}\}, \{y^{56}, w^{56}, \bar{y}^{56}, \bar{w}^{34}\} & \end{cases} \tag{8.100}$$

As mentioned in Section 8.3, the condition for odd number generations 8.32 is a necessary, but not sufficient, condition for the possibility of having 3 generation models within a class. We can check which of the 3 pairing possibilities in (8.100) can give

rise to 3 generations by checking whether eq. (8.49) is satisfiable with our SMT solver for each $\boldsymbol{A}$. Doing this tells us that none of the pairings can give rise to 3 generation models. Despite this, we will choose the pairing $\boldsymbol{A} = \{\bar{w}^{34}, \bar{w}^{56}\}$ with $\boldsymbol{D} = (4,2,1)$ to classify systematically, and in Section 8.5.1 we will demonstrate the origin of the absence of three generations.

The basis for this class of models will then be

$$\begin{aligned}
\mathbb{1} &= \{\psi^\mu, \chi^{1,\dots,6}, y^{1,\dots,6}, w^{1,\dots,6} \mid \overline{y}^{1,\dots,6}, \overline{w}^{1,\dots,6}, \overline{\psi}^{1,\dots,5}, \overline{\eta}^{1,2,3}, \overline{\phi}^{1,\dots,8}\},\\
\boldsymbol{S} &= \{\psi^\mu, \chi^{1,\dots,6}\},\\
\boldsymbol{e_1} &= \{y^1, w^1 \mid \overline{y}^1, \overline{w}^1\},\\
\boldsymbol{e_2} &= \{y^2, w^2 \mid \overline{y}^2, \overline{w}^2\},\\
\boldsymbol{b_1} &= \{\psi^\mu, \chi^{12}, y^{34}, y^{56} \mid \overline{y}^{34}, \overline{y}^{56}, \overline{\eta}^1, \overline{\psi}^{1,\dots,5}\},\\
\boldsymbol{b_2} &= \{\psi^\mu, \chi^{34}, y^{12}, w^{56} \mid \overline{y}^{12}, \overline{w}^{56}, \overline{\eta}^2, \overline{\psi}^{1,\dots,5}\},\\
\boldsymbol{b_3} &= \{\psi^\mu, \chi^{56}, w^{1234} \mid \overline{w}^{1234}, \overline{\eta}^3, \overline{\psi}^{1,\dots,5}\},\\
\boldsymbol{z_1} &= \{\overline{\phi}^{1,\dots,4}\},\\
\boldsymbol{x} &= \{\overline{\psi}^{1,\dots,5}, \overline{\eta}^{1,2,3}\},\\
\gamma &= \{\bar{y}^{56}, \bar{w}^{34}, \bar{\psi}^{1,\dots,5} = \bar{\eta}^{1,2,3} = \bar{\phi}^{1,2,6,7} = \frac{1}{2}, \bar{\phi}^8\},
\end{aligned} \tag{8.101}$$

where we have the same $\boldsymbol{z_2}$ combination as eq. (8.21) and the untwisted gauge group is

$$\text{Observable: } SU(5) \times U(1) \times U(1)_{i=1,2,3} \times U(1)_{j=4,5} \tag{8.102}$$

$$\text{Hidden: } SU(2) \times U(1)_{H_1} \times SO(4) \times U(1)_{H_2} \times SU(2) \times U(1)_{H_3} \times U(1)_{H_4}. \tag{8.103}$$

There are two horizontal symmetries associated to the antiholomorphic currents from the pairings $\bar{y}^{5,6}$ and $\bar{w}^3\bar{w}^4$. Since there are 10 basis vectors we naively have 2^{45} independent GGSO configurations but the following 10 phases do not affect the projection criteria for the phenomenological criteria we investigate

$$C\begin{bmatrix}\mathbb{1}\\ \boldsymbol{b_1}\end{bmatrix}, C\begin{bmatrix}\mathbb{1}\\ \boldsymbol{b_2}\end{bmatrix}, C\begin{bmatrix}\mathbb{1}\\ \boldsymbol{b_3}\end{bmatrix}, C\begin{bmatrix}\mathbb{1}\\ \boldsymbol{z_1}\end{bmatrix}, C\begin{bmatrix}\mathbb{1}\\ \gamma\end{bmatrix}, C\begin{bmatrix}\boldsymbol{S}\\ \gamma\end{bmatrix}, C\begin{bmatrix}\boldsymbol{b_1}\\ \gamma\end{bmatrix}, C\begin{bmatrix}\boldsymbol{b_3}\\ \gamma\end{bmatrix}, C\begin{bmatrix}\boldsymbol{z_1}\\ \gamma\end{bmatrix}, C\begin{bmatrix}\boldsymbol{x}\\ \gamma\end{bmatrix}. \tag{8.104}$$

This leaves just 35 free GGSO phases generating a space of $2^{35} \sim 3.4 \times 10^{10}$ independent configurations to classify. The supersymmetric subspace of which is subject to conditions (8.37) and (8.38).

8.5.1 Class B Phenomenological Features

Observable Spinorials Representations and Absence of Three Generation

The following sectors give rise to the fermion generations

$$\boldsymbol{F}_t^1 = \boldsymbol{b_1} + t\boldsymbol{e_{3456}} \tag{8.105}$$

$$\boldsymbol{F}_{pq}^2 = \boldsymbol{b_2} + p\boldsymbol{e_1} + q\boldsymbol{e_2} \tag{8.106}$$

$$\boldsymbol{F}_{pq}^3 = \boldsymbol{b_3} + p\boldsymbol{e_1} + q\boldsymbol{e_2}, \tag{8.107}$$

and the degeneracies $\boldsymbol{D}$ tell us that $\boldsymbol{F}_0^1$ generate 4 copies of the **16** or $\overline{\mathbf{16}}$, $\boldsymbol{F}_1^1$ generate 2 copies of the **16** *and* 2 copies of the $\overline{\mathbf{16}}$, whilst $\boldsymbol{F}_{pq}^2$ generate 2 copies of either $\left(\mathbf{10}, +\frac{1}{2}\right)$, $(\bar{\mathbf{5}}, -\frac{3}{2}) + (\mathbf{1}, \frac{5}{2})$, $\left(\overline{\mathbf{10}}, -\frac{1}{2}\right)$ or $(\mathbf{5}, +\frac{3}{2}) + (\mathbf{1}, -\frac{5}{2})$. Lastly, $\boldsymbol{F}_{pq}^3$ generates 1 copy of the **16** or $\overline{\mathbf{16}}$.

As mentioned above, three generation models do not arise in this class, and to see why it will be useful to write the projection equations for these spinorial sectors. We can first construct the projectors for these sectors by utilising eq. (8.44)

$$\mathbb{P}_{\boldsymbol{F}_t^1} = \frac{1}{2^5} \prod_{i=1,2} \left(1 - C\begin{bmatrix} \boldsymbol{F}_t^{(1)} \\ \boldsymbol{e_i} \end{bmatrix}\right) \left(1 - C\begin{bmatrix} \boldsymbol{F}_t^{(1)} \\ \boldsymbol{2\gamma + x} \end{bmatrix}\right) \prod_{a=1,2} \left(1 - C\begin{bmatrix} \boldsymbol{F}_t^{(1)} \\ \boldsymbol{z_a} \end{bmatrix}\right) \tag{8.108}$$

$$\mathbb{P}_{\boldsymbol{F}_{pq}^2} = \frac{1}{2^3} \left(1 - C\begin{bmatrix} \boldsymbol{F}_{pq}^2 \\ \boldsymbol{2\gamma + x} \end{bmatrix}\right) \prod_{a=1,2} \left(1 - C\begin{bmatrix} \boldsymbol{F}_{pq}^2 \\ \boldsymbol{z_a} \end{bmatrix}\right) \tag{8.109}$$

$$\mathbb{P}_{\boldsymbol{F}_{pq}^3} = \frac{1}{2^3} \left(1 - C\begin{bmatrix} \boldsymbol{F}_{pq}^3 \\ \boldsymbol{2\gamma + x} \end{bmatrix}\right) \prod_{a=1,2} \left(1 - C\begin{bmatrix} \boldsymbol{F}_{pq}^3 \\ \boldsymbol{z_a} \end{bmatrix}\right), \tag{8.110}$$

Next we can apply eq. (8.45) to get the chirality phases

$$\boldsymbol{X}_{t=0}^1 = -C\begin{bmatrix} \boldsymbol{F}_0^1 \\ \boldsymbol{b_2} \end{bmatrix}^*,$$

$$\boldsymbol{X}_{pq}^2 = -C\begin{bmatrix} \boldsymbol{F}_{pq}^2 \\ \boldsymbol{b_1} \end{bmatrix}^*$$

$$\boldsymbol{X}_{pq}^3 = -C\begin{bmatrix} \boldsymbol{F}_{pq}^3 \\ \boldsymbol{b_1} \end{bmatrix}^*,$$

where we have chosen $\mathrm{ch}(\psi^\mu) = +1$ for the spacetime fermion chirality and note the $\boldsymbol{F}_1^1$ does not have a chirality operator as it gives rise to 2 copies of the **16** and the $\overline{\mathbf{16}}$. By

applying eq. (8.47), we can write the quantum numbers of the $SU(5) \times U(1)$ representations as

$$\begin{aligned}
n_{10} &= \sum_{t=0,1} 2\mathbb{P}_{\boldsymbol{F}_t^1} \frac{1}{2}\left(1+t+(1-t)\boldsymbol{X}_t^1\right) + \sum_{p,q=0,1} 2\mathbb{P}_{\boldsymbol{F}_{pq}^2} \frac{1}{4}\left(1+\boldsymbol{X}_{pq}^2\right)\left(1+C\begin{bmatrix}\boldsymbol{F}_{pq}^2\\ \boldsymbol{\gamma}\end{bmatrix}\right) \\
&\quad + \sum_{p,q=0,1} \mathbb{P}_{\boldsymbol{F}_{pq}^3} \frac{1}{2}\left(1+\boldsymbol{X}_{pq}^3\right) \\
n_{\bar{5}} &= \sum_{t=0,1} 2\mathbb{P}_{\boldsymbol{F}_t^1} \frac{1}{2}\left(1+t+(1-t)\boldsymbol{X}_t^1\right) + \sum_{p,q=0,1} 2\mathbb{P}_{\boldsymbol{F}_{pq}^2} \frac{1}{4}\left(1+\boldsymbol{X}_{pq}^2\right)\left(1-C\begin{bmatrix}\boldsymbol{F}_{pq}^2\\ \boldsymbol{\gamma}\end{bmatrix}\right) \\
&\quad + \sum_{p,q=0,1} \mathbb{P}_{\boldsymbol{F}_{pq}^3} \frac{1}{2}\left(1+\boldsymbol{X}_{pq}^3\right) \\
n_{\overline{10}} &= \sum_{t=0,1} 2\mathbb{P}_{\boldsymbol{F}_t^1} \frac{1}{2}\left(1+t-(1-t)\boldsymbol{X}_t^1\right) + \sum_{p,q=0,1} 2\mathbb{P}_{\boldsymbol{F}_{pq}^2} \frac{1}{4}\left(1-\boldsymbol{X}_{pq}^2\right)\left(1+C\begin{bmatrix}\boldsymbol{F}_{pq}^2\\ \boldsymbol{\gamma}\end{bmatrix}\right) \\
&\quad + \sum_{p,q=0,1} \mathbb{P}_{\boldsymbol{F}_{pq}^3} \frac{1}{2}\left(1-\boldsymbol{X}_{pq}^3\right) \\
n_{5} &= \sum_{t=0,1} 2\mathbb{P}_{\boldsymbol{F}_t^1} \frac{1}{2}\left(1+t-(1-t)\boldsymbol{X}_t^1\right) + \sum_{p,q=0,1} 2\mathbb{P}_{\boldsymbol{F}_{pq}^2} \frac{1}{4}\left(1-\boldsymbol{X}_{pq}^2\right)\left(1-C\begin{bmatrix}\boldsymbol{F}_{pq}^2\\ \boldsymbol{\gamma}\end{bmatrix}\right) \\
&\quad + \sum_{p,q=0,1} \mathbb{P}_{\boldsymbol{F}_{pq}^3} \frac{1}{2}\left(1-\boldsymbol{X}_{pq}^3\right),
\end{aligned} \tag{8.111}$$

where we note the singlets have the same projection as $\mathbf{5}$ and $\bar{\mathbf{5}}$. Imposing the condition for complete generations $n_{10} - n_{\overline{10}} = n_{\bar{5}} - n_5$ results in the condition

$$\sum_{p,q} \mathbb{P}_{\boldsymbol{F}_{pq}^2} C\begin{bmatrix}\boldsymbol{F}_{pq}^2\\ \boldsymbol{\gamma}\end{bmatrix} X_{pq}^2 = 0, \tag{8.112}$$

and $n_{10} - n_{\overline{10}} = 3$ for three generations tells us

$$3 = \sum_t 2\mathbb{P}_{F_t^1} X_t^1 + \sum_{p,q} 2\mathbb{P}_{F_{pq}^2} \frac{1}{2}\left(1+C\begin{bmatrix}\boldsymbol{F}_{pq}^2\\ \boldsymbol{\gamma}\end{bmatrix}\right) X_{pq}^2 + \sum_{p,q} \mathbb{P}_{\boldsymbol{F}_{pq}^3} X_{pq}^3, \tag{8.113}$$

which is only possible if

$$\sum_{p,q} \mathbb{P}_{\boldsymbol{F}_{pq}^3} X_{pq}^3 \in \{1,3\}, \tag{8.114}$$

but $\sum_{p,q} \mathbb{P}_{\boldsymbol{F}_{pq}^3} X_{pq}^3 = 3$ we can show is impossible by inspecting (8.110), which only depends on nine phases

$$C\begin{bmatrix}\boldsymbol{b_3}\\ \boldsymbol{z_1}\end{bmatrix}, C\begin{bmatrix}\boldsymbol{b_3}\\ \boldsymbol{z_2}\end{bmatrix}, C\begin{bmatrix}\boldsymbol{b_3}\\ \boldsymbol{x}\end{bmatrix}, C\begin{bmatrix}\boldsymbol{e_1}\\ \boldsymbol{z_1}\end{bmatrix}, C\begin{bmatrix}\boldsymbol{e_1}\\ \boldsymbol{z_2}\end{bmatrix}, C\begin{bmatrix}\boldsymbol{e_1}\\ \boldsymbol{x}\end{bmatrix}, C\begin{bmatrix}\boldsymbol{e_2}\\ \boldsymbol{z_1}\end{bmatrix}, C\begin{bmatrix}\boldsymbol{e_2}\\ \boldsymbol{z_2}\end{bmatrix}, C\begin{bmatrix}\boldsymbol{e_2}\\ \boldsymbol{x}\end{bmatrix}, \tag{8.115}$$

and if 3 of the 4 sectors, $\boldsymbol{F}_{pq}^3$, have $\mathbb{P}_{\boldsymbol{F}_{pq}^3} = 1$ then all 9 phases are fixed and ensures the fourth also has $\mathbb{P}_{\boldsymbol{F}_{pq}^3} = 1$.

Therefore, the only way to satisfy (8.113) is if $\sum_{p,q} \mathbb{P}_{\boldsymbol{F}^3_{pq}} X^3_{pq} = 1$. This further implies $\sum_{p,q} \mathbb{P}_{\boldsymbol{F}^2_{pq}} C[^{\boldsymbol{F}^2_{pq}}_{\gamma}] X^2_{pq} \in \{2,4\}$, from (8.112). If we assume $\sum_{p,q} \mathbb{P}_{\boldsymbol{F}^2_{pq}} C[^{\boldsymbol{F}^2_{pq}}_{\gamma}] X^2_{pq} = 2$ then the constraints this imposes on the phases in $\mathbb{P}_{\boldsymbol{F}^2_{pq}}$ necessitates

$$\sum_{p,q} \mathbb{P}_{\boldsymbol{F}^3_{pq}} X^3_{pq} \in \{0,2\}, \tag{8.116}$$

making 3 generations impossible. Similarly if $\sum_{p,q} \mathbb{P}_{\boldsymbol{F}^2_{pq}} C[^{\boldsymbol{F}^2_{pq}}_{\gamma}] X^2_{pq} = 4$ this imposes

$$\sum_{p,q} \mathbb{P}_{\boldsymbol{F}^3_{pq}} X^3_{pq} \in \{0,4\}, \tag{8.117}$$

which again makes 3 generations impossible.

Not only does the Z3 SMT solver confirm the unsatisfiability of 3 generation configurations, it also generates a proof written in computer language[3]. There are also additional tools available in Z3 to explore unsatisfiability such as identifying a minimal 'unsatisfiable core' [123], isolating the contradiction by giving a (locally) minimal subset of constraints, where dropping either of them results in a satisfiable constraint system. In Figure 8.5 the distribution of n_g is plotted for a random sample of 10^7 Class B models showing empirically the absence of $n_g = 3$ models.

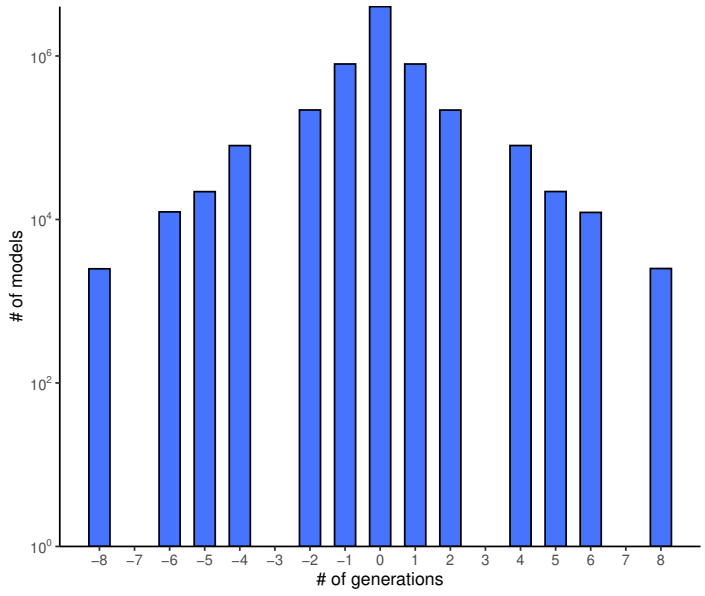

Figure 8.5: *Frequency plot for number of generations from a sample of* 10^7 *Class B vacua.*

The origin of this contradiction can be traced to the projection of moduli in the 2nd and 3rd tori which means there are no $\boldsymbol{e_i}$ vectors to project $\boldsymbol{F}^2_{pq}$ and $\boldsymbol{F}^3_{pq}$. This results in constraining and correlating their presence in the massless spectrum.

[3] Available at https://github.com/BenjaminPercival/AsymmetricOrbifolds.git

Heavy Higgs

As in Class A we will demand the presence of at least one heavy Higgs to break the FSU5 gauge symmetry in our classification. The number of Heavy Higgs $\#\left[(\mathbf{10},\frac{1}{2})+(\overline{\mathbf{10}},-\frac{1}{2})\right]$ can again be calculated through the projections of sectors $\boldsymbol{S}+\boldsymbol{F}^{k}_{pq}$.

Top Quark Mass Couplings

As in Class A, in classifying vacua from Class B we will account for all the three untwisted type TQMC and all 3 twisted type when checking whether a potentially viable TQMC arises from a model.

To check the presence of a viable TQMC we, again, account for the twisted Light Higgs sectors, which can be checked through analogous projection conditions for Class B as in Class A. It is simply the number of $[(\mathbf{5},-1)+(\bar{\mathbf{5}},+1)]$ from the sectors $\boldsymbol{V}^{k}_{pq}$ in the massless spectrum.

Tachyonic Sector Analysis

Class A models have significantly fewer tachyonic sectors than Class B. Specifically, there are 27 sectors producing on-shell tachyons for Class B, compared with the 78 of Class A.

The following 3 sectors will produce on-shell tachyons with a right-moving oscillator should they be present in the spectrum of a model

$$T_1=\begin{Bmatrix}\{\bar{\lambda}\}_{\frac{1}{2}}: & |\boldsymbol{e_1}\rangle & |\boldsymbol{e_2}\rangle\\ \{\bar{\lambda}\}_{\frac{1}{2}}: & |\boldsymbol{e_1}+\boldsymbol{e_2}\rangle & \end{Bmatrix}. \tag{8.118}$$

Further to this, the following on-shell tachyonic sectors arise with no oscillator

$$T_2=\left\{\begin{array}{ccc} |\boldsymbol{z_1}\rangle & |\boldsymbol{z_2}\rangle & |\boldsymbol{x}+2\boldsymbol{\gamma}\rangle\\ |\boldsymbol{e_i}+\boldsymbol{z_1}\rangle & |\boldsymbol{e_i}+\boldsymbol{z_2}\rangle & |\boldsymbol{e_i}+\boldsymbol{x}+2\boldsymbol{\gamma}\rangle\\ |\boldsymbol{e_1}+\boldsymbol{e_2}+\boldsymbol{z_1}\rangle & |\boldsymbol{e_1}+\boldsymbol{e_2}+\boldsymbol{z_2}\rangle & |\boldsymbol{e_1}+\boldsymbol{e_2}+\boldsymbol{x}+2\boldsymbol{\gamma}\rangle\\ & & \\ |\boldsymbol{z_1}+\boldsymbol{x}+2\boldsymbol{\gamma}\rangle & |\boldsymbol{z_2}+\boldsymbol{x}+2\boldsymbol{\gamma}\rangle & |\boldsymbol{z_1}+\boldsymbol{z_2}+\boldsymbol{x}+2\boldsymbol{\gamma}\rangle\\ |\boldsymbol{e_i}+\boldsymbol{z_1}+\boldsymbol{x}+2\boldsymbol{\gamma}\rangle & |\boldsymbol{e_i}+\boldsymbol{z_2}+\boldsymbol{x}+2\boldsymbol{\gamma}\rangle & |\boldsymbol{e_i}+\boldsymbol{z_1}+\boldsymbol{z_2}+\boldsymbol{x}+2\boldsymbol{\gamma}\rangle\\ |\boldsymbol{e_1}+\boldsymbol{e_2}+\boldsymbol{z_1}+\boldsymbol{x}+2\boldsymbol{\gamma}\rangle & |\boldsymbol{e_1}+\boldsymbol{e_2}+\boldsymbol{z_2}+\boldsymbol{x}+2\boldsymbol{\gamma}\rangle & |\boldsymbol{e_1}+\boldsymbol{e_2}+\boldsymbol{z_1}+\boldsymbol{z_2}+\boldsymbol{x}+2\boldsymbol{\gamma}\rangle \end{array}\right\}, \tag{8.119}$$

where $i\in\{1,2\}$.

The condition for the absence of such tachyonic sectors can be compactly written

$$\forall\, t\in T_1\cup T_2:\ \ \mathbb{P}_t=0. \tag{8.120}$$

Enhancements

As in Class A we will ensure the absence of enhancements to the observable gauge factors given from sectors listed in eq. (8.59), as well as the model-dependent sectors

$$\psi^{\mu}\{\bar{\lambda}\}_{\frac{1}{4}}\begin{cases}|\boldsymbol{z_1}+(3)\boldsymbol{\gamma}\rangle =: \mathbf{O}_1\\ |\boldsymbol{z_1}+\boldsymbol{x}+(3)\boldsymbol{\gamma}\rangle =: \mathbf{O}_2\\ |\boldsymbol{z_1}+\boldsymbol{z_2}+(3)\boldsymbol{\gamma}\rangle =: \mathbf{O}_3\\ |\boldsymbol{z_1}+\boldsymbol{z_2}+\boldsymbol{x}+(3)\boldsymbol{\gamma}\rangle =: \mathbf{O}_4,\end{cases} \tag{8.121}$$

and as in Class A we ensure the generalised projectors of these sectors are zero, which can be written

$$\forall\, i \in [1,4]: \quad \mathbb{P}_{\mathbf{O}_i} = 0. \tag{8.122}$$

Exotics

Along with the $(\boldsymbol{\alpha}_L\cdot\boldsymbol{\alpha}_L, \boldsymbol{\alpha}_R\cdot\boldsymbol{\alpha}_R) = (4,4)$ exotic sectors (8.62), there are 112 sectors at the level $(4,6)$ that can produce exotic massless states with a right-moving oscillator with $\nu_f = \frac{1}{2}$ or $\nu_{f^*} = -\frac{1}{2}$. As in Model A, these all arise in pairs with $+\boldsymbol{\gamma}$ and $+3\boldsymbol{\gamma}$ of equal and opposite gauge charges and therefore do not contribute to any chiral anomaly. Similarly for 176 sectors at level $(4,8)$. Therefore, we conveniently do not need to implement a condition on chiral exotics in the classification.

8.5.2 Class B Results

We wish to implement the constraints listed in (8.95) for the case of Class B. However, the absence of 3 generation models in this class means all models break at constraint (4). For completeness, we still present the reduced results in Table 8.4. In order to do a complete scan, we choose to impose condition (8.39) such that SUSY is broken by phases beyond the NAHE-set for the $\mathcal{N}=0$ models. This condition reduces the parameter space to $2^{31} \sim 2.15\times10^9$. We then enumerate all possible configurations of these 31 phases that give both $\mathcal{N}=1$ and $\mathcal{N}=0$ models.

	Total models in sample: $2^{31} = 2147483648$				
	SUSY or Non-SUSY:	$\mathcal{N}=1$	Probability	$\mathcal{N}=0$	Probability
	Total	134217728	6.25×10^{-2}	2013265920	9.38×10^{-1}
(1)	+ Tachyon-Free			518921216	2.42×10^{-1}
(2)	+ No Obs. Enhancements	121896960	5.68×10^{-2}	478915840	2.23×10^{-1}
(3)	+ Complete Generations	74317824	3.46×10^{-2}	271702016	1.27×10^{-1}
(8)	+ $a_{00} = N_b^0 - N_f^0 = 0$			326042	1.51×10^{-4}

Table 8.4: *Phenomenological statistics from a complete scan of* 2^{31} *Class B models. Note that the number of* $a_{00}=0$ *models is an estimate based on extrapolating from a sample of* 2.5×10^3 *of the 1245265024* $\mathcal{N}=0$ *models satisfying (1)-(3).*

In order to compare the efficiency of the SMT solver to that of a random scan we can search for four generation models, rather than three, that satisfy criteria (1)-(3) and (5)-(7) from (8.95). The results of this comparison are shown in Figure 8.6. We see that

the efficiency gained from the SMT is lower for Class B than the Class A case, with efficiency approximately 5.5 times higher compared to the random approach after 3 minutes, reducing to approximately 1.5 times after 1 hour. This reduced efficiency for Class B seems to result from the fewer constraints imposed from the absence of tachyons, evidenced by the probability 2.42×10^{-1} for Table 8.4 compared to 3.08×10^{-2} for Table 8.3, as well as the smaller space of models and higher degeneracy, meaning the SMT algorithm's search saturates more quickly than in Class A.

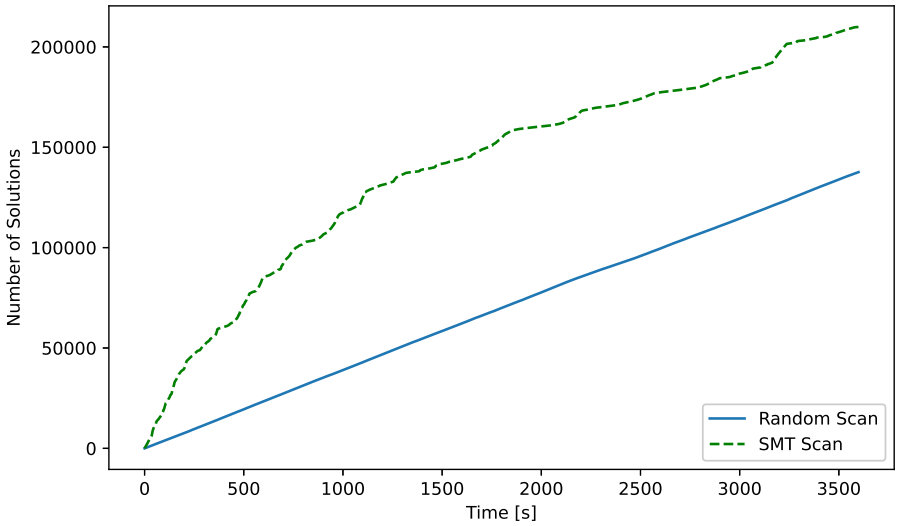

Figure 8.6: *Rate at which the Z3 SMT finds 4 generation models satisfying constraints (1)-(3) and (5)-(7) compared with a random generation approach over a 1 hour period.*

As in the case of Class A models, it is also interesting to perform a statistical analysis at the level of the partition function. Figure 8.7 shows the distribution of the cosmological constant for a batch of 1.5×10^3 Class B models, satisfying conditions (1)-(3) of Table 8.4. We again note the slight tendency to negative values even though positive values are not excluded. In Figure 8.8, we see that the SMT algorithm finds relatively more degenerate models as compared to the Class A case. This is mostly due to the reduced number of constraints on the GGSO phases and the increased frequency of solutions as discussed above.

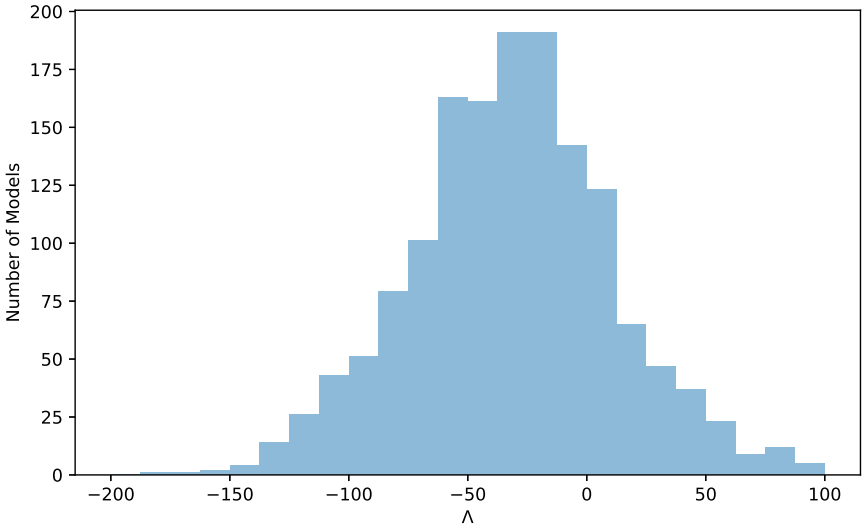

Figure 8.7: *The distribution of the cosmological constant Λ_{ST} for a sample off 1.5×10^3 Class B models satisfying conditions (1)-(3) of Table 8.4. To gain the physical value, a factor of $\mathcal{M}^4$ must be reinstated. These values are evaluated at the free fermionic point using methods discussed in Section 8.3.4.*

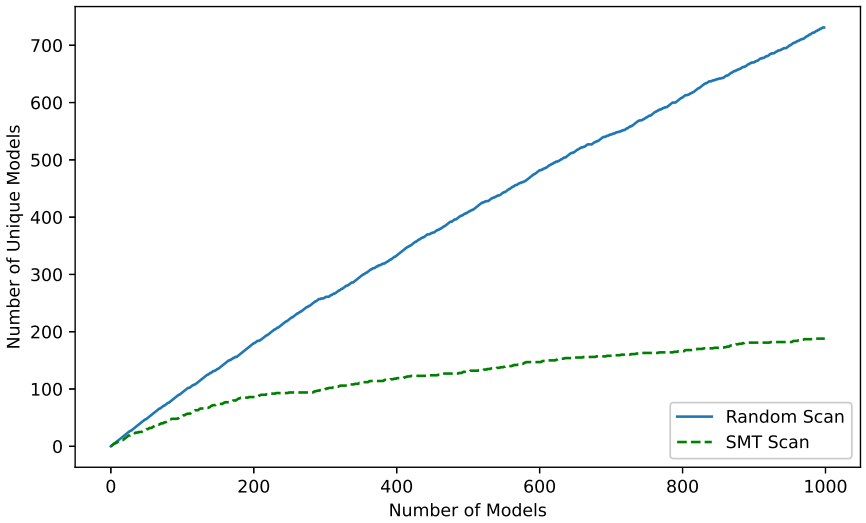

Figure 8.8: *The degeneracy of models in a Random versus an SMT scan for Class B.*

8.5.3 Class B Example Model with 4 Generations

Having discussed the absence of three generation models in this class, we give an example four generation model and discuss its key characteristics. We emphasize that,

although this class of models is not phenomenological, they are of particular interest due to the fact that the untwisted moduli of the 2nd and 3rd tori are fixed. The chosen model is defined by the basis (8.101) and the GGSO phases

$$C\begin{bmatrix} v_i \\ v_j \end{bmatrix} = \begin{array}{c} \\ \mathbf{1} \\ \boldsymbol{S} \\ \boldsymbol{e_1} \\ \boldsymbol{e_2} \\ \boldsymbol{b_1} \\ \boldsymbol{b_2} \\ \boldsymbol{b_3} \\ \boldsymbol{z_1} \\ \boldsymbol{x} \\ \boldsymbol{\gamma} \end{array} \begin{array}{c} \begin{array}{cccccccccc} \mathbf{1} & \boldsymbol{S} & \boldsymbol{e_1} & \boldsymbol{e_2} & \boldsymbol{b_1} & \boldsymbol{b_2} & \boldsymbol{b_3} & \boldsymbol{z_1} & \boldsymbol{x} & \boldsymbol{\gamma} \end{array} \\ \begin{pmatrix} 1 & -1 & 1 & 1 & -1 & -1 & -1 & -1 & 1 & -i \\ -1 & -1 & 1 & 1 & -1 & -1 & -1 & 1 & 1 & -1 \\ 1 & 1 & -1 & 1 & -1 & 1 & -1 & -1 & 1 & 1 \\ 1 & 1 & 1 & -1 & -1 & 1 & 1 & 1 & 1 & 1 \\ -1 & 1 & -1 & -1 & -1 & -1 & -1 & -1 & -1 & -1 \\ -1 & 1 & 1 & 1 & -1 & -1 & 1 & 1 & -1 & -i \\ -1 & 1 & -1 & 1 & -1 & 1 & -1 & -1 & 1 & -1 \\ -1 & 1 & -1 & 1 & -1 & 1 & -1 & -1 & 1 & -i \\ 1 & 1 & 1 & 1 & 1 & 1 & -1 & 1 & -1 & -1 \\ 1 & -1 & 1 & 1 & -1 & -1 & -1 & 1 & -1 & -i \end{pmatrix} \end{array}, \tag{8.123}$$

The states from sector $\boldsymbol{b_1}$ generate four copies of fermion generations in the **16**. We obtain a Heavy Higgs from the sector $\boldsymbol{S}+\boldsymbol{b_3}+\boldsymbol{e_1}+\boldsymbol{e_2}$. There is an untwisted-type TQMC from the first orbifold plane and we note the existence of an additional hidden sector gauge boson from $\psi^\mu\{\bar{y}^1\}\,|\boldsymbol{z_1}\rangle$ which enhances the hidden gauge group

$$\begin{aligned} &SU(2)\times U(1)_{H_1}\times SO(4)\times U(1)_{H_2}\times SU(2)\times U(1)_{H_3}\times U(1)_{H_4} \\ &\rightarrow\ U(1)_{H_1}\times SO(5)\times SU(2)\times U(1)_{H_2}\times SU(2)\times U(1)_{H_3}\times U(1)_{H_4}. \end{aligned} \tag{8.124}$$

The partition function for this model can be calculated similarly to the Class A model presented in Section 8.4.3. The main difference in this case is that the asymmetric shifts introduced by $\boldsymbol{A}$ only explicitly include the anti-holomorphic part of the internal lattice in the first and third orbifold plane. That is, the lattice becomes

$$\begin{aligned} \Gamma^{\gamma}_{(6,6)} =&\ \Gamma^{\gamma}_1\times\Gamma^{\gamma}_2\times\Gamma^{\gamma}_3 \\ =&\quad \vartheta_{y^{3,4}}\begin{bmatrix} r+h_2 \\ s+g_2 \end{bmatrix}\vartheta_{y^{5,6}}\begin{bmatrix} r+h_2 \\ s+g_2 \end{bmatrix} \\ &\times\ \vartheta_{\bar{y}^{3,4}}\begin{bmatrix} r+h_2 \\ s+g_2 \end{bmatrix}\bar{\vartheta}_{\bar{y}^{5,6}}\begin{bmatrix} r+h_2+2H' \\ s+g_2+2G' \end{bmatrix} \\ &\times\ \vartheta_{y^1}\begin{bmatrix} r+h_1+H_1 \\ s+g_1+G_1 \end{bmatrix}^{1/2}\vartheta_{y^2}\begin{bmatrix} r+h_1+H_2 \\ s+g_1+G_2 \end{bmatrix}^{1/2}\vartheta_{w^{5,6}}\begin{bmatrix} r+h_1 \\ s+g_1 \end{bmatrix} \\ &\times\ \bar{\vartheta}_{\bar{y}^1}\begin{bmatrix} r+h_1+H_1 \\ s+g_1+G_1 \end{bmatrix}^{1/2}\bar{\vartheta}_{\bar{y}^2}\begin{bmatrix} r+h_1+H_2 \\ s+g_1+G_2 \end{bmatrix}^{1/2}\bar{\vartheta}_{\bar{w}^{5,6}}\begin{bmatrix} r+h_1 \\ s+g_1 \end{bmatrix} \\ &\times\ \vartheta_{w^1}\begin{bmatrix} r-h_1-h_2+H_1 \\ s-g_1-g_2+G_1 \end{bmatrix}^{1/2}\vartheta_{w^2}\begin{bmatrix} r-h_1-h_2+H_2 \\ s-g_1-g_2+G_2 \end{bmatrix}^{1/2}\vartheta_{w^{3,4}}\begin{bmatrix} r-h_1-h_2 \\ s-g_1-g_2 \end{bmatrix} \\ &\times\ \vartheta_{\bar{w}^1}\begin{bmatrix} r-h_1-h_2+H_1 \\ s-g_1-g_2+G_1 \end{bmatrix}^{1/2}\bar{\vartheta}_{\bar{w}^2}\begin{bmatrix} r-h_1-h_2+H_2 \\ s-g_1-g_2+G_2 \end{bmatrix}^{1/2}\bar{\vartheta}_{\bar{w}^{3,4}}\begin{bmatrix} r-h_1-h_2+2H' \\ s-g_1-g_2+2G' \end{bmatrix}, \end{aligned} \tag{8.125}$$

where Γ^{γ}_i again denotes the terms corresponding to the i^{th} orbifold plane. We see that, indeed, Γ^{γ}_2 remains left-right symmetric and the absence of $\boldsymbol{e_{3,4,5,6}}$ simplifies the lattice.

Based on this lattice, we can gain the q-expansion of the model, which is now given by

$$\begin{aligned} Z = & 2\,q^0\bar{q}^{-1} + 56\,q^{1/2}\bar{q}^{-1/2} + 208\,q^{-1/2}\bar{q}^{1/2} \\ & + 8\,q^0\bar{q}^0 - 192\,q^{1/8}\bar{q}^{1/8} + 1280\,q^{1/4}\bar{q}^{1/4} - 5632\,q^{1/2}\bar{q}^{1/2}, \end{aligned} \tag{8.126}$$

including all terms up to at most $\mathcal{O}(q^{1/2})$ and $\mathcal{O}(\bar{q}^{1/2})$. We note again the presence of the protograviton term with the correct factor and the presence of a constant term $q^0\bar{q}^0$. There was no model found with $N_b^0 = N_f^0$ in a sample of 2.5×10^3 4 generation models.

Integrating this q-expansion over the fundamental domain of the modular group gives the spacetime cosmological constant

$$\Lambda_{\rm ST} = 31.86 \times \mathcal{M}^4, \tag{8.127}$$

calculated to $\mathcal{O}(q^4\bar{q}^4)$. As in the Class A case, this value is evaluated at the free fermionic point in moduli space.

8.6 Discussion

In this chapter we initiated the extension of the fermionic $\mathbb{Z}_2 \times \mathbb{Z}_2$ orbifold classification method to string vacua with asymmetric boundary conditions. There are notable phenomenological advantages for string models with asymmetric boundary conditions, among them the stringy Higgs doublet–triplet splitting mechanism [126] and the top–bottom quark mass hierarchy [130]. Of particular interest is the fact that asymmetric boundary conditions fix many of the untwisted moduli by projecting out moduli fields from the massless spectrum [124]. In this respect, we note that there exist cases in which all the untwisted moduli are projected out [124], as well as cases in which it has been argued the string vacuum is entirely fixed, *i.e.* cases in which the twisted, as well as the supersymmetric moduli , are fixed [70]. We note that from the point of view of the free fermionic classification methodology, these cases are futile because it entails that they are not compatible with any of the $\boldsymbol{e_i}$ vectors discussed in Section 8.2. Our purpose here was therefore to analyse configurations in which some, but not all, of the moduli are fixed. This approach is particularly suited to the search for string vacua with positive cosmological constant, á la [43, 44]. In these cases, the potential of some of the remaining unfixed moduli is analysed away from the self-dual point with the aim of finding a vacuum state with a positive vacuum energy at a stable minimum. Thus, whereas in the case of [43, 44] the other moduli are unfixed, in the case of vacua with asymmetric boundary conditions the possibility exists of finding such vacua in which the other moduli are fixed.

In both Class A and Class B models we saw the incorporation of asymmetric boundary conditions was done through a single basis vector, whereas the remaining basic set, aside from the set of the $\boldsymbol{e_i}$ basis vectors that are compatible with the given

pairings, were identical in the two cases. We note that in principle this can be relaxed, *e.g.* by not including the vector z_1 in the basis. Such a variation may affect the possibility of three generations models in cases such as Class B, where they are impossible, but we leave such variations for future work. We note, however, that the program initiated herein opens the door to the systematic investigation of quasi-realistic vacua that are intrinsically non-geometric. We furthermore demonstrated effective applications of SMT algorithms to the space of free fermionic models under investigation. Not only do they provide significant efficiency increases, as demonstrated in Figure 8.2 and 8.6, but they also allowed for immediate evaluation of unsatisfiable constraints, such as proving the absence of three generation models in Class B.

Other than the systematic study of the one-loop potential for asymmetric models, mentioned as a key motivation for this work, future work classifying Standard-like models (SLMs) with asymmetric boundary conditions is a natural extension of this work. In that context, the role of asymmetric pairings in the (untwisted) Doublet-Triplet splitting mechanism [126] will be evident, in a way it is not for the FSU5 models studied here. The space of asymmetric SLMs will be larger and phenomenologically viable models more sparsely distributed, thus the application of SMT algorithms could prove instrumental in effective searches of this landscape. The analysis of Section 8.2, can be extended so that the SMT can explicitly interpret phenomenological constraints as a function of all asymmetric pairings and provide generic results, including no-go theorems, over a varied space of models. It will furthermore be interesting to explore different possibilities for how to implement the asymmetric boundary conditions, other than solely through the $SO(10)$ breaking vector as studied in this work.

Chapter 9

Reflections

A central theme of this thesis is non-supersymmetric string vacua. As Ioannis Rizos has remarked [137], life without SUSY seems like opening Pandora's box and turning your back on your only friend on the path towards reconciling some of the many mysteries of the Standard Model. For several decades, SUSY has been the most promising route towards solutions to issues such as stabilising the Higgs mass, unifying gauge couplings and being able to compute quantum corrections using holomorphy properties of BPS states. Not only this, SUSY has also given rise to beautiful mathematical structures and concepts. At the worldsheet level, SUSY is even baked into the very foundation of superstring theories.

It is not merely what you gain from having (spacetime) SUSY, but also what you lose without it. The absence of SUSY introduces the threat of tachyonic modes in the string spectrum introducing tree level instabilities into the theory. Although this issue is discussed in various setups in this thesis at the free fermionic point, a more thorough stability analysis of the classical vacuum is required for generic points in the moduli space, see e.g. [138, 139, 140]. A further significant problem, not discussed in this thesis, is the presence of a one-loop tadpole back-reacting on the classical vacuum [141, 142]. This issue has been analysed in certain non-supersymmetric setups, including the $SO(16) \times SO(16)$ case, in [143]. A further obvious problem to address is the issue of the smallness of the cosmological constant, discussed in various parts of this thesis.

With all these issues considered, we may worry that our situation is hopeless. Apart from the obvious fact that we know the world is non-supersymmetric (below the upper threshold of current LHC energies, at least), in recent years it has become increasingly clear that the world of non-SUSY strings contains new and exciting mathematical structures and hopeful avenues for resolving the big mysteries of particle physics. The progress made in the analysis in the one-loop potentials of non-supersymmetric strings [144, 145, 146, 147] and the possibility of finding models with suppressed cosmological constant [43, 44, 73, 74, 148, 149, 150, 151], being just two examples discussed within this thesis. We can add the uncovering of misaligned SUSY [95, 96] as another example, in which refs [97, 99] have uncovered exciting mathematical relationships in the full string spectrum. Further to this, the analysis of gauge thresholds in [152, 153], demonstrating

how certain classes of models enjoy a universal structure to their gauge threshold corrections, provides further evidence of deep structures in the non-SUSY string landscape and new possibilities for making quantum correction calculations tractable.

In this work, I have presented steps towards how we can build and classify concrete non-SUSY models from the $\mathbb{Z}_2 \times \mathbb{Z}_2$ heterotic string in the free fermionic formulation. I have helped introduce viable models descending from a tachyonic 10D string and emphasized how asymmetric shifts may well be instrumental in providing realistic models, ripe for productive analysis in regard to deeper issues of stability mentioned above. There have, indeed, been several others who have suspected that asymmetric orbifolds may play a key role in non-SUSY model building with regard to, for example, suppressing the cosmological constant [154, 155, 156, 157, 158, 159]. However, their role in constraining the moduli space has been of particular interest in this work. It will certainly be interesting to further develop the analysis of asymmetric orbifold models in future work.

I have also emphasized the use of sophisticated computational tools, in particular the SAT/SMT solvers, in helping to solve and declare satisfiability for constraint systems such as those associated to various phenomenological characteristics. It is good to see that ideas from big data and machine learning are making there way into the String Phenomenology community. It is already clear that such approaches will be especially helpful in understanding the string landscape in general, and the non-SUSY landscape in particular.

It seems that researchers in non-SUSY strings are doomed to some (potentially misaligned) oscillation between feeling overwhelmed by the Pandora's box of problems opened up in the absence of SUSY and feeling excited by the opportunities offered by this very lightly explored terrain. There are certainly a wide range of new discoveries to find in the world of non-SUSY strings, and this work can hopefully function as a baby step towards starting to understand this world.

Bibliography

[1] K. Popper. *The Logic of Scientific Discovery*. Basic Books. ISBN: 9781614277439.

[2] J. Halverson and P. Langacker. "TASI Lectures on Remnants from the String Landscape". In: *PoS* TASI2017 (2018), p. 019. DOI: 10.22323/1.305.0019.

[3] M. R. Douglas. "The Statistics of string / M theory vacua". In: *JHEP* 05 (2003), p. 046. DOI: 10.1088/1126-6708/2003/05/046.

[4] F. Ruehle. "Data science applications to string theory". In: *Phys. Rept.* 839 (2020), pp. 1–117. DOI: 10.1016/j.physrep.2019.09.005.

[5] E. Palti. "The Swampland: Introduction and Review". In: *Fortsch. Phys.* 67.6 (2019), p. 1900037. DOI: 10.1002/prop.201900037.

[6] M. van Beest, J. Calderón-Infante, D. Mirfendereski, and I. Valenzuela. *Lectures on the Swampland Program in String Compactifications*. Feb. 2021. arXiv: 2102.01111 [hep-th].

[7] A. E. Faraggi, V. G. Matyas, and B. Percival. "Towards the classification of tachyon-free models from tachyonic ten-dimensional heterotic string vacua". In: *Nuclear Physics B* 961 (2020), p. 115231. ISSN: 0550-3213. DOI: https://doi.org/10.1016/j.nuclphysb.2020.115231.

[8] A. Faraggi, V. Matyas, and B. Percival. "Type 0 $\mathbb{Z}_2 \times \mathbb{Z}_2$ heterotic string orbifolds and misaligned supersymmetry". In: *International Journal of Modern Physics A* 36 (2021), p. 2150174. DOI: 10.1142/S0217751X21501748.

[9] A. E. Faraggi, V. G. Matyas, and B. Percival. "Type $\bar{0}$ heterotic string orbifolds". In: *Physics Letters B* 814 (2021), p. 136080. ISSN: 0370-2693. DOI: https://doi.org/10.1016/j.physletb.2021.136080.

[10] A. Faraggi, B. Percival, S. Schewe, and D. Wojtczak. "Satisfiability modulo theories and chiral heterotic string vacua with positive cosmological constant". In: *Physics Letters B* 816 (2021), p. 136187. DOI: 10.1016/j.physletb.2021.136187.

[11] A. E. Faraggi, V. G. Matyas, and B. Percival. "Towards Classification of $\mathcal{N} = 1$ and $\mathcal{N} = 0$ Flipped $SU(5)$ Asymmetric $\mathbb{Z}_2 \times \mathbb{Z}_2$ Heterotic String Orbifolds". In: (2022). arXiv: 2202.04507 [hep-th].

[12] D. Israel. *Lecture notes on String Theory*. 2019. URL: https://www.lpthe.jussieu.fr/~israel/notes.pdf.

[13] E. Kiritsis. *String theory in a nutshell*. USA: Princeton University Press, 2019. ISBN: 978-0-691-15579-1.

[14] R. Blumenhagen, D. Lüst, and S. Theisen. *Basic concepts of string theory*. Theoretical and Mathematical Physics. Heidelberg, Germany: Springer, 2013. ISBN: 978-3-642-29496-9. DOI: 10.1007/978-3-642-29497-6.

[15] A. N. Schellekens. *Introduction to String Theory*. Nikhef, Amsterdam, 2014. URL: https://www.nikhef.nl/~t58/StringLectures2014.pdf.

[16] D. Tong. *String Theory*. Jan. 2009. arXiv: 0908.0333 [hep-th].

[17] G. Arutyunov. *Lectures on String Theory*. Utrecht University, 2009. URL: https://www2.physik.uni-muenchen.de/lehre/vorlesungen/wise_19_20/TD1_-String-Theory-I/arutyunov_notes.pdf.

[18] T. Mohaupt. *A Short Introduction to String Theory*. Cambridge University Press, 2022.

[19] T. E. Regge. "Introduction to complex orbital momenta". In: *Il Nuovo Cimento (1955-1965)* 14 (1959), pp. 951–976.

[20] A. Sen. "Tachyon dynamics in open string theory". In: *Int. J. Mod. Phys. A* 20 (2005), pp. 5513–5656. DOI: 10.1142/S0217751X0502519X.

[21] F. Gliozzi, J. Scherk, and D. I. Olive. "Supergravity and the Spinor Dual Model". In: *Phys. Lett. B* 65 (1976), pp. 282–286. DOI: 10.1016/0370-2693(76)90183-0.

[22] F. Gliozzi, J. Scherk, and D. I. Olive. "Supersymmetry, Supergravity Theories and the Dual Spinor Model". In: *Nucl. Phys. B* 122 (1977), pp. 253–290. DOI: 10.1016/0550-3213(77)90206-1.

[23] D. J. Gross, J. A. Harvey, E. J. Martinec, and R. Rohm. "The Heterotic String". In: *Phys. Rev. Lett.* 54 (1985), pp. 502–505. DOI: 10.1103/PhysRevLett.54.502.

[24] D. J. Gross, J. A. Harvey, E. J. Martinec, and R. Rohm. "Heterotic String Theory. 1. The Free Heterotic String". In: *Nucl. Phys. B* 256 (1985), p. 253. DOI: 10.1016/0550-3213(85)90394-3.

[25] D. J. Gross, J. A. Harvey, E. J. Martinec, and R. Rohm. "Heterotic String Theory. 2. The Interacting Heterotic String". In: *Nucl. Phys. B* 267 (1986), pp. 75–124. DOI: 10.1016/0550-3213(86)90146-X.

[26] P. Athanasopoulos, A. E. Faraggi, S. G. Nibbelink, and V. M. Mehta. "Heterotic free fermionic and symmetric toroidal orbifold models". In: *Journal of High Energy Physics* 2016 (2016), pp. 1–51.

[27] E. Sharpe. "Discrete torsion in perturbative heterotic string theory". In: *Phys. Rev. D* 68 (12 2003), p. 126005. DOI: 10.1103/PhysRevD.68.126005.

[28] E. Sharpe. "Discrete torsion". In: *Phys. Rev. D* 68 (12 2003), p. 126003. DOI: 10.1103/PhysRevD.68.126003.

[29] I. Antoniadis, C. P. Bachas, and C. Kounnas. "Four-dimensional superstrings". In: *Nuclear Physics* 289 (1987), pp. 87–108.

[30] I. Antoniadis and C. P. Bachas. "4D fermionic superstrings with arbitrary twists". In: *Nuclear Physics* 298 (1988), pp. 586–612.

[31] H. Kawai, D. C. Lewellen, and S.-H. Henry Tye. "Construction of fermionic string models in four dimensions". In: *Nuclear Physics B* 288 (1987), pp. 1–76. ISSN: 0550-3213. DOI: https://doi.org/10.1016/0550-3213(87)90208-2.

[32] K. R. Dienes. "New string partition functions with vanishing cosmological constant". In: *Phys. Rev. Lett.* 65 (16 1990), pp. 1979–1982. DOI: 10.1103/PhysRevLett.65.1979.

[33] L. Dixon and J. Harvey. "String theories in ten dimensions without spacetime supersymmetry". In: *Nuclear Physics B* 274.1 (1986), pp. 93–105. ISSN: 0550-3213. DOI: https://doi.org/10.1016/0550-3213(86)90619-X.

[34] L. Alvarez-Gaumé, P. Ginsparg, G. Moore, and C. Vafa. "An $O(16)timesO(16)$ heterotic string". In: *Physics Letters B* 171.2 (1986), pp. 155–162. ISSN: 0370-2693. DOI: https://doi.org/10.1016/0370-2693(86)91524-8.

[35] A. E. Faraggi and M. Tsulaia. "Interpolations among NAHE-based supersymmetric and nonsupersymmetric string vacua". In: *Physics Letters B* 683.4 (2010), pp. 314–320. ISSN: 0370-2693. DOI: https://doi.org/10.1016/j.physletb.2009.12.039.

[36] A. Faraggi. "String phenomenology from a worldsheet perspective". In: *The European Physical Journal C* 79 (2019). DOI: 10.1140/epjc/s10052-019-7222-5.

[37] A. Faraggi, V. Matyas, and B. Percival. "Stable three generation standard-like model from a tachyonic ten dimensional heterotic-string vacuum". In: *The European Physical Journal C* 80 (2020). DOI: 10.1140/epjc/s10052-020-7894-x.

[38] H. Kawai, D. C. Lewellen, and S. H. H. Tye. "Classification of closed-fermionic-string models." In: *Physical Review D* 34 (1986), pp. 3794–3804.

[39] A. Gregori, C. Kounnas, and J. Rizos. "Classification of the $N = 2$, $Z_2 \times Z_2$-symmetric type II orbifolds and their type II asymmetric duals". In: *Nuclear Physics B* 549.1 (1999), pp. 16–62. ISSN: 0550-3213. DOI: https://doi.org/10.1016/S0550-3213(99)00135-2.

[40] H. K. Dreiner, J. L. Lopez, D. V. Nanopoulos, and D. B. Reiss. "String Model Building in the Free Fermionic Formulation". In: *Nucl. Phys. B* 320 (1989), pp. 401–439. DOI: 10.1016/0550-3213(89)90256-3.

[41] D. Chang and A. Kumar. "Twisted Thirring Interaction and Gauge Symmetry Breaking in $N = 1$ Supersymmetric Superstring Models". In: *Phys. Rev. D* 38 (1988), p. 3734. DOI: 10.1103/PhysRevD.38.3734.

[42] I. Florakis. "Théorie de Cordes et Applications Phénoménologiques et Cosmologiques". In: *PhD Thesis, Université Pierre et Marie Curie* (2011).

[43] I. Florakis and J. Rizos. "Chiral Heterotic Strings with Positive Cosmological Constant". In: *Nuclear Physics* 913 (2016), pp. 495–533.

[44] I. Florakis, J. Rizos, and K. Violaris-Gountonis. "Super no-scale models with Pati-Salam gauge group". In: *Nuclear Physics B* 976 (2022), p. 115689. ISSN: 0550-3213. DOI: https://doi.org/10.1016/j.nuclphysb.2022.115689.

[45] A. E. Faraggi. "$Z_2 \times Z_2$ orbifold compactification as the origin of realistic free fermionic models". In: *Physics Letters B* 326.1 (1994), pp. 62–68. ISSN: 0370-2693. DOI: https://doi.org/10.1016/0370-2693(94)91193-2.

[46] E. Kiritsis and C. Kounnas. "Perturbative and non-perturbative partial supersymmetry breaking: $N = 4 \to N = 2 \to N = 1$". In: *Nuclear Physics* 503 (1997), pp. 117–156.

[47] A. E. Faraggi, S. Forste, and C. Timirgaziu. "$Z_2 \times Z_2$ heterotic orbifold models of non factorisable six dimensional toroidal manifolds". In: *Journal of High Energy Physics* 2006 (2006), pp. 057–057.

[48] R. Y. Donagi and K. Wendland. "On orbifolds and free fermion constructions". In: *Journal of Geometry and Physics* 59 (2009), pp. 942–968.

[49] A. E. Faraggi. "Toward the classification of the realistic free fermionic models". In: *Int. J. Mod. Phys. A* 14 (1999), pp. 1663–1702. DOI: 10.1142/S0217751X99000841.

[50] A. E. Faraggi, C. Kounnas, S. E. M. Nooij, and J. Rizos. "Classification of the chiral Z(2) x Z(2) fermionic models in the heterotic superstring". In: *Nucl. Phys. B* 695 (2004), pp. 41–72. DOI: 10.1016/j.nuclphysb.2004.06.030.

[51] A. E. Faraggi, C. Kounnas, and J. Rizos. "Chiral family classification of fermionic $Z_2 \times Z_2$ heterotic orbifold models". In: *Physics Letters B* 648.1 (2007), pp. 84–89. ISSN: 0370-2693. DOI: https://doi.org/10.1016/j.physletb.2006.09.071.

[52] A. E. Faraggi, C. Kounnas, and J. Rizos. "Spinor-vector duality in fermionic $Z_2 \times Z_2$ heterotic orbifold models". In: *Nuclear Physics B* 774.1 (2007), pp. 208–231. ISSN: 0550-3213. DOI: https://doi.org/10.1016/j.nuclphysb.2007.03.029.

[53] A. E. Faraggi, C. Kounnas, and J. Rizos. "Spinor-vector duality in $N = 2$ heterotic string vacua". In: *Nuclear Physics B* 799.1 (2008), pp. 19–33. ISSN: 0550-3213. DOI: https://doi.org/10.1016/j.nuclphysb.2008.02.009.

[54] T. Catelin-Jullien, A. E. Faraggi, C. Kounnas, and J. Rizos. "Spinor–vector duality in heterotic SUSY vacua". In: *Nuclear Physics B* 812.1 (2009), pp. 103–127. ISSN: 0550-3213. DOI: https://doi.org/10.1016/j.nuclphysb.2008.12.007.

[55] C. Angelantonj, A. E. Faraggi, and M. Tsulaia. "Spinor-Vector duality in heterotic string orbifolds". In: *Journal of High Energy Physics* 2010 (2010), pp. 1–17.

[56] A. E. Faraggi, I. Florakis, T. Mohaupt, and M. Tsulaia. "Conformal aspects of Spinor–Vector duality". In: *Nuclear Physics B* 848.2 (2011), pp. 332–371. ISSN: 0550-3213. DOI: https://doi.org/10.1016/j.nuclphysb.2011.03.002.

[57] G. B. Cleaver, A. E. Faraggi, and S. Nooij. "NAHE based string models with SU(4) x SU(2) x U(1) SO(10) subgroup". In: *Nucl. Phys. B* 672 (2003), pp. 64–86. DOI: 10.1016/j.nuclphysb.2003.09.012.

[58] B. Assel, K. Christodoulides, A. E. Faraggi, C. Kounnas, and J. Rizos. "Classification of heterotic Pati–Salam models". In: *Nuclear Physics B* 844.3 (2011), pp. 365–396. ISSN: 0550-3213. DOI: https://doi.org/10.1016/j.nuclphysb.2010.11.011.

[59] A. E. Faraggi, J. Rizos, and H. Sonmez. "Classification of flipped $SU(5)$ heterotic-string vacua". In: *Nuclear Physics B* 886 (2014), pp. 202–242. ISSN: 0550-3213. DOI: https://doi.org/10.1016/j.nuclphysb.2014.06.025.

[60] A. E. Faraggi, J. Rizos, and H. Sonmez. "Classification of standard-like heterotic-string vacua". In: *Nuclear Physics B* 927 (2018), pp. 1–34. ISSN: 0550-3213. DOI: https://doi.org/10.1016/j.nuclphysb.2017.12.006.

[61] A. E. Faraggi, G. Harries, and J. Rizos. "Classification of left–right symmetric heterotic string vacua". In: *Nuclear Physics B* 936 (2018), pp. 472–500. ISSN: 0550-3213. DOI: https://doi.org/10.1016/j.nuclphysb.2018.09.028.

[62] X.-G. Wen and E. Witten. "Electric and magnetic charges in superstring models". In: *Nuclear Physics B* 261 (1985), pp. 651–677. ISSN: 0550-3213. DOI: https://doi.org/10.1016/0550-3213(85)90592-9.

[63] G. G. Athanasiu, J. J. Atick, M. Dine, and W. Fischler. "Remarks on Wilson lines, modular invariance and possible string relics in Calabi-Yau compactifications". In: *Physics Letters B* 214.1 (1988), pp. 55–62. ISSN: 0370-2693. DOI: https://doi.org/10.1016/0370-2693(88)90451-0.

[64] A. Schellekens. "Electric charge quantization in string theory". In: *Physics Letters B* 237 (1990), pp. 363–369. DOI: 10.1016/0370-2693(90)91190-M.

[65] S. Chang, C. Corianò, and A. E. Faraggi. "Stable superstring relics". In: *Nuclear Physics B* 477.1 (1996), pp. 65–104. ISSN: 0550-3213. DOI: https://doi.org/10.1016/0550-3213(96)00371-9.

[66] C. Corianò, A. E. Faraggi, and M. Plümacher. "Stable superstring relics and ultrahigh energy cosmic rays". In: *Nuclear Physics B* 614.1 (2001), pp. 233–253. ISSN: 0550-3213. DOI: https://doi.org/10.1016/S0550-3213(01)00420-5.

[67] B. Assel, K. Christodoulides, A. E. Faraggi, C. Kounnas, and J. Rizos. "Exophobic quasi-realistic heterotic string vacua". In: *Physics Letters B* 683.4 (2010), pp. 306–313. ISSN: 0370-2693. DOI: https://doi.org/10.1016/j.physletb.2009.12.033.

[68] B. Assel, K. Christodoulides, A. Faraggi, C. Kounnas, and J. Rizos Ioannis. "Exophobic Quasi-Realistic Heterotic String Vacua". In: *Physics Letters B* 683 (2010), pp. 306–313. DOI: 10.1016/j.physletb.2009.12.033.

[69] L. Bernard, A. E. Faraggi, I. Glasser, J. Rizos, and H. Sonmez. "String derived exophobic $SU(6) \times SU(2)$ GUTs". In: *Nuclear Physics B* 868.1 (2013), pp. 1–15. ISSN: 0550-3213. DOI: https://doi.org/10.1016/j.nuclphysb.2012.11.001.

[70] G. B. Cleaver, A. E. Faraggi, E. Manno, and C. Timirgaziu. "Quasi-realistic heterotic-string models with vanishing one-loop cosmological constant and perturbatively broken supersymmetry?" In: *Phys. Rev. D* 78 (4 2008), p. 046009. DOI: 10.1103/PhysRevD.78.046009.

[71] P. Athanasopoulos, A. E. Faraggi, and D. Gepner. "Spectral flow as a map between N=(2,0)-models". In: *Physics Letters B* 735 (2014), pp. 357–363.

[72] P. Athanasopoulos and A. E. Faraggi. "Niemeier Lattices in the Free Fermionic Heterotic–String Formulation". In: *Adv. Math. Phys.* 2017 (2017), p. 3572469. DOI: 10.1155/2017/3572469. arXiv: 1610.04898 [hep-th].

[73] C. Kounnas and H. Partouche. "Super no-scale models in string theory". In: *Nucl. Phys. B* 913 (2016), pp. 593–626. DOI: 10.1016/j.nuclphysb.2016.10.001.

[74] C. Kounnas and H. Partouche. "$\mathcal{N} = 2 \to 0$ super no-scale models and moduli quantum stability". In: *Nucl. Phys. B* 919 (2017), pp. 41–73. DOI: 10.1016/j.nuclphysb.2017.03.011.

[75] C. Kounnas and M. Porrati. "Spontaneous Supersymmetry Breaking in String Theory". In: *Nucl. Phys. B* 310 (1988), pp. 355–370. DOI: 10.1016/0550-3213(88)90153-8.

[76] C. Kounnas and B. Rostand. "Coordinate Dependent Compactifications and Discrete Symmetries". In: *Nucl. Phys. B* 341 (1990), pp. 641–665. DOI: 10.1016/0550-3213(90)90543-M.

[77] S. Ferrara, C. Kounnas, and M. Porrati. "Superstring Solutions With Spontaneously Broken Four-dimensional Supersymmetry". In: *Nucl. Phys. B* 304 (1988), pp. 500–512. DOI: 10.1016/0550-3213(88)90639-6.

[78] S. Ferrara, C. Kounnas, and M. Porrati. "$N = 1$ Superstrings With Spontaneously Broken Symmetries". In: *Phys. Lett. B* 206 (1988), pp. 25–31. DOI: 10.1016/0370-2693(88)91257-9.

[79] S. Ferrara, C. Kounnas, M. Porrati, and F. Zwirner. "Superstrings with Spontaneously Broken Supersymmetry and their Effective Theories". In: *Nucl. Phys. B* 318 (1989), pp. 75–105. DOI: 10.1016/0550-3213(89)90048-5.

[80] J. Scherk and J. H. Schwarz. "Spontaneous Breaking of Supersymmetry Through Dimensional Reduction". In: *Phys. Lett. B* 82 (1979), pp. 60–64. DOI: 10.1016/0370-2693(79)90425-8.

[81] J. Scherk and J. H. Schwarz. "How to Get Masses from Extra Dimensions". In: *Nucl. Phys. B* 153 (1979), pp. 61–88. DOI: 10.1016/0550-3213(79)90592-3.

[82] A. Faraggi, V. Matyas, and B. Percival. "Classification of nonsupersymmetric Pati-Salam heterotic string models". In: *Physical Review D* 104 (2021). DOI: 10.1103/PhysRevD.104.046002.

[83] H. K. Dreiner, J. L. Lopez, D. V. Nanopoulos, and D. B. Reiss. "No Massless Scalar Adjoints for $N = 1$, $D = 4$ Heterotic Strings in the Free Fermionic Formulation". In: *Phys. Lett. B* 216 (1989), pp. 283–288. DOI: 10.1016/0370-2693(89)91116-7.

[84] D. C. Lewellen. "Embedding Higher Level Kac-Moody Algebras in Heterotic String Models". In: *Nucl. Phys. B* 337 (1990), pp. 61–86. DOI: 10.1016/0550-3213(90)90251-8.

[85] K. R. Dienes and J. March-Russell. "Realizing Higher-Level Gauge Symmetries in String Theory: New Embeddings for String GUTs". In: *Nuclear Physics* 479 (1996), pp. 113–172.

[86] E. Plauschinn. "Non-geometric backgrounds in string theory". In: *Phys. Rept.* 798 (2019), pp. 1–122. DOI: 10.1016/j.physrep.2018.12.002. arXiv: 1811.11203.

[87] A. E. Faraggi, G. Harries, B. Percival, and J. Rizos. "Doublet-triplet splitting in fertile left-right symmetric heterotic string vacua". In: *Nuclear Physics B* 953

(2020), p. 114969. ISSN: 0550-3213. DOI: https://doi.org/10.1016/j.nuclphysb.2020.114969.

[88] S. Abel and J. Rizos. "Genetic algorithms and the search for viable string vacua". In: *Journal of High Energy Physics* 2014 (2014), pp. 1–22.

[89] Y.-H. He. *The Calabi–Yau Landscape: From Geometry, to Physics, to Machine Learning*. 2021. DOI: 10.1007/978-3-030-77562-9.

[90] L. de Moura and N. Bjørner. "Z3: An efficient SMT solver". In: *In Conference on Tools and Algorithms for the Construction and Analysis of Systems (TACAS '08)* (2008).

[91] G. B. Cleaver and A. E. Faraggi. "On the anomalous U(1) in free fermionic superstring models". In: *Int. J. Mod. Phys. A* 14 (1999), pp. 2335–2356. DOI: 10.1142/S0217751X99001172.

[92] A. E. Faraggi. "Generation mass hierarchy in superstring derived models". In: *Nucl. Phys. B* 407 (1993), pp. 57–72. DOI: 10.1016/0550-3213(93)90273-R.

[93] A. E. Faraggi, C. Kounnas, and H. Partouche. "Large volume susy breaking with a solution to the decompactification problem". In: *Nucl. Phys. B* 899 (2015), pp. 328–374. DOI: 10.1016/j.nuclphysb.2015.08.001.

[94] J. M. Ashfaque, P. Athanasopoulos, A. E. Faraggi, and H. Sonmez. "Non-tachyonic semi-realistic non-supersymmetric heterotic-string vacua". In: *The European Physical Journal C* 76 (2015), pp. 1–17.

[95] K. R. Dienes. "Modular invariance, finiteness, and misaligned supersymmetry: New constraints on the numbers of physical string states". In: *Nucl. Phys. B* 429 (1994), pp. 533–588. DOI: 10.1016/0550-3213(94)90153-8.

[96] K. R. Dienes, M. Moshe, and R. C. Myers. "String theory, misaligned supersymmetry, and the supertrace constraints". In: *Phys. Rev. Lett.* 74 (1995), pp. 4767–4770. DOI: 10.1103/PhysRevLett.74.4767.

[97] C. Angelantonj, M. Cardella, S. Elitzur, and E. Rabinovici. "Vacuum stability, string density of states and the Riemann zeta function". In: *JHEP* 02 (2011), p. 024. DOI: 10.1007/JHEP02(2011)024.

[98] N. Cribiori, S. Parameswaran, F. Tonioni, and T. Wrase. "Modular invariance, misalignment and finiteness in non-supersymmetric strings". In: *JHEP* 01 (2022), p. 127. DOI: 10.1007/JHEP01(2022)127.

[99] N. Cribiori, S. Parameswaran, F. Tonioni, and T. Wrase. "Misaligned Supersymmetry and Open Strings". In: *JHEP* 04 (2021), p. 099. DOI: 10.1007/JHEP04(2021)099.

[100] R. Hagedorn. "Statistical thermodynamics of strong interactions at high-energies". In: *Nuovo Cim. Suppl.* 3 (1965), pp. 147–186.

[101] S. Abel, K. R. Dienes, and E. Mavroudi. "Towards a nonsupersymmetric string phenomenology". In: *Physical Review D* 91 (2015), p. 126014.

[102] L. Delle Rose, A. E. Faraggi, C. Marzo, and J. Rizos. "Wilsonian dark matter in string derived $Z^{'}$ model". In: *Phys. Rev. D* 96 (5 2017), p. 055025. DOI: 10.1103/PhysRevD.96.055025.

[103] A. E. Faraggi. "Fractional charges in a superstring derived standard like model". In: *Phys. Rev. D* 46 (1992), pp. 3204–3207. DOI: 10.1103/PhysRevD.46.3204.

[104] C. Kounnas. "Massive Boson-Fermion Degeneracy and the Early Structure of the Universe". In: *Fortsch. Phys.* 56 (2008), pp. 1143–1156. DOI: 10.1002/prop.200810570.

[105] I. Florakis and C. Kounnas. "Orbifold Symmetry Reductions of Massive Boson-Fermion Degeneracy". In: *Nucl. Phys. B* 820 (2009), pp. 237–268. DOI: 10.1016/j.nuclphysb.2009.05.022.

[106] I. Florakis, C. Kounnas, and N. Toumbas. "Marginal Deformations of Vacua with Massive boson-fermion Degeneracy Symmetry". In: *Nucl. Phys. B* 834 (2010), pp. 273–315. DOI: 10.1016/j.nuclphysb.2010.03.020.

[107] J. J. Atick, L. J. Dixon, and A. Sen. "String Calculation of Fayet-Iliopoulos d Terms in Arbitrary Supersymmetric Compactifications". In: *Nucl. Phys. B* 292 (1987), pp. 109–149. DOI: 10.1016/0550-3213(87)90639-0.

[108] M. Bianchi and A. Sagnotti. "On the systematics of open string theories". In: *Phys. Lett. B* 247 (1990), pp. 517–524.

[109] C. Angelantonj. "Nontachyonic open descendants of the 0B string theory". In: *Phys. Lett. B* 444 (1998), pp. 309–317. DOI: 10.1016/S0370-2693(98)01430-0.

[110] R. Blumenhagen, A. Font, and D. Lust. "Tachyon free orientifolds of type 0B strings in various dimensions". In: *Nucl. Phys. B* 558 (1999), pp. 159–177. DOI: 10.1016/S0550-3213(99)00381-8.

[111] R. Blumenhagen and A. Kumar. "A Note on orientifolds and dualities of type 0B string theory". In: *Phys. Lett. B* 464 (1999), pp. 46–52. DOI: 10.1016/S0370-2693(99)01002-3.

[112] O. Bergman and M. R. Gaberdiel. "Dualities of type 0 strings". In: *JHEP* 07 (1999), p. 022. DOI: 10.1088/1126-6708/1999/07/022.

[113] K. Forger. "On nontachyonic Z(N) x Z(M) orientifolds of type 0B string theory". In: *Phys. Lett. B* 469 (1999), pp. 113–122. DOI: 10.1016/S0370-2693(99)01285-X.

[114] E. Dudas and J. Mourad. "D-branes in nontachyonic 0B orientifolds". In: *Nucl. Phys. B* 598 (2001), pp. 189–224. DOI: 10.1016/S0550-3213(00)00781-1.

[115] C. Angelantonj and A. Armoni. "Nontachyonic type 0B orientifolds, nonsupersymmetric gauge theories and cosmological RG flow". In: *Nucl. Phys. B* 578 (2000), pp. 239–258. DOI: 10.1016/S0550-3213(00)00136-X.

[116] D. Israel and V. Niarchos. "Tree-Level Stability Without Spacetime Fermions: Novel Examples in String Theory". In: *JHEP* 07 (2007), p. 065. DOI: 10.1088/1126-6708/2007/07/065.

[117] R. Grena, S. Lelli, M. Maggiore, and A. Rissone. "Confinement, asymptotic freedom and renormalons in type 0 string duals". In: *Journal of High Energy Physics* 2000 (2000), pp. 005–005.

[118] M. Akhond, A. Armoni, and S. Speziali. "Phases of $\mathbf{U}(\mathbf{N_c})$ QCD_3 from Type 0 Strings and Seiberg Duality". In: *JHEP* 09 (2019), p. 111. DOI: 10.1007/JHEP09(2019)111.

[119] S. A. Cook. "The Complexity of Theorem-Proving Procedures". In: Association for Computing Machinery, 1971. DOI: 10.1145/800157.805047.

[120] L. A. Levin. "Universal Sequential Search Problems". In: Problems of Information Transmission, 1973.

[121] R. Impagliazzo and R. Paturi. "Complexity of k-SAT". In: *Proceedings. Fourteenth Annual IEEE Conference on Computational Complexity (Formerly: Structure in Complexity Theory Conference) (Cat.No.99CB36317)* (1999), pp. 237–240.

[122] A. Bradley and Z. Manna. *The calculus of computation: Decision procedures with applications to verification*. Springer, 2007. ISBN: 3-540-74112-7. DOI: 10.1007/978-3-540-74113-8.

[123] A. Cimatti, A. Griggio, and R. Sebastiani. "Computing Small Unsatisfiable Cores in Satisfiability Modulo Theories". In: *J. Artif. Intell. Res. (JAIR)* 40 (2014). DOI: 10.1613/jair.3196.

[124] A. E. Faraggi. "Moduli fixing in realistic string vacua". In: *Nuclear Physics B* 728.1 (2005), pp. 83–108. DOI: https://doi.org/10.1016/j.nuclphysb.2005.08.028.

[125] A. E. Faraggi. "Yukawa couplings in superstring-derived standard-like models". In: *Phys. Rev. D* 47 (11 1993), pp. 5021–5028. URL: https://link.aps.org/doi/10.1103/PhysRevD.47.5021.

[126] A. E. Faraggi. "Doublet–triplet splitting in realistic heterotic string derived models". In: *Physics Letters B* 520.3 (2001), pp. 337–344. ISSN: 0370-2693. DOI: https://doi.org/10.1016/S0370-2693(01)01165-0.

[127] A. E. Faraggi, D. V. Nanopoulos, and K. Yuan. "A standard-like model in the four-dimensional free fermionic string formulation". In: *Nuclear Physics* 335 (1990), pp. 347–362.

[128] A. E. Faraggi. "A new standard-like model in the four dimensional free fermionic string formulation". In: *Physics Letters B* 278.1 (1992), pp. 131–139. ISSN: 0370-2693. DOI: https://doi.org/10.1016/0370-2693(92)90723-H.

[129] A. E. Faraggi. "Hierarchical top - bottom mass relation in a superstring derived standard - like model". In: *Phys. Lett. B* 274 (1992), pp. 47–52. DOI: 10.1016/0370-2693(92)90302-K.

[130] A. E. Faraggi. "Top quark mass prediction in superstring derived standard - like model". In: *Phys. Lett. B* 377 (1996), pp. 43–47. DOI: 10.1016/0370-2693(96)00310-3.

[131] I. Antoniadis, J. Ellis, J. Hagelin, and D. V. Nanopoulos. "The flipped $SU(5) \times U(1)$ string model revamped". In: *Physics Letters B* 231 (1989), pp. 65–74.

[132] A. E. Faraggi and D. V. Nanopoulos. "Naturalness of three generations in free fermionic Z(2)-n x Z(4) string models". In: *Phys. Rev. D* 48 (1993), pp. 3288–3296. DOI: 10.1103/PhysRevD.48.3288.

[133] A. E. Faraggi. "Toward the classification of the realistic free fermionic models". In: *Int. J. Mod. Phys. A* 14 (1999), pp. 1663–1702. DOI: 10.1142/S0217751X99000841.

[134] I. Antoniadis, J. Rizos, and K. Tamvakis. "Gauge symmetry breaking in the hidden sector of the flipped SU(5) × U(1) superstring model". In: *Physics Letters B* 278 (1992), pp. 257–265.

[135] A. E. Faraggi and E. Halyo. "Cabibbo-Kobayashi-Maskawa mixing in superstring derived Standard - like Models". In: *Nucl. Phys. B* 416 (1994), pp. 63–86.

[136] J. Rizos. "Top-quark mass coupling and classification of weakly coupled heterotic superstring vacua". In: *European Physical Journal C* 74 (2014), p. 2905. DOI: 10.1140/epjc/s10052-014-2905-4.

[137] J. Rizos. Workshop on Testing Fundamental Physics Principles. Corfu, 2017. URL: http://www.physics.ntua.gr/corfu2017/Talks/irizos@uoi_gr_01.pdf.

[138] C. Angelantonj, M. Cardella, and N. Irges. "An Alternative for Moduli Stabilisation". In: *Phys. Lett. B* 641 (2006), pp. 474–480. DOI: 10.1016/j.physletb.2006.08.072.

[139] D. Kutasov and N. Seiberg. "Number of degrees of freedom, density of states and tachyons in string theory and CFT". In: *Nucl. Phys. B* 358 (1991), pp. 600–618. DOI: 10.1016/0550-3213(91)90426-X.

[140] C. Angelantonj, C. Kounnas, H. Partouche, and N. Toumbas. "Resolution of Hagedorn singularity in superstrings with gravito-magnetic fluxes". In: *Nucl. Phys. B* 809 (2009), pp. 291–307. DOI: 10.1016/j.nuclphysb.2008.10.010.

[141] W. Fischler and L. Susskind. "Dilaton Tadpoles, String Condensates and Scale Invariance". In: *Phys. Lett. B* 171 (1986), pp. 383–389. DOI: 10.1016/0370-2693(86)91425-5.

[142] W. Fischler and L. Susskind. "Dilaton Tadpoles, String Condensates and Scale Invariance. 2." In: *Phys. Lett. B* 173 (1986), pp. 262–264. DOI: 10.1016/0370-2693(86)90514-9.

[143] I. Basile, J. Mourad, and A. Sagnotti. "On Classical Stability with Broken Supersymmetry". In: *JHEP* 01 (2019), p. 174. DOI: 10.1007/JHEP01(2019)174.

[144] C. Angelantonj, I. Florakis, and B. Pioline. "A new look at one-loop integrals in string theory". In: *Commun. Num. Theor. Phys.* 6 (2012), pp. 159–201. DOI: 10.4310/CNTP.2012.v6.n1.a4.

[145] C. Angelantonj, I. Florakis, and B. Pioline. "Rankin-Selberg methods for closed strings on orbifolds". In: *JHEP* 07 (2013), p. 181. DOI: 10.1007/JHEP07(2013)181.

[146] C. Angelantonj, I. Florakis, and B. Pioline. "One-Loop BPS amplitudes as BPS-state sums". In: *JHEP* 06 (2012), p. 070. DOI: 10.1007/JHEP06(2012)070.

[147] C. Angelantonj, I. Florakis, and B. Pioline. "A new look at one-loop integrals in string theory". In: *Commun. Num. Theor. Phys.* 6 (2012), pp. 159–201. DOI: 10.4310/CNTP.2012.v6.n1.a4.

[148] H. Itoyama and S. Nakajima. "Marginal deformations of heterotic interpolating models and exponential suppression of the cosmological constant". In: *Physics*

Letters B 816 (2021), p. 136195. DOI: https://doi.org/10.1016/j.physletb.2021.136195.

[149] H. Itoyama and S. Nakajima. "Stability, enhanced gauge symmetry and suppressed cosmological constant in 9D heterotic interpolating models". In: *Nuclear Physics* 958 (2020), p. 115111.

[150] H. Itoyama and S. Nakajima. "Exponentially suppressed cosmological constant with enhanced gauge symmetry in heterotic interpolating models". In: *Progress of Theoretical and Experimental Physics* 2019.12 (2019). DOI: 10.1093/ptep/ptz123. URL: https://doi.org/10.1093/ptep/ptz123.

[151] S. Abel and R. J. Stewart. "Exponential suppression of the cosmological constant in nonsupersymmetric string vacua at two loops and beyond". In: *Phys. Rev. D* 96 (10 2017), p. 106013. URL: https://link.aps.org/doi/10.1103/PhysRevD.96.106013.

[152] C. Angelantonj, I. Florakis, and M. Tsulaia. "Universality of Gauge Thresholds in Non-Supersymmetric Heterotic Vacua". In: *Phys. Lett. B* 736 (2014).

[153] I. Florakis. "Universality of radiative corrections to gauge couplings for strings with spontaneously broken supersymmetry". In: *J. Phys. Conf. Ser.* 631.1 (2015). Ed. by N. E. Mavromatos, V. A. Mitsou, D. Skliros, and A. Di Domenico, p. 012079. DOI: 10.1088/1742-6596/631/1/012079.

[154] C. Angelantonj, I. Antoniadis, and K. Forger. "Nonsupersymmetric type I strings with zero vacuum energy". In: *Nucl. Phys. B* 555 (1999), pp. 116–134. DOI: 10.1016/S0550-3213(99)00344-2.

[155] J. A. Harvey. "String duality and nonsupersymmetric strings". In: *Phys. Rev. D* 59 (1999), p. 026002. DOI: 10.1103/PhysRevD.59.026002.

[156] S. Kachru and E. Silverstein. "4-D conformal theories and strings on orbifolds". In: *Phys. Rev. Lett.* 80 (1998), pp. 4855–4858. DOI: 10.1103/PhysRevLett.80.4855.

[157] G. Shiu and S. H. H. Tye. "Bose-Fermi degeneracy and duality in nonsupersymmetric strings". In: *Nucl. Phys. B* 542 (1999), pp. 45–72. DOI: 10.1016/S0550-3213(98)00775-5.

[158] K. Aoyama and Y. Sugawara. "Non-SUSY Heterotic String Vacua of Gepner Models with Vanishing Cosmological Constant". In: *PTEP* 2021.3 (2021). DOI: 10.1093/ptep/ptab016.

[159] N.-P. Chang, D.-X. Li, and J. Perez Mercader. "The Cosmological Constant and Asymmetric Orbifolds". In: *Phys. Rev. Lett.* 60 (1988), p. 882. DOI: 10.1103/PhysRevLett.60.882.